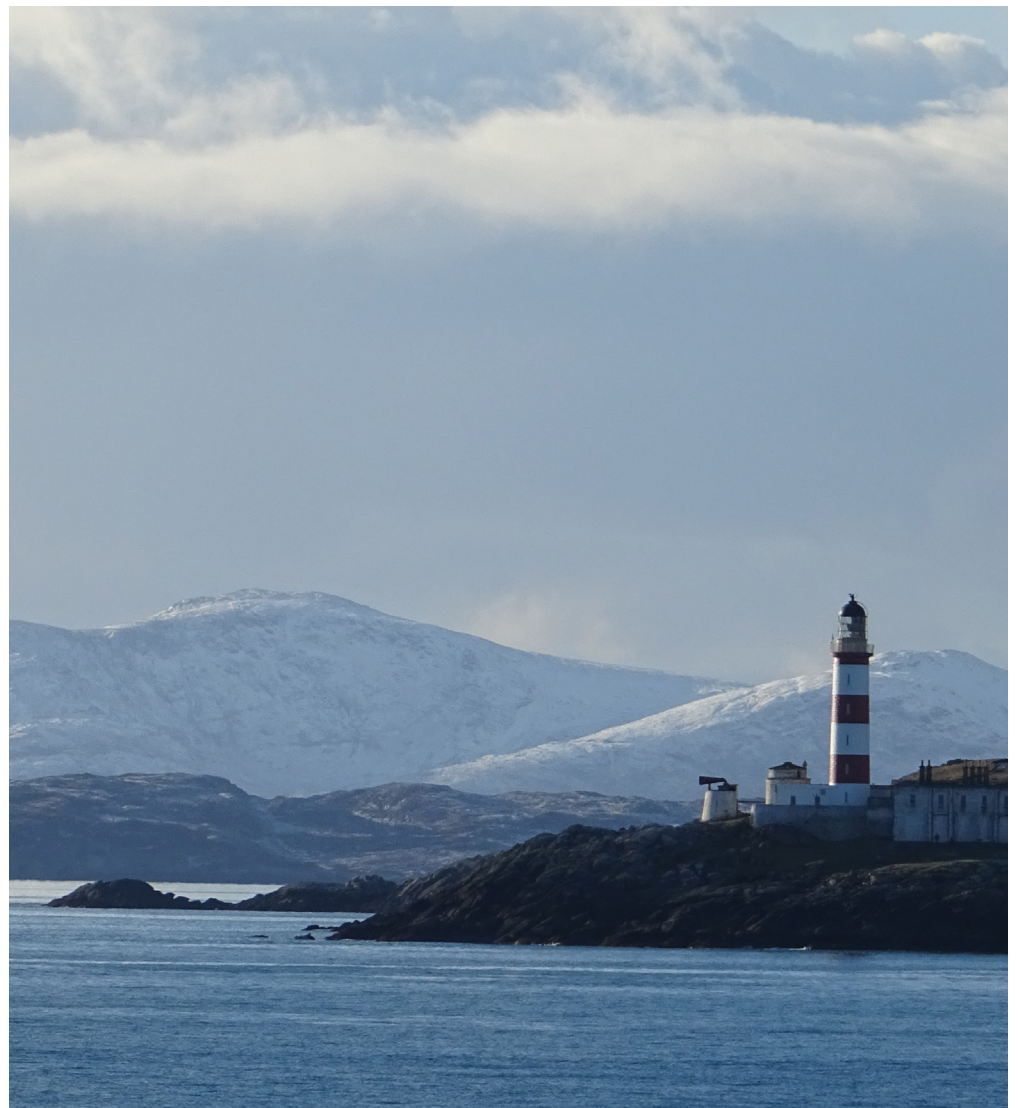


# ICES REPORT ON OCEAN CLIMATE 2021

Volume 358 | December 2023

**ICES COOPERATIVE  
RESEARCH REPORT**

**RAPPORT  
DES RECHERCHES  
COLLECTIVES**



## International Council for the Exploration of the Sea Conseil International pour l'Exploration de la Mer

H. C. Andersens Boulevard 44–46  
DK-1553 Copenhagen V  
Denmark  
Telephone (+45) 33 38 67 00  
Telefax (+45) 33 93 42 15  
[www.ices.dk](http://www.ices.dk)  
[info@ices.dk](mailto:info@ices.dk)

Series editor: Emory Anderson

Prepared under the auspices of ICES Working Group on Oceanic Hydrography (WGOH)

ISBN number: 978-87-7482-985-0

ISSN number: 2707-7144

Cover image: © Crown Copyright / Marine Scotland. All rights reserved.

This document has been produced under the auspices of an ICES Expert Group or Committee.  
The contents therein do not necessarily represent the view of the Council.

© 2023 International Council for the Exploration of the Sea.

This work is licensed under the Creative Commons Attribution 4.0 International License (CC BY 4.0). For citation of datasets or conditions for use of data to be included in other databases, please refer to ICES data policy.



# ICES Cooperative Research Report

Volume 358 | December 2023

## ICES Report on Ocean Climate 2021

### Editors

Cesar González-Pola • Karin M. H. Larsen • Paula Fratantoni •  
Agnieszka Beszczynska-Möller

Recommended format for purpose of citation:

González-Pola, C., Larsen, K. M. H., Fratantoni, P., and Beszczynska-Möller, A.  
(Eds.). 2023. ICES Report on ocean climate. ICES Cooperative Research  
Reports Vol. 358. 123 pp. <https://doi.org/10.17895/ices.pub.24755574>



**ICES**  
**CIEM**

International Council for  
the Exploration of the Sea  
Conseil International pour  
l'Exploration de la Mer

# Contents

I	Summary .....	i
II	Foreword .....	ii
III	Acknowledgements .....	iv
1	Introduction .....	1
	Highlights for the North Atlantic 2021 .....	1
2	Summary of upper ocean conditions in 2021 .....	3
	2.1 <i>In situ</i> stations and sections .....	3
	2.2 Sea surface temperature .....	9
	2.4 ARGO gridded temperature and salinity fields .....	10
	2.4.1 ISAS: Gridded temperature and salinity fields .....	10
	2.4.2 Method .....	11
	2.4.3 Highlights of 2021 .....	13
	2.4.4 Surface layers .....	13
	Seasonal patterns of T/S 2021 anomaly .....	13
	Seasonal cycle and monthly anomalies .....	13
	Interannual variability and long-term tendency .....	15
	Mixed layer depth .....	16
	2.5 Intermediate and deep layers .....	18
3	The North Atlantic atmosphere .....	20
	3.1 The North Atlantic Oscillation (NAO) index .....	20
	3.2 Sea level pressure and wind speed .....	21
	3.3 Surface air temperature .....	22
4	Detailed area descriptions, part I: The upper ocean .....	22
	Introduction .....	26
	4.1 West Greenland .....	29
	4.2 Labrador Sea .....	32
	Oceanographic monitoring of the Labrador Sea .....	32
	Deep convection, water ventilation, and hydrographic trends .....	34
	Hydrographic changes in the Labrador Sea over the past 82 years .....	35
	4.3 Newfoundland-Labrador Shelf .....	36
	4.4 Gulf of St Lawrence .....	39
	4.5 Scotian Shelf .....	42
	4.6 Northeast US continental shelf .....	46
	4.7 Icelandic waters .....	52
	4.8 Bay of Biscay and Iberian coast .....	55
	4.9 Gulf of Cadiz .....	58
	4.10 Canary Basin .....	61
	4.11 Southwest Approaches .....	63

4.12	Celtic Seas .....	65
4.13	Rockall Trough.....	67
4.14	Hatton–Rockall Basin .....	68
4.15	Iceland Basin .....	70
4.16	Irminger Sea .....	71
4.17	Faroese Waters and the Faroe–Shetland Channel.....	72
4.18	North Sea .....	76
4.19	Skaggerak, Kattegat, and the Baltic Sea .....	82
4.20	Norwegian Sea .....	87
4.21	Barents Sea .....	90
4.22	Fram Strait.....	93
5	Detailed area descriptions, part II: The intermediate and deep ocean .....	98
	Introduction.....	98
	5.1 Nordic Seas.....	99
	5.1.1 Greenland Sea .....	99
	5.1.2 Norwegian Sea .....	100
	5.1.3 Iceland Sea .....	102
	5.2 North Atlantic.....	102
	5.2.1 Iceland–Scotland Ridge overflow waters .....	102
	5.2.2 Iceland Basin .....	103
	5.2.3 Rockall Trough.....	105
	5.2.4 Irminger Basin .....	105
	5.2.5 Labrador Basin.....	107
	5.2.6 West Iberian margin.....	107
	5.2.7 Gulf of Cadiz .....	110
	5.2.8 Canary Basin .....	112
	References.....	114
	Annex 1: Contact information for authors by section.....	117
	Annex 2: List of abbreviations .....	123

# I Summary

ICES Report on Ocean Climate (IROC) combines decades of ocean observations across the North Atlantic ICES regions to describe the current status of sea temperature, salinity, and atmospheric conditions, as well as observed trends and recent variability. Regional analyses are prepared by the local experts who are directly involved in the monitoring programmes responsible for collecting the data presented in the report. The report describes in detail the status of 2021 conditions, including how the record-low salinities first observed in the Subpolar Gyre in 2016/2017 have continued to spread along the main circulation pathways both towards the north (into the North Sea, Nordic Seas, Barents Sea, and Fram Strait) and the south (into the Subtropical Gyre). Salinities in the Subpolar Gyre itself and in the immediate downstream pathways (e.g. Atlantic Water in the Faroe Current, Faroe Bank Channel, and deep regions west of Scotland) have increased to near-average. Regional record warming in some regions and minimum sea-ice extents are also discussed.

The 2021 IROC marks the final annual release in this series since the late 1990s. The IROC will subsequently shift to a triennial publication schedule.

## II Foreword

We are pleased to present the 2021 issue of the ICES Report on Ocean Climate (IROC). The report was written by a group of experts cooperating in the International Council for the Exploration of the Sea (ICES) Working Group on Oceanic Hydrography (WGOH). In the report, you will find hydrographic analyses and interpretations of long-time data series through 2021.

Despite some continued operational restrictions related to the COVID-19 pandemic, ocean observations were collected much more efficiently in 2021 than in 2020. Advances in safety procedures, introduced by the institutions conducting the measurements, ensured the continuation of data time-series in many regions. WGOH held meetings online in 2022, with the main meeting held in spring and an additional meeting in autumn. An increase in attendance was observed for these virtual meetings, because they enabled more people to participate, and there is a very strong possibility that hybrid and online meetings will become standard for WGOH. Online communication brings more opportunities to develop the IROC text and content (e.g. map unification), coordinate data exchange, and develop common research and data standards.

A decision has been made to change the publishing rhythm of the IROC in future years. Annual production deadlines have become increasingly difficult to meet due to a combination of limited human resources and the extremely compressed production time-line. Ideally, we aim to release the report during summer, prior to the ICES Annual Science Conference. This requires contributors to submit data and descriptive text during early spring so that the editorial team can assemble and review the report before it is passed to the ICES production team. An earlier deadline for data submission is not feasible due to data collection time-lines. A three-year publication frequency is consistent with publication time-lines for other ICES reports. The change will allow the WGOH to work on the report at a more reasonable pace while also allowing time to make desired improvements to the product. We would like to note that, despite these changes, the WGOH membership is still committed to meeting each year to review the latest oceanographic and atmospheric observations for the North Atlantic and Nordic Seas, and continuing to utilize the online IROC portal to publish annual highlights summarizing conditions as an outcome of these meetings. In addition, WGOH will continue to update the observational time-series served on the IROC portal at an annual frequency so that these valuable data are available to the broader ICES community.

The IROC 2021 was written by the following members of WGOH with support from a number of data providers:

Jon Albretsen (IMR, Bergen, Norway), Wilken-Jon von Appen (AWI, Bremerhaven, Germany), Barbara Berx (MSS, Aberdeen, UK), Agnieszka Beszczynska-Möller (IOPAN, Sopot, Poland), Boris Cisewski (TI-SF, Bremerhaven, Germany), Caroline Cusack (Marine Institute, Galway, Ireland), Frédéric Cyr (DFO, St. John's, Newfoundland and Labrador, Canada), Eoghan Daly (Marine Institute, Ireland), Magnus Danielsen (MFRI, Iceland), Damien Desbruyères (Ifremer/LOPS, Brest, France), Femke de Jong (NIOZ, Texel, Netherlands), Stephen Dye (Cefas, Lowestoft, UK), Almudena Fontán (AZTI, San Sebastian, Spain), Paula Fratantoni (NOAA, Woods Hole, MA, USA), Peter Galbraith (DFO, Mont-Joli, Quebec, Canada), César González-Pola (IEO, Gijón, Spain), Rocío Graña (IEO, Gijón, Spain), David Hebert (DFO, Dartmouth, Nova Scotia, Canada), Jenny Hindson (MSS, Aberdeen, UK), Billy Hunter (AFBI, UK), Randi Ingvaldsen (IMR, Bergen, Norway), Sam Jones (SAMS, Oban, UK), Dagmar Kieke (BSH, Hamburg, Germany), Inga Kirstein (AWI, Bremerhaven, Germany), Holger Klein (BSH, Hamburg, Germany), Manuela Köllner (BSH, Hamburg, Germany), Nicolas Kolodziejczyk (UBO, Brest, France), Tim Kruschke (BSH, Hamburg, Germany), Karin Margretha H. Larsen

(FAMRI, Tórshavn, Faroes), K. Latarius (BSH, Hamburg, Germany), C. Layton (DFO, Dartmouth, Nova Scotia, Canada), Taavi Liblik (TalTech, Tallinn, Estonia), Johanna Linders (SMHI, Göteborg, Sweden), Peter Loewe (BSH, Hamburg, Germany), Kieran Lyons (Marine Institute, Galway, Ireland), Kjell-Arne Mork (IMR, Bergen, Norway), Ángela Mosquera (IEO, Tenerife, Spain), Sólveig R. Ólafsdóttir (MFRI, Reykjavik, Iceland), Hjalte Parner (ICES, Copenhagen, Denmark), Carmen Presas-Navarro (IEO, Tenerife, Spain), Berit Rabe (Scottish Government, Aberdeen, UK), Ricardo Sánchez-Leal (IEO, Cadiz, Spain), Tim Smyth (PML, Plymouth, UK), Raquel Somavilla (IEO, Santander, Spain), Alexander Trofimov (PINRO, Murmansk, Russian Federation), Pedro Vélez-Belchí (IEO, Tenerife, Spain), Karen Wiltshire (AWI, Bremerhaven, Germany), Tycjan Wodzinowski (MIR-PIB, Gdynia, Poland), Igor Yashayaev (BIO, Bedford, Canada), and Svein Østerhus (NORCE, Bergen, Norway).

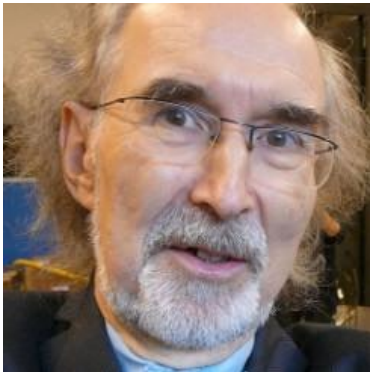
For a list of authors by section, including full affiliation and contact details, see Annex 1.

Technical assistance during the assembly of this report was provided by Eneko Aierbe and Rocío Graña (IEO, Gijón, Spain).

### III Acknowledgements

This year, we are introducing a new IROC section to pay tribute to the work of past WGOH colleagues who have contributed considerable time and effort to the expert group activities and the content of past reports. We commend our WGOH colleagues listed below (alphabetical order by surname) and wish them all the very best in the future.

#### **Pekka Alenius**



Pekka Alenius, born in 1954, began studying oceanography at the University of Helsinki in 1973. Pekka started his career in the Finnish Institute of Marine Research (FIMR) in 1975, first as a summer research assistant, then as a scientist and later as a senior scientist. His first touch of real ICES work was a possibility to participate in the Working Group on Marine Data Management (WGMDM) meeting in 1983 in Brest as deputy for Pentti Mälkki. During 1988–1992, he represented Finland in WGMDM and again, after a break, on from 1999. When Bert Rudels was nominated to WGOH, Pekka assisted him in reporting on ocean climate data from the northern Baltic Sea. Pekka continued to be the Finnish contact when preparing the IROC until his retirement in spring 2022 from the Finnish Meteorological Institute (FMI). Pekka says that having the possibility to visit several Member State data centres in WGMDM meetings and later take part in meetings of ICES Working Group on Data and Information (WGDIM) and ICES Data and Information Group (DIG) in ICES Headquarters in Copenhagen has been a great privilege and joy. Pekka always remembers to stress the importance of ICES Data Centre for maintaining a long time-series of quality controlled data and for the many kinds of data products, like IROC, that ICES has in its repertoire. Pekka has always been an inspirational colleague, and he is always available to share both his vast experience and enthusiasm for oceanography with younger scientists.

#### **Eugene Colbourne**



Eugene Colbourne began his career in marine science in the late 1980s and shortly thereafter accepted a position as lead physical oceanographer for Fisheries and Oceans Canada (DFO) at the Northwest Atlantic Fisheries Centre in St. John's, Newfoundland and Labrador. Eugene has led and contributed to numerous oceanographic missions in the Northwest Atlantic aboard a variety of Canadian Coast Guard ships and charter research vessels. He also distinguished himself through active participation and publication of research reports on numerous ocean climate and hydrographic studies throughout the Northwest Atlantic over three decades. Eugene was a founding member of DFO's Atlantic Zone Monitoring Program (AZMP) and a main contributor to WGOH and the NAFO Standing Committee on Fisheries Environment (STACFEN). He contributed to the online ocean climate status summaries for the Northwest Atlantic and to annual state-of-the-ocean reports for physical oceanographic conditions over the North Atlantic. Eugene has contributed to a number of ICES

and NAFO symposia over the years that investigated a variety of aspects of the links between ocean climate and fisheries stock dynamics. Eugene retired from DFO in 2018.

## Holger Klein



Holger Klein, our retired colleague and former member of WGOH, worked for decades at the Federal Maritime and Hydrographic Agency (BSH) in Hamburg, Germany. Being passionate about the ocean since childhood, Holger loved to be at sea either on a sailing boat or on board a research vessel. Experimental oceanography, team spirit, and getting to the bottom of physical processes has always been a keen interest of Holger's. The North Sea proved to be the perfect scientific 'playground' for him. With so many scientific partners and partner institutions addressing changes in the North Sea and the North Atlantic, and potential causes of these changes, WGOH was a scientific 'home' for Holger since 2006. Therein, he acted as an enthusiastic advocate for ocean and climate topics related to the North Sea. As an active WGOH member, he enjoyed engaging in the annual meetings, and

one particular meeting was organised by him in Hamburg in April 2014. Holger always strived to establish and maintain long-term time-series of climate-relevant parameters bringing people and time-series from various observational sites together.

## Victor Valencia



Victor Valencia, a former member of WGOH, worked for decades at the Marine Research Division of AZTI until he retired in 2018. During his professional career, he worked in a broad range of disciplines including physical, biological, and chemical oceanography, fisheries research, and analytical and environmental chemistry. He established the long-term hydrographic monitoring programme "VARIACIONES, short- and long-term oceanographic and meteorological variability in relation to the Bay of Biscay fisheries" (Basque

Government, Spain) in the southeastern Bay of Biscay. Through this programme, repeated hydrographic surveys have been carried out nearly monthly since April 1986. In the mid-1990s, Victor also contributed to the establishment of the physicochemical and biological long-term monitoring network (Basque Water Agency) consisting of 32 coastal and estuarine stations sampled since 1995, and an additional 19 stations since 2002. He has been an active member of WGOH since the beginning of the 2000s. We would like to thank him for his enthusiasm and commitment for maintaining long-term measurements and especially for sharing knowledge, data, and ideas.

# 1 Introduction

Long time-series of ocean properties are rare in the surface ocean and even more uncommon in the deep ocean. The North Atlantic region is unique, having a relatively large number of locations where oceanographic data have been collected repeatedly for multiple years or decades. The longest records extend back more than a century.

The ICES Report on Ocean Climate (IROC) combines decades of ocean observations across the North Atlantic ICES region to describe the current status of sea temperature and salinity and atmospheric conditions, as well as observed trends and recent variability. The production of the IROC is the primary focus of the International Council for the Exploration of the Sea (ICES) Working Group on Oceanic Hydrography (WGOH; González-Pola *et al.*, 2019).

Section 1 provides an overview of changes across the entire ICES Area, synthesizing information from the longest available time-series. The main focus of this report is the observed variability of the upper ocean (upper 1 000 m); a summary of upper ocean conditions is presented in Section 2. Section 2.3 presents spatially gridded fields constructed by optimal analysis of Argo float data, distributed by the Coriolis data centre in France. Section 3 provides a brief description of atmospheric conditions, and the subsequent two sections contain short regional summaries of the variability of North Atlantic upper waters (Section 4) and intermediate and deep waters (Section 5). Although the focus of the report is on temperature and salinity measurements, additional complementary datasets are included throughout the report, such as sea level pressure (SLP), air temperature, and ice cover.

The data presented here represent an accumulation of knowledge collected by many individuals and institutions over decades of observations. Much of the data included in this report, and additional data, are available to download via a web tool <sup>1</sup>. A more detailed overview of a particular region and a full description of some of the datasets used to develop the time-series presented in this report can be found in the annual meeting reports of WGOH <sup>2</sup>.

WGOH met via video conference 11–21 April 2022 to review oceanographic conditions in the North Atlantic in 2021. WGOH members are custodians of some of the longest sustained time-series of ocean observations, with many now extending more than 40 years. Their joint analysis has strengthened individual organizational efforts to provide the following highlights for the North Atlantic 2021.

## Highlights for the North Atlantic 2021

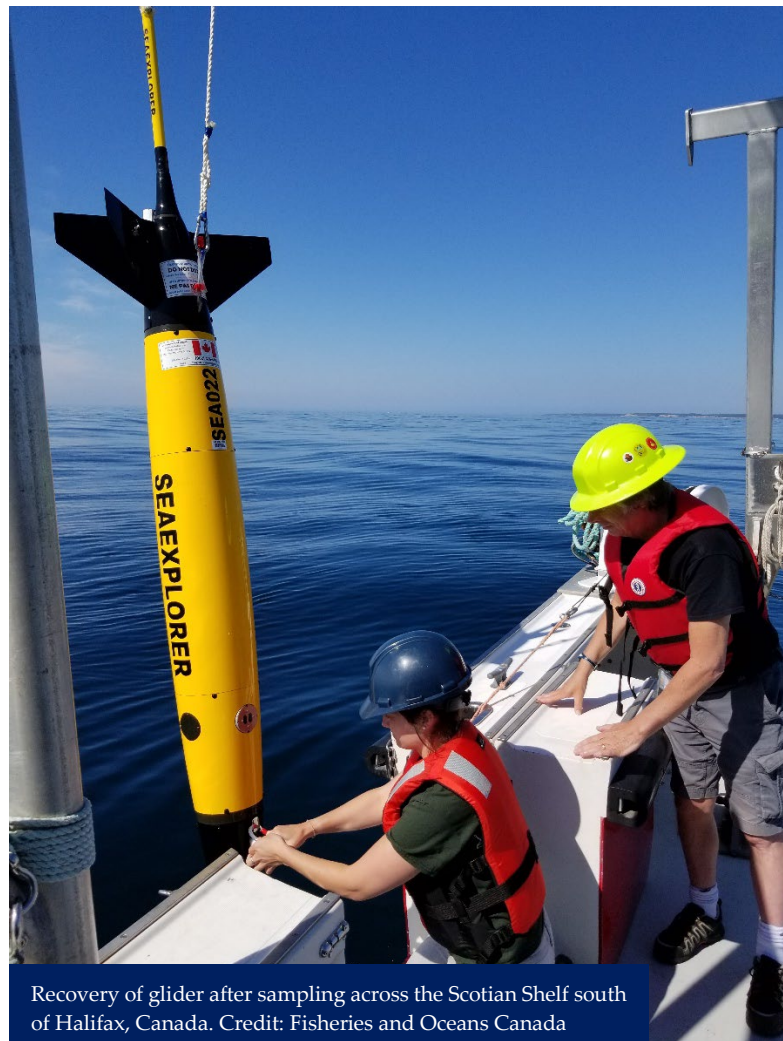
- The record-low salinities, first observed in the Subpolar Gyre in 2016/2017, have continued to spread (within expected time-lines) along the main circulation pathways both towards the north (into the North Sea, Nordic Seas, Barents Sea, and Fram Strait) and the south (into the Subtropical Gyre).
- Low-salinity anomalies are now also apparent deeper in the water column, meaning this is no longer a feature exclusive to surface waters.

---

<sup>1</sup>ICES report on ocean climate (IROC). 2023. ICES, Copenhagen, Denmark. <http://ocean.ices.dk/iroc>

<sup>2</sup>Working Group on Oceanic Hydrography. 2023. ICES, Copenhagen, Denmark. <http://www.ices.dk/community/groups/Pages/WGOH.aspx>

- Salinities in the Subpolar Gyre itself and in the immediate downstream pathways [e.g. Atlantic Water (AW) in the Faroe Current, Faroe Bank Channel, and deep regions west of Scotland] have increased to near average.
- Record-low salinity in surface waters of the Bay of Biscay, the Iberian coast, the Gulf of Cadiz, and the Canary Islands is changing water column stratification (i.e. increasing the buoyancy anomaly). For example, in the Bay of Biscay and Iberian coast, the salinity of the upper 500 m is the lowest observed in approximately the last three decades.
- Temperatures across the surface waters of the North Atlantic and the inflowing AW to the Norwegian and Barents seas remain close to the long-term average. However, the deep waters in the Nordic Seas, and associated overflow branches, have continued to warm. In some regions (e.g. the Greenland Sea at 700–2 000 m), this warming appears to have slowed or even stopped.
- Record warming was observed on the continental shelves of the western North Atlantic in 2021. Ocean temperatures close to the seabed were substantially above normal across the region, including record highs in the northern Gulf of St Lawrence, off southern Newfoundland, and across the northeast US Shelf.
- The sea ice area in the Barents Sea was much lower in 2021 compared to previous years. A new seasonal low record for sea ice volume occurred in the Gulf of St Lawrence (considering the period since records began in 1969).



Recovery of glider after sampling across the Scotian Shelf south of Halifax, Canada. Credit: Fisheries and Oceans Canada

## 2 Summary of upper ocean conditions in 2021

This section summarizes conditions in the upper layers of the North Atlantic during 2021 using data from (i) a selected set of sustained observations, (ii) gridded sea surface temperature (SST) data, and (iii) gridded vertical profiles of temperature and salinity from Argo floats.

### 2.1 *In situ* stations and sections

Where *in situ* section and station data are presented in the summary tables and figures, normalized anomalies have been provided to allow better comparison of trends across regions (figures 2.1, 2.2, and 2.3; Table 2.1). The anomalies have been normalized by dividing the values by the standard deviation (s.d.) of the data during 1991–2020 (or the closest time-period available). Please note that, following standard practice in climate science, the 30-year reference average shifted with the turn of the decade (which differs from previous IROC reports). A value of +2 thus represents temperature or salinity data measuring 2 s.d. higher than normal.

#### Information Box 2.1. Definitions

**Sustained observations or time-series:** Regular measurements of ocean temperature and salinity made over 10–100 years. Most measurements are made 1–4 times a year, but some are made more frequently.

**Anomalies:** Mathematical differences between each individual measurement and the average value of temperature, salinity, or other variables at each location and time. Positive anomalies in temperature and salinity imply warm or saline conditions; negative anomalies imply cool or fresh conditions.

**Normalized anomalies:** anomalies that have been normalized by dividing the values for a given year by the standard deviation (s.d.) of the 1981–2010 data (or the closest time-period available). A value of +2 thus represents temperature or salinity data measuring 2 s.d. higher than normal.

**Seasonal cycle:** The short-term changes at the surface of the ocean brought about by the passing of the seasons – the ocean surface is cold in winter and warms through spring and summer. Temperature and salinity changes caused by the seasonal cycle are usually much greater than the prolonged year-to-year changes we describe here.



R.V. Celtic Explorer during subsurface mooring deployment. Credit: Paul Stapleton

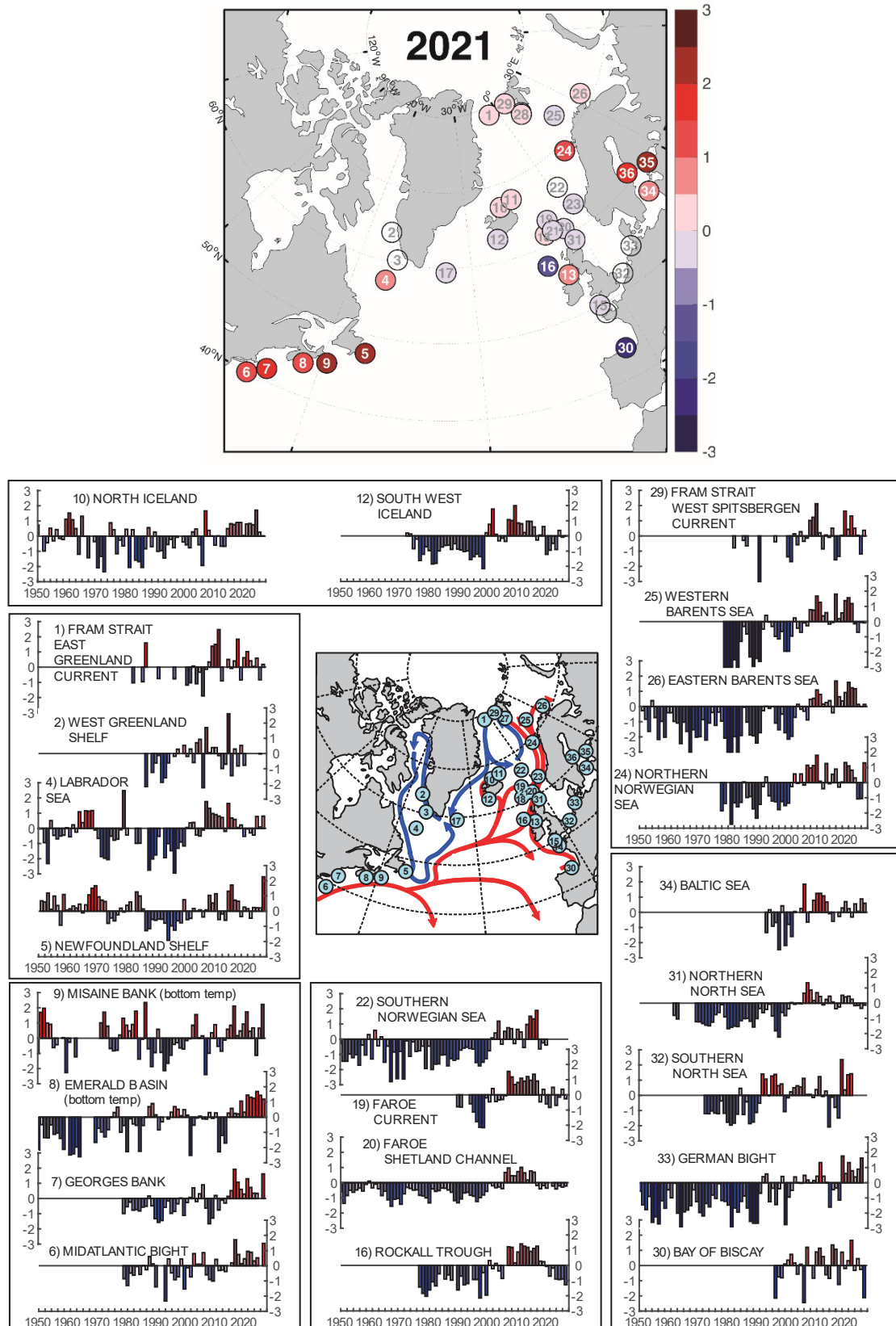
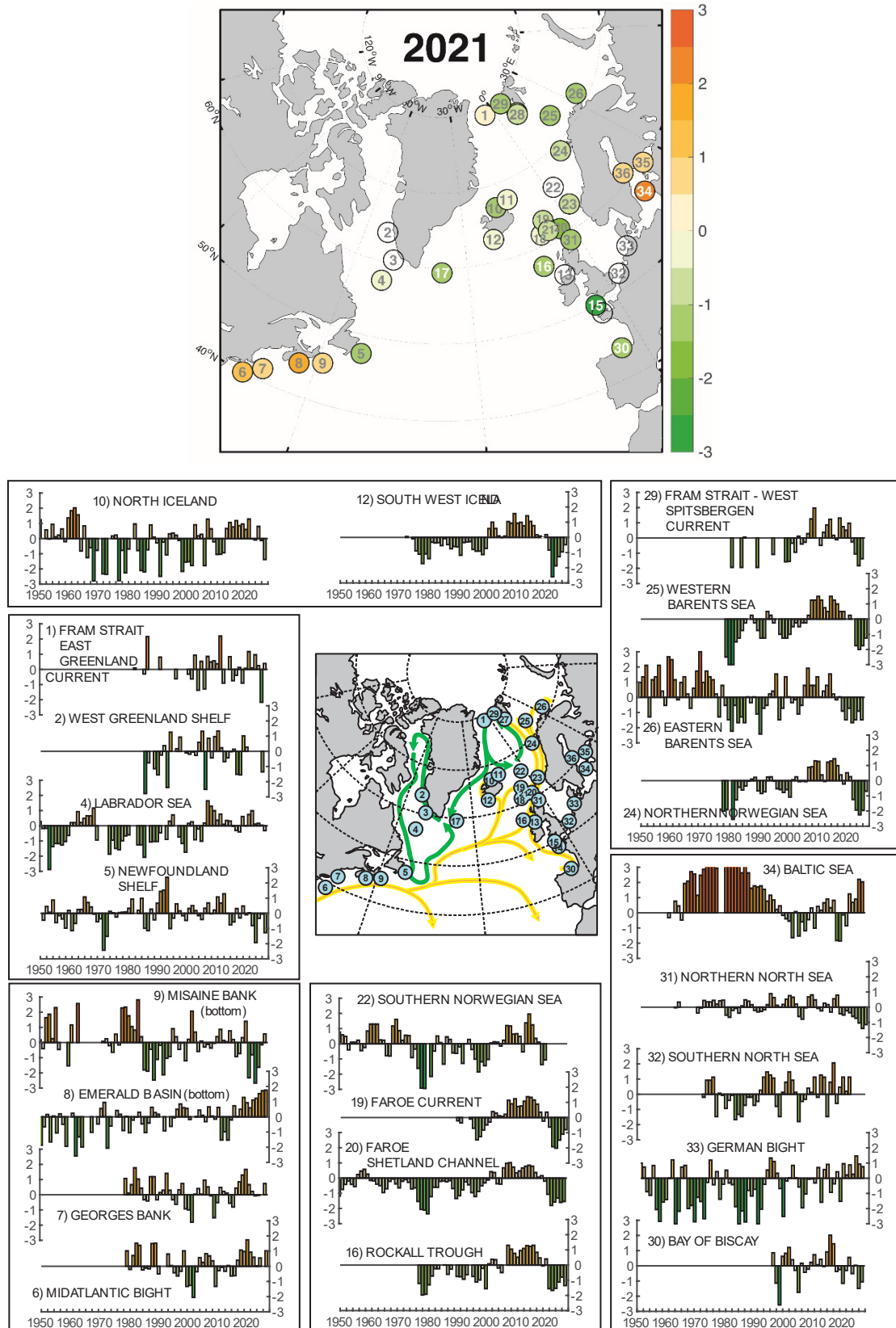


Figure 2.1. Upper ocean temperature anomalies at selected locations across the North Atlantic. The anomalies are normalized with respect to the standard deviation (s.d.; e.g. a value of +2 indicates 2 s.d. above normal). Upper panels: maps of conditions in 2021. Lower panels: time-series of normalized anomalies at each of the selected stations. Colour intervals: 0.5 s.d.; reds: positive/warm; blues: negative/cool. More details can be found in Section 4.



**Figure 2.2.** Upper ocean salinity anomalies at selected locations across the North Atlantic. The anomalies are calculated relative to a long-term mean and normalized with respect to the s.d. (e.g. a value of +2 indicates 2 s.d. above normal). Upper panel: map of conditions in 2021. Lower panels: time-series of normalized anomalies at each of the selected stations. Colour intervals: 0.5 s.d.; oranges: positive/saline; greens: negative/fresh. More details can be found in Section 4.

**Table 2.1. Changes in temperature (upper panel) and salinity (lower panel) at selected stations in the North Atlantic region during the past decade, 2012–2021. The index numbers on the left can be used to cross-reference each point with information in figures 2.1 and 2.2, and in Table 2.2. Unless specified, these are upper-layer anomalies. The anomalies are normalized with respect to the s.d. (e.g. a value of +2 indicates that the data observation of temperature or salinity for that year was 2 s.d. above normal). Blank boxes indicate that data were unavailable for a particular year at the time of publication. Note that no salinity data are available for station 13. Colour intervals: 0.5 s.d.; red: warm; blue: cold; orange: saline; green: fresh.**

	2012	2013	2014	2015	2016	2017	2018	2019	2020	2021	
1	0.41	1.84	-0.84	0.62	1.02	0.42	0.05	0.59	-0.83	0.18	3
2	0.30	-0.82	0.53	-0.77					-0.03		
3	1.12	-0.21	0.58	-1.01	-0.94			0.05			
4	0.59	0.06	0.22	-0.53	-0.04	-0.29	-0.44	0.78	0.09	0.81	
5	0.73	0.66	-0.35	0.27	0.16	-0.46	0.24	0.22	0.21	2.26	
6	1.71	0.74	0.14	0.46	0.95	0.89	0.32	0.52		1.47	
7	0.52	1.92	1.07	0.60	0.29	1.30	0.73	0.35	0.34	1.62	
8	0.25	0.22	1.06	0.33	1.45	1.31	1.25	1.89	1.44	1.19	
9	2.12	0.17	0.48	0.93	1.73	0.46	0.68	-1.13	0.66	2.23	
10	0.77	0.90	0.90	0.04	0.80	0.83	0.75	1.71	0.26	0.02	
11	0.20	0.33	1.29	0.41	0.64	1.93	2.06	1.38	-0.23	0.33	
12	-0.27	0.06	0.61	-1.21	-0.94	-0.49	-0.90	0.36	-0.08	-0.01	
13	0.10	-0.10	1.21	0.19	1.07	1.45	-0.10	1.45	0.41	0.70	
14	0.24	-1.02	1.50	0.94	0.48						
15	0.23	-0.81	0.37	-0.18	-0.26	0.29	0.20	-0.29	1.01	-0.25	
16	1.26	0.28	0.24	-0.06	-0.71	-0.18	-0.90	-0.93	-0.90	-1.27	
17	-0.27		0.05	-0.42	-0.79		-0.42		-0.17	-0.49	
18	-0.12	-0.04	0.55	0.06	-0.11	0.16	-0.78	-0.30	0.45	0.35	
19	0.91	-0.46	0.36	-0.59	-0.83	0.50	-0.69	-0.15	0.37	-0.26	
20	-0.18	-0.40	-0.19	-0.36	0.00	-0.22	-0.41	-0.21	-0.29	-0.22	
21	0.18	0.29	0.39	0.01	-0.29	-0.01	-0.23	-1.02	-0.09	-0.07	
22	1.90	-0.64	-0.24	-0.38							
23	0.11	0.25	-0.01	0.21	0.05	0.48	-1.03	0.22	-0.33	-0.25	
24	0.89	-0.29	0.04	1.32	1.10	0.82	0.31	-1.07	-1.05	1.30	
25	1.81	0.19	0.57	1.38	1.57	1.19	-0.14	-0.70	-0.05	-0.08	
26	1.68	0.64	0.37	0.92	1.59	1.23	1.17	0.14	-0.01	0.14	
27	0.57	-0.35	0.80	0.62	1.12	1.20	1.15	-0.07	0.04	-0.21	
28	0.15	-0.93	0.88		0.51	2.39	0.79	-0.11	-1.10	0.35	
29	-1.57	-1.34	0.04	1.63	0.44	1.31	0.51	0.04	-1.18	0.37	
30	1.07	-1.25	0.88	-0.19	0.32	1.66	-0.32	0.46	-0.26	2.11	
31	-0.36	-0.25	0.52	0.42	0.46	0.26	-0.16	-0.15	-0.34	-0.13	
32	-0.79	-1.49	2.35	0.36	1.35	1.42					
33	-0.35	-1.14	1.76	0.61	1.33	0.79	0.39	0.89	1.63		
34		-0.27	0.29	0.70	0.24	-0.31	0.55	0.06	0.88	0.60	
35	0.44	0.76	-0.23	-0.02	0.75	0.68	1.05	1.96	1.22	2.37	
36	-0.42	-0.24	1.10	1.06	1.21	0.80	0.80	0.62	1.83	1.88	

	2012	2013	2014	2015	2016	2017	2018	2019	2020	2021	
1	-0.39	0.13	-0.91	0.07	1.18	0.10	0.97	0.25	-2.17	0.39	3
2	-1.52	-1.55	1.01	0.27					-1.35		
3	-0.51	0.72	-0.93	-0.12	-1.98			-0.37			
4	-0.31	-0.40	0.61	0.00	0.75	0.99	0.11	0.17	0.04	-0.32	
5	0.32	-0.30	0.48	-0.09	0.04	-0.81	-1.93	-0.33	-0.05	-1.27	
6	0.40	1.07	0.98	1.74	0.93	0.60	0.02	0.55		1.02	
7	-0.81	0.44	0.85	1.30	1.67	0.67	0.22	-0.07	-0.04	0.74	
8	0.02	0.50	1.28	0.93	0.59	1.11	1.22	1.53	1.72	1.76	
9	-0.92	-0.73	0.32	1.40	-2.32	-0.81	-2.57	-1.63	-0.15	0.56	
10	1.18	0.85	0.96	0.60	1.29	-0.02	-0.09	0.81	-0.13	-1.38	
11	1.22	0.91	-0.34	0.59	0.75	0.71	-0.40	0.54	0.15	-0.01	
12	0.17	0.09	-0.00	0.18	-0.83	-2.59	-1.88	-1.27	-0.96	-0.48	
13											
14	0.02	-0.10	-0.17	-0.06	-0.10						
15	0.35	0.40	-0.17	1.39	0.42	1.28	-1.39	-0.76	-1.89	3.11	
16	0.84	0.47	-0.06	0.40	-1.56	-1.67	-1.53	-1.12	-0.80	-1.35	
17	0.41		0.30	0.70	0.44		-0.18		-0.66	-1.32	
18	0.44	0.56	0.10	0.46	-1.14	-1.78	-2.20	-1.34	-0.82	-0.22	
19	0.88	0.35	-0.23	0.35	-0.63	-1.92	-2.02	-1.49	-1.10	-0.80	
20	0.37	0.06	0.16	-0.20	-1.07	-1.80	-1.57	-1.32	-1.60	-1.54	
21	0.78	0.29	-0.22	-0.25	-1.06	-1.83	-2.16	-2.32	-1.09	-0.87	
22	0.36	0.11	-1.37	-1.06							
23	0.68	0.38	-0.34	0.28	-0.59	-1.81	-2.19	-1.29	-1.21	-0.94	
24	0.99	0.38	-0.22	0.52	0.26	-1.24	-1.94	-2.25	-1.96	-0.70	
25	1.00	0.50	0.50	0.00	0.25	0.00	-1.75	-2.00	-1.75	-1.25	
26	0.22	-0.16	0.03	-0.91	-1.48	-0.72	-1.67	-1.48	-0.91	-1.48	
27	1.37	0.67	1.24	0.37	0.71	0.71	-0.02	-1.21	-1.16	-1.48	
28	1.22	0.80	1.50		1.00	0.75	-0.85	-1.15	-1.50	-0.80	
29	0.17	-0.11	1.31	0.74	0.51	0.97	-0.26	-1.06	-1.83	-1.37	
30	1.45	-0.37	-0.25	-1.16	-0.31	0.56	-0.51	0.04	-1.49	-1.06	
31	0.79	-0.43	-0.52	-0.24	-0.37	-0.62	-0.74	-1.04	-1.40	-1.15	
32	2.07	-0.60	0.47	1.13	0.20	1.13					
33	0.42	-1.52	0.96	0.22	0.88	0.26	1.47	0.93	0.76		
34	0.82	-1.83	-1.86	-0.14	-0.85	1.24	0.69	0.90	2.21	2.04	
35	-1.27	0.52	0.13	-0.37	-0.13	0.71	1.50	1.36	0.25	0.69	
36	0.56	0.01	0.55	-0.91	-0.51	0.83	2.08	1.14	1.36	0.60	

**Table 2.2. Details of the datasets included in [figures 2.1](#) and [2.2](#) and in [Table 2.1](#). Blank boxes indicate that no information was available for the area at the time of publication. T: temperature; S: salinity. Some data are calculated from an average of more than one station; in such cases, the latitudes and longitudes presented here represent a nominal midpoint along that section.**

Index	Description	Section	Measurement depth (m)	Reference period	Lat	Lon	Mean T	s.d.	Mean S	s.d.
1	Fram Strait East Greenland Current	4.21	50–500	1993–2020	78.83	–6.00	0.73	0.47	34.618	0.126
2	Fylla Section – Station 4 – Greenland Shelf	4.1	0–50	1993–2020	63.88	–53.37	2.95	0.82	33.236	0.339
3	Cape Desolation Section – Station 3 – Greenland Shelf	4.1	75–200	1993–2020	60.47	–50.00	5.95	0.54	34.939	0.048
4	Central Labrador Sea	4.2	15–50	1991–2020	57.07	–50.92	4.68	0.69	34.635	0.176
5	Station 27 – Newfoundland Shelf T – Canada	4.3	0–175	1991–2020	47.55	–52.59	0.60	0.50	32.4	0.1
6	NE US continental shelf – Northern Middle Atlantic Bight	4.5	1–30	1991–2020	40.00	–71.00	11.54	1.04	32.720	0.420
7	NE US continental shelf – Northwest Georges Bank	4.5	1–30	1991–2020	41.50	–68.30	10.30	0.91	32.580	0.270
8	Emerald Basin – Central Scotian Shelf – Canada	4.4	250 (near bottom)	1991–2020	44.00	–63.00	9.43	0.92	34.972	0.174
9	Misaine Bank – Northeast Scotian Shelf – Canada	4.4	100 (near bottom)	1991–2020	45.00	–59.00	1.62	0.57	32.513	0.115
10	Siglunes Station 2–4 – North Iceland –North Icelandic Irminger Current – Spring	4.6	50–150	1991–2020	67.00	–18.00	3.99	1.00	34.909	0.099
11	Langanes Station 2–6 – Northeast Iceland –East Icelandic Current – Spring	4.6	T: 0–50 S: 0–50	1991–2020 1981–2010	67.50	–13.50	1.47	0.70	34.749	0.068
12	Selvogsbanki Station 5 –Southwest Iceland –Irminger Current – Spring	4.6	0–200	1991–2020	63.00	–21.47	7.93	0.45	35.185	0.060
13	Point 33 – Astan	4.10	5	1998–2020	48.78	–3.94	10.78	0.45		
14	Western Channel Observatory (WCO) –E1 – UK	4.10	0–40	1991–2020	50.03	–4.37	12.85	0.3	35.204	0.112
15	Malin Head Weather Station	4.11	Surface	1991–2020	55.37	–7.34	12.80	0.76	35.260	0.06
16	Ellett Line – Rockall Trough – UK (Section Average)	4.12	30–800	1991–2020	56.75	–11.00	9.42	0.27	35.351	0.043
17	Central Irminger Sea Sub Polar Mode Water	4.15	200–400	1991–2020	59.40	–36.80	4.32	0.46	34.903	0.027
18	Faroe Bank Channel – West Faroe Islands	4.16	Upper layer High salinity core	1991–2020	61.40	–8.30	8.82	0.32	35.293	0.05
19	Faroe Current – North Faroe Islands (Modified North Atlantic Water)	4.16	Upper layer High salinity core	1991–2020	63.00	–6.00	8.15	0.36	35.240	0.051

**Table 2.2. (continued)**

Index	Description	Section	Measurement depth (m)	Reference period	Lat	Lon	Mean T	s.d.	Mean S	s.d.
20	Faroe Shetland Channel – Shetland Shelf (North Atlantic Water)	4.16	Upper layer High salinity core	1991–2020	61.00	–3.00	9.97	0.43	35.392	0.048
21	Faroe Shetland Channel – Faroe Shelf (Modified North Atlantic Water)	4.16	Upper layer High salinity core	1991–2020	61.50	–6.00	8.41	0.54	35.251	0.055
22	Ocean Weather Station Mike	4.19	50	1991–2020	66.00	2.00	7.71	0.44	35.176	0.036
23	Southern Norwegian Sea – Svinøy Section – Atlantic Water	4.19	50–200	1991–2020	63.00	3.00	8.23	0.34	35.238	0.051
24	Central Norwegian Sea – Gimsøy Section – Atlantic Water	4.19	50–200	1991–2020	69.00	12.00	7.05	0.32	35.166	0.046
25	Fugløya – Bear Island Section – Western Barents Sea – Atlantic Inflow	4.19	50–200	1991–2020	73.00	20.00	5.85	0.37	35.083	0.040
26	Kola Section – Eastern Barents Sea	4.20	0–200	1991–2020	71.50	33.50	4.57	0.47	34.778	0.053
27	Greenland Sea section – West of Spitsbergen 76.5N	4.19	200	1996–2020	76.50	10.50	3.4	0.57	35.070	0.044
28	Northern Norwegian Sea – Sorkapp Section – Atlantic Water	4.19	50–200	1991–2020	76.33	10.00	4.38	0.46	35.079	0.04
29	Fram Strait – West Spitsbergen Current	4.21	50–500	1993–2020	78.83	7.00	3.25	0.61	35.038	0.035
30	Santander Station 6 (Shelf Break) – Bay of Biscay – Spain	4.7	0–30	1993–2020	43.71		15.82	0.32	35.460	0.170
31	Fair Isle Current Water (waters entering North Sea from Atlantic)	4.17	0–100	1991–2020	59.00		10.15	0.57	34.870	0.150
32	Section Average – Felixstowe – Rotterdam – 52N	4.17	Surface	1981–2010	52.00	3.00	12.21	0.55	34.760	0.150
33	North Sea – Helgoland Roads	4.17	Surface	1991–2020	54.18	7.90	10.68	0.67	32.387	0.409
34	Baltic Proper – East of Gotland – Baltic Sea	4.18	Surface T Surface S	1990–2010 1981–2010	57.50	19.50	9.27	1.03	7.172	0.196
35	Baltic – LL7 – Baltic Sea	4.18	70	1991–2020	59.51	24.50	4.25	0.94	8.063	1.031
36	Baltic – SR5 – Baltic Sea	4.18	110	1991–2020	61.05	19.35	3.53	0.84	6.481	0.157

## 2.2 Sea surface temperature

Satellites have been measuring SST for approximately 40 years, which has led to the creation of gridded datasets. [Figure 2.3](#) shows seasonal SST anomalies for 2021 extracted from the Optimum Interpolation SST dataset version 2 (OISST.v2) provided by the NOAA–CIRES Climate Diagnostics Center, USA. The data may be less reliable at high latitudes where *in situ* data are sparse and satellite data are hindered by cloud cover. Regions with > 50% ice cover over the averaging period appear blank.

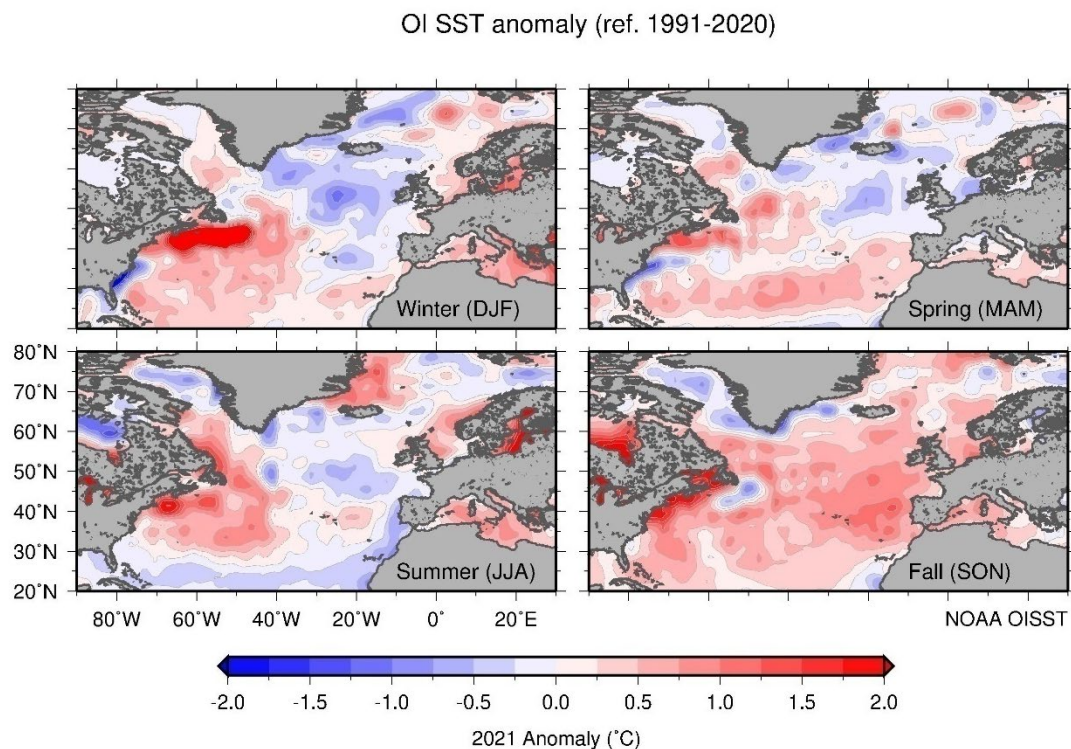


**Figure 2.3.** Maps of seasonal sea surface temperature anomalies (°C) over the North Atlantic for 2021 from the NOAA OISST.v2 dataset provided by the NOAA–CIRES Climate Diagnostics Center, USA. The data are produced on a 1° grid from a combination of satellite and *in situ* temperature data. The colour-coded temperature scale is the same in all panels, and the anomaly is calculated with respect to mean conditions for 1991–2020. Regions with ice cover for > 50% of the averaging period appear blank.



## 2.3 ARGO gridded temperature and salinity fields

*N. Kolodziejczyk and D. Desbruyères*

The ARGO network of profiling floats has been established to monitor the large-scale global ocean variability (<http://www.argo.ucsd.edu>). Argo data are transmitted in real time and rapidly made available by the two Global Data Assembly Centres (Argo-GDAC). Delayed-mode data undergo expert calibration and are delivered later, on average with a delay between one and several years. In the North Atlantic, temperature and salinity conditions have been adequately described over the upper 2 000 m since 2002 when the Argo network began to be implemented. The dataset is thus suitable for an overview of deep-sea oceanographic conditions in this basin and provides the general context for the data collected at stations and sections mostly located at the periphery of the basin.

### 2.3.1 ISAS: Gridded temperature and salinity fields

Temperature and salinity gridded fields are estimated on a regular 0.5° grid using the *In situ* Analysis System (ISAS; Gaillard *et al.*, 2016). The dataset used for generating ISAS-gridded fields is downloaded from the Coriolis Argo GDAC1. It should be noted that Coriolis assembles many types of data transmitted in real time, merging the Argo dataset with data collected by the Global Telecommunications System (GTS), such as data from moorings and CTDs and data on marine animals. However, the Argo dataset remains the main contributor to the ISAS gridded fields in the open ocean. The ISAS optimal interpolation (OI) procedure is as follows: the *in situ* temperature and salinity profiles are vertically interpolated on 152 standard levels between the surface and 2 000 m depth. The horizontal mapping to produce gridded fields is performed independently at each standard level. The mapping method is based on an optimal estimation algorithm and includes a horizontal smoothing through specified covariance scales. The results presented here were produced with the last version of ISAS, named ISAS20 (Kolodziejczyk *et al.*, 2021). The reference state used for this ISAS release was the World Ocean Atlas 2018 (WOA18) climatology, and the *a priori* variances were computed from the same Argo dataset. Two ISAS gridded temperature and salinity products are used:

- For the period 2002–2020, ISAS20 product is used (using ISASv8 tool; Kolodziejczyk *et al.*, 2021). For this period, only Argo delayed-mode and real-time profiles are used. Due to the long lasting task of Delayed Mode Quality Control processing from Argo principal investigators and experts, the most recent fields (2017–present) still include a large number of real-time profiles. Thus, this last period should be considered with caution. In order to minimize this issue, an extra quality control based on a detailed climatology check and the verification of grey lists of suspiciously functioning buoys is applied to *in situ* profiles delayed-mode and remaining real-time data before they are included in the analysis.
- The last year of the analysed series, i.e. 2021, uses the Near Real Time (NRT) dataset prepared by Coriolis at the end of each month from real-time data. For this period, data are interpolated using ISASv7 tool including only real-time mode data (i.e. only from automatic QC processing). Because Argo salinity data require advanced quality checks and validation, NRT salinity fields have to be used with caution. Therefore, time-series of monthly salinity anomalies are not considered herein, and the focus is rather made on their seasonally averaged and annually averaged patterns.

### 2.3.2 Method

The ISAS interpolated fields are used to compute seasonal to interannual maps of temperature and salinity anomalies averaged within an upper layer (0–100 m depth) and intermediate and deep layers (700–1 000 m; 1 000–1 500 m; 1 500–2 000 m depth). Note that the temperature and salinity anomalies throughout this section are computed using the climatological ISAS15 fields (2006–2015). In order to compute temperature and salinity anomalies, the climatological monthly temperature and salinity fields are removed from each monthly ISAS field over the period 2002–2021. Note that the temperature and salinity fields are blanked in regions with water depths deeper than 1 000 m where the Argo coverage is either too sparse or unavailable. The seasonal time-windows are defined as winter (JFM), spring (AMJ), summer (JAS), and autumn (OND). The seasonal and interannual variability is monitored in selected areas ([Figure 2.4](#)), representative of the North Atlantic polar, subpolar, and subtropical regions, and named: Greenland Sea; Labrador Sea; Irminger Basin; Eastern Atlantic Region; Gulf Stream Region; and Azores Region. Within each selected area, the number of temperature and salinity profiles used in the monthly objective analyses is shown in [Figure 2.5](#). This provides an assessment of the robustness of the temperature and salinity time-series in each area.

The mixed-layer depth (MLD) is an indicator of winter convection location and intensity in the North Atlantic and Nordic Seas. In order to compare the MLD among areas throughout the decade, an *ad hoc* MLD criterion for Greenland Sea was chosen following Brakstad *et al.* (2019). This criterion is based on a density-difference with respect to the 10-m depth value. The base of the mixed layer is identified as the depth where the increase in potential density reaches:

$$\Delta\rho = \rho(T_0 - \Delta T, S_0) - \rho(T_0, S_0) \quad (1)$$

where  $T_0$  and  $S_0$  are surface temperature and salinity. Consensus from the literature indicates that the criterion  $\Delta T = 0.2^\circ\text{C}$  is the most appropriate for the Greenland Sea. The resulting observed climatological mixed layer for the Greenland Sea ([Figure 2.9](#)) is in line with Brakstad *et al.* (2019). For clarity, the same criterion is used for the other boxes in the North Atlantic Subtropical and Subpolar gyres. Comparing MLD calculated using the criterion of  $0.03 \text{ kg m}^{-3}$ , previously used in these regions (de Boyer Montégut *et al.*, 2004), and  $0.01 \text{ kg m}^{-3}$ , recommended based on individual profiles in the Subpolar Gyre (Piron *et al.*, 2016), results in small differences, but does not change the interannual variability. To compute the MLD 2002–2021 average and 2021 anomaly ([Figure 2.9](#)), the month of March has been chosen as the common period for maximum MLD, i.e. at the end of the winter season and before spring restratification. Note that a mixed layer computed from smoother interpolated T/S fields may slightly underestimate the MLD relative to those computed using individual profiles.

It should be noted that the deepest MLD does not always occur in March, but can vary from year to year at a single location and might not occur at the same time of year across the whole basin (generally between February and April in the North Atlantic). Therefore, in order to compute the interannual MLD time-series ([Figure 2.10](#)):

- i) The 50% monthly deepest MLD is averaged in selected winter convection areas in the North Atlantic ([Figure 2.9](#)). Note that the selected deep convection areas differ from the ones in [Figure 2.4](#). Six regions are selected: the Greenland convection zone in the Nordic Seas, western and eastern regions in the Labrador Sea area, the Irminger Basin convection zone, and the eastern Subpolar Gyre ([Figure 2.9](#)).
- ii) For each year since 2002, the deepest monthly average MLD between February and April was plotted ([Figure 2.10](#)).

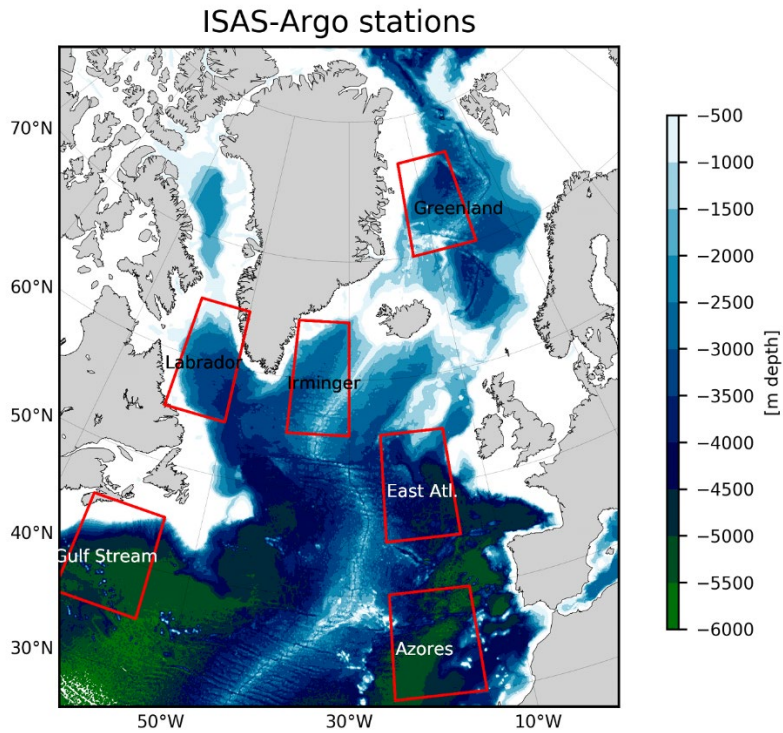


Figure 2.4. Location of the six regions in the North Atlantic used for computing averaged temperature and salinity profile time-series: Azores, Gulf Stream, Eastern Atlantic, Irminger Sea, Labrador Sea, and Greenland Sea.

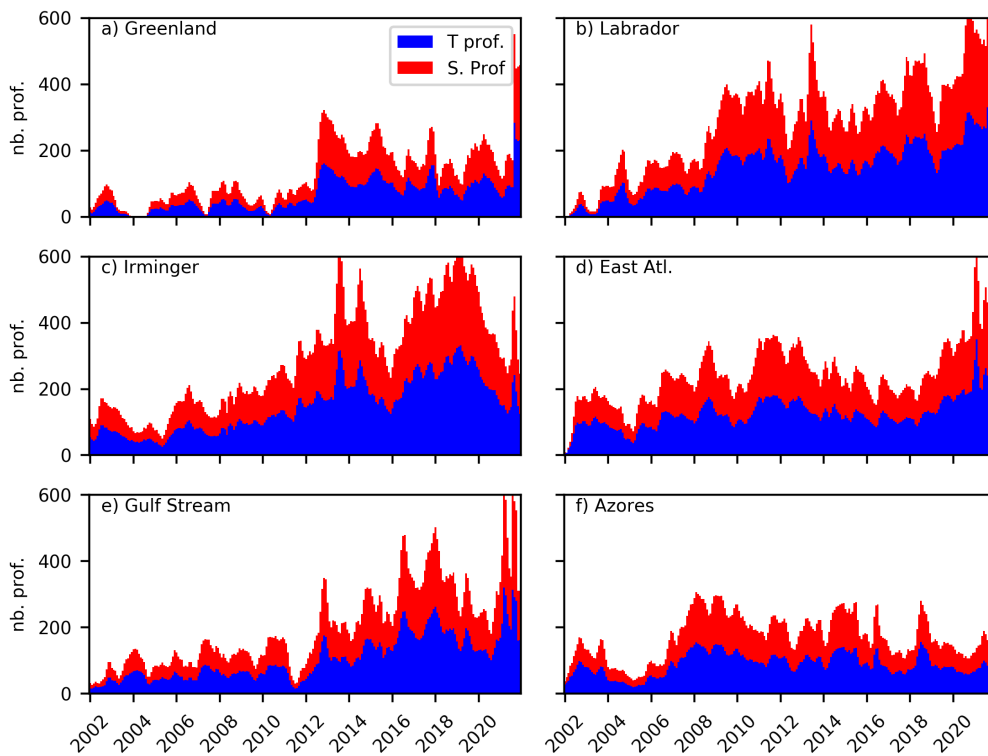


Figure 2.5. Number of temperature (blue) and salinity (red) profiles used in monthly objective analysis for 2002–2021 in each selected region from Figure 2.4. a) Greenland Sea; b) Labrador Sea; c) Irminger Basin; d) East Atlantic Region; e) Gulf Stream Region; and f) Azores Region.

### 2.3.3 Highlights of 2021

- The Greenland Sea surface was still warmer than usual (reference 2006–2015), but the warming of its intermediate layer (700–2 000 m depth) appeared to have stopped in 2021.
- The surface layer of the Subpolar Gyre showed continued warming, while its deep layer has started to warm again since 2018 after a period of cooling since 2014.

### 2.3.4 Surface layers

#### Seasonal patterns of T/S 2021 anomaly

The broad pattern of temperature and salinity anomalies in 2021 (with respect to the 2006–2015 climatological mean) shows a relatively warm and salty subtropical region, a relatively cold and fresh subpolar region, and contrasted conditions in the Nordic Seas ([Figure 2.6](#)). However, there were significant subregional and intra-annual changes in each of these regions. The warm subtropical anomalies appear to spread over the width of the basin from west (in JFM) to east (in OND), while a cold and fresh anomaly is observed off Newfoundland (45°N) in AMJ and JAS. In the subpolar region, negative temperature and salinity anomalies are observed in the Irminger Basin and eastern Subpolar Gyre during JFM and AMJ. This pattern is sustained over the years for salinity alone. The upper layer temperature appears to increase in the eastern Subpolar Gyre in JAS and OND. In contrast, the Labrador Sea is warmer and saltier than usual around its northern (during JFM and AMJ) and eastern (JAS and OND) boundaries. The warm and salty anomaly was probably advected southward by the Labrador Current along the upper North American continental slope. In the Nordic Seas, warm and salty anomalies primarily developed within the western portion of the domain (Iceland and Greenland seas) in JAS and OND, while a weak cold anomaly developed along the eastern margin (Norwegian Sea).

#### Seasonal cycle and monthly anomalies

The 2021 seasonal cycle of temperature anomalies is depicted in [Figure 2.7](#), averaged within the six areas representative of the main sub-basins of the North Atlantic domain ([Figure 2.4](#)). The 2006–2015 climatology (solid) and the spread (dashed) over the period 2002–2021 is also shown.

- In 2021, the surface layer of the Greenland Sea (panel a in [Figure 2.7](#)) was slightly warmer than the reference period of 2006–2015 during the winter months (JFMA), and then became significantly warmer than usual during the rest of the year (spring–summer–autumn).
- The surface layer of the Labrador Sea (panel b in [Figure 2.7](#)) was warmer than normal over the whole seasonal cycle.
- In the Irminger Sea (panel c in [Figure 2.7](#)), the surface layer was generally colder than normal throughout the year, especially during winter, but warmer than usual during July.
- In the eastern Atlantic (panel d in [Figure 2.7](#)), the 2021 surface layer exhibited significant colder temperature than the 2006–2015 average during the first half of the year and warmer during the second half.
- The surface layers of the Gulf Stream and Azores regions, i.e. western and eastern Subtropical Gyre, respectively (panels e and f in [Figure 2.7](#)) were warmer than normal over the whole seasonal cycle.

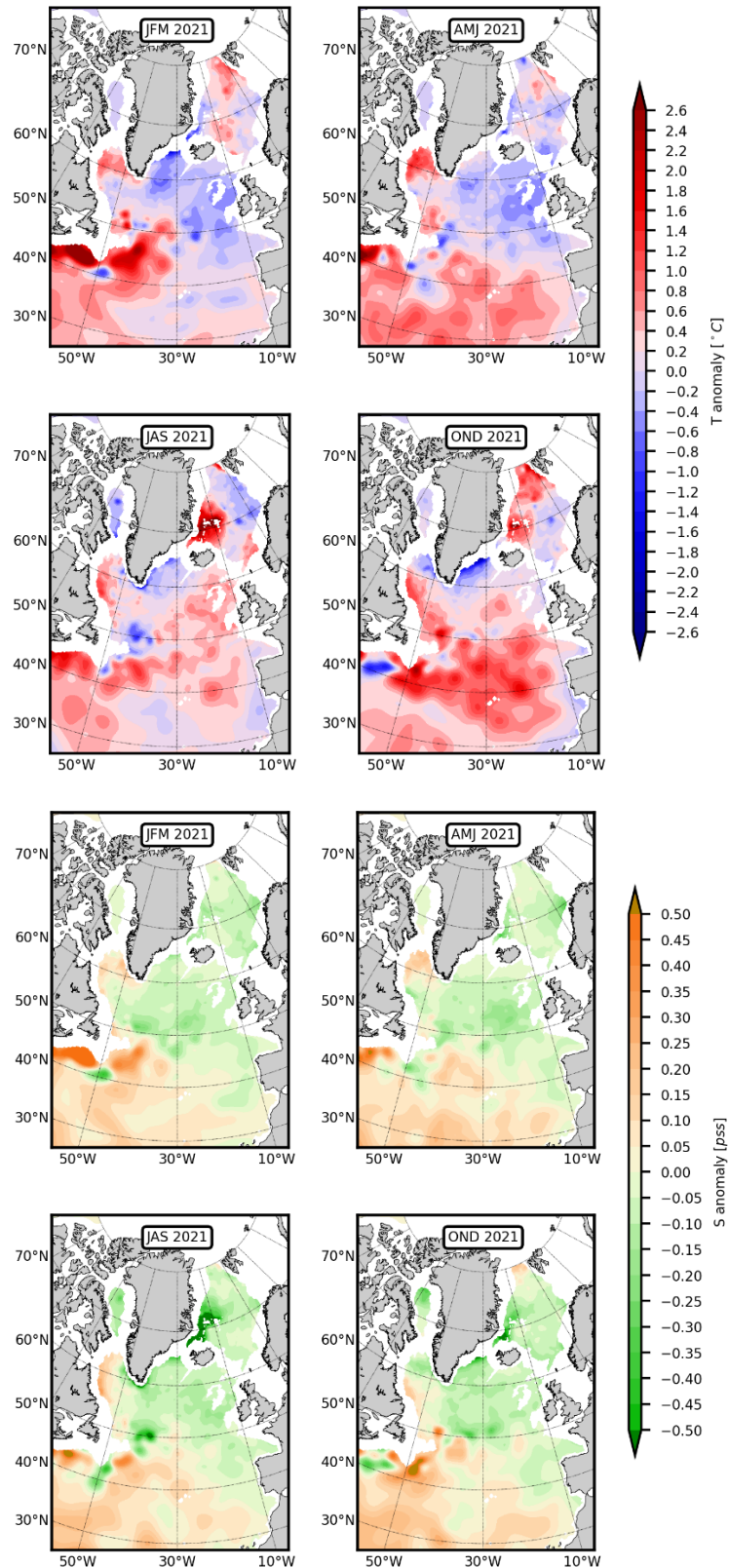


Figure 2.6. Near-surface temperature (upper panel) and salinity (lower panel) anomalies (0–100 m average) averaged over winter (JFM), spring (AMJ), summer (JAS), and autumn (OND) 2021. Anomalies are the differences between the ISAS monthly mean values and the reference climatology ISAS15 2006–2015. Data prepared from the Coriolis, ISAS monthly analysis of Argo data.

In conclusion, the observed seasonal cycle of temperature in the main North Atlantic sub-basins revealed a year (2021) warmer than usual for the western subpolar basin (Labrador) and Nordic Seas (Greenland), while the eastern subpolar basin (Iceland Sea and Irminger and Rockall basins) remained colder than usual for most of the year. The Subtropical Gyre also showed a sustained positive anomaly over the whole seasonal cycle.

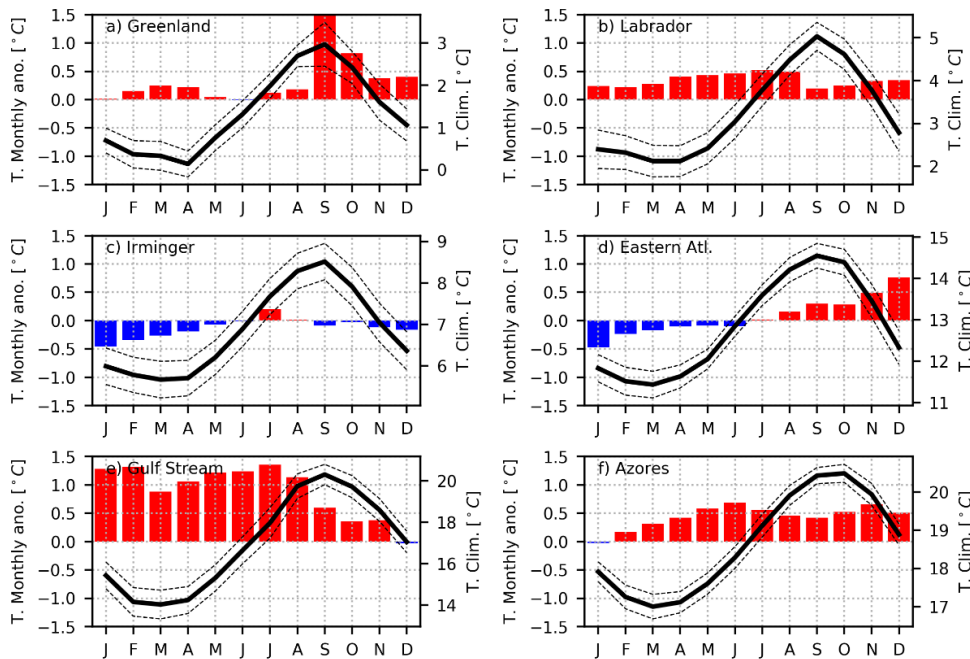
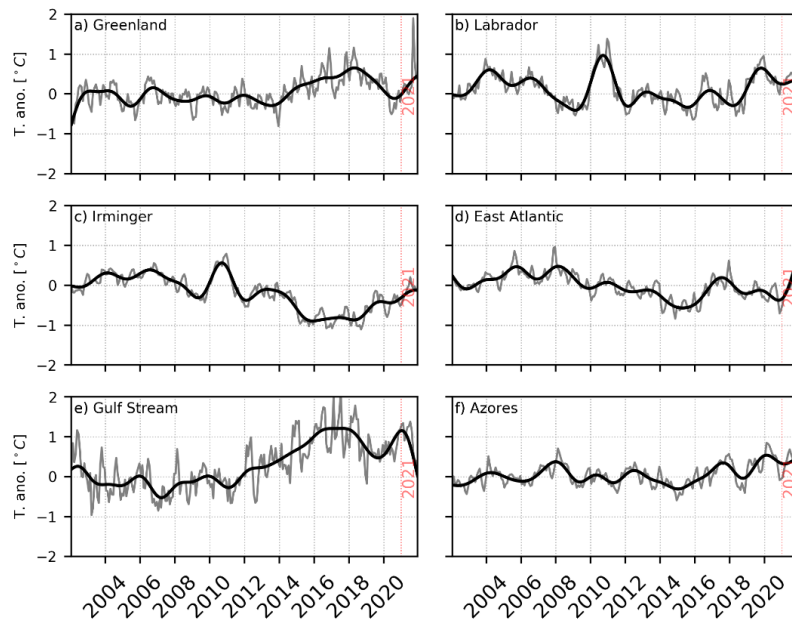


Figure 2.7. 2021 near-surface temperature (0–100 m average) monthly anomalies (bars) and climatological seasonal cycle (thick line) with its standard deviation (dashed lines) over the period 2006–2015. Anomalies are the differences between the ISAS monthly mean values and the reference climatology ISAS15 2006–2015. Data prepared from the Coriolis, ISAS monthly analysis of Argo data.

### Interannual variability and long-term tendency

The interannual variability of the upper layer (0–100 m) temperature anomaly (relative to 2006–2015) over the period 2002–2021 in the six North Atlantic areas is depicted in Figure 2.8. The Greenland Sea region, although warmer than average over the last five years, has shown a continued cooling tendency since 2018 and reached average 2006–2015 surface temperature conditions in 2020 (panel a in Figure 2.8). In 2020–2021, the upper layer of the Greenland Sea again showed a warming tendency. In 2021, the Labrador Basin (panel b in Figure 2.8) remained warmer than usual due to a warming tendency that has been observed since 2018 and which is now mainly seen along the western boundary of the Basin (Figure 2.6). This recent warming event in the Labrador Basin has occurred after a decade (since 2008) that was slightly colder than usual, except for the remarkable 2010 warm event. Although the Irminger Basin (panel c in Figure 2.8) has exhibited similar relative warming events since 2018, temperature in 2021 reached the 2006–2015 average. This is due to the unabated cooling observed since 2008, despite the 2010 exceptional warming event. The eastern Atlantic region; panel d in Figure 2.8), has shown a similar upper ocean temperature decrease, but a very strong warming was observed in 2021. When compared to the long-term 2006–2015 mean, the subtropical region was generally warmer in recent years, with warming being particularly significant over the Gulf Stream region since 2015 (panel e in Figure 2.8). However, surprisingly, a strong cooling was observed in 2021 in the Gulf Stream region (panel e in Figure 2.8). In the eastern Subtropical Gyre (Azores; panel

f in [Figure 2.8](#)), a warming trend has been observed since 2015, with the 2020–2021 surface temperatures being the warmest recorded since 2002 in this region.



**Figure 2.8.** Upper ocean (0–100 m depth) temperature interannual anomalies (reference climatology: 2006–2015 over the 2002–2021 period (19 years) in the basin areas defined in [Figure 2.4](#). a) Greenland Sea; b) Labrador Sea; c) Irminger Basin; d) Eastern Atlantic Basin; e) Gulf Stream Region; and f) Azores Region. Thin grey line: monthly interannual anomaly. Thick black curve: 24-month low pass filtered (with a Butterworth filter) time-series.

### Mixed layer depth

The MLD is an indicator of winter convection intensity in the North Atlantic and Nordic Seas. Winter heat and freshwater fluxes control the sea surface buoyancy loss (increase in density) of the ocean surface layers and trigger deep convection.

Winter in 2021 ([Figure 2.9](#)) was characterized by a noticeable increase in MLD in both the Labrador and Greenland seas. However, in the Labrador Basin, the centre of the deepest MLD anomaly retracted toward the northern part of the Basin, while the Irminger Basin and southern Labrador Basin present shallower MLDs (relative to 2002–2021 ([Figure 2.9](#))). In the Greenland Sea, the deep convection area appeared to be smaller, but deeper, than usual and confined to the eastern part of the Greenland Sea Gyre. In 2021, in the Irminger and western Iceland basins, the March MLD was shallower than usual, while in the eastern Iceland Basin, it appeared to be deeper than usual.

[Figure 2.10](#) shows the deepest MLD averaged in the different regions depicted in [Figure 2.9](#) over the period 2002–2021. In 2021, the MLD was still shallower than usual since the stronger convection period before 2014. In the Irminger Basin (panel b in [Figure 2.10](#)), maximum MLD was still lower than usual, especially since the strong events period between 2015 and 2017. In 2021, the MLD was shallower in the Labrador Sea in the eastern region (panel c in [Figure 2.10](#)) than in the western region (panel d in [Figure 2.10](#)). Overall, MLDs in the Subpolar Gyre have remained shallower than average since 2017 (panels c and d in [Figure 2.10](#)). Interestingly, the deepest MLD in the eastern Labrador Basin was less common before 2014 (one-third of the events). In 2021, and since 2016, MLDs in the Iceland Basin are shallower than usual. In contrast, the Rockall region presents deeper MLDs than usual.

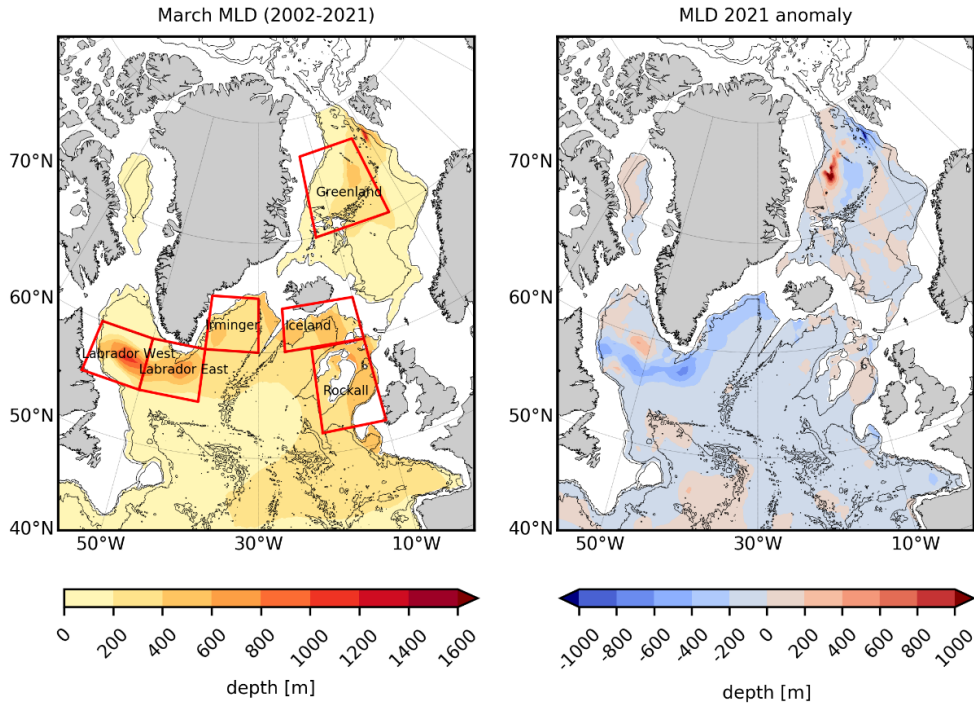


Figure 2.9. Left panel: Climatological March Mixed Layer Depth (MLD) for winter 2006–2015. The selected areas to compute the yearly deepest MLD time-series in [Figure 2.10](#) are as follows: western and eastern Labrador Sea, Irminger, Greenland, Iceland, and Rockall basins. Right panel: the 2021 March MLD anomaly (in m). Isobath 1 000 m, 2 000 m and 4 000 m depth are plotted. Regions shallower than 1 000 m depth are blanked.

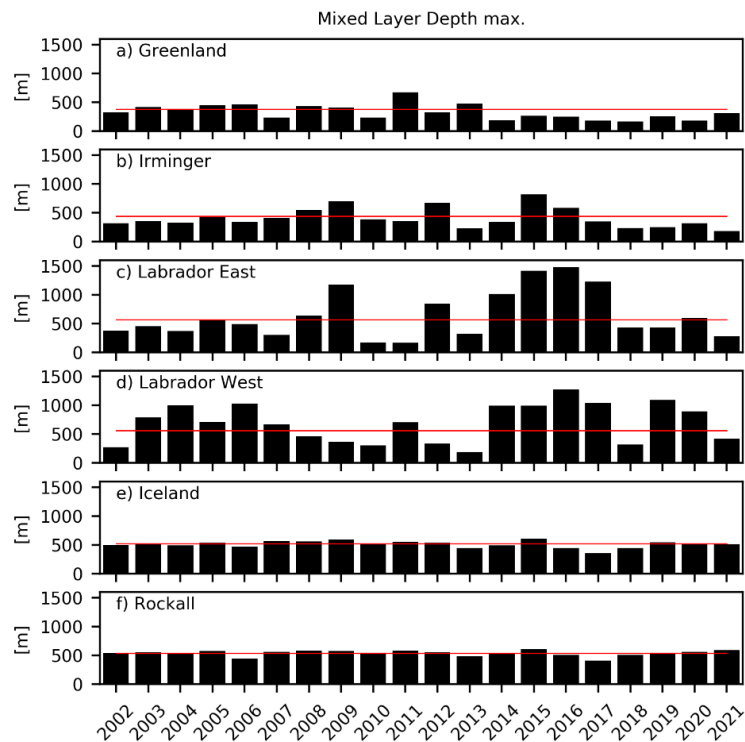
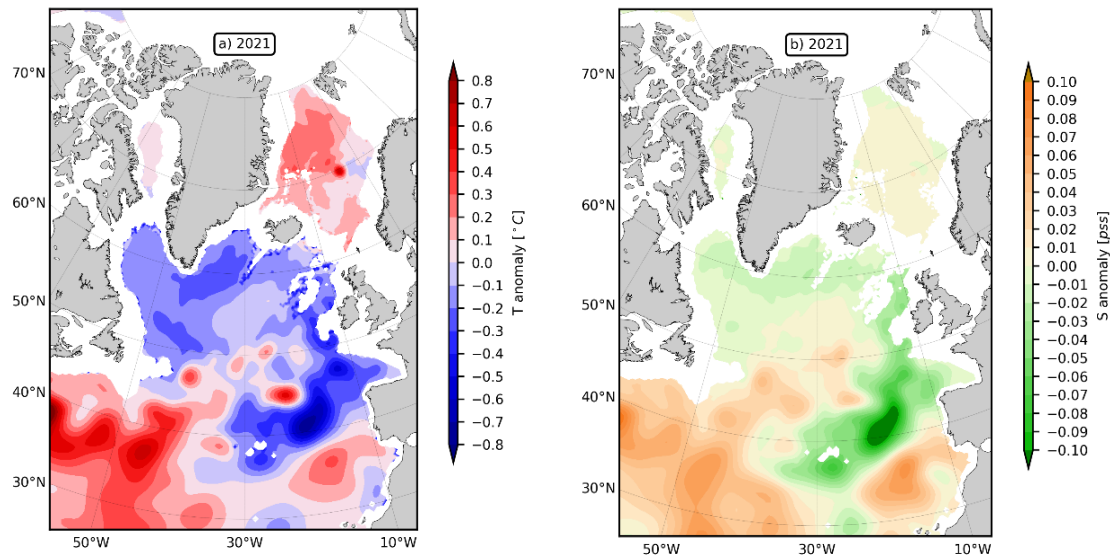


Figure 2.10. Yearly deepest MLD over the period 2002–2021 averaged in the selected area from [Figure 2.9](#): a) Greenland Sea; b) Irminger Basin; c) eastern and d) western Labrador Sea; e) Iceland Basin; f) Rockall Basin. Red line is the average deepest MLD over 2002–2021.

## 2.4 Intermediate and deep layers

The maps of 2021 interannual temperature and salinity anomalies in the intermediate layer (700–1 500 m) of the North Atlantic are shown in [Figure 2.11](#). [Figure 2.12](#) shows time-series of temperature anomalies in the intermediate layers (700–2 000 m depth) averaged in each area ([Figure 2.4](#)) for the period 2002–2021.



**Figure 2.11.** 2021 maps of annual (a) temperature and (b) salinity anomalies averaged within 700–1 500 m in the North Atlantic. Anomalies are the differences between the ISAS monthly mean values and the reference climatology ISAS15 2006–2015. Data prepared from the Coriolis ISAS monthly analysis of Argo data.

In 2021, the overall spatial pattern was one of a relatively warm western subtropical region, a relatively cold subpolar region, and a relatively warm Nordic Seas (when compared to the 2006–2015 climatological period; panel a in [Figure 2.11](#)). In 2021, the northeastern Subtropical Gyre dramatically cooled. The North Atlantic intermediate salinity anomalies showed a similar pattern, with saltier anomalies in the western Subtropical Gyre, fresher anomalies in the northeastern Subtropical Gyre, and a fresher Subpolar Gyre. (panel b in [Figure 2.11](#)). The cold anomaly pattern that can be observed at 40°N off the Iberian Peninsula and is associated with a fresh anomaly pattern (panels a and b in [Figure 2.11](#)) has been sustained since 2020. This is probably due to the southward shift of the warm and salty Mediterranean water panache at intermediate depth. The contrasting interannual behaviour of temperature in those regions is striking ([Figure 2.12](#)). Since 2012, the deep layer of the Gulf Stream area has warmed by nearly 0.05°C (at 1 500–2 000 m depth), 0.1°C (at 1 000–1 500 m depth) and 0.5°C (at 700–1 000 m depth) in the intermediate layers (panel e in [Figure 2.12](#)). However, in 2021, this warming tendency seemed to have reversed, with temperatures 0.3°C cooler than in 2020 in the 700–1 000 m level. The subpolar area (Labrador and Irminger seas) has cooled by about 0.3°C in the intermediate layers since 2012 (700–1 500 m depth; panels b and c in [Figure 2.12](#)). In the Labrador Sea, even the deepest layers (1 500–2 000 m depth) have cooled by nearly 0.1°C during the same period. Interestingly, since 2016, the intermediate layer cooling trend seems to have stopped in the Labrador Seas (panel b in [Figure 2.12](#)), and since 2019 in the Irminger Sea (panel c in [Figure 2.12](#)), and is now observed to warm again. In contrast, temperatures in the intermediate and deep layers of the Greenland Sea (panel a in [Figure 2.12](#)) are characterized by an unabated positive trend (increase of 0.1 and 0.3°C since 2002 for the deep and intermediate layers,

respectively). Strikingly, in 2021, this warming trend was interrupted for the first time since 2002 (to be confirmed in 2022). In the eastern Atlantic (panel d in [Figure 2.12](#)), the intermediate layers (700–1 500 m depth) appear to have slightly cooled since 2012, but there is significant interannual variability. In contrast, the deep layer showed a warming trend for 2002–2017 (accumulated 0.15°C) and cooling conditions afterwards.

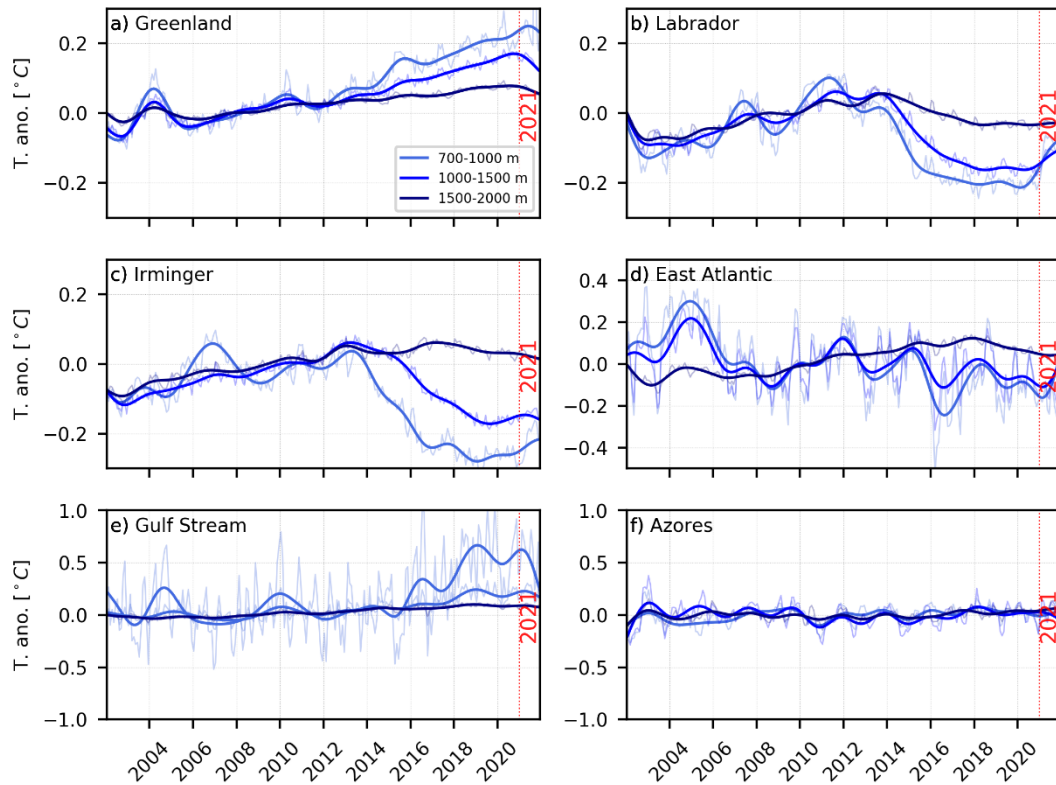


**Figure 2.12.** Time-series of temperature anomalies (using 2006–2015 as reference) averaged over the 700–1 000 m (light blue), 1 000–1 500 m (blue), and 1 500–2 000 m (dark blue) layers over the period 2002–2022 in (a) East Atlantic, (b) Irminger Sea, (c) Labrador Sea, (d) Greenland Sea, (e) Gulf Stream Region, and (f) Azores Region. The thin lines are monthly anomalies, and the 24-month low pass filtered (with Butterworth filter) time-series of monthly anomalies is plotted in thick lines.

### 3 The North Atlantic atmosphere

*L. C. Harrison and S. R. Dye*

The North Atlantic Oscillation (NAO) is a pattern of atmospheric variability that has a significant impact on oceanic conditions. It affects wind speed, precipitation, evaporation, and the exchange of heat between ocean and atmosphere, and its effects are most strongly felt in winter. The NAO index is a simple device used to describe the state of the NAO. It is a measure of the strength of the sea level air pressure gradient between Iceland and Lisbon, Portugal. When the NAO index is positive, there is a strengthening of the Icelandic low-pressure system and the Azores high-pressure system. This produces stronger mid-latitude westerly winds, with colder and drier conditions over the western North Atlantic and warmer and wetter conditions in the eastern North Atlantic. When the NAO index is negative, there is a reduced pressure gradient, and the effects tend to be reversed.

There are several slightly different versions of the NAO index calculated by climate scientists. The Hurrell winter (December/January/February/March, or DJFM) NAO index (Hurrell *et al.*, 2003) is the most commonly used, and is particularly relevant to the eastern North Atlantic. Previous editions of the IROC (Gonzalez-Pola *et al.*, 2022 and earlier editions) quoted instrumental NAO index values, but this edition of the IROC presents pattern index values that are calculated using a different method. Consequently, all NAO indices for past winters provided in this report differ slightly from the indices shown in previous editions of the IROC. Note that although people may think of winter as coming at the end of the year, here the 'winter season' spans the annual boundary and precedes the year of interest. Thus, the winter of December 2019 to March 2020 sets up conditions for the summer of 2020.

The NAO is the dominant pattern of atmospheric pressure variability in the North Atlantic. However, when the NAO itself is weak (i.e. the dominant atmospheric pattern is not a NAO-type pattern), this may be because a different pattern is occurring. Two other dominant atmospheric regimes have been identified as useful descriptors: (i) the Atlantic Ridge mode, when a strong anticyclonic ridge develops off western Europe (similar to the East Atlantic pattern); and (ii) the Blocking regime, when the anticyclonic ridge develops over Scandinavia. The four regimes (positive NAO, negative NAO, Atlantic Ridge, and Blocking) have all been occurring at around the same frequency (20–30% of all winter days) since 1950 (Hurrell and Deser, 2010). These modes of variability are revealed through cluster analysis of sea level pressure (SLP), rather than by examining point-to-point SLP gradients. For this reason, this report also includes maps of SLP, windspeed, and air temperature as this offers a more detailed understanding of the North Atlantic atmospheric variability than the NAO index alone.

#### 3.1 The North Atlantic Oscillation (NAO) index

The Hurrell NAO index underwent a long period of increase from a mostly negative phase in the 1960s to a persistent positive phase during the late 1980s and early 1990s. This was followed by a large and rapid decrease during winter 1995/1996. In many of the years between 1996 and 2009, the Hurrell winter NAO index was fairly weak and was a less useful descriptor of

atmospheric conditions, mainly because SLP patterns were not typical for the NAO. In winter 2009/2010, the index was strongly negative ([Figure 3.1](#)), and its anomaly pattern exerted a dominant influence on atmospheric conditions. This was the strongest negative anomaly since 1969 and the second strongest negative value for the Hurrell winter NAO index on record (starting in 1899). Winter 2014/2015 saw the strongest positive NAO index since 1990 and the third most positive NAO index in the last 123 years [Hurrell and National Center for Atmospheric Research Staff (Eds.), 2017]. In winter 2016/2017, the NAO index was positive (+0.87) for the fourth consecutive winter, the first firmly positive run of greater than two years since 1989–1995. Winter 2017/2018 experienced a negative, but near neutral (−0.17), NAO index before returning to positive values in the winters of 2018/2019 (+0.74) and 2019/2020 (+1.78). The winter of 2020/2021 then reversed this positive trend with a return to a negative NAO index (−0.72).

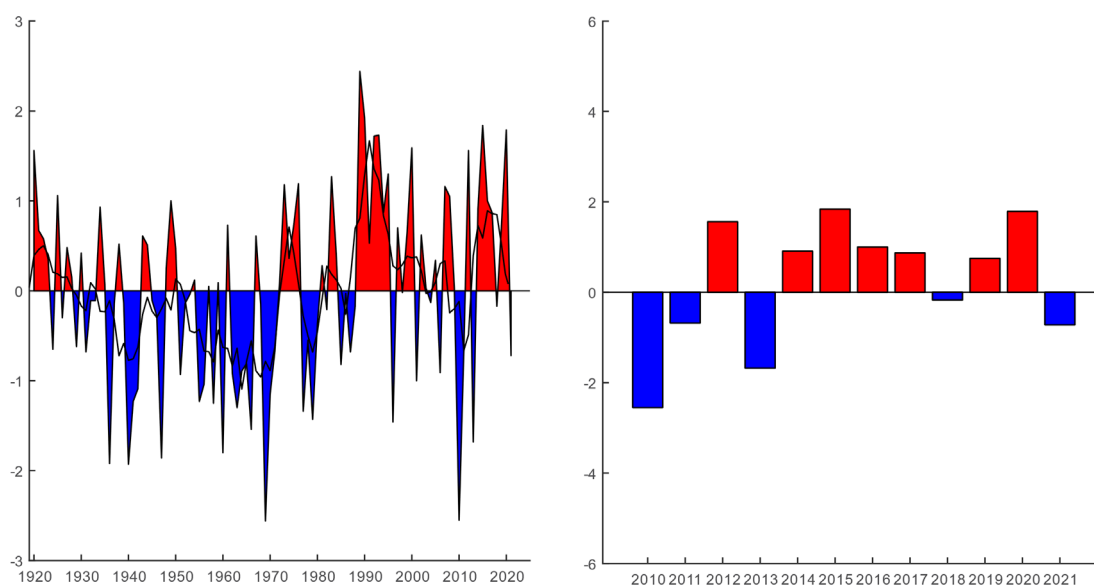


**Figure 3.1.** The Hurrell winter (DJFM) NAO index for the past 100 years with a two-year running mean applied (left panel) and for the current decade (right panel). Data source: NAO Index Data provided by the Climate Analysis Section, NCAR, Boulder, USA, (Hurrell *et al.*, 2003).

## 3.2 Sea level pressure and wind speed

The spatial pattern of atmospheric conditions indicated by a particular NAO index value are more understandable when the anomaly fields are mapped. Impacts on ocean properties are particularly dominated by winter conditions; hence, the inclusion of SLP and windspeed maps for winter ([figures 3.2](#) and [3.3](#); Kalnay *et al.*, 1996).

The top panel of [Figure 3.2](#) shows the winter SLP averaged over 30 years (1991–2020). The dominant features ('action centres') are the Iceland Low, situated southwest of Iceland, and the Azores High, west of Gibraltar. The middle panel of [Figure 3.2](#) shows the mean SLP for winter 2020/2021 (December 2020 through March 2021), and the bottom panel shows the 2020/2021 winter SLP anomaly (i.e. the difference between the top and middle panels).

The SLP pattern is closely related to wind patterns. The geostrophic or gradient wind blows parallel to the isobars, with lower pressure to the left in the northern hemisphere. The closer the

isobars are, the stronger the wind. The strength of the winter mean surface wind averaged over the 30-year period (1991–2020) is shown in the upper panel of [Figure 3.3](#), while the middle panel shows the mean surface wind for winter 2020/2021 and the lower panel the anomaly in winter 2020/2021.

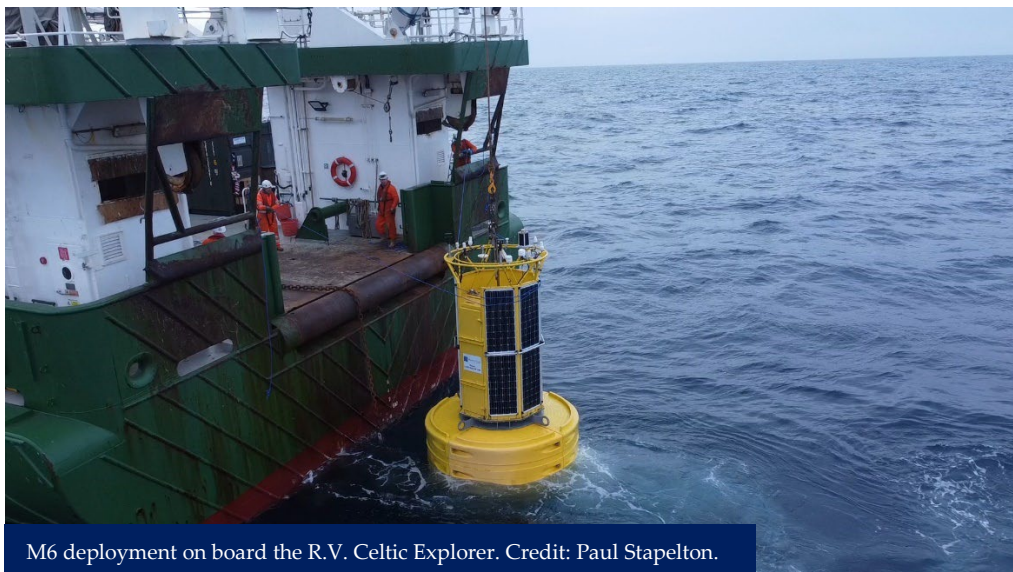
The SLP anomaly for winter 2020/2021 ([Figure 3.2](#)) shows a stronger-than-average anticyclonic anomaly over Iceland and the North Atlantic stretching from the Labrador Sea in the west to the Kara Sea in the east, with the anomaly strengthening over the Barents Sea. A low-pressure anomaly was observed in the mid-Atlantic, north of the Azores, and across western Europe, centring around the English Channel. This pattern is consistent with the negative NAO index for this winter period ( $-0.72$ ).

A negative NAO implies weaker westerly winds in the mid-latitude regions, compared with the 30-year climatology, which can be seen in [Figure 3.3](#). Windspeeds were slower over the North Sea, parts of the Norwegian Sea, and over the Atlantic between Newfoundland and the west coast of the UK and Ireland. A strengthening of winds south of Ireland broke this mid-latitude pattern of weaker-than-average winds. Stronger winds were also seen in the southern part of the region centred around the Azores, as well as in the North Atlantic west of Iceland.

### 3.3 Surface air temperature

North Atlantic winter mean surface–air temperatures are shown in [Figure 3.4](#) (Kalnay *et al.*, 1996). The 1991–2020 mean conditions (top panel in [Figure 3.4](#)) show warm temperatures penetrating far to the north on the eastern side of the North Atlantic and the Nordic Seas caused by the northward movement of warm oceanic water. The middle panel of [Figure 3.4](#) shows the conditions in winter 2020/2021, and the bottom panel shows the difference between the two.

Surface air temperatures in the east over the southern Barents and Kara seas were much colder than the 1991–2020 average, and temperatures were slightly lower than average in the east Atlantic over the Azores. In contrast, winter conditions were significantly warmer in the western part of the region, particularly across the Labrador Sea and into the Arctic. Mildly warmer-than-average temperatures were also seen over the Baltic Sea, while the North Sea and Northeast Atlantic experienced average surface air temperatures.



M6 deployment on board the R.V. Celtic Explorer. Credit: Paul Stapelton.

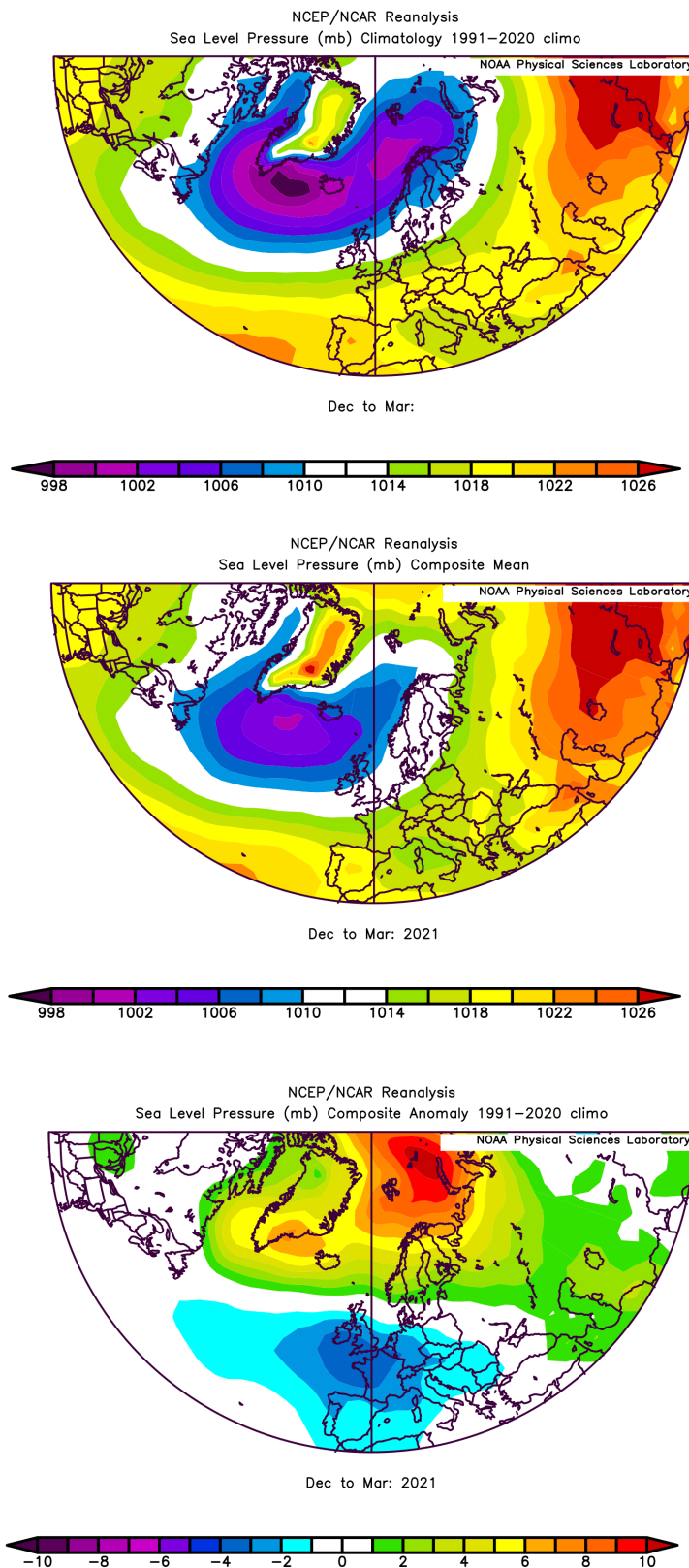


Figure 3.2. Winter (DJFM) sea level pressure fields. Top panel: sea level pressure averaged over 30 years (1991–2020). Middle panel: sea level pressure in winter 2020/2021. Bottom panel: winter 2020/2021 sea level pressure anomaly calculated as the difference between the top and middle panels. Images provided by the NOAA/ESRL Physical Sciences Division, Boulder, CO, USA (available online at <https://www.cdc.noaa.gov>).

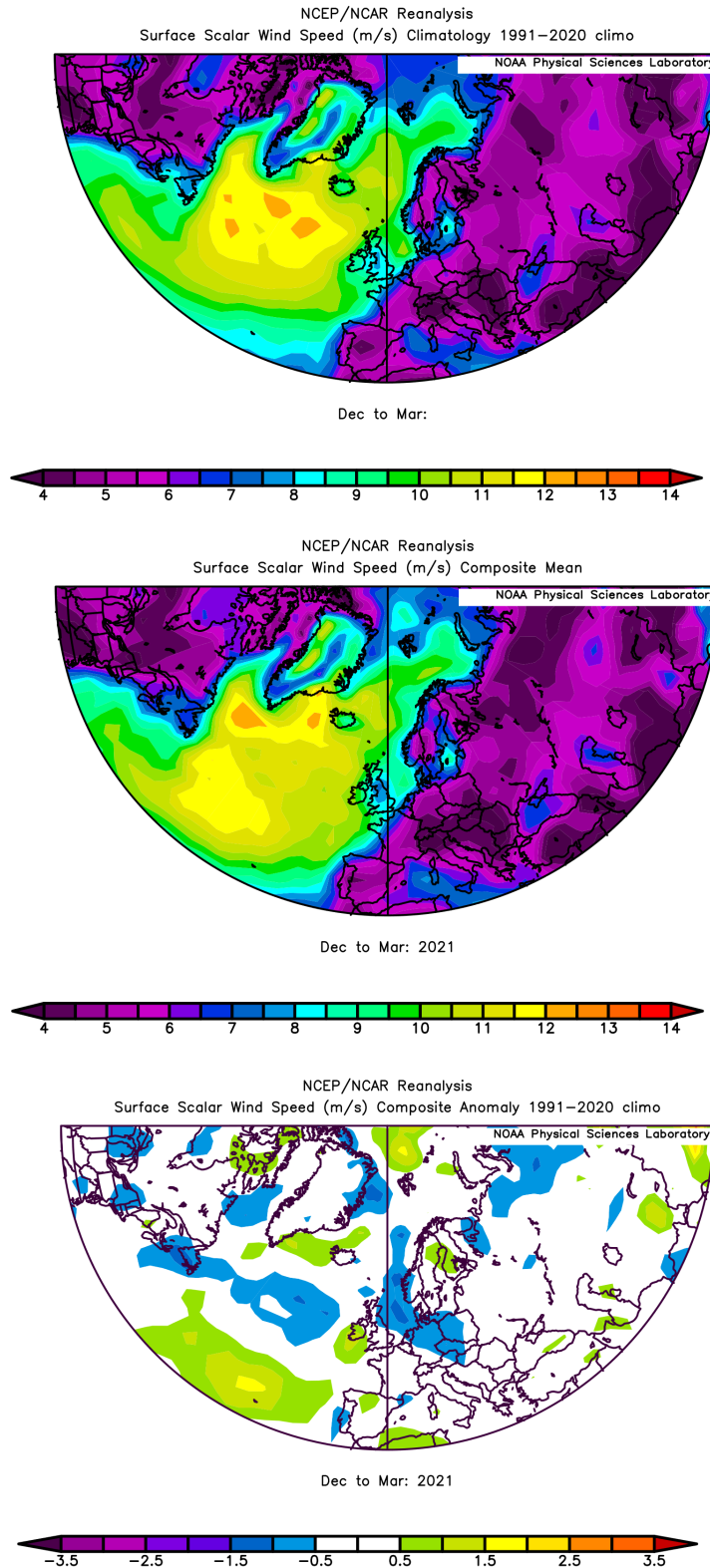


Figure 3.3. Winter (DJFM) windspeed fields. Top panel: scalar windspeed averaged over 30 years (1991–2020). Middle panel: scalar windspeed in winter 2020/2021. Bottom panel: winter 2020/2021 scalar windspeed anomaly calculated as the difference between the top and middle panels. Images provided by the NOAA/ESRL Physical Sciences Division, Boulder, CO, USA (available online at <https://www.cdc.noaa.gov/>).

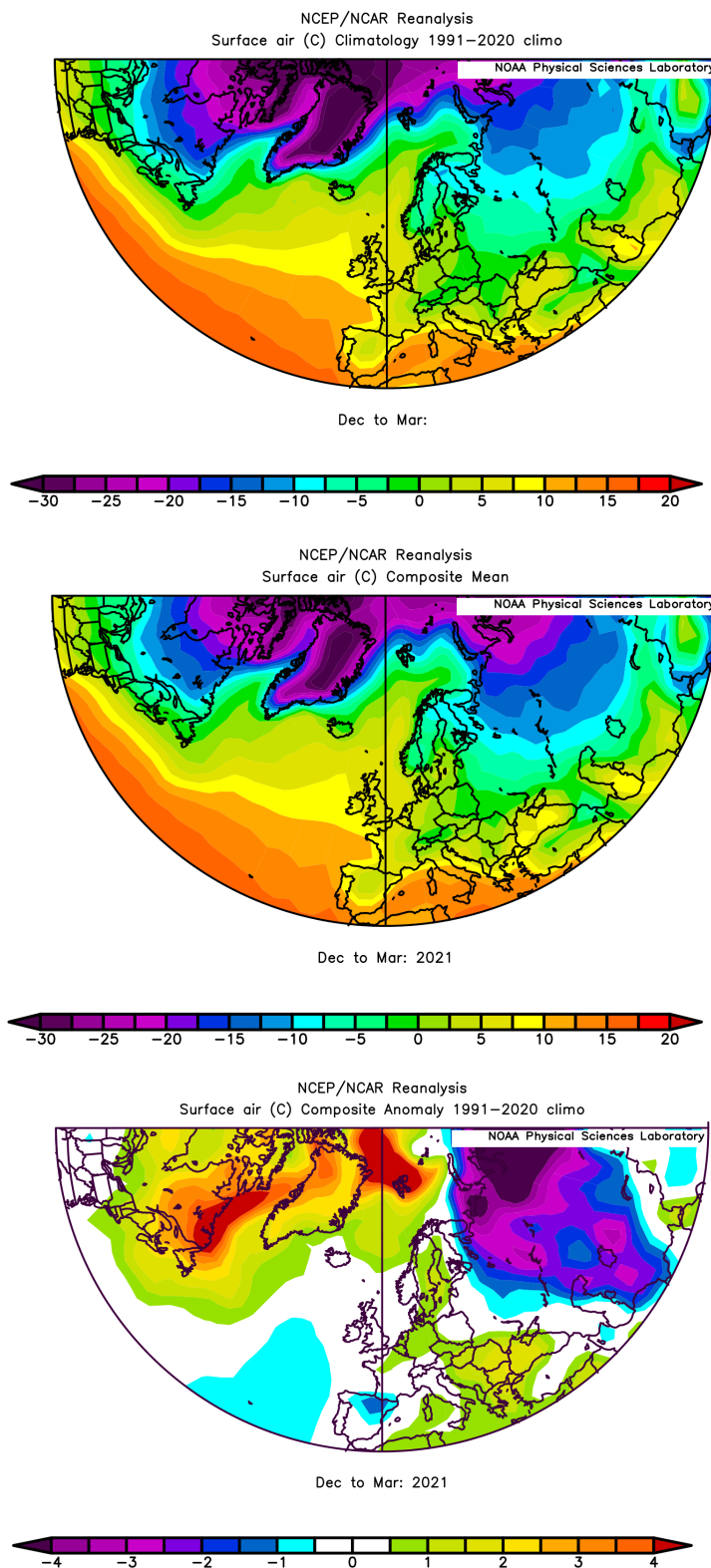


Figure 3.4. Winter (DJFM) surface air temperature fields. Top panel: surface air temperature averaged over 30 years (1991–2020). Middle panel: surface air temperatures in winter 2020/2021. Bottom panel: winter 2020/2021 surface air temperature anomaly calculated as the difference between the top and middle panels. Images provided by the NOAA/ESRL Physical Sciences Division, Boulder, CO, USA (available online at <http://www.cdc.noaa.gov/>).

## 4 Detailed area descriptions, part I: The upper ocean

### Introduction

In this section, time-series from sustained observations are presented for each of the areas shown in [Figure 4.1](#). The general pattern of oceanic circulation in the upper layers of the North Atlantic in relation to the areas described here is shown in [Figure 4.2](#). In addition to temperature and salinity, other indices are presented where available, such as air temperature and sea ice extent. Regional characteristics of the sections and stations are summarized, noting any significant changes.

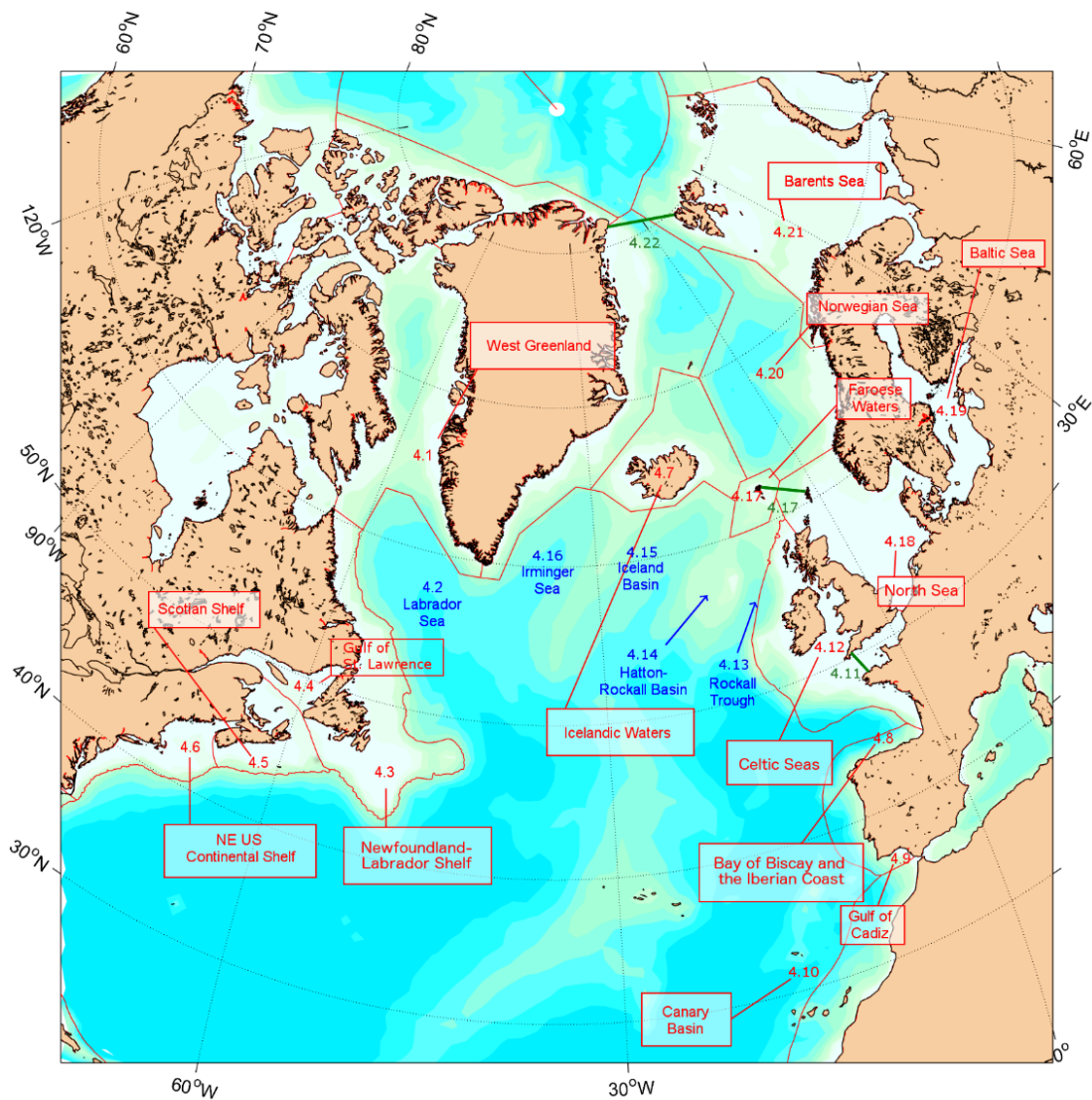


Figure 4.1. Schematic of marine areas used to organize data presented in this section. The numbers refer to the section number within this report. Regions are labelled in red. Ocean basins are labelled in blue. Straits are labelled in green. NOAA Large Marine Ecosystems (LME) boundaries are shown for background reference, but the hydrographic regions used here are loosely defined and do not perfectly overlap with the LMEs.

Most standard sections or stations are sampled annually or more frequently. Many of the time-series presented here have been extracted from larger datasets and have been chosen as indicators of the conditions in a particular area. Where appropriate, data are presented as anomalies to demonstrate how the values compare with the average or 'normal' conditions (usually the long-term mean of each parameter during 1991–2020). For datasets that do not extend as far back as 1991, the average conditions have been calculated from the start of the dataset through to 2020.

In places, the seasonal cycle has been removed from a dataset either by calculating the average seasonal cycle during 1991–2020 or by drawing on other sources such as regional climatology datasets. Smoothed versions of most time-series are included using a Loess smoother, a locally weighted regression with a two- or five-year window (chosen depending on which was most appropriate to each time-series).

In some areas, data are sampled regularly enough to allow a good description of the seasonal cycle. Where possible, monthly data from 2021 are presented and compared with the average seasonal conditions and statistics.

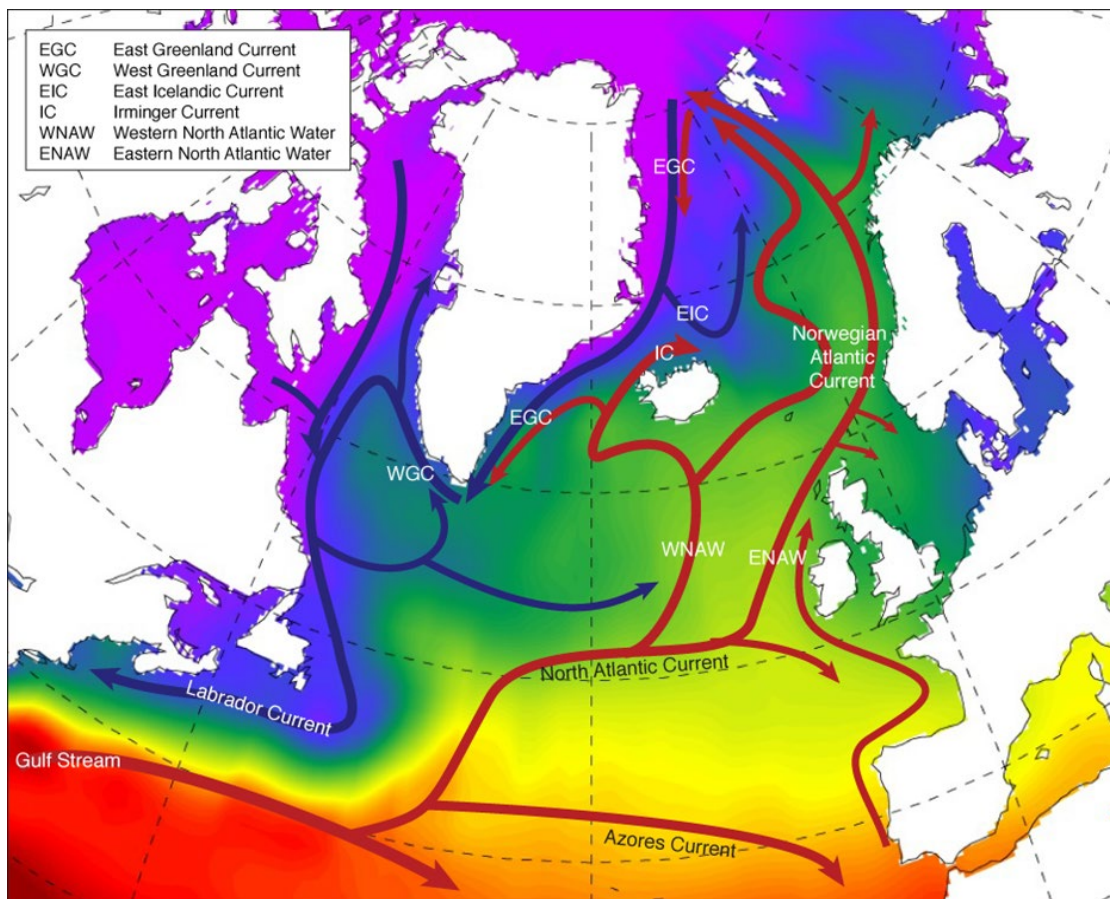
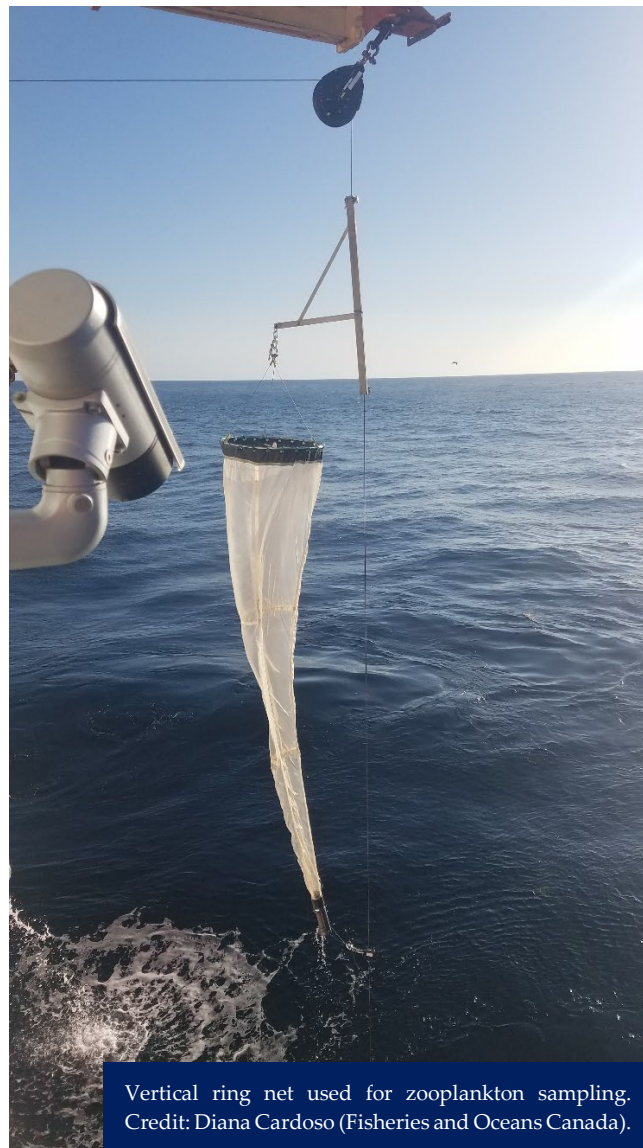


Figure 4.2. Schematic of the general circulation of the upper ocean (0–1 000 m) in the North Atlantic. Blue arrows: movement of cooler waters of the Subpolar Gyre; red arrows: movement of warmer waters of the Subtropical Gyre.

Although there are no real boundaries in the ocean, it is intended that the data presented represent conditions in a particular area. This section groups datasets into areas based on existing definitions. The NOAA Large Marine Ecosystems (LMEs) <sup>3</sup> serve as an overall reference as they cover all regions. However, ICES marine ecoregions <sup>4</sup>, the bathymetry of ocean basins <sup>5</sup>, and the general pattern of ocean circulation are also considered (Figure 4.2). While the data presented offer the best available indicative time-series within a region, it should be noted that, in large areas with complex circulation patterns, consideration should be given to how representative these data are of the whole ecoregion.



Vertical ring net used for zooplankton sampling.  
Credit: Diana Cardoso (Fisheries and Oceans Canada).

---

<sup>3</sup>Large Marine Ecosystems Hub. 2023. <https://iwlearn.net/marine/services/lme-hub>

<sup>4</sup>ICES ecoregions and advisory areas. 2023. ICES, Copenhagen, Denmark. <https://www.ices.dk/advice/ICES%20ecoregions%20and%20advisory%20areas/Pages/ICES-ecosystems-and-advisory-areas.aspx>

<sup>5</sup>Undersea feature names. 2023. General bathymetric chart of the ocean (GEBCO). [https://www.gebco.net/data\\_and\\_products/undersea\\_feature\\_names/](https://www.gebco.net/data_and_products/undersea_feature_names/)

## 4.1 West Greenland

*B. Cisewski and J. Mortensen*

The NOAA LME project identifies the ecosystem of the Canadian eastern Arctic–western Greenland as a single LME. Here, only conditions in the western Greenland portion of the region are examined. The hydrographic conditions presented are monitored at two oceanographic sections across the continental slope of West Greenland in the southwestern part of the ecoregion at a position that is influenced by the West Greenland Current (WGC; [Figure 4.3](#)). The WGC carries water north along the west coast of Greenland and consists of two components: a cold, fresh, inshore component which is a mixture of Polar Water and melt water, and a warmer, saltier, offshore component which is called Irminger Sea Water. Being part of the cyclonic Subpolar Gyre, the WGC is subject to hydrographic variations on time-scales associated with variability in the gyre.

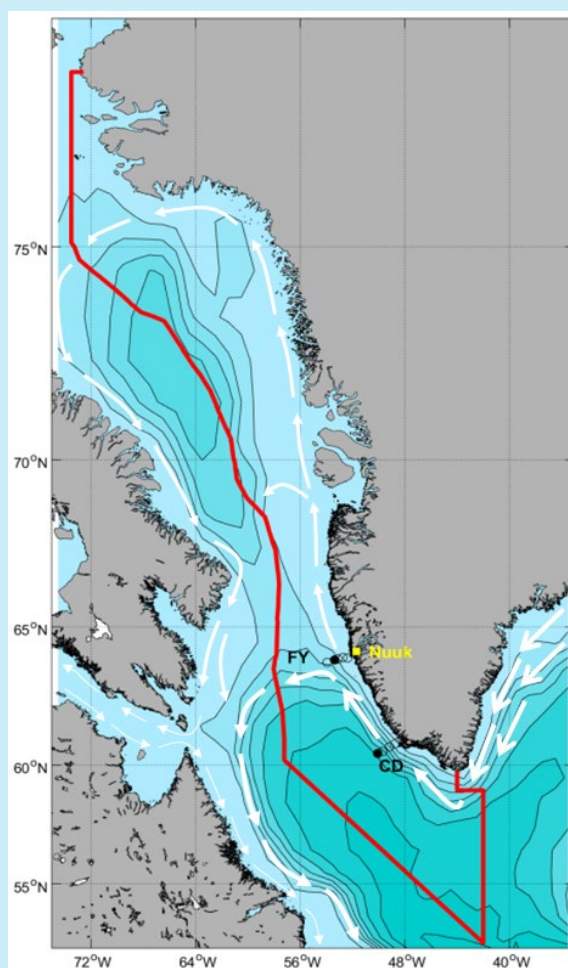
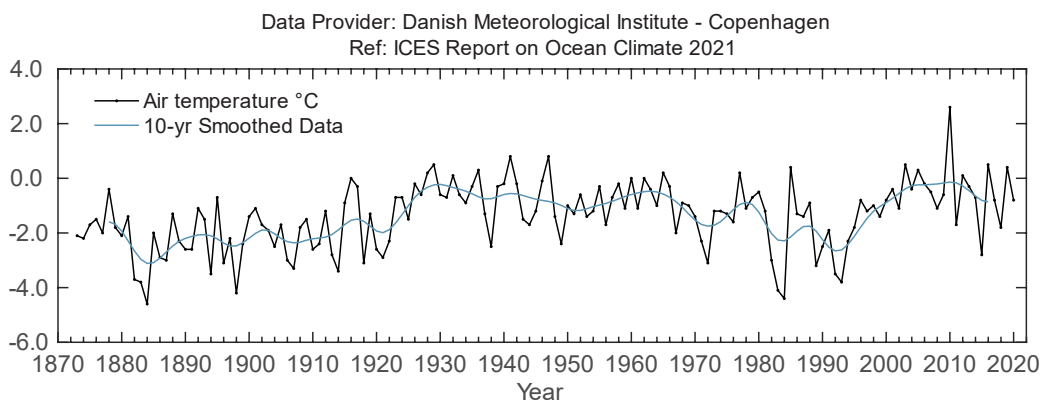


Figure 4.3. Circulation schematic for the Labrador Sea and Davis Strait. The location of Nuuk is marked in yellow. White arrows show the path of the surface circulation. The thick arrows are the West Greenland Current (WGC). The red lines show the extent of NAFO Area 1a, western Greenland. Circles labelled 'FY' are the stations of the Fyllas Bank hydrographic section; station 4 is marked as a black circle. Circles labelled 'CD' are the stations of the Cape Desolation hydrographic section; station 3 is marked as a black circle.

The West Greenland shelf and adjacent seas are delineated in the north by the NOAA LME boundaries and in the south by ICES marine ecoregion boundaries. The data presented here are from two hydrographic sections located across the southwest Greenland continental shelf, which are sampled twice annually (in June/July by the Greenland Institute of Natural Resources, Greenland, and in autumn by the Thünen Institute of Sea Fisheries, Germany). The time-series shown are from the continental slope influenced by the WGC. In autumn 2021, the Cape Desolation and Fyllas Bank sections had to be cancelled due to ship engine failures and severe weather conditions. In winter 2020/2021, the NAO index was negative. The annual mean air temperature at Nuuk Weather Station in West Greenland was 0.2°C in 2021, 1.2°C above the long-term mean (1991–2020:  $T_{\text{mean}} = -1.0^\circ\text{C}$ ; Cappelen and Drost Jensen, 2021; [Figure 4.4](#)). The mean water properties between 0 and 50 m depth at Fyllas Bank Station 4 ([Figure 4.5](#)) are used to monitor variability of the fresh surface water component of the WGC in June/July. In 2021, the temperature of this water mass was 1.59°C, 0.1°C below its long-term mean (1981–2010:  $T_{\text{mean}} = 1.69^\circ\text{C}$ ; [Figure 4.6](#)). Salinity increased in 2021, being 0.31 above its long-term mean (1981–2010  $S_{\text{mean}} = 33.27$ ; Mortensen, 2022; [Figure 4.6](#)).



**Figure 4.4. West Greenland. Annual mean air temperature at Nuuk station (64.16°N 51.75°W). Data source: Cappelen (2021).**



CCGS Hudson's fast rescue craft with both DFO and CCG staff securing a line to the AZMP's Viking Buoy for its recovery. Credit: Diana Cardoso (DFO).

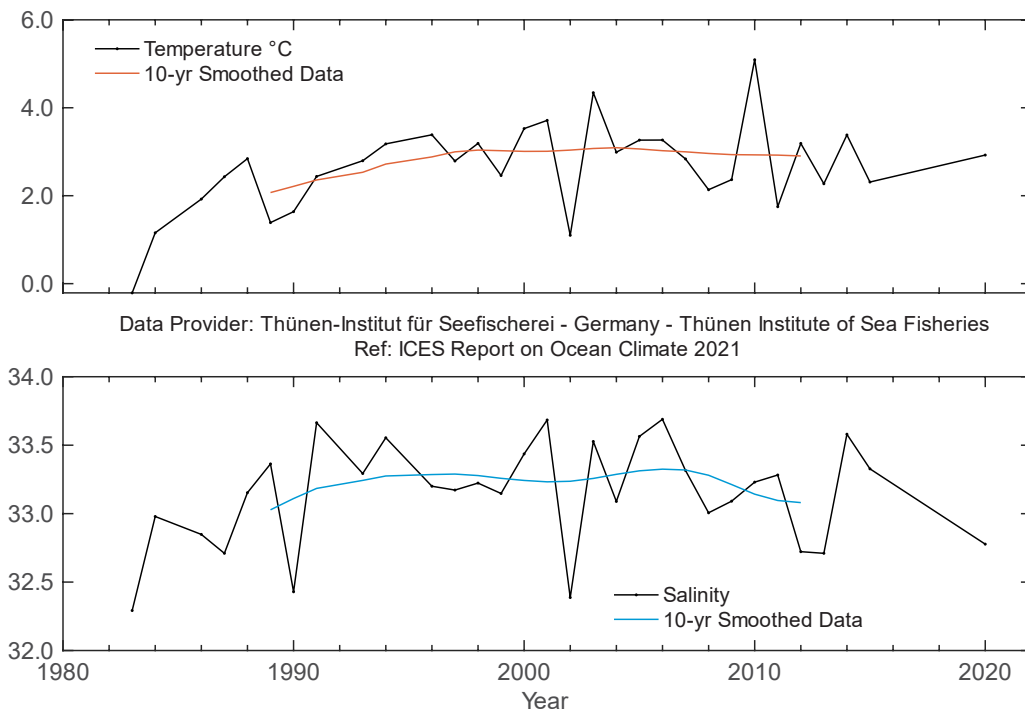


**Figure 4.5. West Greenland. Mean temperature (upper panel) and salinity (lower panel) in the 0–50 m water layer at Fyllas Bank Station 4 (63.88°N 53.37°W). Data until 2020.**

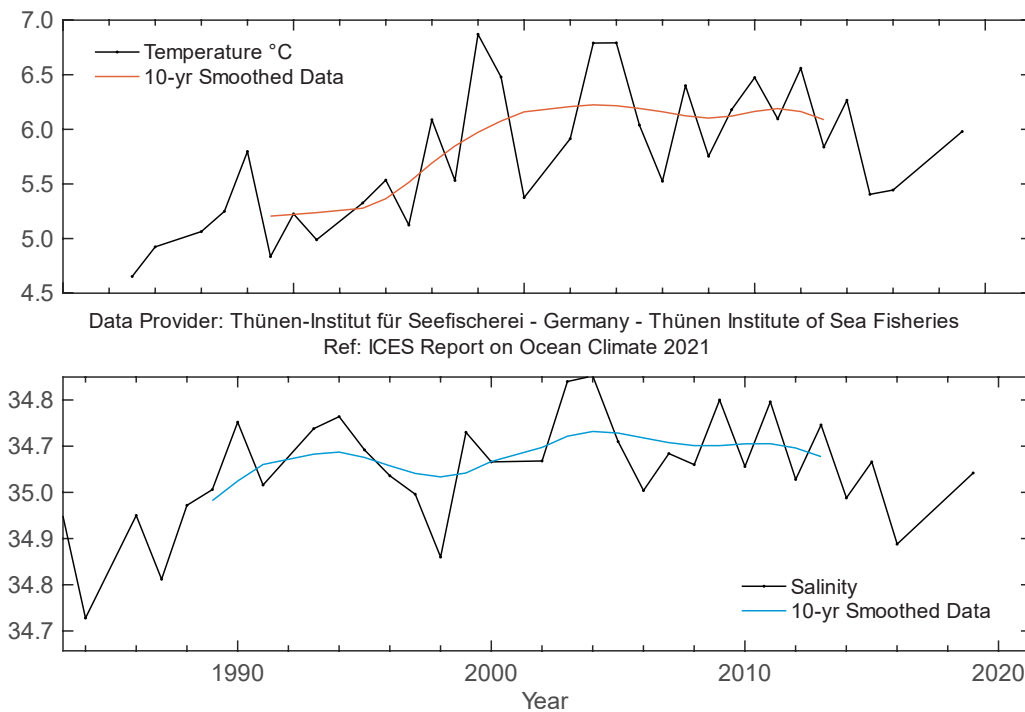


**Figure 4.6. West Greenland. Temperature (upper panel) and salinity (lower panel) in the 75–200 m water layer at Cape Desolation Station 3 (60.47°N 50°W). Data until 2019.**

## 4.2 Labrador Sea

*I. Yashayaev*

---

**IN 2021, WINTER CONVECTION AND INTERMEDIATE WATER-MASS PRODUCTION IN THE LABRADOR SEA STOPPED SHORT OF REACHING 900 M FOR THE FIRST TIME IN THE PAST 10 YEARS.**

---

The Labrador Sea is located between Greenland and the Labrador coast of eastern Canada. Its deep semi-enclosed basin is bounded by the West Greenland and the Newfoundland–Labrador shelves. Cold, low-salinity waters of polar origin circle the Labrador Sea in a counterclockwise current system that includes both the north-flowing WGC on the eastern side and the south-flowing Labrador Current on the western side. Patches of warmer and saltier AW, typically found under the offshore extension of the WGC, can be traced to their origin in the low latitudes of the North Atlantic by following the North Atlantic Current (NAC) and Gulf Stream. The AW mixes with other water masses and progressively becomes colder and fresher as it flows north into the Labrador Sea, following its eastern boundary, and eventually circuits the sea’s northern and western peripheries.

Interannual changes in the hydrographic conditions of the Labrador Sea are controlled by a number of factors, including annual heat loss to the atmosphere, heat and salt gain from the AW, and freshwater gains from the Arctic outflow, sea-ice melt, precipitation, and continental run-off. In addition, instantaneous conditions and process development depend on the cumulative effect of past heat, salt, and freshwater gains and their respective temperature, salinity, and density changes, also termed ocean preconditioning (Yashayaev and Loder, 2017). The Labrador Sea has a significant role in the subpolar region and climate system as a whole. Its extreme winter surface heat losses result in the formation of cold and dense intermediate depth waters which can reach a depth of 2500 m. This process makes the Labrador Sea the primary location in the northern hemisphere for the atmospheric ventilation of the intermediate and deep layers of the Atlantic Ocean. Through winter cooling of surface and subsurface waters and their subsequent mixing and sinking to depths of 500–2 500 m (depending on winter severity), a relatively dense and deep intermediate water mass is formed known as Labrador Sea Water (LSW). This water spreads over the Atlantic Ocean ventilating its deep layers and feeding and driving the global ocean’s overturning circulation or ocean conveyor belt.

### Oceanographic monitoring of the Labrador Sea

There were no oceanographic ship surveys covering the central Labrador Sea in 2021. However, the Argo, Deep Argo, and Biological Argo floats provided sufficient measurements to resolve the full seasonal cycle for the upper- and deep-water time-series. Before the year-round Argo data became readily available in the early 2000s, the Labrador Sea was mainly assessed through observations from the Atlantic Repeat 7-West (AR7W) repeat hydrography line, conducted primarily in support of the World Ocean Circulation Experiment (WOCE). This key Atlantic transect has been occupied and sampled at least yearly since 1990, except for 2017 and 2021,

resulting in a 31-year record (1990–2020) of deep-sea observations. [Figure 4.7](#) shows an example of the AR7W surveys, comprising CTD, water sampling, expendable bathythermograph (XBT), and Moving Vessel Profiler (MVP) casts, and Argo float deployments.

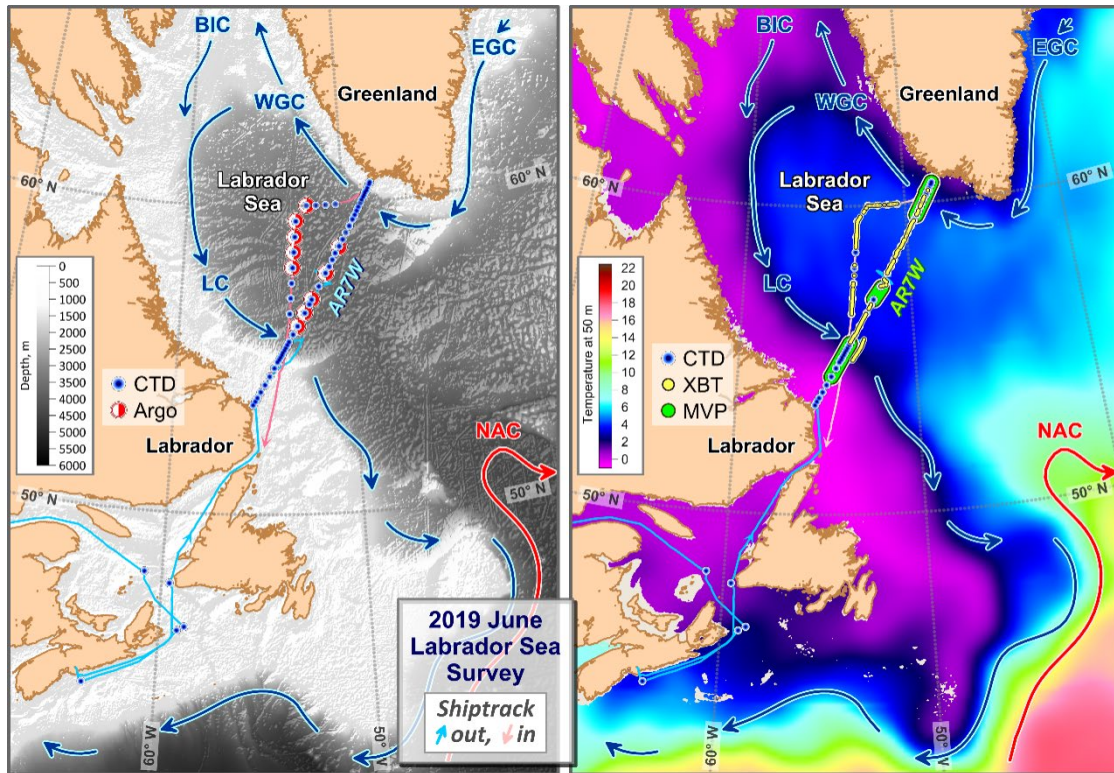


**Figure 4.7. Labrador Sea. Topography, surface currents, and temperature at 50 m. CTD, water sampling, expendable bathythermograph (XBT) and Moving Vessel Profiler (MVP) casts, and Argo float deployments conducted in the Labrador Sea in June 2019 by the Bedford Institute of Oceanography (Fisheries and Oceans Canada).**

The International Argo Program has provided the oceanographic community with unprecedented year-round monitoring of key oceanographic variables from the sea surface to 2 000 m. The central Labrador Sea ship survey and Argo float observations have been used to construct time-series of temperature, salinity, and density absolute values and anomalies averaged annually, revealing interannual-to-multidecadal changes in regional conditions over nearly eight decades. Examples of these series for the upper (50–200 m) and deep intermediate (1 000–1 800 m) layers are presented in [figures 4.8](#) and [5.11](#) (see Section 5.2.5), respectively. Key factors causing these properties to change are (i) advection of freshwater from the Arctic, continental run-off, and precipitation, as well as heat and salt from other Atlantic basins; and (ii) local atmospheric forcing mainly, but not exclusively, projected onto the deep Labrador Sea through winter convection. In order to better understand the appearance and causes of interannual-to-multidecadal changes in the region, the progressive developments of deep convection alternated with periods of ocean ‘relaxation’ over the past thirty years are described in more detail.

## Deep convection, water ventilation, and hydrographic trends

A sequence of severe winters in the early 1990s led to deep convection, with the maximum depth reached in 1994. This process filled the upper 2 500 m of the water column with cold, fresh, and dense water. Conditions have generally become milder since the mid-1990s. During 1995–2011, the upper and deep layers of the Labrador Sea became warmer and more saline as net annual surface heat loss decreased, while the influence of the AW on these layers increased ([figures 4.8](#) and [5.11](#); see Section 5.2.5). This tendency reversed in 2011 and, during 2011–2018, the upper and intermediate layers cooled and freshened. The cooling and freshening stopped in 2019, and winter temperatures evolved to normal in 2020 and above normal in 2021.

A closer examination of temperature and salinity records shows that the observed warming and cooling trends were not always uniform. A short spike in cooling and freshening in the deep intermediate series ([Figure 5.11](#); Section 5.2.5) was associated with the deep convection event of 2008 (Yashayaev and Loder, 2009). The 2010 and 2011 winter heat losses were low in magnitude and were matched by record weak convection, with the MLD typically not exceeding 800 m. The situation changed abruptly in 2012, starting a new and important trend in LSW production and regional hydrographic properties. In winter 2012, convection reached, and possibly exceeded, 1 400 m in depth, evident from both Argo float and ship survey temperature and salinity profile data. Interestingly, 2012 salinity in the top 50 m was the lowest since 2003, possibly influencing the strength of convection in winter 2013, which was not as deep as in the previous year. The situation reversed once again in 2014 when a strong winter cooling triggered convective mixing in the Labrador Sea reaching deeper than 1600 m. Convection continued to deepen over the following four winters reaching, and probably exceeding, 2 000 m depth at the end of the period. The mixed part of the water column became colder and denser with each cooling cycle. Finally, as mentioned in the previous paragraph, the deepening of convection and water column cooling and densification stopped in 2019. While convection still remained fairly strong, it reached, at most, 1 500 m in 2019, 1 600 m in 2020, and 850 m in 2021.

The observed multiyear development in convection is the result of recurring, relatively strong, winter surface cooling (often, but not always, coinciding with high NAO index values), which causes deep mixing and results in the preconditioning of the water column. This may, in turn, facilitate a deeper convection the next year under a weaker winter cooling. Water column preconditioning can also be viewed as the ocean's 'memory' or ability to carry forward some information from past winter cooling events. This suggests that certain properties imposed on the water column by a stronger-than-usual convective mixing in previous years, such as low temperature, weak vertical stability, and weak overall stratification, may result in the kind of preconditioning that facilitated the strengthening and deepening of convection observed in winter 2018. The residual imprint of deep convective preconditioning on density stratification decreased over the following three years which, combined with an extremely weak surface winter cooling in 2021, resulted in the shallowest convection observed for 2012–2021.

In the winters of 2016–2018, the mid-high latitude North Atlantic experienced a more moderate cumulative loss of oceanic heat to the atmosphere than the two-decade record-high observed in winter of 2015 (Yashayaev and Loder, 2017). Winter heat losses in the Labrador Sea in 2018 were the lowest since winter 2014. However, despite the reduction in cumulative winter heat losses, the depth of winter convection has been steadily increasing since 2015, reaching and exceeding 2 000 m in 2018 (the deepest since the record-deep cooling down to 2 400 m in 1994), and forming the most significant class of LSW since 1994, in terms of volume, depth, and density. A reservoir filled with this well-ventilated, record-deep, cold, and fairly fresh LSW is evident in

seawater property sections (data not shown). LSW formed in 2018 is characterized by low temperature ( $< 3.3^{\circ}\text{C}$ ) and salinity ( $< 34.86$ ) between 1 000 and 2 000 m.

The winter NAO index was slightly positive in 2019, but exceptionally high in 2020 (the highest since 2015 and third highest since 1995). The latter presents an exemplary case of net surface heat loss over the central Labrador Sea that is uncorrelated with the respective winter NAO index. The reason for this disparity is the character of the atmospheric forcing in winter 2020. The higher-than-normal NAO index was associated with stronger winds, but these were from a more northerly rather than westerly direction, and the zone of most intense winds shifted to the east. This atmospheric situation did not favour high surface heat losses in the convection zone. In 2021, on the other hand, the NAO index was negative for the first time since 2013, which is consistent with the lowest winter surface cooling over the same period.

## Hydrographic changes in the Labrador Sea over the past 82 years

The long-term changes observed in the Labrador Sea until 2016 have been extensively discussed in a series of publications (Yashayaev *et al.*, 2007; Yashayaev and Loder, 2009, 2016, 2017). Here, the series is updated ([figures 4.8](#) and [5.11](#); see Section 5.2.5) and the earlier statement concerning the long-term variability of temperature and salinity is revisited.

The deep intense winter mixing during the five consecutive winters from 2014 to 2018 and the associated progressive cooling of the top 2 000 m have interrupted the general warming and stratification-building trend that has persisted in the intermediate waters of the Labrador Sea since the mid-1990s. Despite the reduction in net surface heat loss after 2015, water column cooling continued until 2018 aided by multiyear convective preconditioning. Responding to winter cooling enhanced by convective preconditioning, both the upper (50–200 m) and deeper (1 000–1 800 m) layers cooled between 2011 and 2018 ([figures 4.8](#) and [5.11](#); see Section 5.2.5). However, in the last two years the situation changed, with temperature increasing in the upper layer to near-normal and stabilizing in the deeper layer.

Events of moderate freshening of the upper layer spread across the central basin in 2013, 2015, and 2018–2021 ([Figure 4.8](#)).

With respect to multidecadal changes in the subpolar North Atlantic, the progressively deepening convective mixing that reoccurred in the Labrador Sea during the period 2012–2018 has reversed the general warming trend observed in the intermediate waters during 1994–2011. The situation changed again in 2019, starting a new period (2019–2021) of weakening of winter convection and warming of the water column. As a result of such a sustained recurrence of stronger-than-normal convection and production of LSW, followed by warming and post-convective relaxation, the annual average temperature and density in the region's upper 2 000 m have predominantly varied on a bi-decadal time-scale, rather than having a long-term trend, as might be expected from anthropogenic climate change.

The above-average regional winter cooling during 2012–2020, enhanced by convective preconditioning, has increased the rate of removal of gas-saturated waters from the top 200 m. The moderately strong winter convection (down to 1 600 m) in winter 2020 further added to increased gas uptake (dissolved oxygen, anthropogenic gases, and carbon dioxide) and consequently increased gas concentrations in the lower half of the Labrador Sea 0–2 000 m layer. However, in 2021, winter conditions abruptly became milder, shutting down renewal and ventilation of the intermediate and deep waters in the North Atlantic.

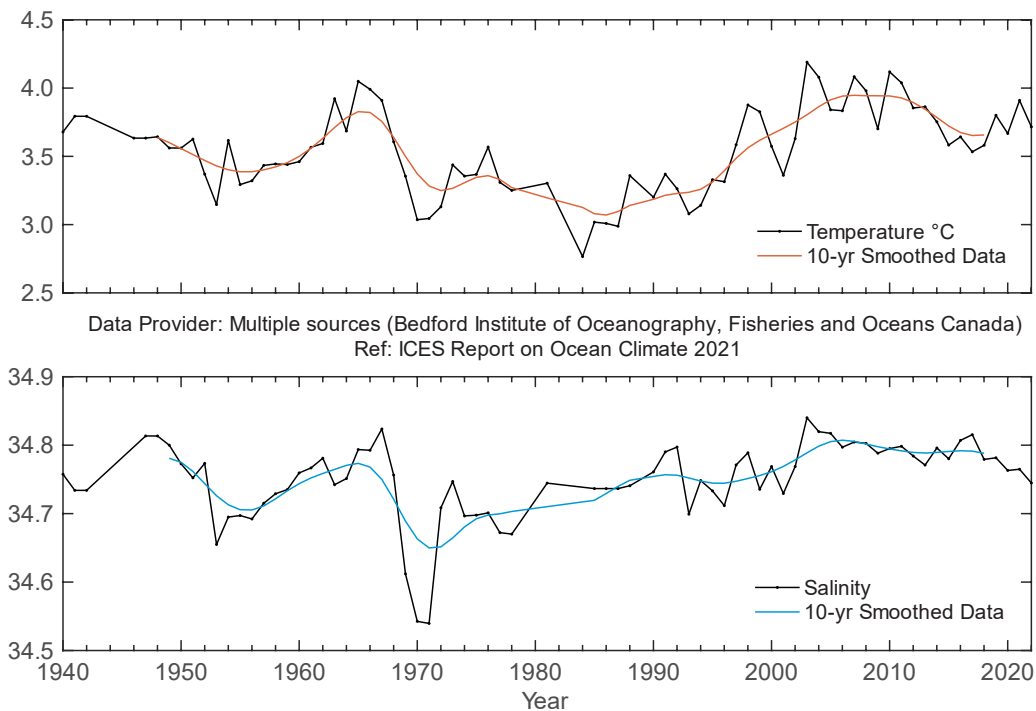


Figure 4.8. Labrador Sea. Annually averaged temperature (upper panel) and salinity (lower panel) anomalies in the 50–200 m vertical layer in the west central region of the Labrador Sea (centred at 56.7°N 52.5°W). Values are based on profiles of reversing thermometer, water sample salinity, CTD, and Argo data. Prior to yearly bin-averaging, estimates of the seasonal cycle (derived from all data in the assembled time-series) have been removed from the vertically interpolated observations at each level in the layer.

### 4.3 Newfoundland-Labrador Shelf

*F. Cyr and P. S. Galbraith*

---

**2021 WAS ONE OF THE WARMEST ON RECORD FOR THE NEWFOUNDLAND AND LABRADOR OCEAN CLIMATE.**

---

The Newfoundland–Labrador Shelf region is located on the western side of the Labrador Sea, stretching from the Hudson Strait to the tail of Grand Banks. The bathymetry on the shelf consists of shallow banks separated by deeper channels or saddles. The ocean circulation is dominated by the southward flowing Labrador Current system, which brings cold and fresh Arctic-origin waters, sea ice, and icebergs on the shelf down the Grand Banks, as well as warmer and saltier LSW along the continental slope.

Hydrographic conditions are determined in part by the strength of the winter atmospheric circulation over the Northwest Atlantic (e.g. winter NAO index), advection by the Labrador Current, freshwater runoff, and cross-shelf exchange with warmer continental slope water. Superimposed are large seasonal and interannual variations in solar heat input, sea ice cover, and storm-forced mixing. The resulting water mass on the shelf exhibits large annual cycles with strong horizontal and vertical temperature and salinity gradients.

The winter NAO index, a key indicator of the direction and intensity of the winter windfield patterns over the Northwest Atlantic, was negative for the first time in eight years. This led to the large majority of the environmental parameters for the Newfoundland–Labrador region being above normal in 2021.

Annual air temperatures were generally above normal across the entire west side of the Atlantic. In Cartwright, southern Labrador, the annual air temperature was 1.6 s.d. above normal, making 2021 the second warmest year on record after 2010 (Figure 4.10). When considering only the winter months (DJF), record-warm temperatures were established at Iqaluit (Baffin Island), Bonavista, and St John’s (Newfoundland), and the second warmest winter on record was observed in Cartwright (data not shown).

The seasonal (DJFMAMJ) mean sea-ice volume in three regions of the Newfoundland–Labrador shelf (northern Labrador, southern Labrador, and Newfoundland) has been generally decreasing since the early 1990s. After a recent rebound to near-normal conditions between 2014 and 2017, sea ice volumes have returned to below normal since 2018 (Figure 4.9), reaching, in 2021, 24.5 km<sup>3</sup> (-1.7s.d.), 15.2 km<sup>3</sup> (-1.7s.d.) and 2.2 km<sup>3</sup> (-1.2 s.d.), respectively. The combined sea ice volume for these three regions was the second lowest in 2021 (-1.6 s.d.), after 2011, since the beginning of the time-series in 1980.

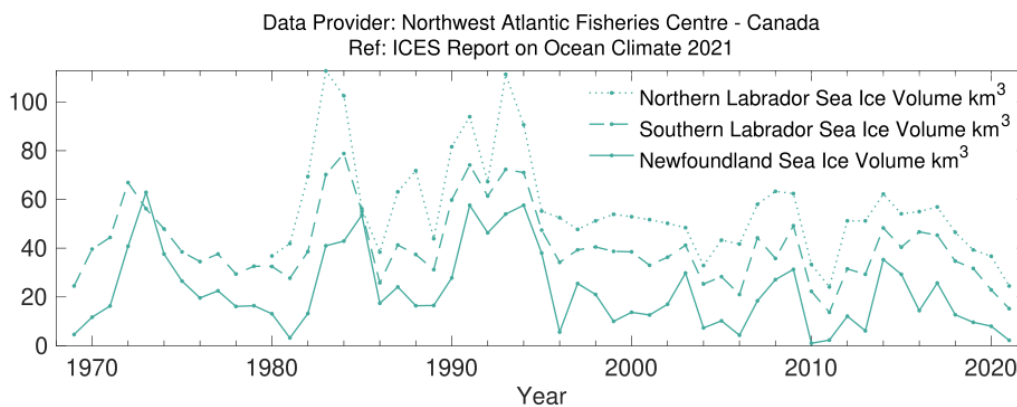


**Figure 4.9. Northwest Atlantic: Newfoundland–Labrador Shelf. Winter and spring sea ice areas off Newfoundland–Labrador between 45°N and 55°N.**

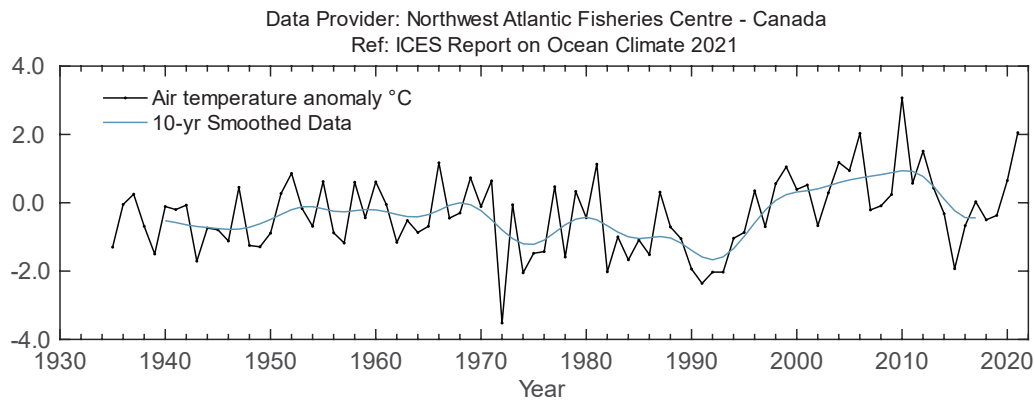


**Figure 4.10. Northwest Atlantic: Newfoundland–Labrador Shelf. Annual air temperature anomalies at Cartwright on the Labrador coast.**

At the standard monitoring site off eastern Newfoundland (Station 27), the depth-averaged annual water temperature established a new warm record in 2021 at  $1.15^{\circ}\text{C}$  (2.2 s.d.) above normal (Figure 4.11). This easily beats the previous record of  $0.85^{\circ}\text{C}$  (1.7 s.d.) established in 2011. Warm years generally correspond to fresher-than-normal conditions on the Newfoundland shelf. This was the case in 2021, when the salinity anomaly was -1.3 s.d., the second freshest anomaly since 1970, after 2018 (-1.9 s.d.).

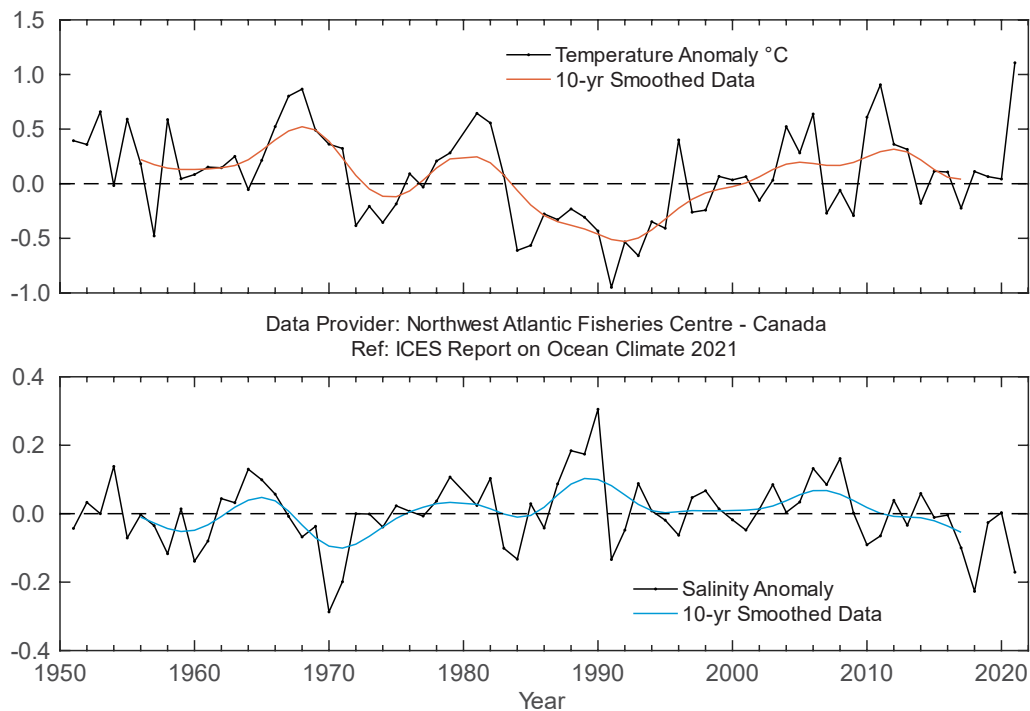


**Figure 4.11. Northwest Atlantic: Newfoundland–Labrador Shelf. Annual depth-averaged Newfoundland Shelf temperature (top panel) and salinity (middle panel) anomalies at Station 27 ( $47.55^{\circ}\text{N}$   $52.59^{\circ}\text{W}$ ).**

A robust index of ocean climate conditions in eastern Canadian waters is the areal extent of the cold intermediate layer (CIL), defined as the continental shelf waters  $< 0^{\circ}\text{C}$  along standard hydrographic sections on the Labrador and Newfoundland shelf (Figure 4.12). After its formation during winter, the CIL remains isolated throughout summer and early autumn

between the seasonally heated upper layer and the warmer shelf–slope water. During the 1960s, when the winter NAO was at the most negative phase of the 20th century, the volume of CIL water was at a minimum (warmer-than-normal conditions), and during the positive winter NAO years of the early 1990s, the CIL volume reached near-record high values (colder-than-normal conditions). From the late 1990s to about 2011, the area of CIL water gradually decreased as a consequence of increased ocean temperatures. Following this period, the CIL area expanded and reached 2.3 s.d. above normal in 2015, the second largest anomaly since the beginning of the time-series in 1984 (+2.35 s.d.). This cooling phase lasted between about 2014 and 2017 and was driven by the beginning of the ongoing positive winter NAO phase. However, since 2018, the CIL area has been shrinking, reaching  $-2.1$  s.d. and  $-1.4$  s.d. in 2021 on the southern Labrador and Newfoundland shelves, respectively, averaged over these two regions. This makes 2021 the third smallest CIL on record, after 1972 and the all-time record low of 1965.

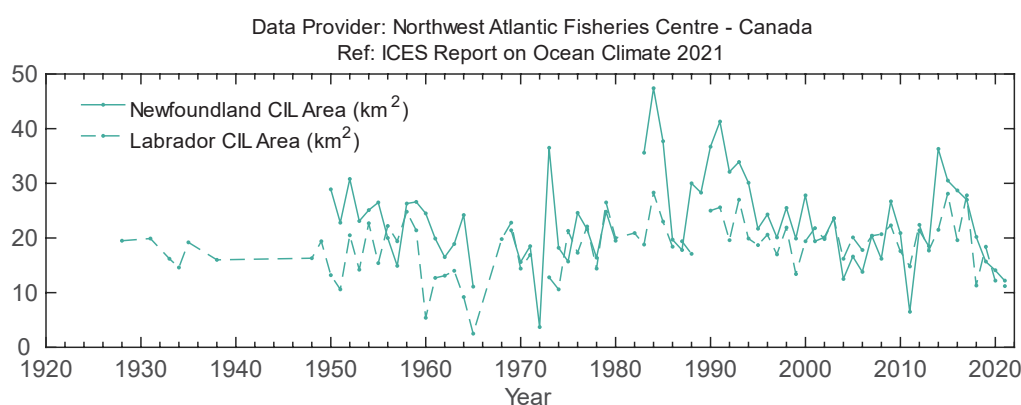


Figure 4.12. Spatial extent of cold intermediate layer (CIL).

## 4.4 Gulf of St Lawrence

*P. S. Galbraith*

**DEEP-WATER TEMPERATURE (300 M) WAS AT A 100+ YEAR RECORD HIGH. THE WINTER COLD-MIXED LAYER HAD THE SECOND LOWEST VOLUME ON RECORD, LEAVING BEHIND THE WARMEST SUMMER COLD-INTERMEDIATE LAYER IN 40 YEARS. THE MAY–NOVEMBER SEA SURFACE TEMPERATURE AVERAGE WAS THE THIRD HIGHEST ON RECORD.**

The Gulf of St. Lawrence is a semi-enclosed Canadian sea covering an area of about 235 000 km<sup>2</sup> and containing 35 000 km<sup>3</sup> of water, which opens to the Atlantic Ocean through Cabot Strait (104 km wide and 480 m at its deepest) and the Strait of Belle Isle (17 km wide and 60 m at its sill). In winter, it can become completely covered by sea ice and nearly half of its water volume usually gets cooled to temperatures below 0°C within the winter mixed layer (Galbraith, 2006). This creates a CIL that persists until late autumn and determines the bottom temperature habitat on the Magdalen Shallows and other shallow (<100 m) areas of the Gulf.

Waters deeper than roughly 150–200 m are entrained inwards from the continental slope by estuarine circulation, taking several years to reach the heads of the Gulf deep channels, during which mixing and diffusion occurs. This layer has been warming since 2009, breaking 100+ year records each year since 2015 and reaching above 7°C in the channels of the northeastern Gulf in recent years.

The maximum sea ice volume of 11 km<sup>3</sup> (–1.4 s.d. against the 1991–2020 climatology) was just shy of the series low record of 2010 (Figure 4.13), and the January–April average volume was a series record low (data not shown). The 12-year span since 2010 contains eight of the 12 lowest maximum sea ice volumes since records began in 1969.

In winter, a near-freezing mixed layer is formed in the Gulf of St Lawrence that averages 75 m in thickness. The layer has been sampled every March since 1996 using a unique helicopter-based survey which now samples around 100 stations to 200 m depth from stationary flight. In March 2021, the volume of the mixed layer colder than –1°C was 4 700 km<sup>3</sup>, which is the second lowest value of the 1996–2021 time-series (Figure 4.14).

The volume of CIL (T < 1°C) present in August and September is estimated from temperature profiles taken mostly during multispecies surveys since the mid-1980s (Figure 4.15). The volume in 2021 of 1 700 km<sup>3</sup> was a time-series record low (–2.9 s.d.; i.e. warmer-than-normal conditions). The last above-normal conditions occurred in 2008.

Sea surface temperatures (SST) averaged monthly over the Gulf were the highest of the satellite record (since 1981) in October and November. The May–November SST average was far above normal (+0.9°C, +1.8 s.d.) and the third highest in the time-series after 2006 and 2012 (Figure 4.16).

Deep-water temperatures have been increasing overall in the Gulf since 2009, with inward advection from Cabot Strait (Figure 4.17). The Gulf-wide average temperature at 300 m has been at a new 100+ year record high every year since 2015, standing in 2021 at 6.9°C (+1.2°C, +2.8 s.d.).

Data and processing methods used for these results are described in Galbraith *et al.* (2021a) for the SST product, and in the annual reporting for Canada’s Atlantic Zone Monitoring Program (e.g. Galbraith *et al.*, 2021b).

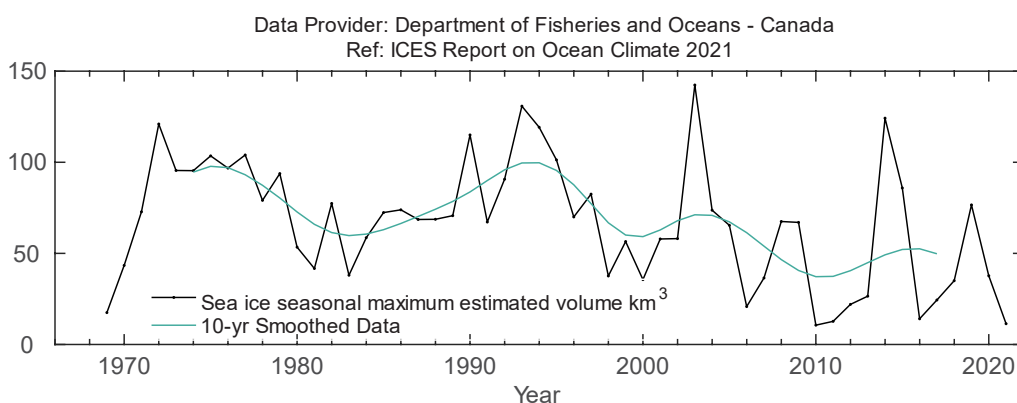
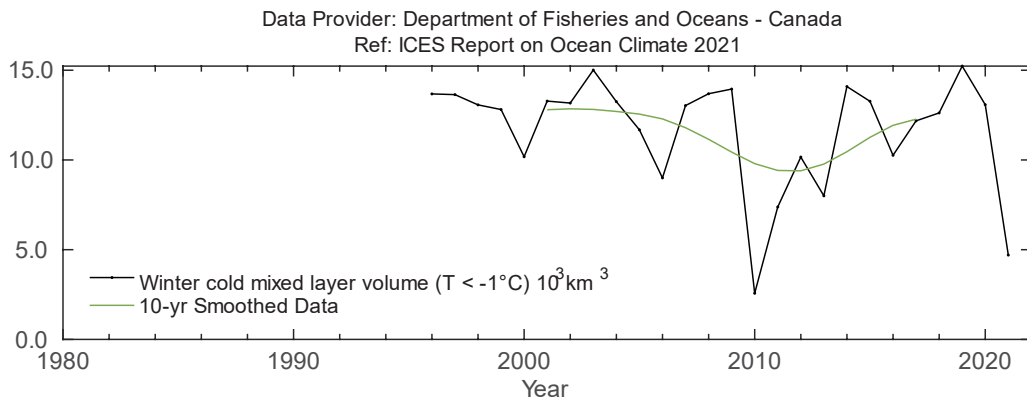
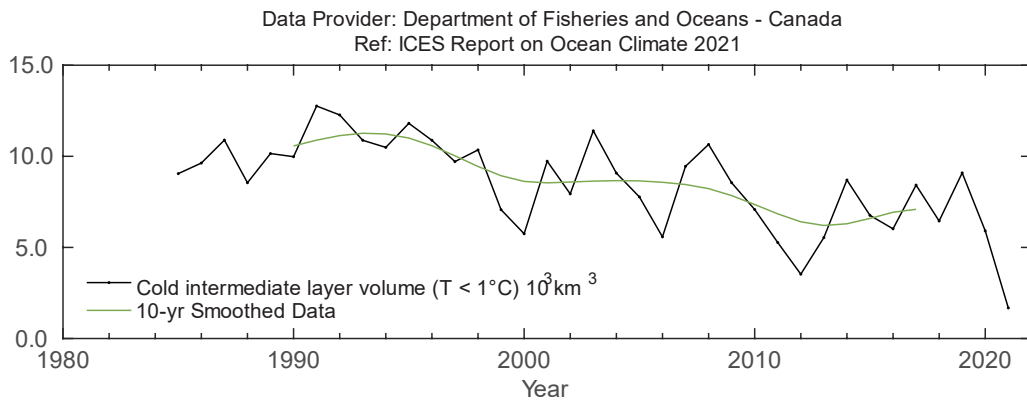


Figure 4.13. Northwest Atlantic: Gulf of St Lawrence. Seasonal maximum sea ice volume in the Gulf of St Lawrence estimated from weekly ice charts.



**Figure 4.14. Northwest Atlantic: Gulf of St Lawrence. Winter mixed-layer ( $T < -1^{\circ}\text{C}$ ) volume in the Gulf of St Lawrence.**



**Figure 4.15. Northwest Atlantic: Gulf of St Lawrence. Cold intermediate layer (CIL) volume ( $T < 1^{\circ}\text{C}$ ) present in August and September in the Gulf of St Lawrence.**

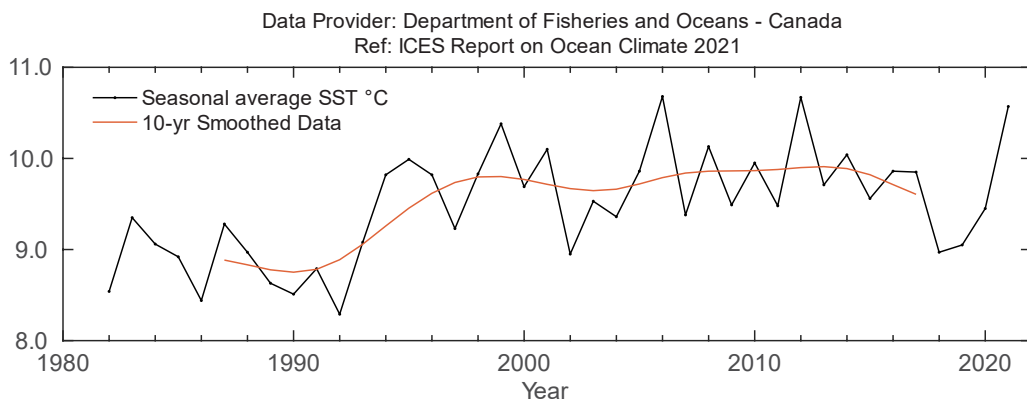


**Figure 4.16. Northwest Atlantic: Gulf of St Lawrence. Seasonally averaged sea surface temperature (SST; May–November) in the Gulf of St Lawrence.**

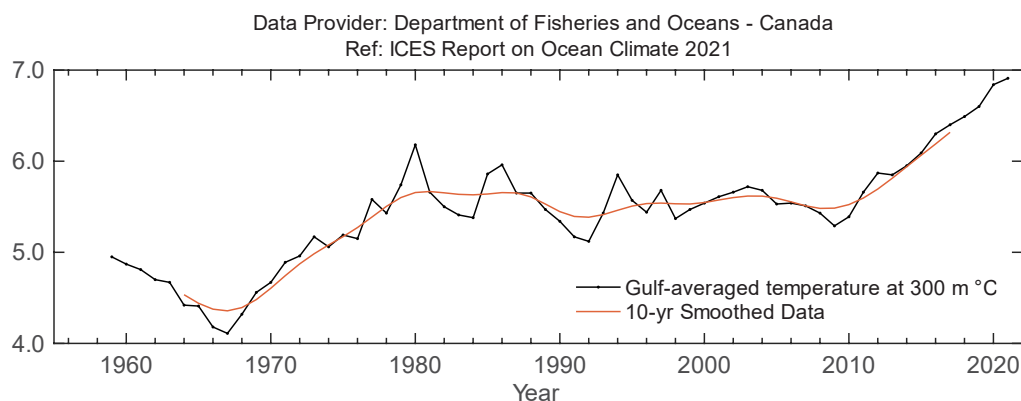


Figure 4.17. Northwest Atlantic: Gulf of St Lawrence. Averaged temperature at 300 m.

## 4.5 Scotian Shelf

*D. Hebert, C. Layton, and P. S. Galbraith*

---

**OCEAN TEMPERATURES AND SALINITY IN THE DEEP WATERS OF THE SCOTIAN SHELF REGION WERE WELL ABOVE NORMAL IN 2021, NEAR RECORD HIGHS, REFLECTIVE OF WARM SALTY CONDITIONS IN THE SLOPE REGION OFFSHORE.**

---

The Scotian Shelf is the continental shelf off the coast of Nova Scotia and is identified as an LME. It is characterized by a complex topography consisting of many offshore shallow banks and deep mid-shelf basins. It is separated from the Newfoundland Shelf in the northeast by the Laurentian Channel and borders the Gulf of Maine to the southwest. Surface circulation is dominated by a general flow towards the southwest interrupted by clockwise movement around the banks and anticlockwise movement around the basins, with the strengths varying seasonally.

Hydrographic conditions on the Scotian Shelf are determined by heat transfer between the ocean and the atmosphere, inflow from the Gulf of St Lawrence and the Newfoundland Shelf, and exchange with offshore slope waters. Water properties have large seasonal cycles and are modified by freshwater run-off, precipitation, and melting of sea ice. Temperature and salinity exhibit strong horizontal and vertical gradients that are modified by diffusion, mixing, currents, and shelf topography.

In 2021, annual mean air temperature over the Scotian Shelf ([Figure 4.18](#)), represented by Sable Island observations, was +1.0°C (+1.4 s.d.) above the long-term mean (1991–2020). The linear trend (and 95% confidence limits) from 1900 to 2020 is +1.4°C 100 years<sup>-1</sup> (+1.1°C 100 years<sup>-1</sup>, +1.8°C 100 years<sup>-1</sup>). The January–April seasonal average of sea ice on the Scotian Shelf in 2021, measured seaward of Cabot Strait between Nova Scotia and Newfoundland, was near zero at 200 km<sup>2</sup>, below (–0.9 s.d.) the 1991–2020 long-term mean of 4 800 km<sup>2</sup>. The maximum weekly area of 2 100 km<sup>2</sup> was also below (–1.0 s.d.) the 15 400 km<sup>2</sup> long-term mean ([Figure 4.19](#)). The interannual variability of sea ice is very high, leading to low standardized anomalies.

Topography separates the northeastern Scotian Shelf from the rest of the Shelf. In the northeast, the seabed tends to be covered by relatively cold water (2–5°C), whereas the basins in the central and southwestern regions typically have bottom temperatures of 6–10°C. The origin of the latter is the offshore slope waters, whereas water in the northeast comes principally from the Gulf of St Lawrence. The interannual variability of the two water masses differs.

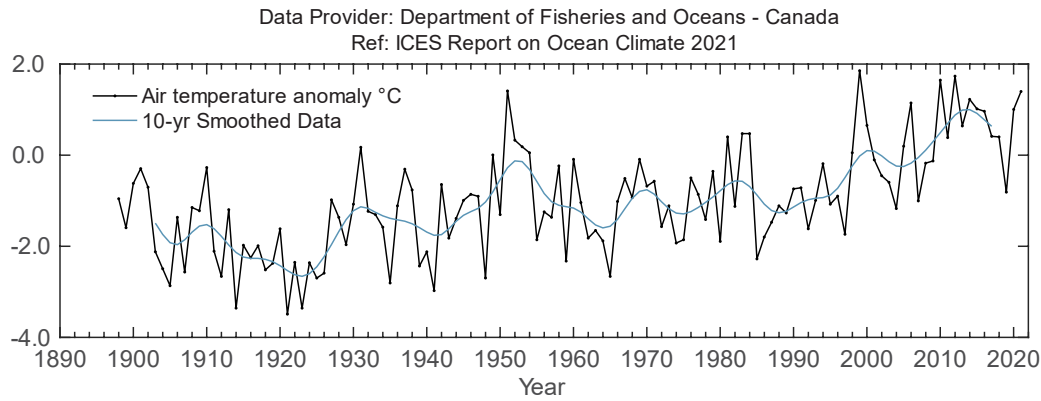


**Figure 4.18. Northwest Atlantic: Scotian Shelf. Air temperature anomalies at Sable Island on the Scotian Shelf.**

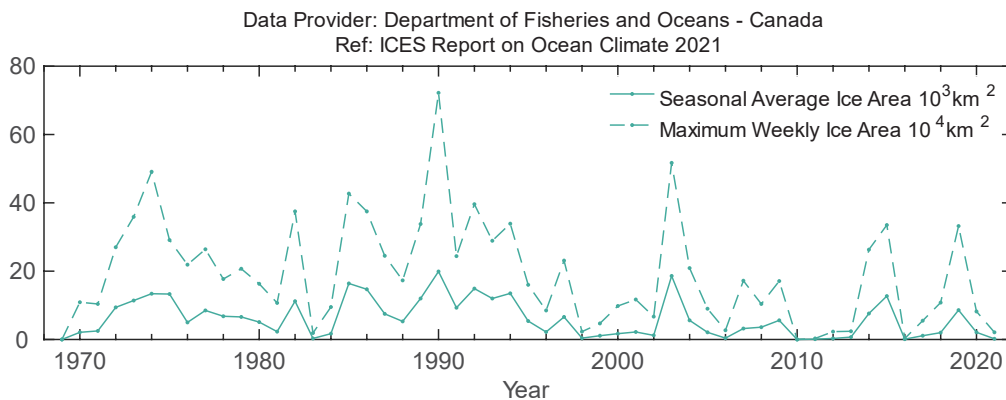


**Figure 4.19. Northwest Atlantic: Scotian Shelf. Monthly ice area means seaward of Cabot Strait.**

Measurements of near-bottom temperatures (100 m) at the Misaine Bank station capture the changes in the shallow northeast Scotian Shelf (Figure 4.20). They revealed an above-average annual temperature anomaly of +1.3°C in 2021 (+2.2 s.d.; relative to the 1991–2020 mean), making it the second warmest year in the record, and near-normal anomaly for salinity of +0.06 (+0.6 s.d.).

Measurements are also taken in the deep water along the Scotian Shelf from Cabot Strait to the Gulf of Maine. The deep Cabot Strait anomalies represent the offshore water intrusions travelling up the Laurentian Channel. In 2021, the 200–300 m annual temperature anomaly was the second warmest on record at +1.3°C (+1.9 s.d.), making five out of the last six years the warmest on record. Similarly, the salinity anomaly was far above normal, +0.2 (+1.7 s.d.), the fourth saltiest on record (Figure 4.21).

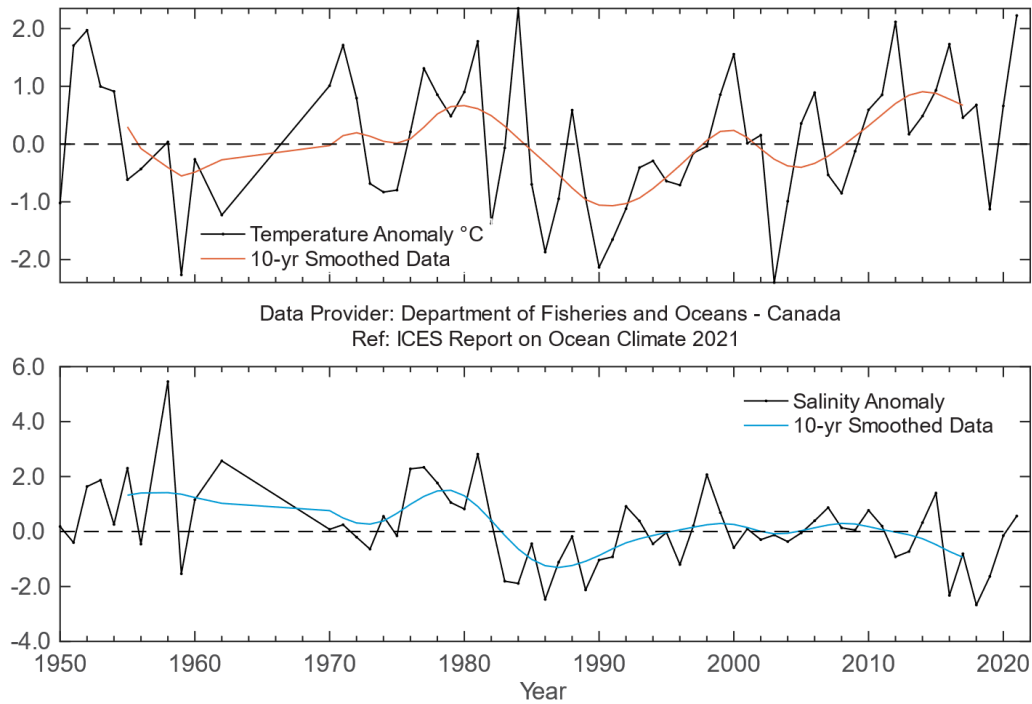


Figure 4.20. Northwest Atlantic: Scotian Shelf. Near-bottom temperature (upper panel) and salinity (lower panel) anomalies at Misaine Bank (100 m).

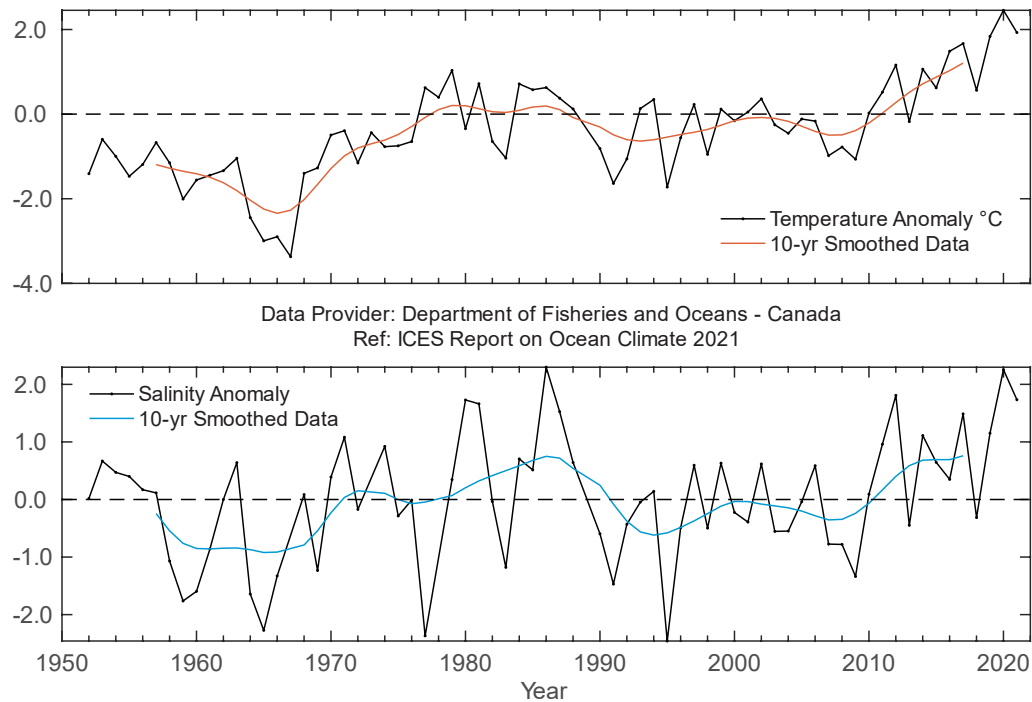
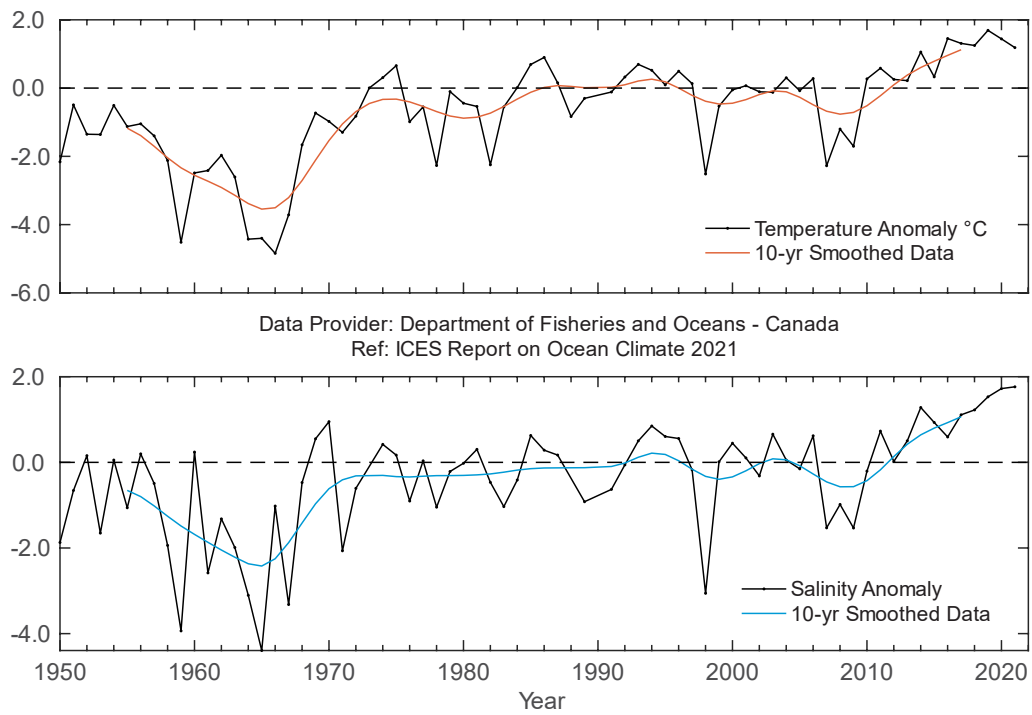
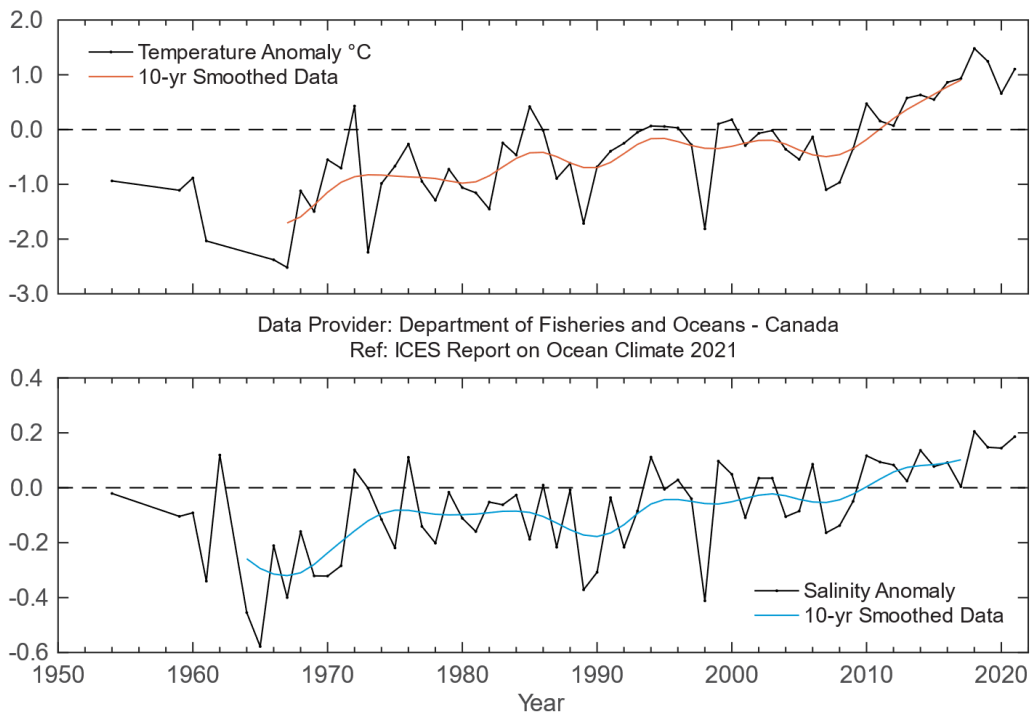


Figure 4.21. Northwest Atlantic: Scotian Shelf. Near-bottom temperature (upper panel) and salinity (lower panel) anomalies in the eastern Scotian Shelf (Cabot Strait, 200-300 m).



**Figure 4.22. Northwest Atlantic: Scotian Shelf. Near-bottom temperature (upper panel) and salinity (lower panel) anomalies in the central Scotian Shelf (Emerald Basin, 250 m).**



**Figure 4.23. Northwest Atlantic: Scotian Shelf. Near-bottom temperature (upper panel) and salinity (lower panel) anomalies in the central Scotian Shelf (Georges Basin, 200 m).**

The deep Emerald Basin anomalies represent the slope water intrusions onto the central Scotian Shelf that are subsequently trapped in the inner basins. In 2021, the 250 m annual temperature anomaly was a near-record high  $+1.1^{\circ}\text{C}$  ( $+1.2$  s.d.), making seven out of the last eight years the warmest years in the record ([Figure 4.22](#)). Similarly, the salinity anomaly was far above normal at  $+0.3$  ( $+1.8$  s.d.), which is a record high. Seven out of the last eight years were the saltiest on record ([Figure 4.22](#)).

The deep Georges Basin anomalies represent the slope water intrusions through the Northeast Channel into the Gulf of Maine that are subsequently trapped in the basins. In 2021, the 200 m annual temperature anomaly was a near-record high at  $+1.1^{\circ}\text{C}$  ( $+1.6$  s.d.), making the last nine years the warmest years on record ([Figure 4.23](#)). Similarly, the salinity anomaly was far above normal at  $+0.2$  ( $+1.4$  s.d.), making 2021 the second saltiest year on record. Four out of the last eight years were the saltiest on record ([Figure 4.23](#)). Model simulations of the region showed a large flux of warm salty water from the slope region.

## 4.6 Northeast US continental shelf

*P. Fratantoni*

---

**2021 WAS CHARACTERIZED BY WARMER-THAN-AVERAGE WATER TEMPERATURES OBSERVED ACROSS THE ENTIRE NORTHEAST US SHELF.**

---

The northeast US continental shelf extends from the southern tip of Nova Scotia, Canada, southwest through the Gulf of Maine and the Middle Atlantic Bight, to Cape Hatteras, North Carolina ([Figure 4.24](#)). Contrasting water masses from the Subtropical and Subpolar gyres influence the hydrography in this region. Located at the downstream end of an extensive interconnected coastal boundary current system, the northeast US continental shelf is the direct recipient of cold and freshwater of Arctic origin, accumulated coastal discharge and ice melt that has been advected thousands of kilometres around the boundary of the subpolar North Atlantic. Likewise, subtropical water masses advected by the Gulf Stream, slope currents, and associated eddies also influence the composition of water masses within this shelf region. The western boundary currents of the Subpolar and Subtropical gyres respond to variations in basin-scale forcing through changes in position, volume transport, and/or water mass composition. It is partly through these changes that basin-scale climate variability is communicated to the local northeast US continental shelf. Shelf-wide, hydrographic conditions have been monitored annually in this region since 1977 as part of quarterly ecosystem monitoring and twice-yearly bottom-trawl surveys conducted by the US National Marine Fisheries Service, Northeast Fisheries Science Center.

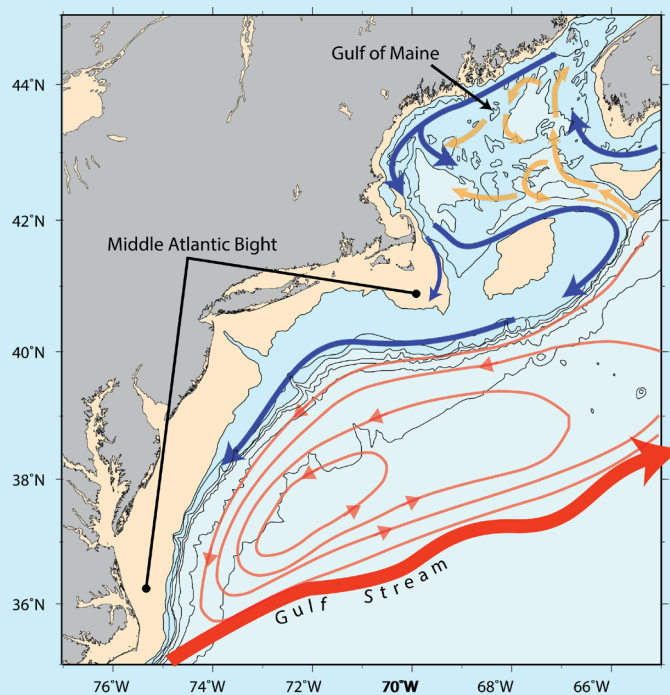


Figure 4.24. Circulation schematic for the northeast US shelf region. Blue arrows: shelf water circulation; orange arrows: deeper slope water circulation pathways. Water depths deeper than 200 m are shaded blue. Water depths shallower than 50 m are shaded tan.

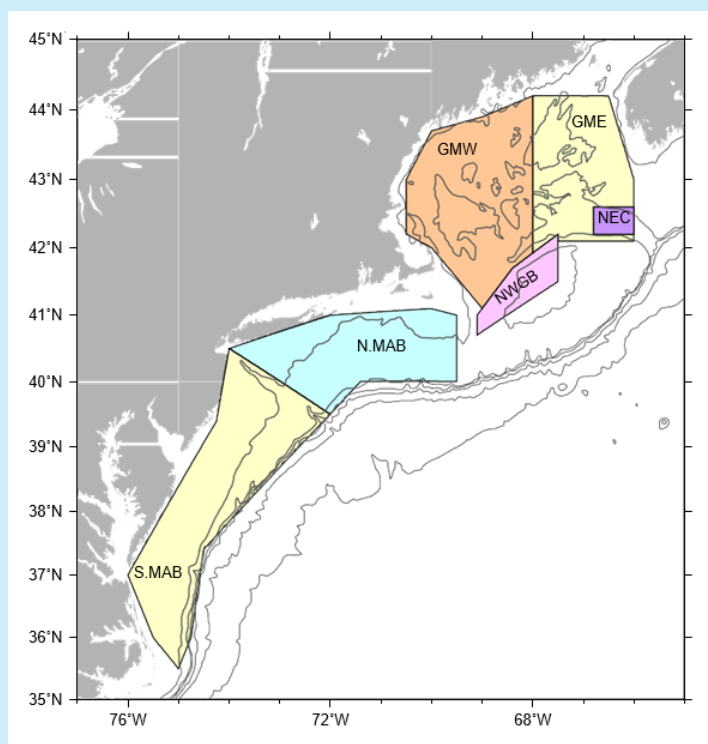
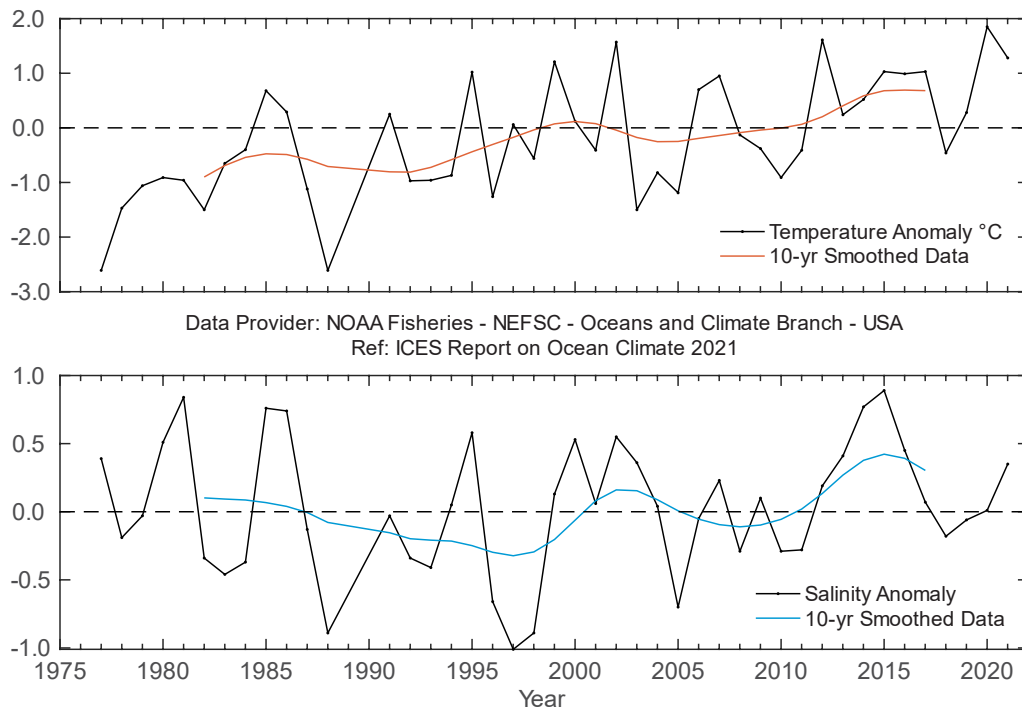


Figure 4.25. The six regions within which CTD observations are used to compute regional average time-series: eastern and western Gulf of Maine - GME and GMW; northern and southern Middle Atlantic Bight - N.MAB and S.MAB; Northeast Channel - NEC; and northwest Georges Bank - NWGB. The 50-, 200-, 500-, 1 000-, 2 000-, and 3 000-m isobaths are shown.

The majority of the northeast US continental shelf was warmer in 2021 than the 1991–2020 mean. Annual 0–30 m temperatures were 1.3–1.5°C warmer than normal everywhere (figures 4.26, 4.27, 4.28, 4.29, and 4.30). Enhanced warming was observed throughout the year, but particularly in summer and early autumn in the northern Middle Atlantic Bight (data not shown). Extremely warm conditions were also observed near the bottom across the entire region, with warm anomalies measuring more than 1 s.d. above normal throughout the year in the Gulf of Maine and northern Middle Atlantic Bight (data not shown). Most notably, anomalies exceeded 2.5°C in surface and bottom waters during September in the northern Middle Atlantic Bight and reached 2°C in surface and bottom waters in the western Gulf of Maine in November.

In 2021, waters in the upper 30 m were saltier than normal everywhere except the eastern Gulf of Maine, where they were near normal (Figure 4.29). Seasonally, large positive anomalies were observed during September and October in the northern Middle Atlantic Bight, where anomalies exceeded 0.7. Similar patterns were observed near the bottom, although with more saline conditions observed in the northern Middle Atlantic Bight and eastern Gulf of Maine. Bottom waters in the northern Middle Atlantic Bight were saltier than normal throughout the year, although anomalies were particularly enhanced during September and October.

Deep waters entering the Gulf of Maine through the Northeast Channel represent one of the dominant water mass sources to the Gulf of Maine slope waters (Mountain, 2012). These deep waters lying between 150 and 200 m are uninfluenced by seasonal atmospheric forcing. On an annual scale, deep inflow to the Gulf of Maine continued to be very warm and salty in 2021 compared to the long-term mean, marking two decades during which southern-source waters have dominated the slope water composition in the region (Figure 4.32).



**Figure 4.26.** Northeast US continental shelf. Time-series plots of 0–30 m averaged temperature anomaly (upper panel) and salinity anomaly (lower panel) in the region between Cape Hatteras, North Carolina, and Hudson Canyon. Anomalies are calculated relative to 1991–2020 using hydrographic data from shelf-wide surveys.

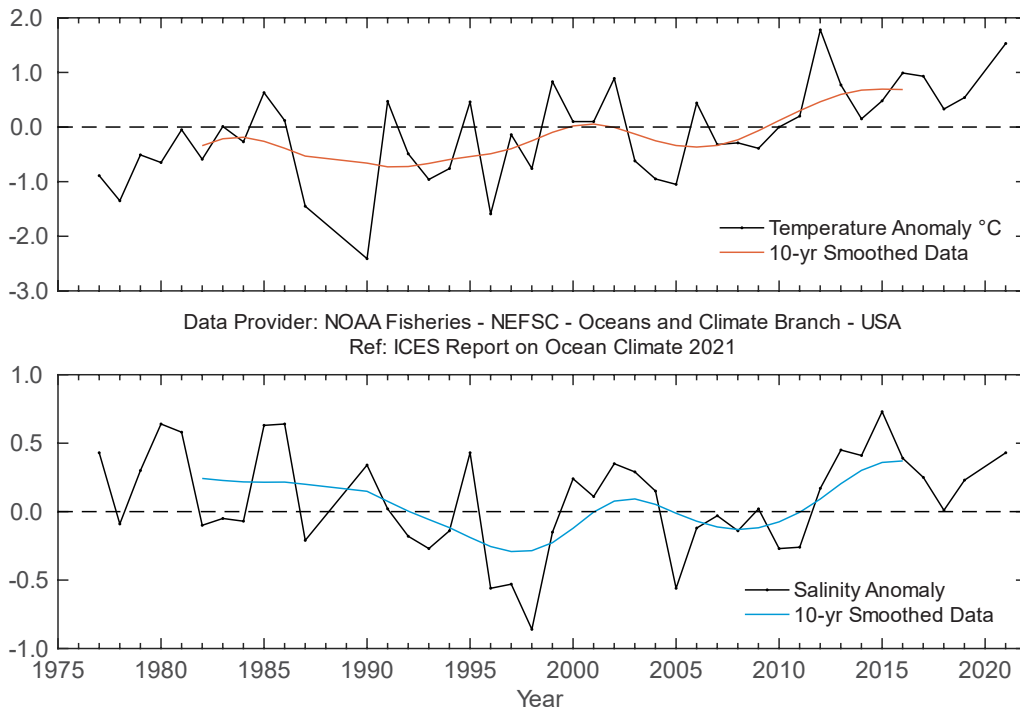


**Figure 4.27. Northeast US continental shelf. Time-series plots of 0–30 m averaged temperature anomaly (upper panel) and salinity anomaly (lower panel) in the region between Hudson Canyon and Cape Cod, Massachusetts. Anomalies are calculated relative to 1991–2020 using hydrographic data from shelf-wide surveys.**

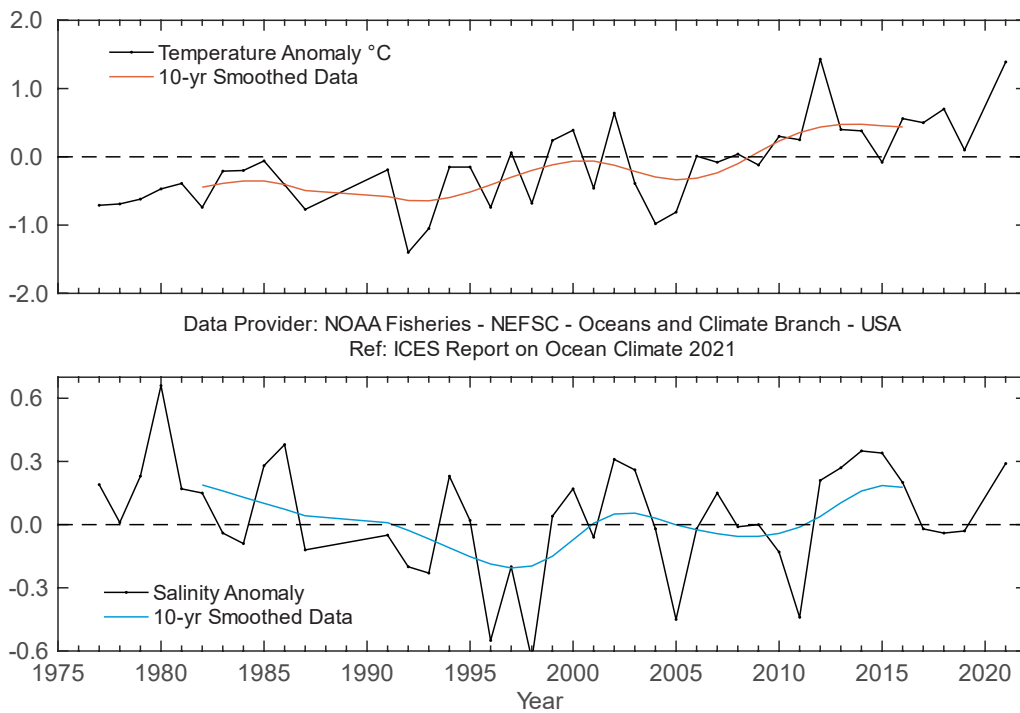


**Figure 4.28. Northeast US continental shelf. Time-series plots of 0–30 m averaged temperature anomaly (upper panel) and salinity anomaly (lower panel) in the western Gulf of Maine. Anomalies are calculated relative to 1991–2020 using hydrographic data from shelf-wide surveys.**

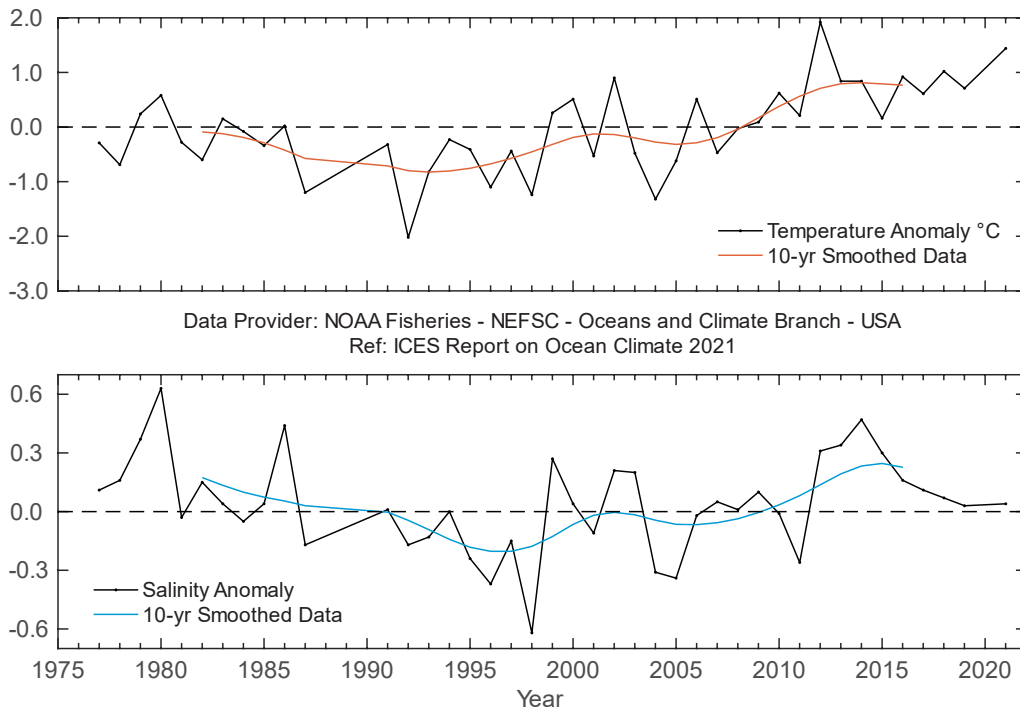


**Figure 4.29. Northeast US continental shelf. Time-series plots of 0–30 m averaged temperature anomaly (upper panel) and salinity anomaly (lower panel) in the eastern Gulf of Maine. Anomalies are calculated relative to 1991–2020 using hydrographic data from shelf-wide surveys.**

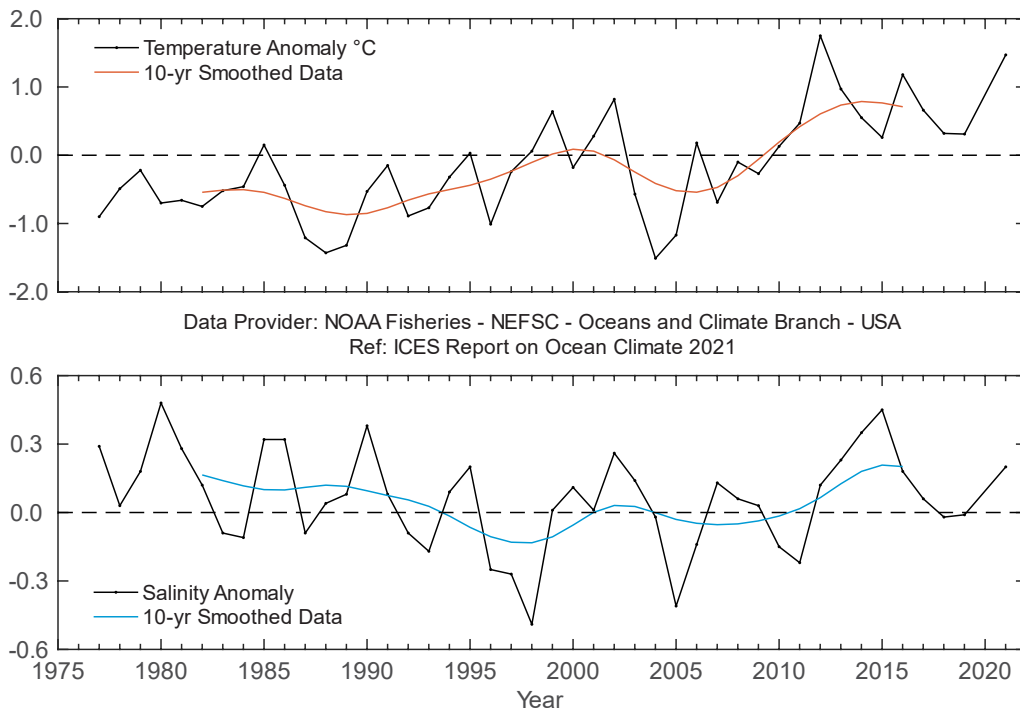


**Figure 4.30. Northeast US continental shelf. Time-series plots of 0–30 m averaged temperature anomaly (upper panel) and salinity anomaly (lower panel) on George Bank. Anomalies are calculated relative to 1991–2020 using hydrographic data from shelf-wide surveys.**

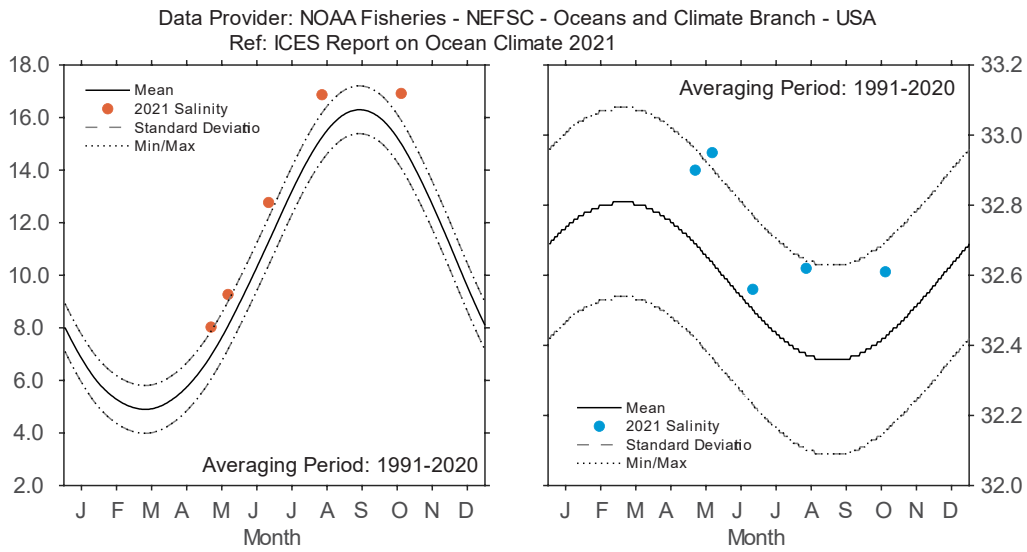


**Figure 4.31.** Northeast US continental shelf. 2021 temperature (left panel) and salinity (right panel) averaged over 0–30 m at northwest Georges Bank, relative to the annual cycle calculated for 1991–2020. The envelope corresponding to the monthly range and 1 s.d. are shown.

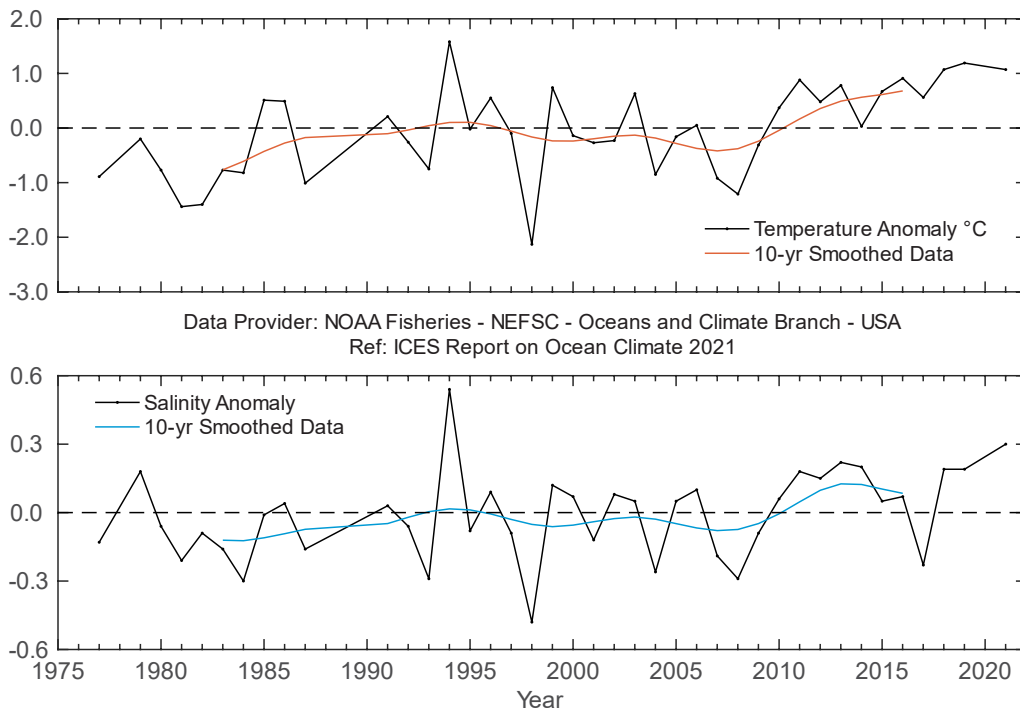


**Figure 4.32.** Northeast US continental shelf. Time-series plots of 150–200 m averaged temperature anomaly (upper panel) and salinity anomaly (lower panel) in the Northeast Channel. Anomalies are calculated relative to 1991–2020 using hydrographic data from shelf-wide surveys.

## 4.7 Icelandic waters

*S. R. Ólafsdóttir and M. Danielsen*

The Icelandic Shelf and surrounding waters are an LME and an ICES ecoregion. In Icelandic waters, mixing of different water masses occurs through convergence at the Greenland–Scotland Ridge and north of Iceland. This mixing process results in a high natural variability in ocean conditions in this area (Figure 4.33). The warm Irminger Current (6–8°C), a branch of the NAC, flows from the south, and the cold East Greenland and East Icelandic currents (–1°C to 2°C) flow from the north. The Greenland–Scotland ridge is a barrier for the exchange of waters between the Nordic Seas and the subpolar North Atlantic.

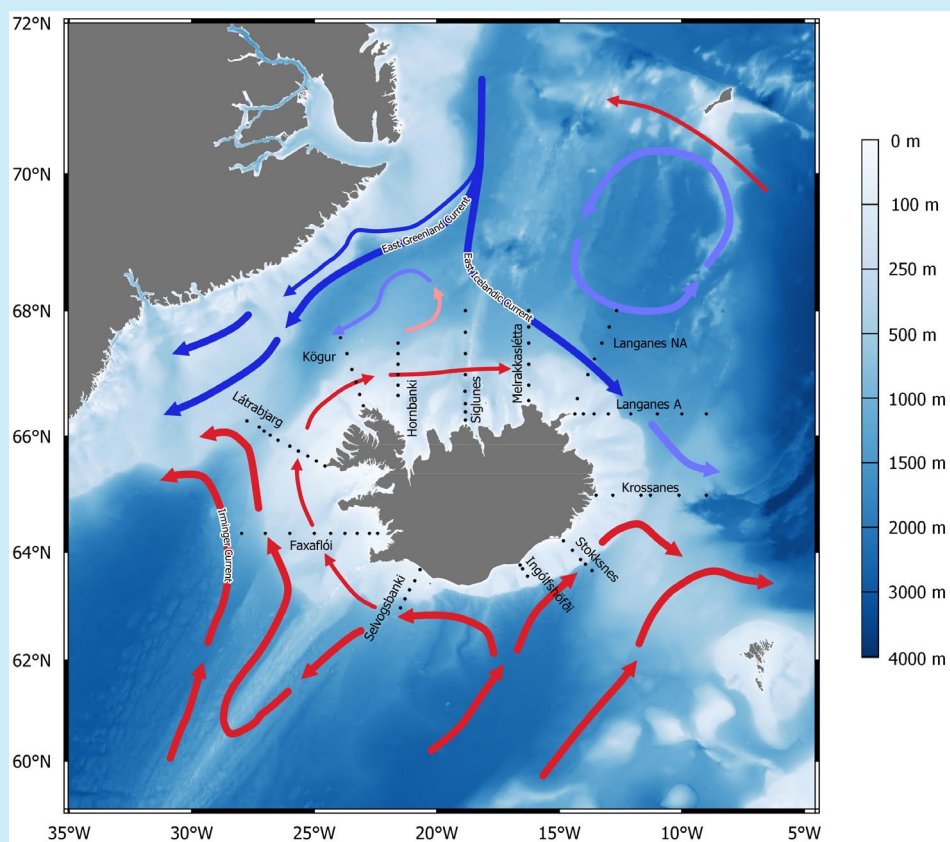


Figure 4.33. Main surface currents and locations of standard sections in Icelandic waters.

Mean annual air temperature in 2021 continued to be slightly above average in southern Iceland (0.3°C; Reykjavik) and above average in northern Iceland (0.4°C; Akureyri; Figure 4.34). The AW temperature south of Iceland in spring was close to the long-term average, as it was the year before (Figure 4.36). Salinity increased by 0.03 between years, but was still below average, as it has been since 2016. On the north Icelandic Shelf, temperature was at the long-term average in spring, but salinity decreased by 0.13 and was below the long-term average. (Figure 4.35). In the surface layer northeast of Iceland in the East Icelandic Current, both temperature and salinity were close to the long-term averages (Figure 4.37).

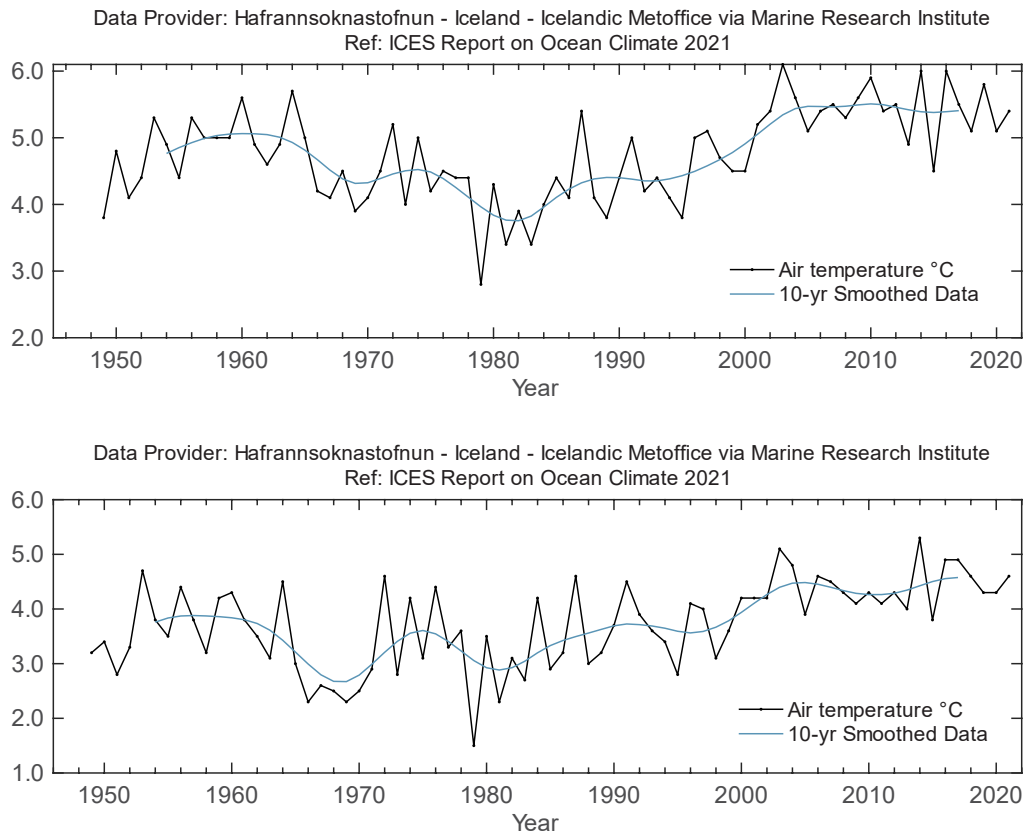


Figure 4.34. Icelandic waters. Mean annual air temperature at Reykjavik (upper panel) and Akureyri (lower panel).

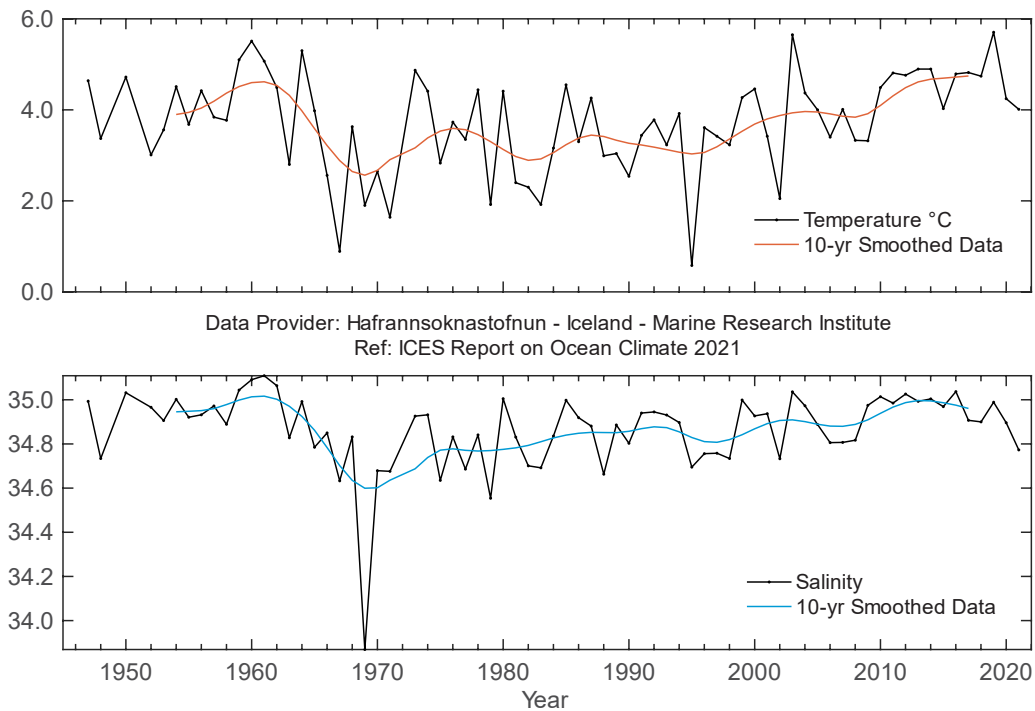


Figure 4.35. Icelandic waters. Temperature (upper panel) and salinity (lower panel) at 50–150 m at Siglunes Stations 2–4 in north Icelandic waters.

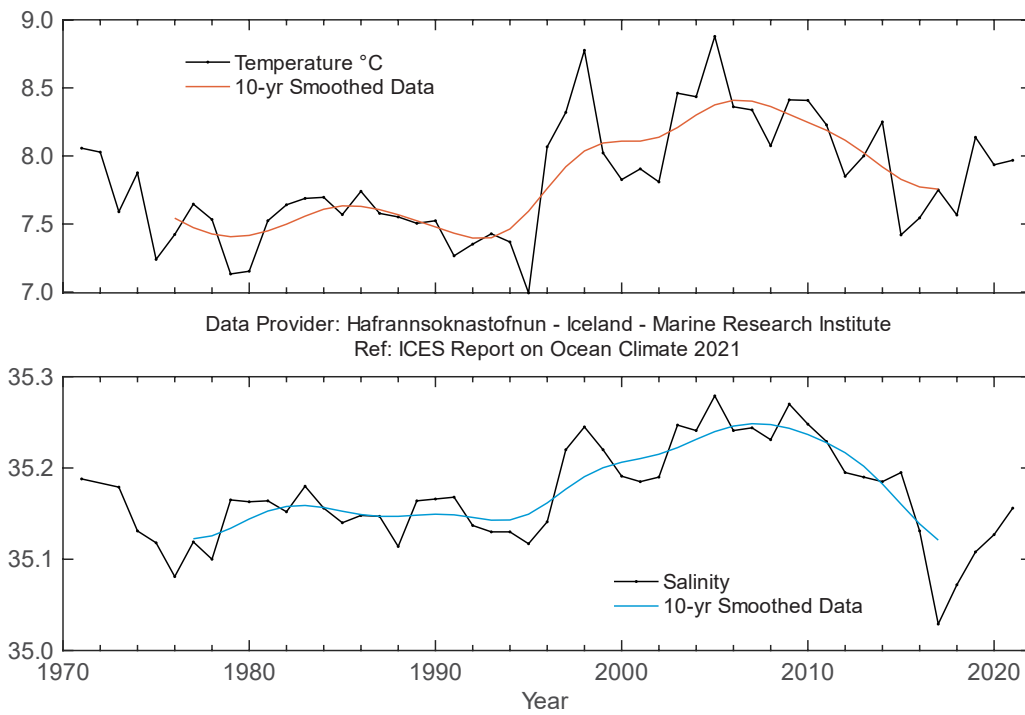


Figure 4.36. Icelandic waters. Temperature (upper panel) and salinity (lower panel) at 0–200 m at Selvogsbanki Station 5 in south Icelandic waters.

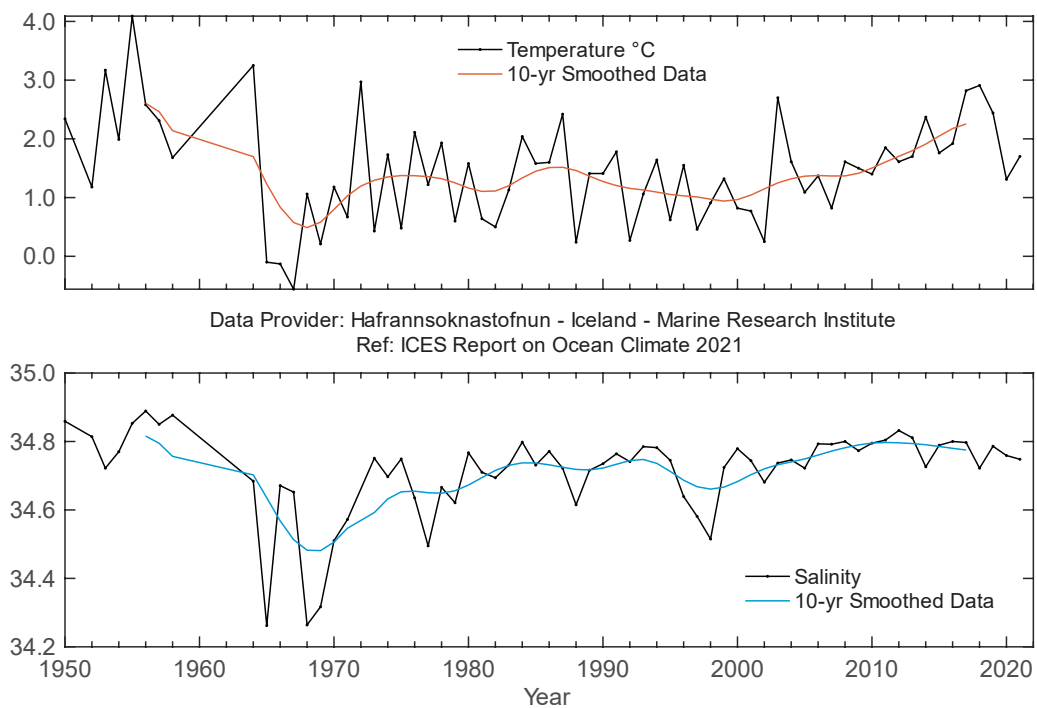


Figure 4.37. Icelandic waters. Temperature (upper panel) and salinity (lower panel) at 0–50 m in the East Icelandic Current (Langanes Stations 2–6).

## 4.8 Bay of Biscay and Iberian coast

*A. Fontán and C. González-Pola*

**SALINITY IN THE UPPER 500 M WAS THE LOWEST OBSERVED IN THE LAST THREE DECADES. THIS SUBSTANTIAL FRESHENING WAS ACCOMPANIED BY BELOW-AVERAGE TEMPERATURES FOR THE UPPER 700 M.**

The western Iberian coast is located at the northeast edge of the Subtropical anticyclonic Gyre, sometimes referred to as the intergyre region. It is characterized by weak upper ocean circulation with mean southward flow of a few  $\text{cm s}^{-1}$  (e.g. Paillet and Mercier, 1997). The Bay of Biscay is considered an adjacent sea with weak anticyclonic circulation (Pingree, 1993; van Aken, 2002). The area also encompasses the northern tip of the northwest Africa upwelling system. Coastal upwelling events dominate in spring/summer, and a geostrophically balanced poleward flow develops in autumn and winter, known as the Iberian Poleward Current (Pingree and Le Cann, 1990). The regional modal waters that comprise the upper permanent thermocline are known as Eastern North Atlantic Central Waters (ENACW). Below them, Mediterranean Water (MW) spreads north from its source in the Gulf of Cadiz, mostly as a slope current. Further below, LSW can be identified at approximately 1 800 m. Finally, the deep ocean is occupied by a mixture of cold polar waters known as North Atlantic Deep Water (NADW).

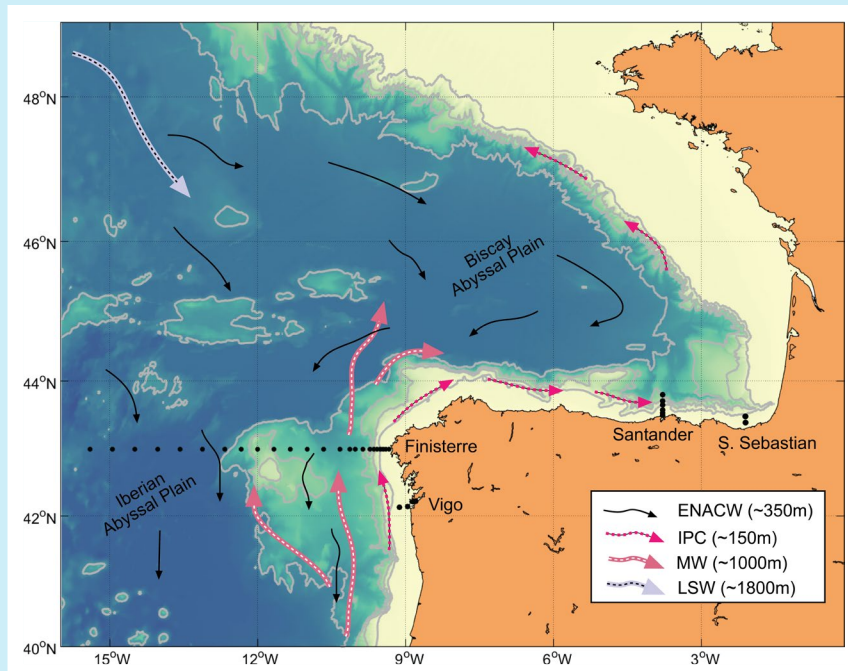


Figure 4.38. Circulation schematic for northwest Iberia and the Bay of Biscay. Black thin arrows show the dominant southward flow in the upper ocean carrying mainly ENACW. The Iberian Poleward Current and the MW pathways are also shown. Black dots show the repeated hydrographic stations, which are either occupied monthly (Vigo, Santander, and San Sebastian) or one or two times a year (Finisterre section).

Air temperature in 2021 was around the long-term average (1991–2020) in the southern Bay of Biscay (Figure 4.39). The seasonal cycle showed a very irregular pattern, combining warmer- and colder-than-normal conditions. 2021 can be considered wet in the southern Bay of Biscay, resulting from very wet conditions in January, February, June, November, and December. The cumulative precipitation in those months constituted more than 65% of the annual total. This pattern was consistent with the seasonal cycle for continental run-off. The annual run-off in 2021 was slightly above the long-term average.

The sea surface temperature was around the long-term average (1991–2020) in San Sebastian (Figure 4.40) and across the Bay of Biscay, corresponding to atmospheric conditions. Upper ocean conditions were the result of such average temperatures and wet conditions, a weak signature of southern-origin waters, and the influence of fresher waters with subpolar origin spreading across the eastern North Atlantic. Unfortunately, the Santander section classically used to track hydrographical changes in the region (figures 4.41 and 4.42) had low occupancy in 2021, so the status is inferred from alternative sources. Subsurface waters influenced by the development of the winter mixed layer (down to 300 m) were very fresh and colder than normal, influenced by the conditions of underlying central waters, described in Section 5.2.6.

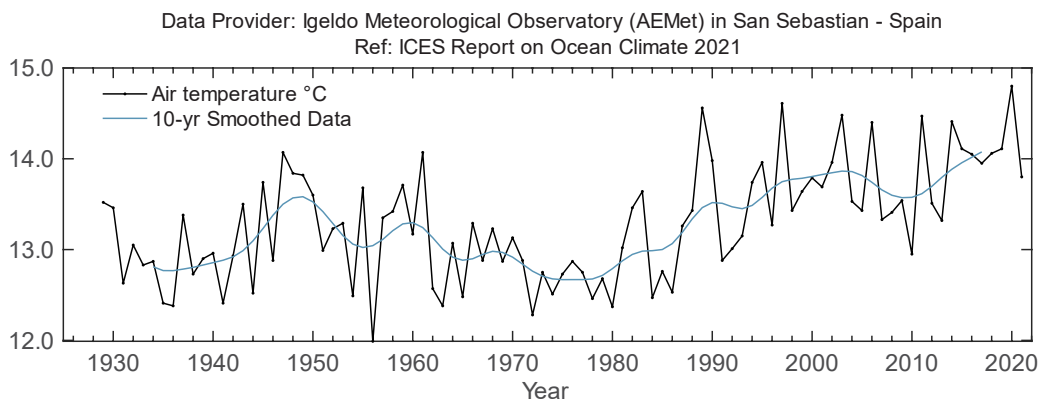


Figure 4.39. Bay of Biscay and eastern Atlantic. Air temperature at San Sebastian (43°18.50'N 002°02.37'W).

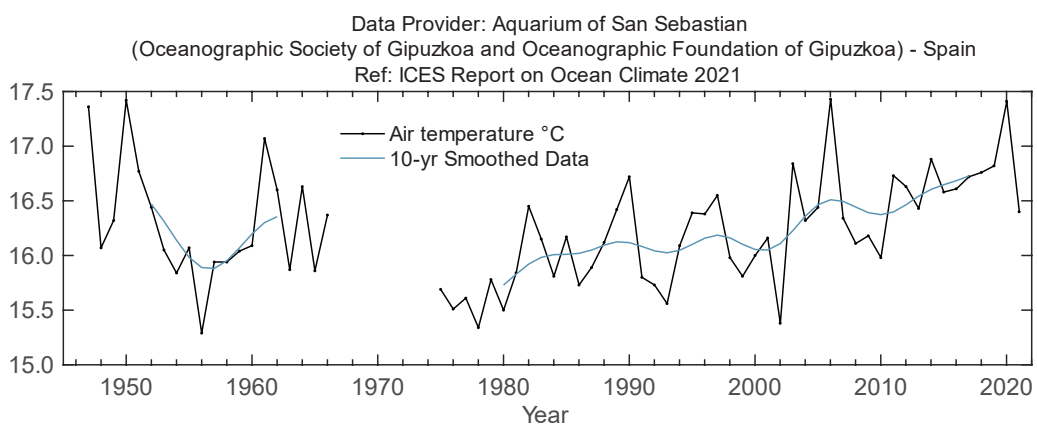
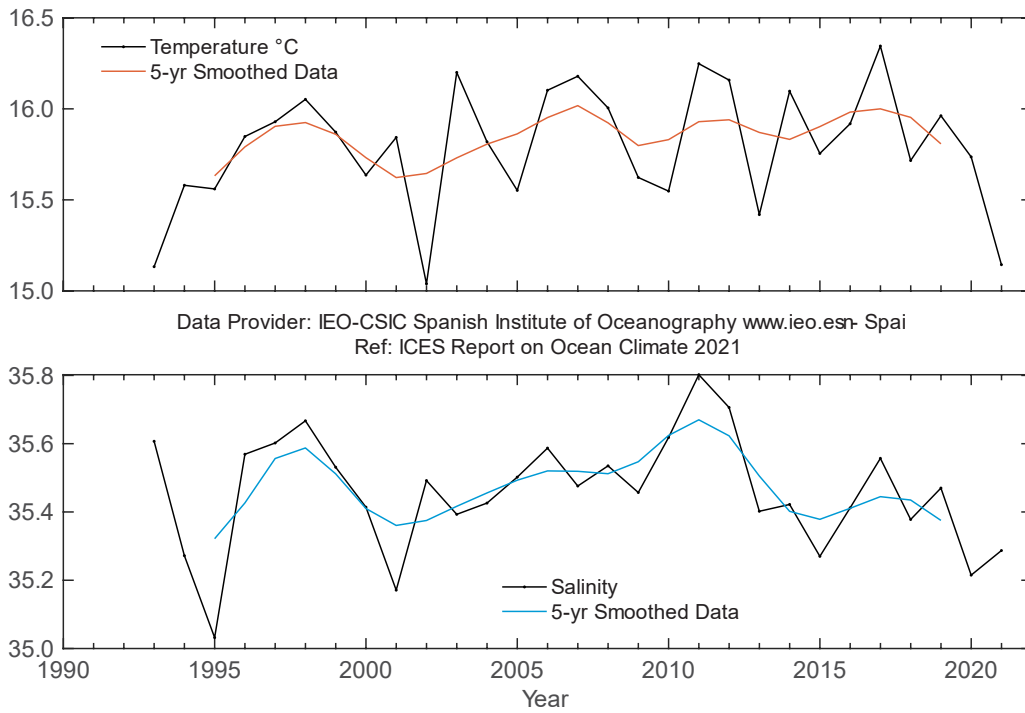
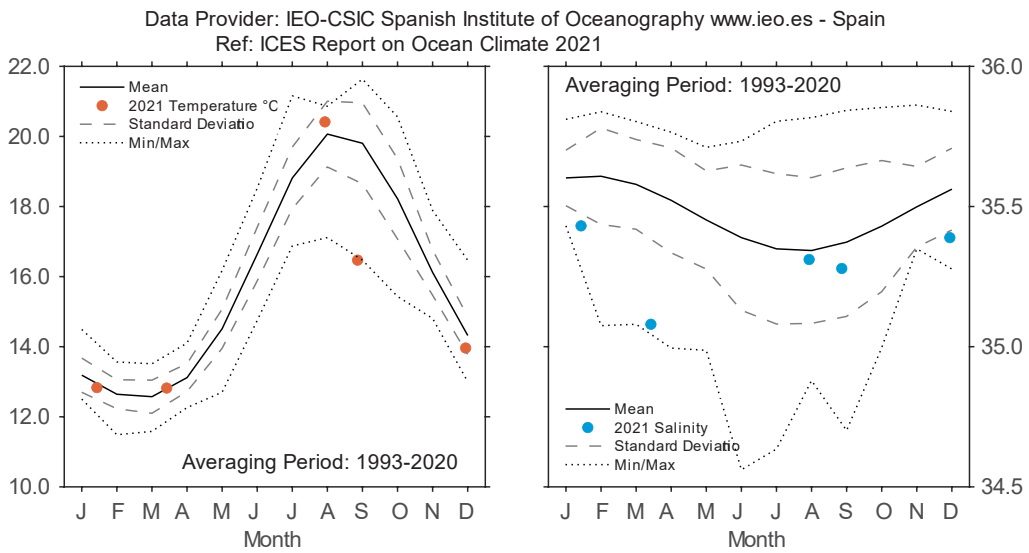


Figure 4.40. Bay of Biscay and eastern Atlantic. Sea surface temperature at San Sebastian (43°18.50'N 002°02.37'W).



**Figure 4.41.** Bay of Biscay and eastern North Atlantic. Temperature (upper panel) and salinity (lower panel) at Santander Station 6, 0–30 m (43°42.50'N 003°47.00'W).



**Figure 4.42.** Bay of Biscay and eastern North Atlantic. 2021 monthly temperature (left panel) and salinity (right panel) at Santander Station 6, 10 m (43°42.50'N 003°47.00'W).

## 4.9 Gulf of Cadiz

*R. Sánchez-Leal*

**ON TOP OF THE STEADY SURFACE WARMING ( $0.20^{\circ}\text{C DECADE}^{-1}$ ), 2021 FEATURED A VERY WARM SPRING AND WINTER AND A COOLER SUMMER, RESULTING IN A FLATTENED ANNUAL THERMAL RANGE WHEN COMPARED TO PREVIOUS YEARS.**

The Gulf of Cadiz is a basin located between the southwest Iberian Peninsula and the northwest African margin. Circulation dynamics are largely governed by water exchange through the Strait of Gibraltar, the ocean gateway between the Atlantic Ocean and the Mediterranean Sea. The exchange features a two-layer inverse estuarine circulation, with dense, saline MW flowing west under the Atlantic inflow (AI) that flows towards the Mediterranean Sea. Dominant features include (i) two Atlantic components that feed the AI: (a) the baroclinic Gulf of Cadiz Current that advects fresh and cool waters from the Portuguese Coastal Transition Zone, and (b) a meridional branch of the Azores Current, a broad barotropic flow that brings warm and saline subtropical AW; (ii) an inshore current system linked with coastal runoff; and (iii) a cyclonic upwelling hotspot generated by tidal stirring over the Trafalgar Banks. Near the slope, the subsurface circulation is dominated by Mediterranean Overflow (MO), a dense gravity current that flows attached to the seabed following the intricate bottom topography. Offshore, the seasonal expansion of the Antarctic Intermediate Water (AAIW) constrains the spread of MO ([Figure 4.43](#)).

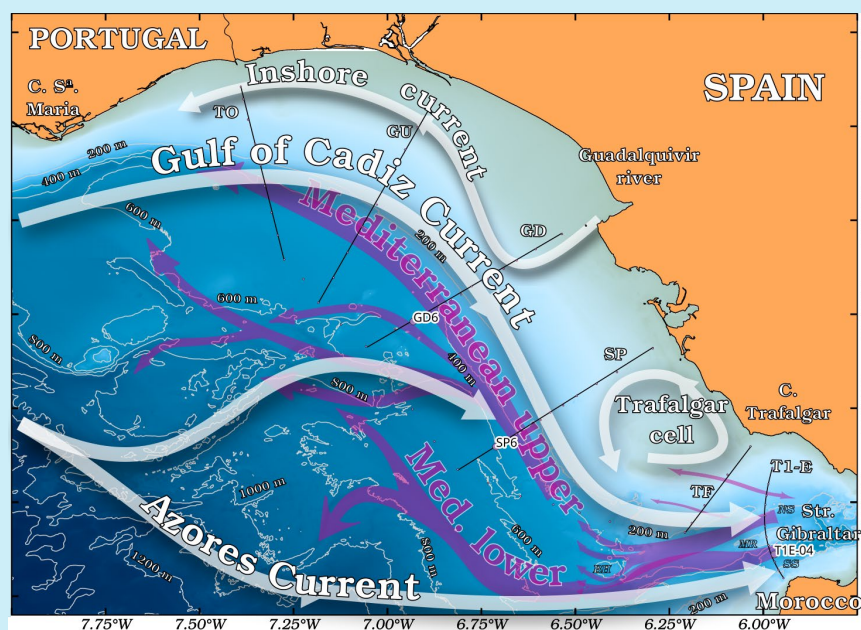


Figure 4.43. Sketch of the main currents in the Gulf of Cadiz. Grey arrows depict the surface circulation. Magenta arrows depict the subsurface circulation. Also included are the STOCA project standard sections (black lines) and fixed oceanographic station under the responsibility of the Spanish Institute of Oceanography, Cadiz, whose data are presented in this report (GD6 and SP6). Puertos del Estado provides data from a weather buoy located at GD6.

The instrumental record in the Gulf of Cadiz suggests a statistically significant warming trend (about  $0.21^{\circ}\text{C decade}^{-1}$ ) of air and ocean SST over the last two decades (data provided from Puertos del Estado, Spain <sup>6</sup>, not shown). The smoothed time-series indicate interannual variability, with colder-than-average SST in 2009, 2013, and 2018/2019. Warmer SST occurred in 2010/2011, 2016/2017, and 2020.

Considering the intra-annual variability, daily SST indicated sustained, very warm conditions from February to May and from October to mid-December. In contrast, colder-than-average conditions were observed from late June to mid-August. This cold period was abruptly interrupted by a two-week heatwave, which raised SSTs by more than  $4.5^{\circ}\text{C}$  in just a few days. From late August through late September, temperatures oscillated around the seasonal average before rebounding from October through mid-December. As a consequence, 2021 was overall slightly cooler than average (about  $-0.20^{\circ}\text{C}$ ), and the annual thermal range was flatter than in previous years.

The monthly time-series for the surface layer (0–20 m) depict the seasonal cycle of temperature and salinity (Figure 4.45) calculated from observations collected at SP6 during 2009–2021. Mean and 95% confidence intervals are derived from the harmonic fit of all available observations during this period. In 2021, both temperature and salinity remained above the seasonal average for most of the year, except for December, when temperature dropped below the seasonal average. Notably, August was anomalously warm, with surface temperatures exceeding  $24^{\circ}\text{C}$ . This measurement was obtained during the STOCA 42 (202108) cruise, which took place following the onset of an intense heatwave. Salinity levels, while generally above the seasonal average, fell within the confidence intervals. The time-series data illustrate that although seasonal variability dominates at the surface, it can be observed at all depth levels of the water column (Figure 4.44). This presents a significant challenge when seeking precise and unbiased calculations of trends and anomalies based only on cruise data.



Sampling work on board the R.V. Celtic Explorer. Credit: Tomasz Szumski.

---

<sup>6</sup>Puertos de Estado. 2023. Ministry of Transport, Mobility and Urban Agenda, Spain. <https://www.puertos.es/es-es/oceanografia/Paginas/portus.aspx>

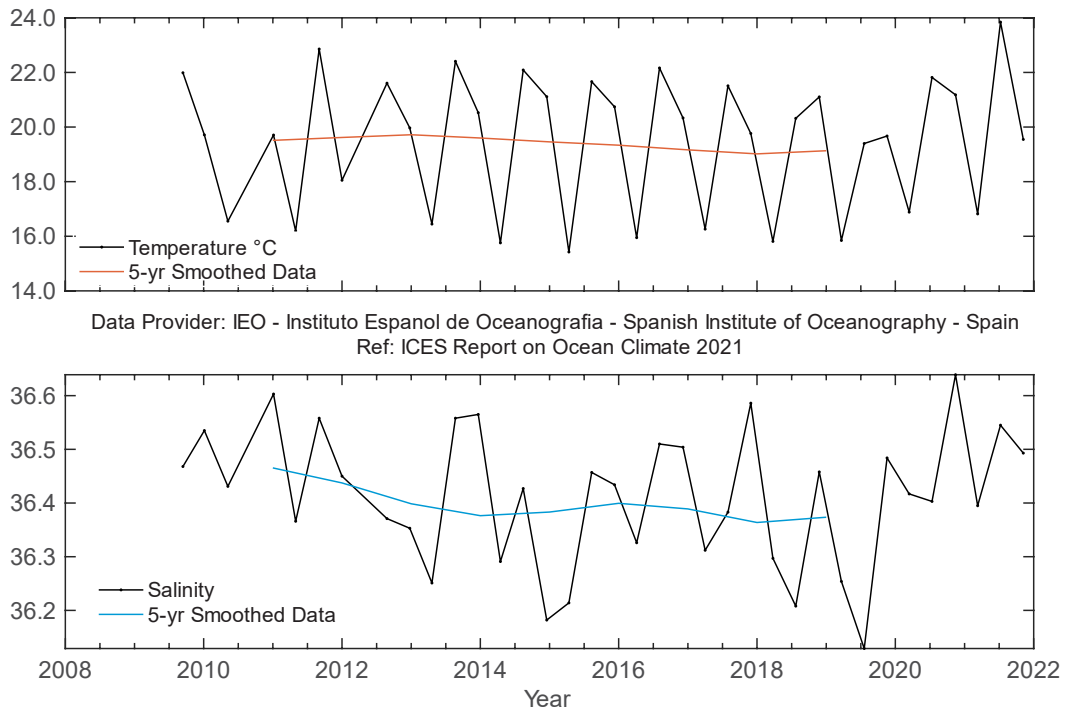


Figure 4.44. Gulf of Cadiz. Potential temperature (upper panel) and salinity (lower panel) for the 0–20 m water column at Station SP6 (36°08.68'N 006°42.76'W) of the STOCA programme.

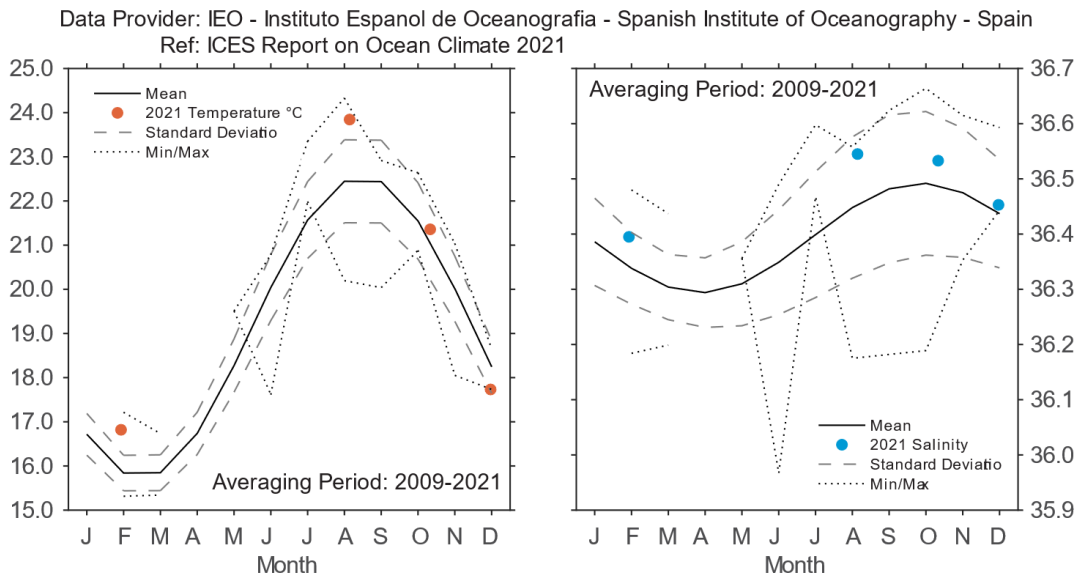


Figure 4.45. Gulf of Cadiz. 2021 monthly temperature (left panel) and salinity (right panel) at STOCASP6 station, 10 m (36°08.68'N006°42.76'W).

## 4.10 Canary Basin

*P. Vélez-Belchí, A. Mosquera, and C. Presas-Navarro*

**2022 CONFIRMS THE END OF THE COOLING AND FRESHENING CYCLE THAT BEGAN IN 2014 FOR THE NACW. HOWEVER, TRENDS OF WARMING AND SALINIFICATION REMAIN LOW, AND CONDITIONS IN THE 200–800 DBAR LAYER ARE SIMILAR TO THOSE OBSERVED AT THE BEGINNING OF THE 2000S. COOLING AND FRESHENING CONTINUES IN THE INTERMEDIATE WATERS (800–1400 DBAR) FOLLOWING THE 2014 MAXIMUM.**

The Canary Basin sits at the boundary between the oceanic waters of the Subtropical Atlantic Gyre and the upwelling waters from the Canary Current Large Marine Ecosystem (CCLME) off the coast of northwest Africa. Since the early 2000s, the Canary Islands archipelago region has been monitored by the Spanish Institute of Oceanography (Tel *et al.*, 2016), specifically for oceanic waters west of Lanzarote (Stations 11–23, [Figure 4.46](#) and the Coastal Transition Zone (CTZ) of the CCLME upwelling region (Stations 1–10, [Figure 4.46](#)).

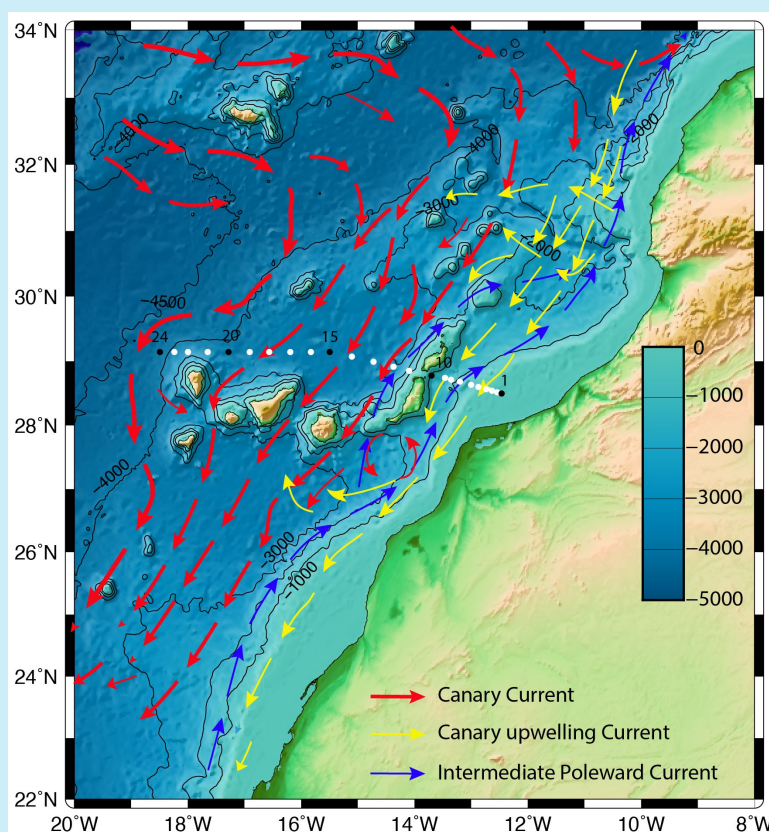


**Figure 4.46.** Circulation schematic for the Canary Basin. Red arrows: southward-flowing Canary Current composed mainly of NACW and intermediate waters. Yellow arrows: the Canary Upwelling Current that flows in the thermocline waters. The white dots show the distribution of the 24 hydrographic stations sampled in the Canary Islands archipelago region since 1997. Stations 5–10 are used to estimate changes in the CTZ and stations west of Lanzarote (11–24) the oceanic waters.

The upper water levels are under the influence of the southward-flowing Canary Current and the Canary Upwelling Current associated with the upwelling front (Figure 4.46). The intermediate water levels are under the influence of the tongue of slowly propagating Mediterranean waters and the slope current known as the Canary Intermediate Poleward Current (Hernández-Guerra *et al.*, 2017; Vélez-Belchí *et al.*, 2017).

The waters above the seasonal thermocline are characterized by scattered temperature and salinity values due to seasonal heating and evaporation. These waters occupy the upper 300 m in the oceanic region and the upper 100 m in the stations under the effect of the coastal upwelling, which are considered surface waters. Below the seasonal thermocline and through the permanent thermocline are the NACW, roughly located between 300 m and 700 m depth. These waters are characterized on the  $\theta/S$  diagram by an approximately straight-line relationship between potential temperature ( $11.4^{\circ}\text{C} < \theta < 14.9^{\circ}\text{C}$ ) and salinity ( $35.6 < S < 36.1$ ). At intermediate levels, roughly between 700 m and 1 200 m, two distinct water masses are found in the Canary Islands region: the fresher ( $S < 35.3$ ) and slightly lighter Antarctic Intermediate Waters (AAIW), and the saltier ( $S > 35.4$ ) and heavier MW.

In the depth stratum that characterizes the NACW waters (200–800 dbar), there has been an overall, non-statistically significant warming of  $0.06 \pm 0.05^{\circ}\text{C decade}^{-1}$  and a weak overall increase in salinity of  $0.002 \pm 0.011^{\circ}\text{C decade}^{-1}$  (Figure 4.47). Between the 1990s and the early 2000s, there was a decrease in temperature and salinity for all upper-layer waters. This trend was followed in the mid-2000s by a marked increase in both temperature and salinity, which peaked in 2014, the warmest and saltiest year on record. A decreasing trend for temperature and salinity was observed between 2014 and 2018, which ended in 2020. There was a small increase in temperature and salinity in 2020/2021, but values are still only slightly higher than those observed in the late 1990s (Vélez-Belchí *et al.*, 2015). The overall increase in temperature and salinity almost compensates in density. Since there are not statistically significant changes in density, it is possible to conclude that the observed trends in temperature and salinity were due to a deepening of the isoneutral surfaces rather than to changes along the isoneutral surfaces. For the same depth stratum, the overall increase in temperature for NACW waters was also observed in the CTZ, although with slightly smaller values ( $0.06 \pm 0.13^{\circ}\text{C decade}^{-1}$ ), but no trend was observed in salinity ( $0.000 \pm 0.020^{\circ}\text{C decade}^{-1}$ ) due to the influence of upwelling (data not shown). The variability and uncertainty in trend estimates is higher in the CTZ due to the proximity of the upwelling region and the frequent intrusions of upwelling filaments.

The surface waters (25–150 dbar) in the CTZ show a long-term, non-statistically significant cooling of  $-0.13 \pm 0.42^{\circ}\text{C decade}^{-1}$  and a non-statistically significant decrease in salinity of  $-0.048 \pm 0.054^{\circ}\text{C decade}^{-1}$ , both consistent with an increase in upwelling in the CCLME. However, this trend is weaker in 1997-2022 than in shorter periods. Upwelling of the CCLME continued to strengthen, with 2015 as the coolest and freshest year on record for the upwelling-influenced surface waters. SST satellite observations corroborate the changes in the upwelling regime inferred from *in situ* observations, with different areas showing increased upwelling. However, the magnitude of the observed trend in the satellite SST is different, because the satellite only observes a very thin surface layer of the ocean.

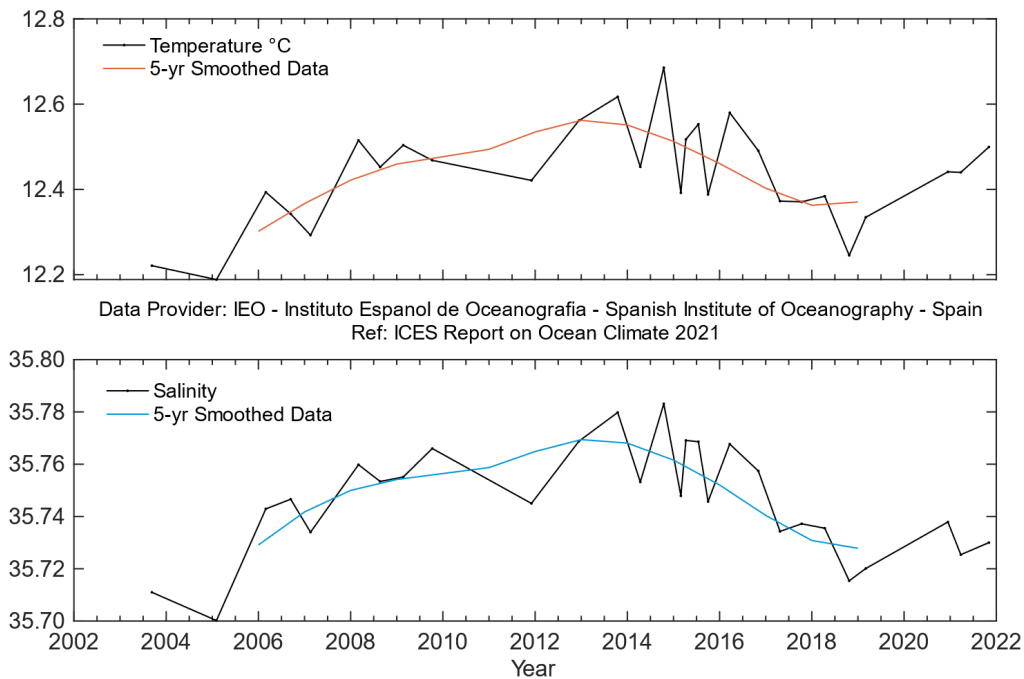


Figure 4.47. Canary Basin. Potential temperature (upper panel) and salinity (lower panel) for the 200–800 m layer in the oceanic waters .

## 4.11 Southwest Approaches

*T. Smyth*

The datasets presented here are from the western end of the English Channel and the boundary of the Celtic Sea and the Bay of Biscay ecoregions. The area is commonly referred to as the Southwest Approaches, which relates to the passage of shipping through the English Channel. As these data come from a boundary between different ecoregions, this term has also been adopted here, as it relates to the region forming a pathway for AW to enter the southern North Sea.

Station E1 (50.03°N 4.37°W) is situated on the southern UK coast in the western English Channel. The water depth is 75 m, and the station is tidally influenced by a 1.1-knot maximum surface stream at mean spring tide. The seabed is mainly sand, resulting in a low bottom stress ( $1\text{--}2 \text{ ergs cm}^{-2} \text{ s}^{-1}$ ). The station may be described as oceanic with the development of a seasonal thermocline. Stratification typically starts in early April, persists throughout summer, and is eroded by the end of October. The typical depth of the summer thermocline is around 20 m. The station is greatly affected by ambient weather.

Measurements have been taken at this station since the end of the 19th century, with data currently available since 1903 (Figure 4.48). The series is unbroken, apart from gaps for the two world wars and a hiatus in funding between 1985 and 2002. The data takes the form of vertical profiles of temperature and salinity. Early measurements were taken with reversing mercury-in-glass thermometers and discrete salinity bottles. More recently, electronic equipment (Seabird CTD) has been utilized. The time-series demonstrates considerable interannual variability in temperature.

E1 was sampled on 16 occasions during 2021: approximately fortnightly in summer and monthly in winter. At the surface, E1 started 2021 with slightly above-average temperatures and only reached a minimum temperature of 9.4°C in February (Figure 4.49). In spring and early summer, temperatures were around the long-term mean at the surface, although there was a notable cold period in late May when surface temperatures decreased to 11.1°C. During July, a short summer heatwave manifested as temperatures in excess of 19°C. At 50 m, temperatures were above average for the first half of the year, and around average for the summer months until the breakdown in stratification vented warmer temperatures throughout the water column. This was similar to the pattern observed during 2020. Autumn and early winter temperatures were slightly above the long-term mean.

For almost the entire duration of 2021, salinity was below the long-term mean throughout the water column, particularly during spring/summer, with salinities  $\approx 0.2$  below the long-term mean (Figure 4.49).

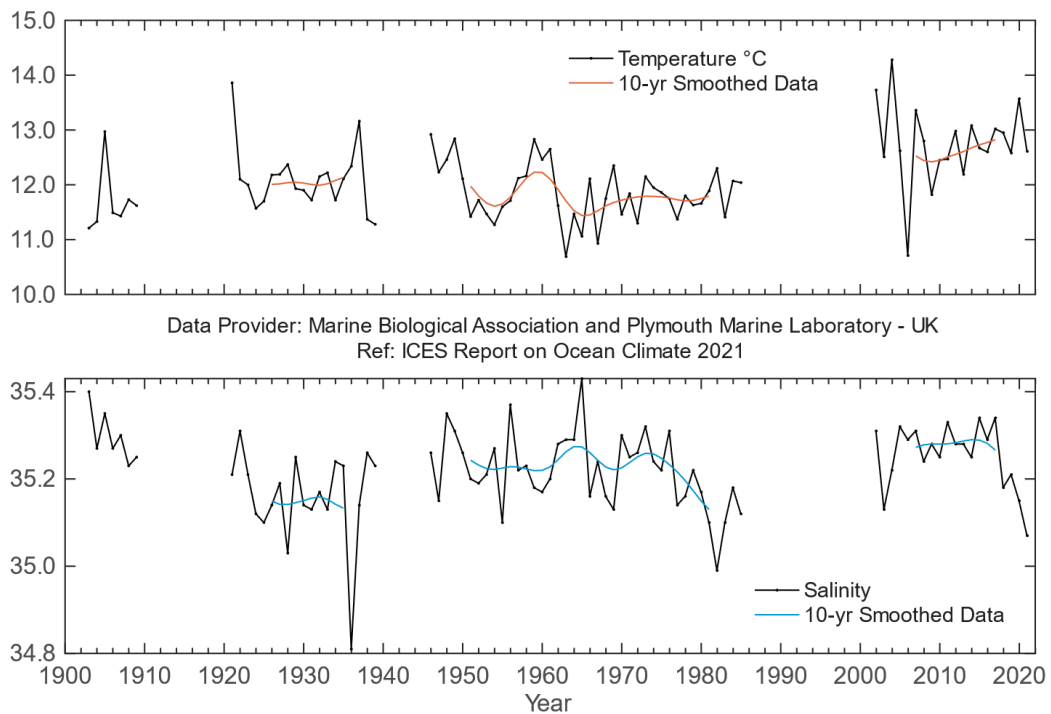
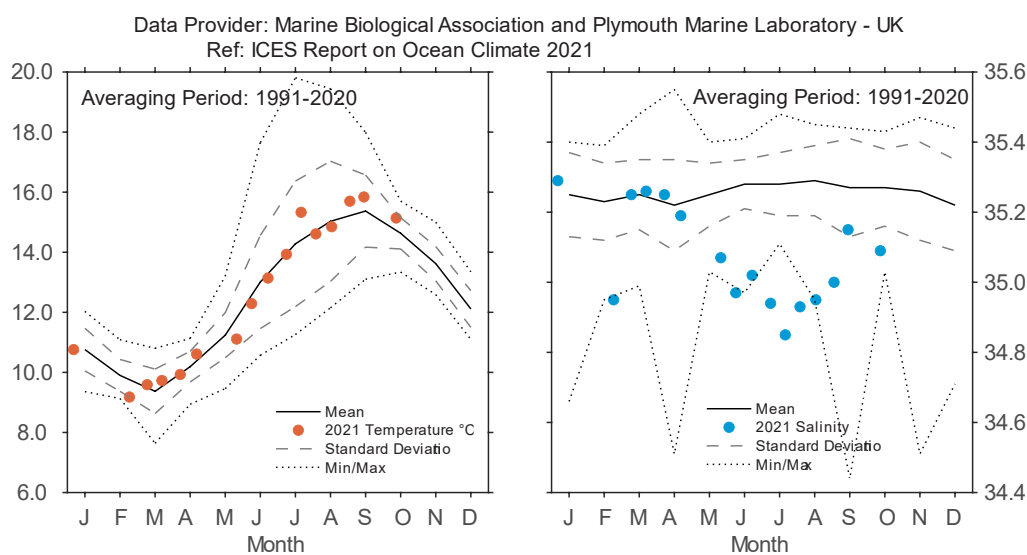


Figure 4.48. Southwest Approaches. Temperature (upper panel) and salinity (lower panel) anomalies of surface water (0–40 m) at Station E1 in the western English Channel (50.03°N 4.37°W).





**Figure 4.49. Southwest Approaches. Monthly average seasonal cycle with 2021 temperature (left panel) and salinity (right panel) observations of surface water (0–40 m) at Station E1 in the western English Channel (50.03°N 4.37°W).**

## 4.12 Celtic Seas

*K. Lyons, C. Cusack, E. Daly, and B. Hunter*

The Celtic Seas is defined as an ICES ecoregion and is included in NOAA LME 24 (Celtic-Biscay Shelf). The Celtic Seas region contains the shelf seas of northwestern Europe and part of the Rockall Trough. The shelf seas are mainly relatively shallow (< 100 m). The structure of the water column on the shelf is primarily driven by (i) vertical mixing due to tides and wind, and (ii) the seasonal variation in solar heating, leading to seasonal (summer) density-driven currents (e.g. Irish Coastal Current). In addition to the influence of coastal waters on the shelf, the area is strongly influenced by the poleward transport of AW, as well as the continental slope current that brings waters north from the Bay of Biscay region.

The Malin Head coastal station (the most northerly point of Ireland), where SST measurements are taken, is inshore of coastal currents and influenced by run-off. The measurement methodology has changed over the years, from the hand-held thermometers used initially to the current high-precision SBE39 temperature sensor (in use since 2008). An offshore data buoy that collects hourly temperature data is maintained off the southwest coast of Ireland (51.22°N 010.55°W) since mid-2002. From the mid-1990s until recently, a strong increasing trend in SST was observed at the Malin Head coastal station, which has since levelled out. The mean annual SST of 11.10°C recorded at Malin Head in 2021 was 0.70°C above the 1991–2020 normalized mean (Figure 4.51). Malin Head monthly mean temperatures for 2021 were all close to the long-term mean (Figure 4.50). For the M3 buoy SST time-series, the annual mean in 2021 of 13.00°C was 0.23°C below the 2003–2020 normalized mean (Figure 4.50). Monthly mean temperatures at this site in 2021 were all close to the long-term mean (Figure 4.50).

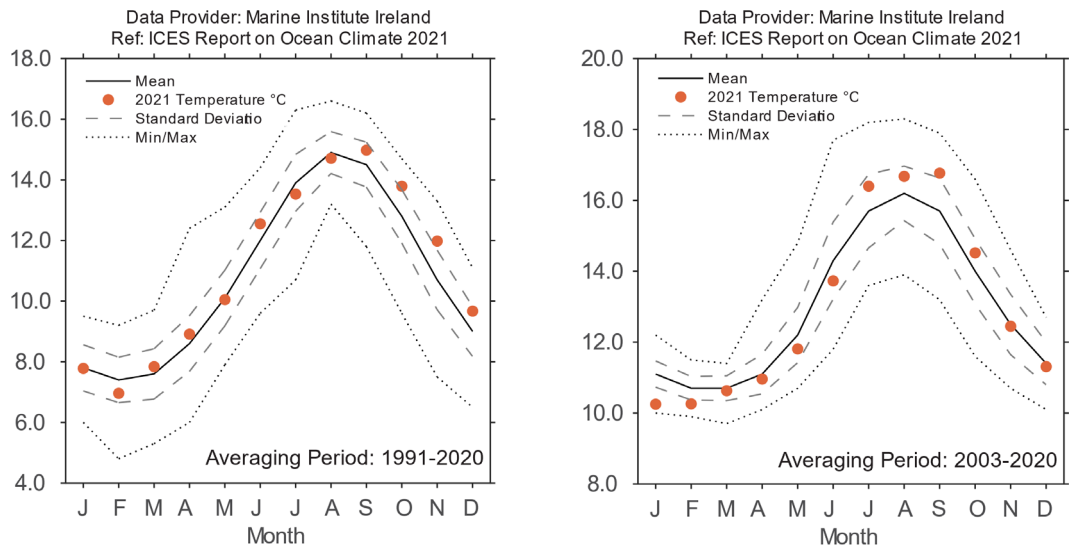


Figure 4.50. Celtic Seas. Monthly average seasonal cycle with 2021 monthly temperature at Malin Head (left panel) and the M3 Weather Buoy southwest of Ireland (right panel; 51.22°N 10.55°W).

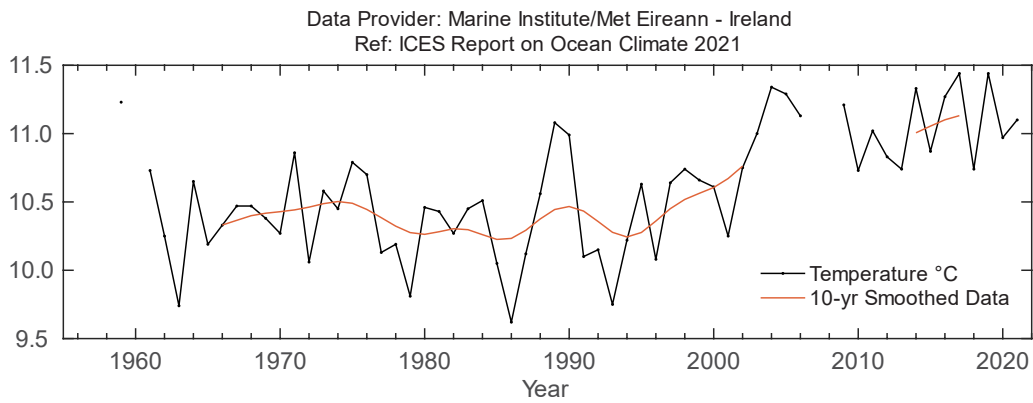
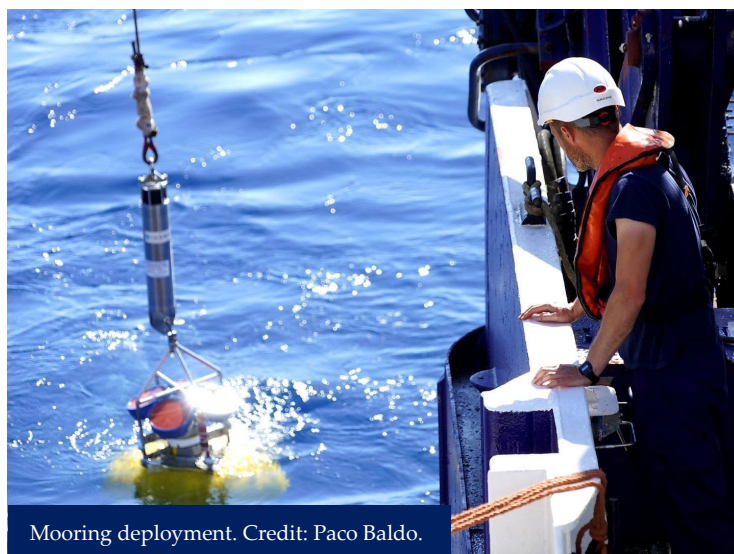


Figure 4.51. Celtic Seas. Temperature at the Malin Head coastal station (55.39°N 7.38°W).



### 4.13 Rockall Trough

*S. Jones*

**FRESH AND NEAR-AVERAGE TEMPERATURE CONDITIONS IN THE ROCKALL TROUGH UPPER OCEAN IN 2021, WITH SALINITY BELOW THE LONG-TERM AVERAGE.**

Rockall Trough is a deep ocean basin situated west of UK and Ireland, within the Celtic Seas and oceanic Northeast Atlantic ecoregions. It has significantly different oceanographic characteristics than the shallower shelf sea areas. Rockall Trough is separated from the Iceland Basin by the Hatton and Rockall banks, and from the Norwegian Sea by the shallow (500 m) Wyville–Thomson Ridge. It is a route for warm North Atlantic upper water to reach the Norwegian Sea, where it is converted into cold, dense overflow water as part of the thermohaline overturning in the North Atlantic. The upper water column is characterized by poleward-moving eastern North Atlantic Water, which is warmer and more saline than the Iceland Basin waters that also contribute to the Norwegian Sea inflow (Figure 4.52).

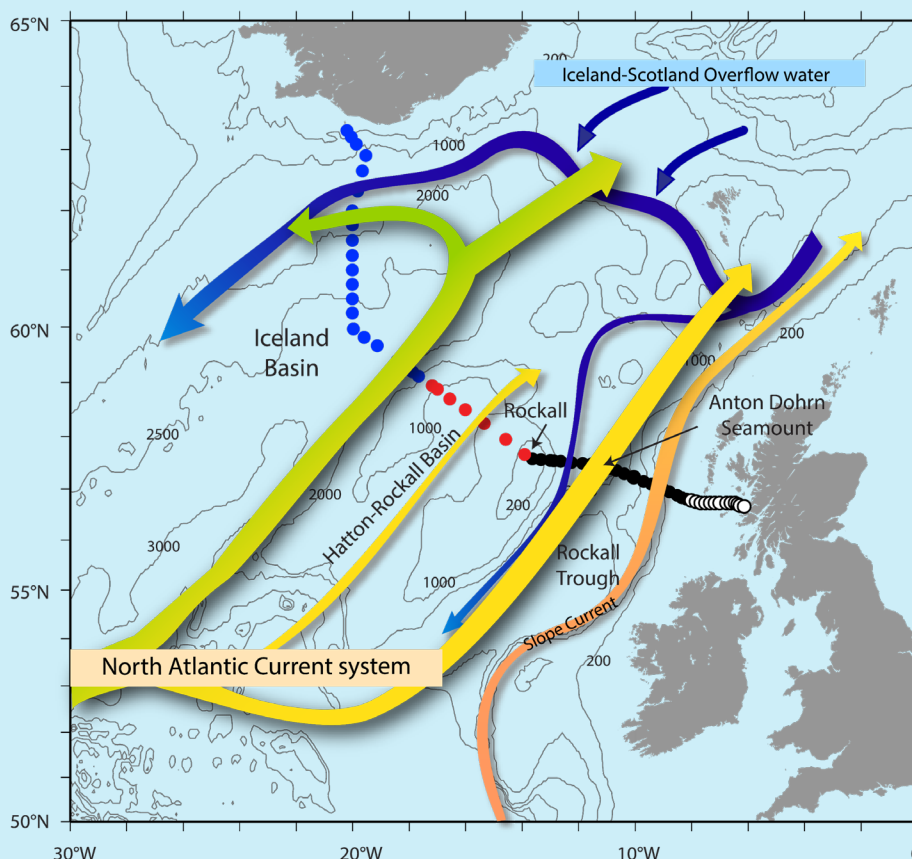


**Figure 4.52. Circulation schematic for the Rockall Trough, Hatton–Rockall Basin, and Iceland Basin. Green, yellow, and orange colours indicate the upper waters of the NAC and the slope current. Dark blue arrows show the approximate locations of the main overflow currents.**

The potential temperature of the upper 800 m remained close to the 1991–2020 mean in 2021 (Figure 4.53). The upper ocean had been cooling relative to a peak of 9.8°C in 2007, but this cooling appears to have halted or slightly reversed since 2019. The salinity of the upper 800 m decreased since the end of the 2000s, with a sharp freshening to a near-record minimum in 2017. In 2019 and 2020, upper ocean salinity increased slightly from this deep minimum, but remained below the 1991–2020 mean. The Ellett Line CTD transect was not occupied between 2019 and 2021, but equivalent data points in the time-series were generated using Argo profiles from within the basin, supported by moorings deployed by the OSNAP project for that year.

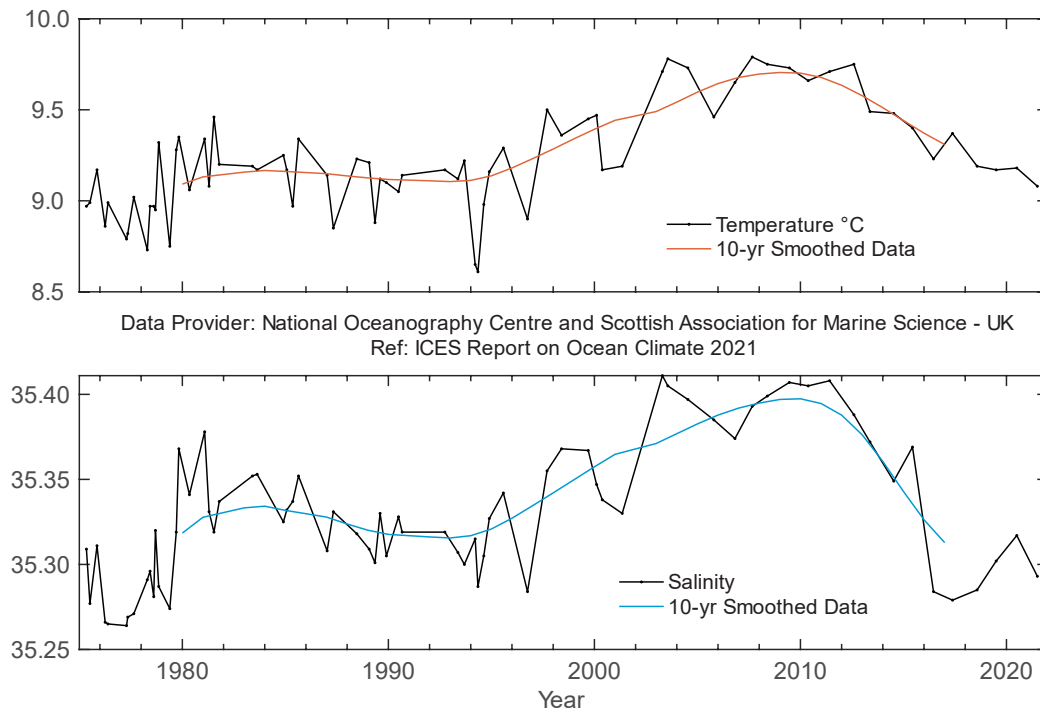


Figure 4.53. Rockall Trough. Temperature (upper panel) and salinity (lower panel) for the upper ocean (potential density 27.2–27.50 kg m<sup>-3</sup>, representing the top 800 m, but excluding the seasonally warmed surface layer).

#### 4.14 Hatton–Rockall Basin

*S. Jones*

The shallow Hatton–Rockall Basin (1 000 m) lies between the Iceland Basin to the west and Rockall Trough to the east and is bounded by the Hatton and Rockall banks. The basin is filled with well-mixed subpolar-mode water moving northward as part of the NAC complex. Winter mixing reaches 800–1 000 m. Temperature and salinity vary considerably depending on the type of NAC water that enters the basin. The region is in the transition zone between cold, fresh, central Subpolar Water and warm, saline, eastern Subpolar Water.

The range in basin mean temperature and salinity in the upper 1 000 m is more than 1°C and 0.1, respectively, higher than in the Iceland Basin to the west and Rockall Trough to the east. This high variability may be due to seasonal-to-decadal changes in the structure and location of the NAC system as it crosses the Hatton–Rockall Basin (Houpert *et al.*, 2020). The lowest temperature and salinity values were seen at the start of the time-series in 1996, followed by a steady rise to maximum values in the late 2000s (Figure 4.54). After 2010, there was a decrease in temperature and salinity, which is consistent with observations from neighbouring basins. Since 2018, salinity has increased substantially, but, as of 2021, it is still lower than the 1991–2020 average. The temperature in 2021 was close to the long-term mean.

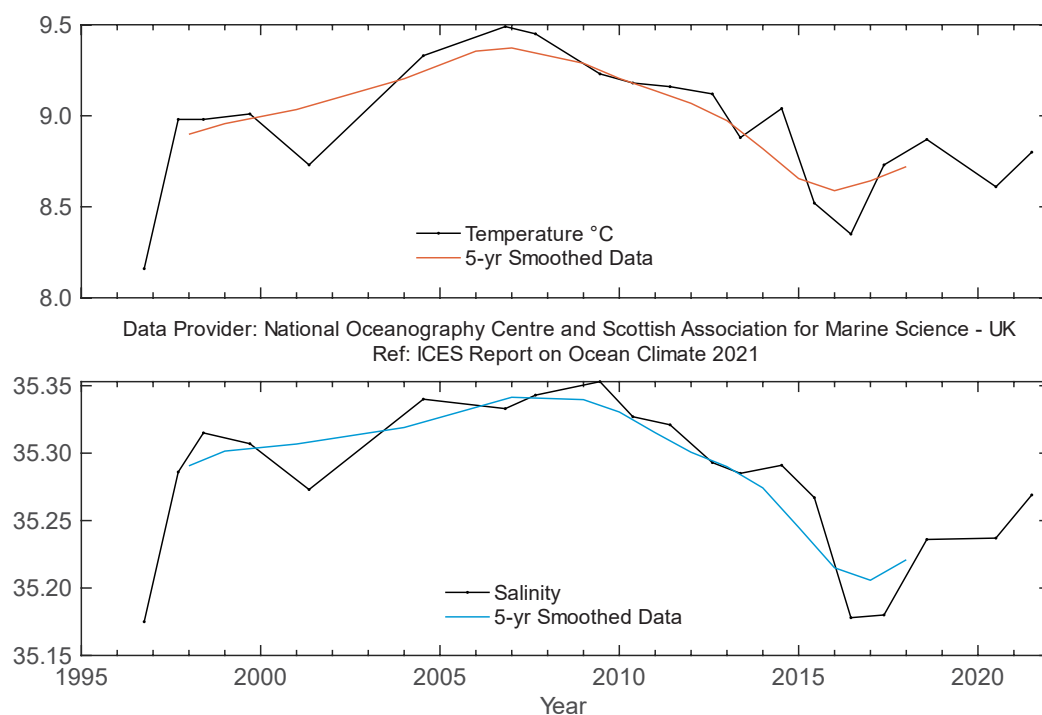


Figure 4.54. Hatton–Rockall Basin. Temperature (upper panel) and salinity (lower panel) for the upper ocean (potential density 27.20–27.50 kg m<sup>-3</sup>, representing the top 600 m and excluding the seasonally warmed surface layer).



## 4.15 Iceland Basin

*S. Jones*

### SALINITY RETURNS TO NEAR-MEAN VALUES IN THE ICELAND BASIN UPPER OCEAN AFTER A PERIOD OF RECORD LOWS.

A major part of the NAC flows into the Iceland Basin, adjacent to the shallow Hatton Bank on the southeast side of the basin ([Figure 4.52](#)). The NAC typically consists of one or two fronts located between warmer, more saline water in the east and colder, fresher water to the north and west. The region is rich in eddy activity, and the water properties are quite variable in time and space. Most of the water entering the Iceland Basin from the south flows through into the Norwegian Sea over the Iceland–Scotland Ridge. A smaller fraction of the NAC water recirculates south of Iceland in the boundary currents of the main anticlockwise circulation of the Subpolar Gyre.

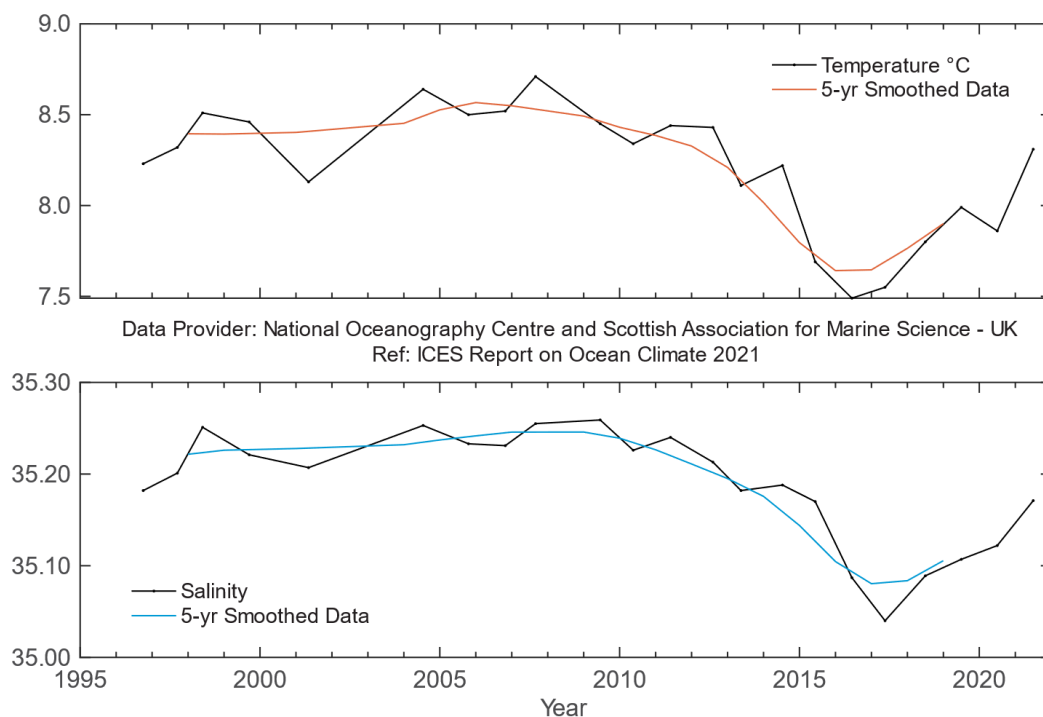


**Figure 4.55. Iceland Basin. Temperature (upper panel) and salinity (lower panel) for the upper ocean (potential density 27.20–27.50 kg m<sup>-3</sup>, representing the top 500 m and excluding the seasonally warmed surface layer).**

Temperature and salinity of the upper ocean (ca. upper 500–600 m) vary from year to year, but also exhibit multiyear changes. From 1996 to the late 2000s, both temperature and salinity increased, followed by a sharp decrease ([Figure 4.55](#)). By 2017, temperature and salinity were the lowest recorded since 1996. The freshening after 2010 implies that the basin was receiving more water originating in the west and central subpolar region and less warm, saline water from the eastern intergyre regions. Superimposed on that multiyear trend was a rapid cooling

observed between 2014 and 2015, caused by a high flux of heat from the ocean to the atmosphere (Duchez *et al.*, 2016) and a rapid freshening in 2015–2017 (Holliday *et al.*, 2020). In recent years, temperatures and salinity have largely recovered from these deep minima. In 2021, upper ocean temperatures were slightly above the 1991–2020 mean, while salinity remained slightly below average. The Ellett Line transect was not occupied from 2018 onwards, but equivalent data points in the time-series were generated using Argo profiles from within the basin for those years.

## 4.16 Irminger Sea

*M. F. de Jong*

The Irminger Sea is the ocean basin between South Greenland, the Reykjanes Ridge, and Iceland. This area forms part of the North Atlantic Subpolar cyclonic Gyre. Due to this gyre, the exchange of water between the Irminger and the Labrador seas proceeds relatively fast. In the bottom layers of the Irminger Sea, cold water originating in the (sub)Arctic seas flows from Denmark Strait and to the south over the continental slope of Greenland.

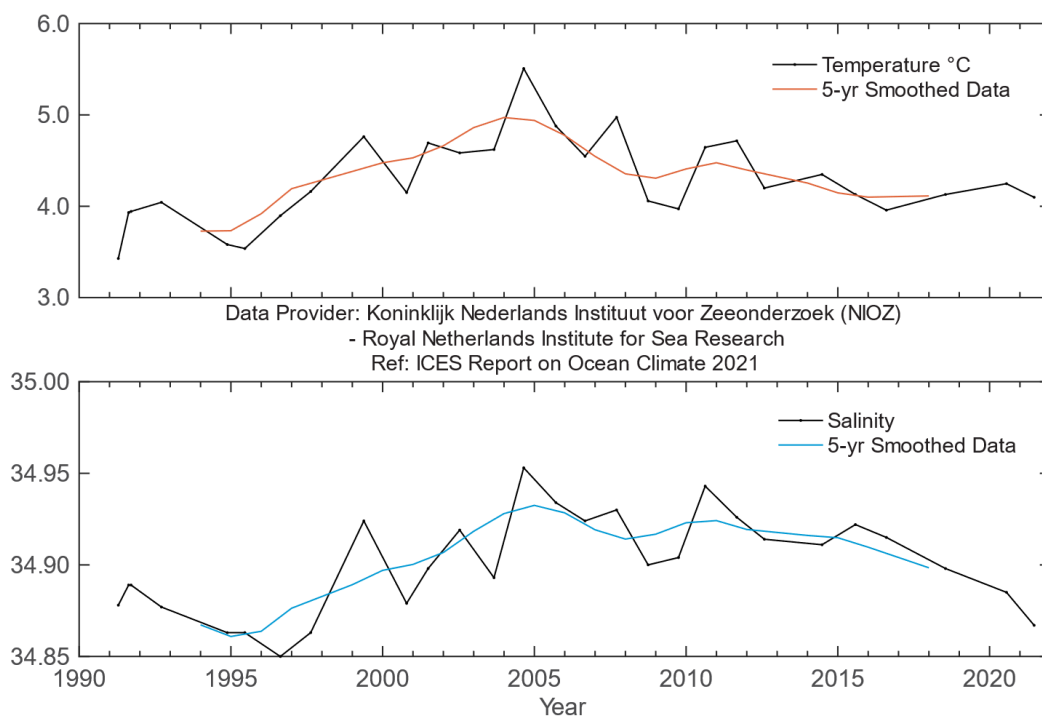


**Figure 4.56. Irminger Sea. Temperature (upper panel) and salinity (lower panel) of Subpolar Mode Water in the central Irminger Sea (averaged over 200–400 m).**

The SPMW, located in the centre of the Irminger Sea in the 200–400 dbar pressure interval, continued to freshen in 2021 (Figure 4.56). Moderate convection has mixed part of the subpolar surface freshwater anomaly into the upper 500 m of the water column. The salinity anomaly is  $-0.036$  compared to the 1990–2020 mean ( $-1.32$  s.d.). As winter cooling has not been particularly

strong these last winters, temperature remains more stable and has even slightly increased since 2016. The temperature anomaly is now  $-0.226$ , approximately  $-0.49$  s.d. [compared to  $-0.367$  ( $-0.79$  s.d.) in 2016]. The decrease in salinity and increase in temperature since 2016 has led to lower densities and a strengthening of the stratification in the central Irminger Sea.

#### 4.17 Faroese Waters and the Faroe–Shetland Channel

*K. M. H. Larsen, B. Berx, and B. Rabe*

---

**MODIFIED NORTH ATLANTIC WATER (MNAW) SALINITY IN THE REGION IS RECOVERING, BUT REMAINS BELOW THE LONG-TERM MEAN. NORTH ATLANTIC WATER (NAW) SALINITY AT THE SCOTTISH SLOPE IS STILL BELOW THE LONG-TERM MEAN. TEMPERATURES IN THE WHOLE REGION ARE CLOSE TO THE LONG-TERM MEAN.**

---

Data from the Faroese Waters ecoregion are grouped together here with data from the Faroe–Shetland Channel. This small region sits at the boundary between the Celtic, North, and Norwegian seas ecoregions and at the boundary between the North Atlantic Ocean and Nordic Seas.

One of the NAC branches crosses the Greenland–Scotland Ridge ([Figure 4.57](#)) on either side of the Faroes. Its properties are sampled in the Faroe Bank Channel before it crosses the ridge and in the Faroe Current after it crosses the ridge. Some of this water recirculates and is sampled within the Faroe–Shetland Channel as MNAW.

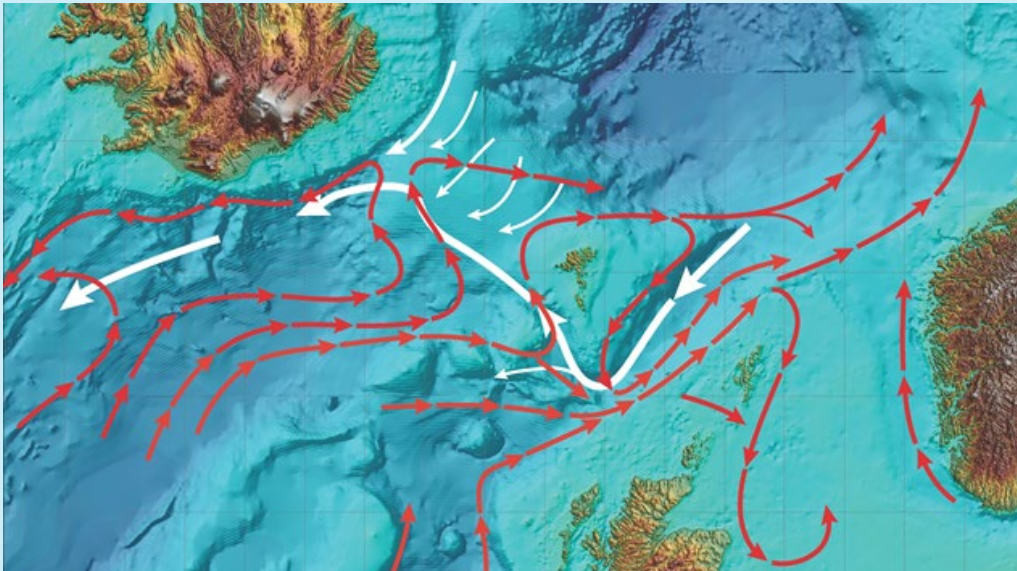


**Figure 4.57. Circulation schematic for Faroese Waters and the Faroe–Shetland Channel. Red lines: poleward movement of AW. Thick white lines: return circulation (at depth) of waters from the Nordic Seas.**

Further east, the continental slope current flows along the edge of the northwest European continental shelf. Originating in the Southern Rockall Trough, it carries warm, saline AW into the Faroe–Shetland Channel. A proportion of this AW crosses onto the shelf itself and enters the North Sea, where it is diluted with coastal water and eventually leaves in the Norwegian Coastal Current. The remainder enters the Norwegian Sea and joins the water coming from north of the Faroes to become the Norwegian Atlantic Water.

In general, both temperature and salinity in all upper-layer waters around the Faroes and in the Faroe–Shetland Channel increased markedly during the 1990s and 2000s and then decreased during the first half of the 2010s. Salinity reached record-low values in the second half of the 2010s.

Record-high salinity was observed in the Faroe Bank Channel ([Figure 4.58](#)) and the Faroe Current ([Figure 4.59](#)) in November 2009, after which salinity decreased at both locations. In autumn and winter 2016/2017, salinity decreased abruptly and continued to decrease at a slower rate in 2017 and 2018. Since 2018, salinity has been increasing, especially in 2021, but is still below the long-term mean. Temperatures in the Faroe Bank Channel and the Faroe Current were relatively high and stable during most of the 2000s. In 2012/2013, they decreased and have since been close to the long-term mean, not accompanying the decrease in salinity in the latter half of the 2010s.

On the Faroe Shelf, the annual average temperature has been relatively high since the early 2000s, but the annual averaged temperature in 2015 was the lowest observed since 2000. Since 2015, temperatures have been slightly higher and above the long-term mean (data not shown). The 2021 monthly mean temperatures were close to the long-term mean, with a colder-than-average winter, spring and summer, and a warmer-than-average autumn [missing information in summer and autumn for the reference series ([Figure 4.60](#)) is inferred from alternative series at Skopun]. A notable exception was March, which was warmer than average by 1.15 s.d. (left panel in [Figure 4.60](#)). The long-term salinity trend on the Faroe Shelf follows the trend observed for off-shelf waters. Salinities increased from the start of the observations in 1995 to record-high values in 2010, after which they decreased until the latter half of the 2010s. The record-low salinity observed in the Faroe Bank Channel in autumn 2016 was already evident in the Faroe Shelf salinity in late summer 2016. Similar to observations off-shelf, the freshening continued on-shelf in subsequent years, particularly during winter months, with record-low salinities observed as late as January 2020. Despite this, annual mean salinities have been increasing since 2018 and were just below the long-term mean in 2021 (right panel in [Figure 4.60](#)).

In the early 1990s in the Faroe–Shetland Channel, surface waters were warmer and more saline than the long-term mean. Driven by basin-scale processes, the salinity of both NAW and MNAW showed a significant freshening in 2017 and 2018 ([Figure 4.61](#) and [Figure 4.62](#)) followed by an increase in salinity in 2020, although they were still below the long-term mean. AW remained much fresher than the long-term mean in 2021, especially along the European Shelf Edge. AW temperatures on both sides of the Faroe–Shetland Channel have decreased significantly since record-high temperatures of 2010. In 2021, NAW and MNAW temperatures were both close to the long-term mean. These patterns were in close agreement with observations in the upper-layer waters around the Faroes.

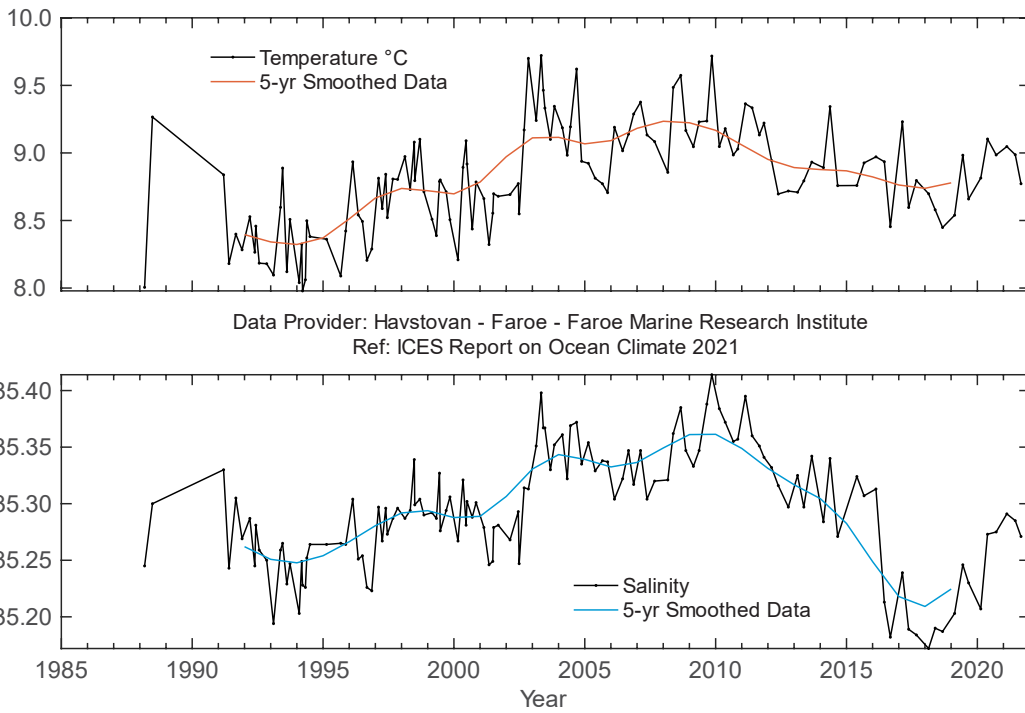


**Figure 4.58. Faroese Waters. Temperature (upper panel) and salinity (lower panel) in the high-salinity core of Atlantic Water over the Faroe Bank Channel (maximum salinity averaged over a 50-m deep layer).**

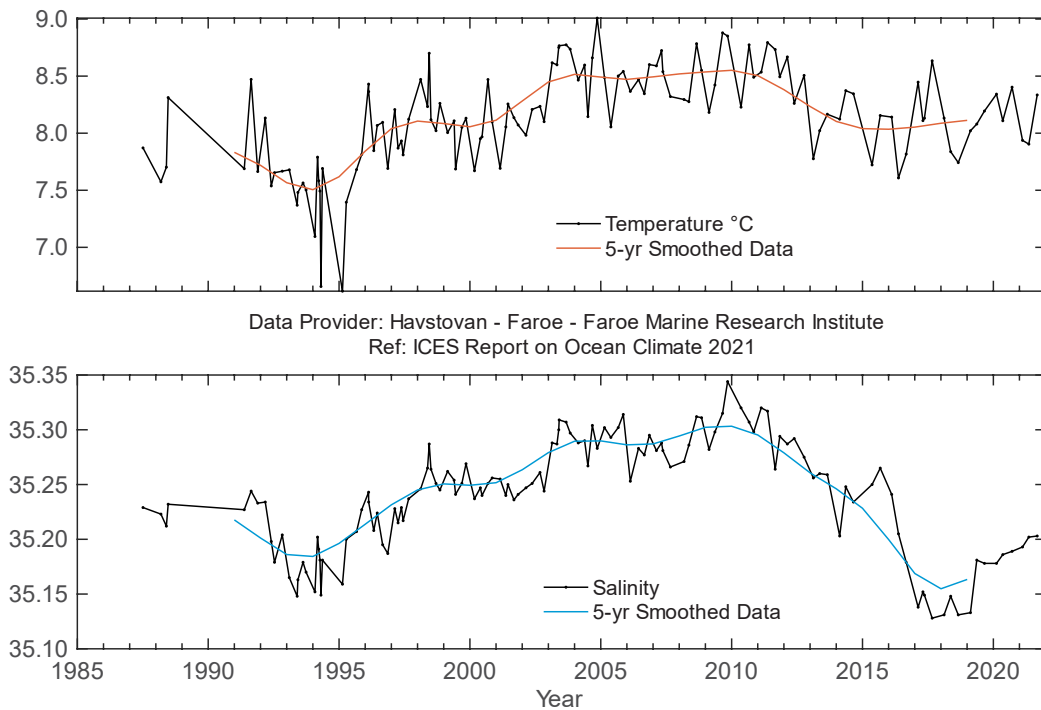


**Figure 4.59. Faroese Waters. Temperature (upper panel) and salinity (lower panel) in the high-salinity core of the Faroe Current north of the Faroes (maximum salinity averaged over a 50-m deep layer).**

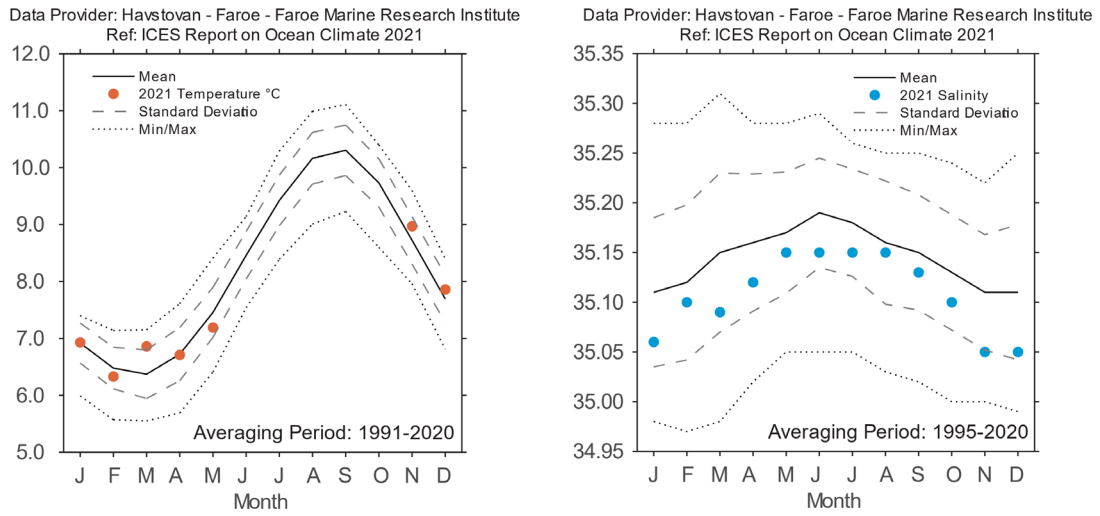


Figure 4.60. Faroe Waters. 2021 monthly temperature (left panel) from the Faroe coastal station at Oyrargjogv (62.12°N 7.17°W) and monthly salinity (right panel) from the Faroe coastal station at Skopun (61.91°N 6.88°W). Due to a technical issue, no data are available from Oyrargjogv for May–September. Note the different averaging periods.

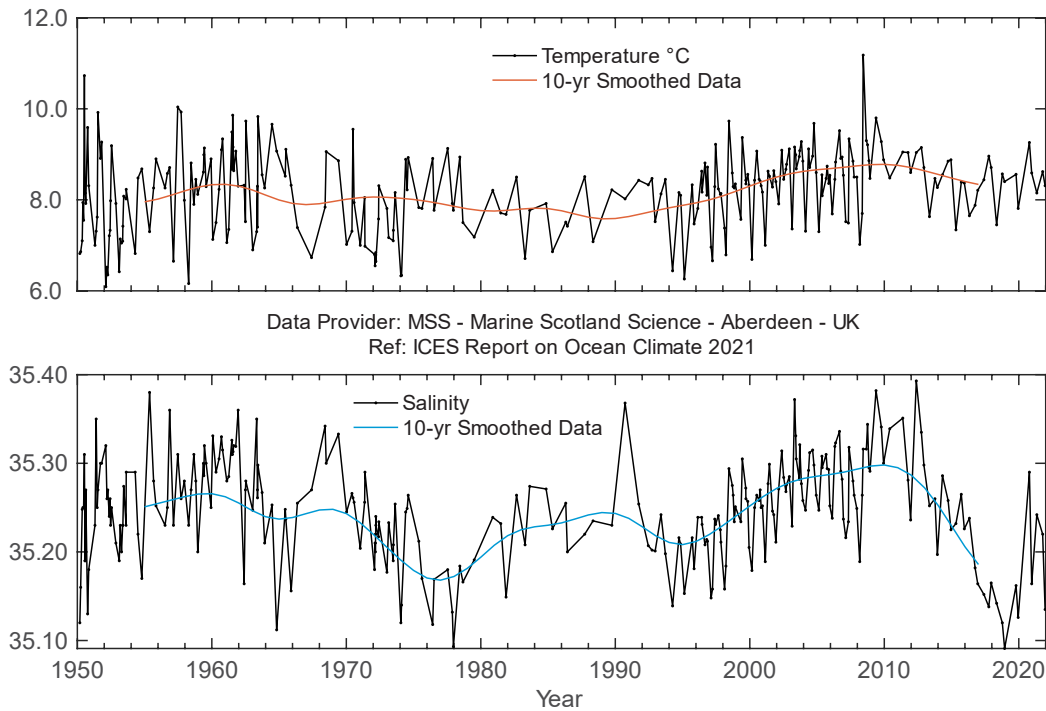


Figure 4.61. Faroe–Shetland Channel. Temperature (upper panel) and salinity (lower panel) in the modified North Atlantic Water (MNAW) entering the Faroe–Shetland Channel from the north after circulating around the Faroes.

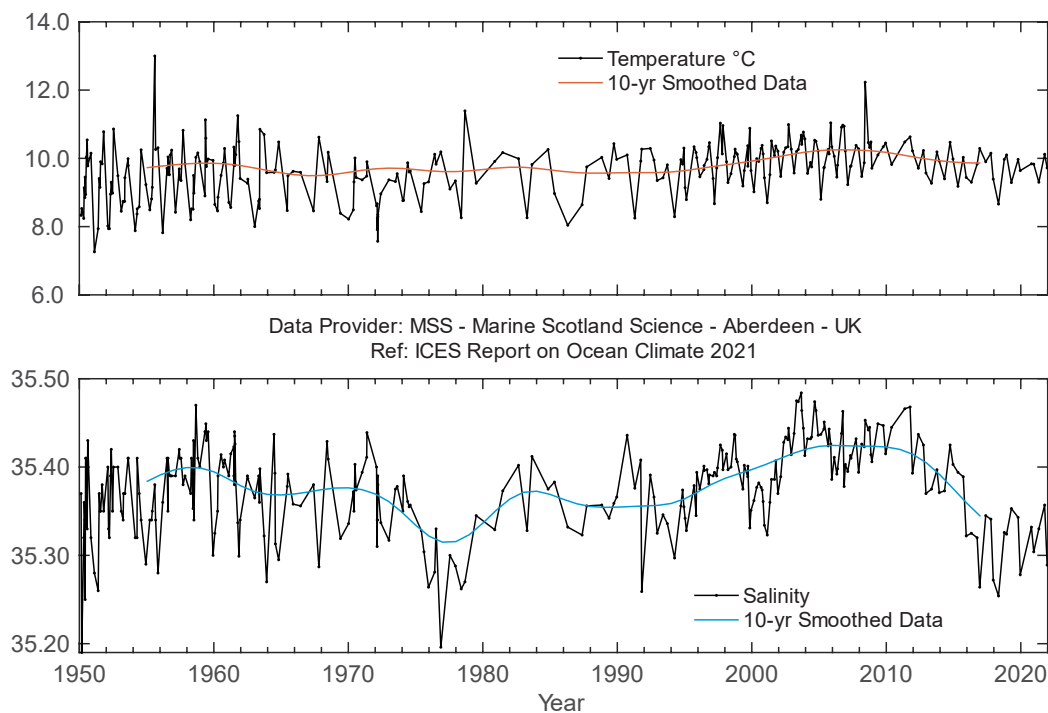


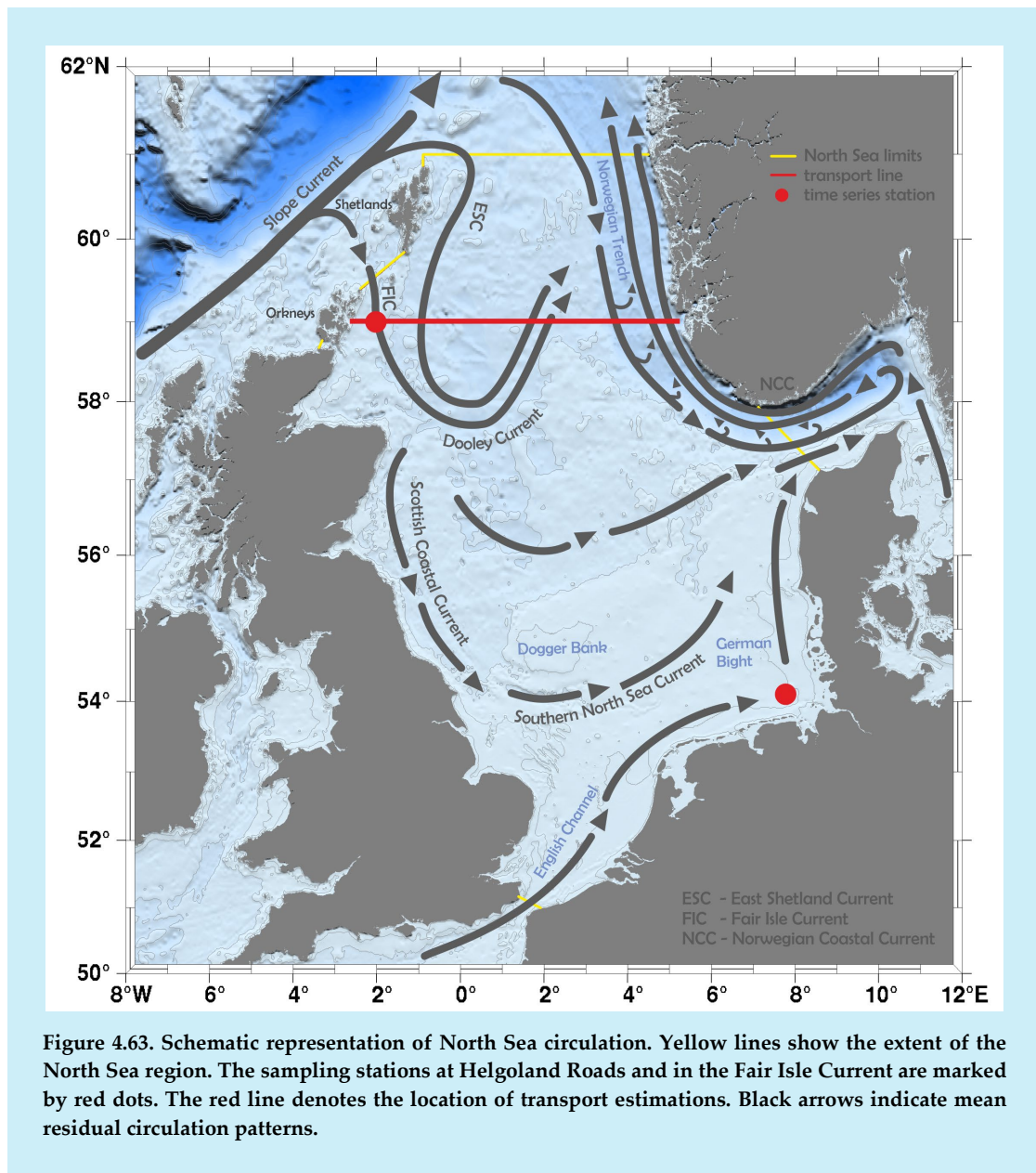
Figure 4.62. Faroe–Shetland Channel. Temperature (upper panel) and salinity (lower panel) in the Atlantic Water in the slope current.

## 4.18 North Sea

*D. Kieke, J. Albrechtsen, B. Berx, B. Rabe, I. Kirstein, K. Wiltshire, H. Klein, P. Loewe, K. Latarius, M. Köllner, and T. Kruschke*

**NORTH SEA TEMPERATURES IN 2021 WERE OVERALL SLIGHTLY ABOVE THE LONG-TERM 1991–2020 MEAN. HOWEVER, WINTER AND SPRING WERE COOLER THAN AVERAGE, WHILE SUMMER AND AUTUMN WERE WARMER. THE INFLOW OF AW FROM THE NORTH WAS RELATIVELY LOW IN 2021, CONTINUING THE TREND OF THE LAST DECADE.**

North Sea oceanographic conditions are determined by the inflow of saline AW (Figure 4.63), run-off from the adjacent land and local ocean–atmosphere heat exchange. Inflow through the northern entrances to the North Sea (Fair Isle Gap, east of Shetland, and Norwegian Trench) and, to a lesser degree, through the southern Channel, can be strongly influenced by the NAO (see Section 3). This phenomenon can also be seen in numerical model simulations. In coastal regions, salinity is lower as a consequence of freshwater input from river run-off. Outflow from the North Sea occurs mainly along the Norwegian coast, where AW has mixed with river run-off and lower-salinity Baltic water. From late spring to autumn, the imbalance between tidal mixing and local heating forces the development of seasonal stratification in most parts of the northern North Sea.



The state of the North Sea in 2021 is described on the basis of hydrographic time-series obtained in the northern and southern North Sea and on data obtained from a large-scale hydrographic survey covering the greater North Sea region in summer 2021. Time-series of modelled AW entering the North Sea at its northern boundary complement the observational dataset.

Annual SST for the North Sea is described from area-averaged estimates for the greater North Sea regions and from local SST measurements in the southern North Sea (Helgoland Roads time-series). Annual values are based on monthly means. The Helgoland Roads time-series used in the IROC report is currently under revision. Results reported refer to the time-series as it was until 2021. In 2021, the SST anomaly for January relative to the long-term mean was slightly positive (+0.3°C; [Figure 4.64](#)). However, late winter to spring months (February–May), showed negative anomalies in the range -0.2°C (March) to -0.7°C (May). From May to June,

North Sea SST anomalies experienced a sharp increase of around 1.5°C. SSTs remained above the long-term average until December, when a negative anomaly of -0.3°C was observed. The largest negative and positive anomalies in 2021 compared to the long-term mean occurred in May (-0.7°C) and July (+1.0°C). The smallest deviation from the long-term mean occurred in August (+0.2°C).

SSTs at Helgoland Roads in the southern North Sea showed a similar pattern locally in 2021 (Figure 4.65), with the difference being that temperatures remained above the long-term mean from July until the end of the year.

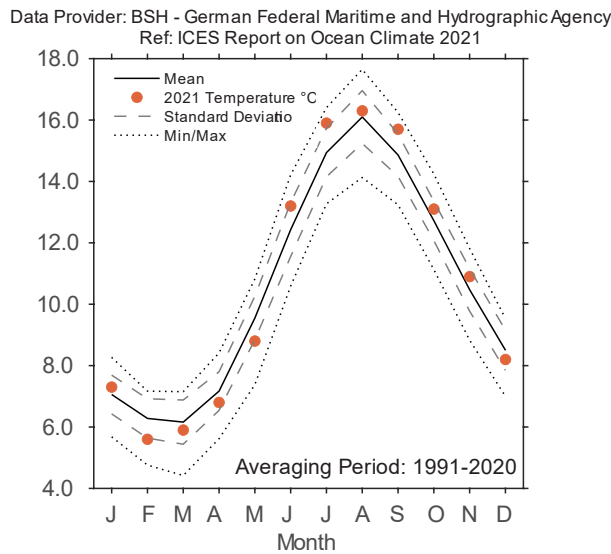


Figure 4.64. North Sea. Monthly means of area-averaged SST. Dashed lines denote the ±0.5 s.d. interval. Data provided by BSH.

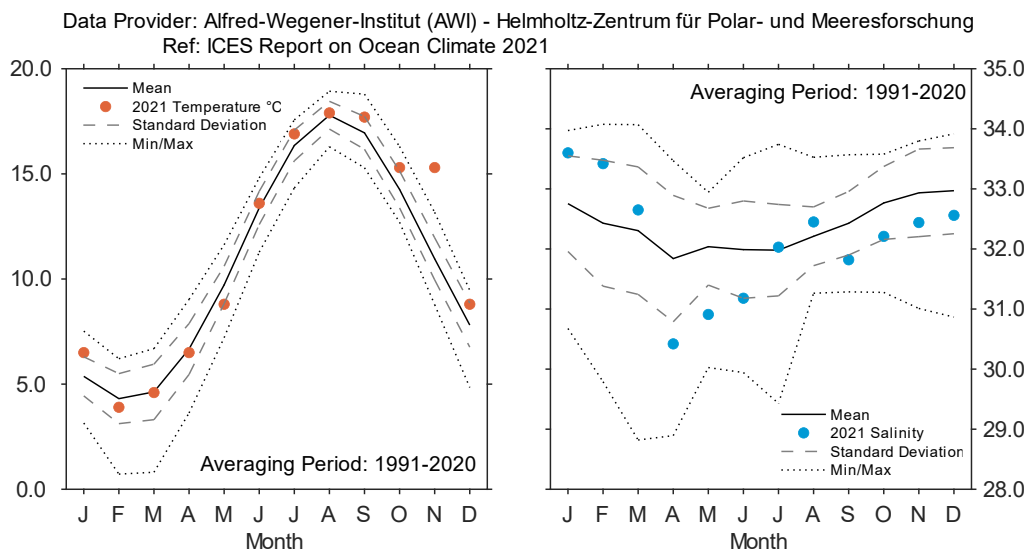


Figure 4.65. Southern North Sea. Monthly surface temperature (left panel) and salinity (right panel) at the station Helgoland Roads. Dashed lines denoted the ±0.5 s.d. interval.

The annual area-averaged mean of North Sea SST in 2021 was 10.6°C (+0.1°C; [Figure 4.66](#)), while the annual local average at Helgoland Roads, in the southern North Sea, was 11.1°C (+0.4°C). Both time-series show the same long-term warming trend, with some year-to-year variability. However, there is a greater temperature range at Helgoland Roads, potentially due to shallower water depths in the German Bight. These local patterns are to be expected, because most of the North Sea SST variability is due to local ocean–atmosphere heat exchange, especially in areas located away from the AW inflow pathways.

The Elbe River run-off into the German Bight slightly increased in 2021 compared to previous years and was closer to the long-term average. This freshwater increase explains the decrease in annual SSS at Helgoland Roads from 2020 to 2021, with SSS falling below the long-term mean at Helgoland Roads ([Figure 4.67](#)).

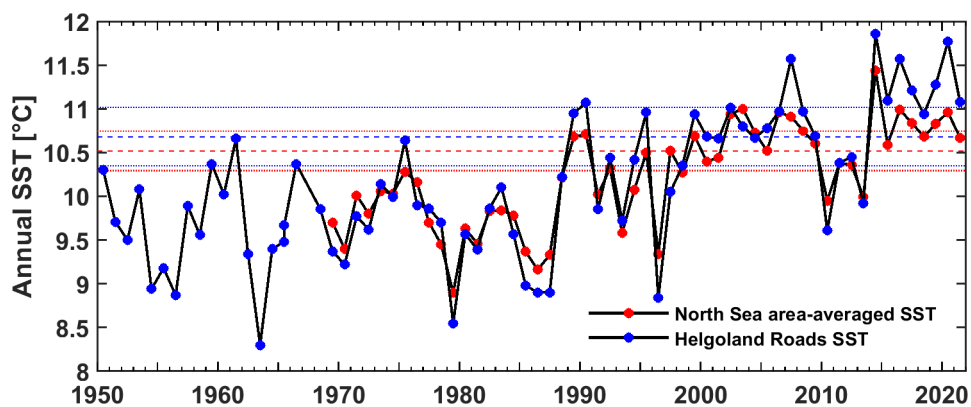


Figure 4.66. North Sea. Annual means of area-averaged SSTs (red) and the local SST at station Helgoland Roads (blue). Dashed lines show the respective long-term mean values, while dotted lines highlight the ± 0.5 s.d. intervals. Data provided by BSH and AWI.

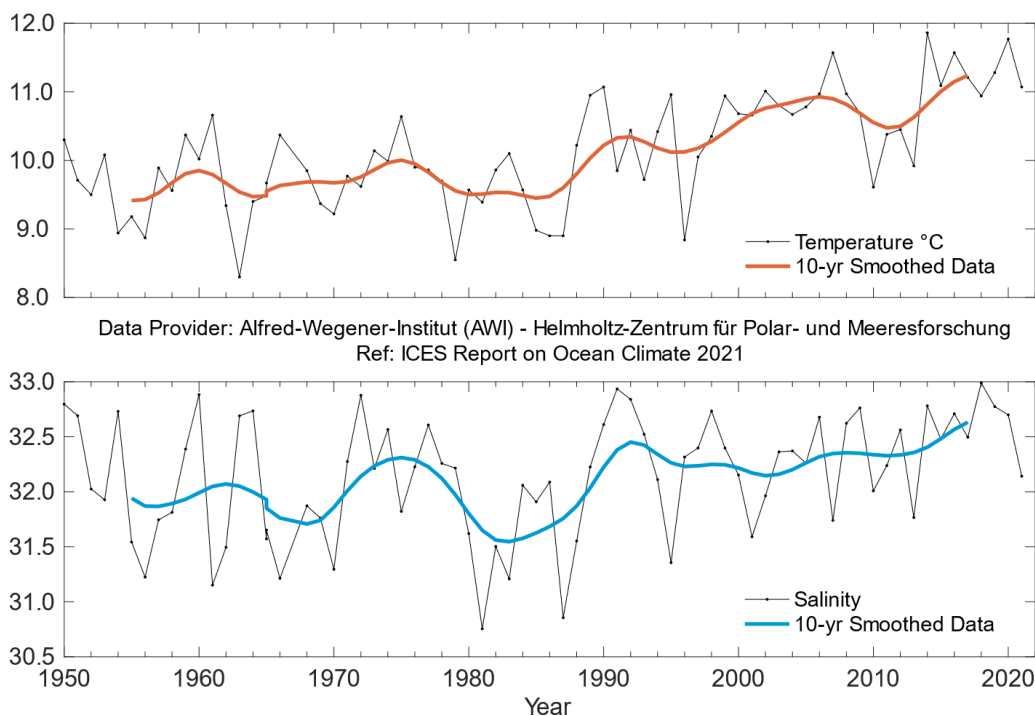


Figure 4.67. Southern North Sea. Annual mean surface temperature (upper panel) and salinity (lower panel) at the station Helgoland Roads. Data provided by AWI.

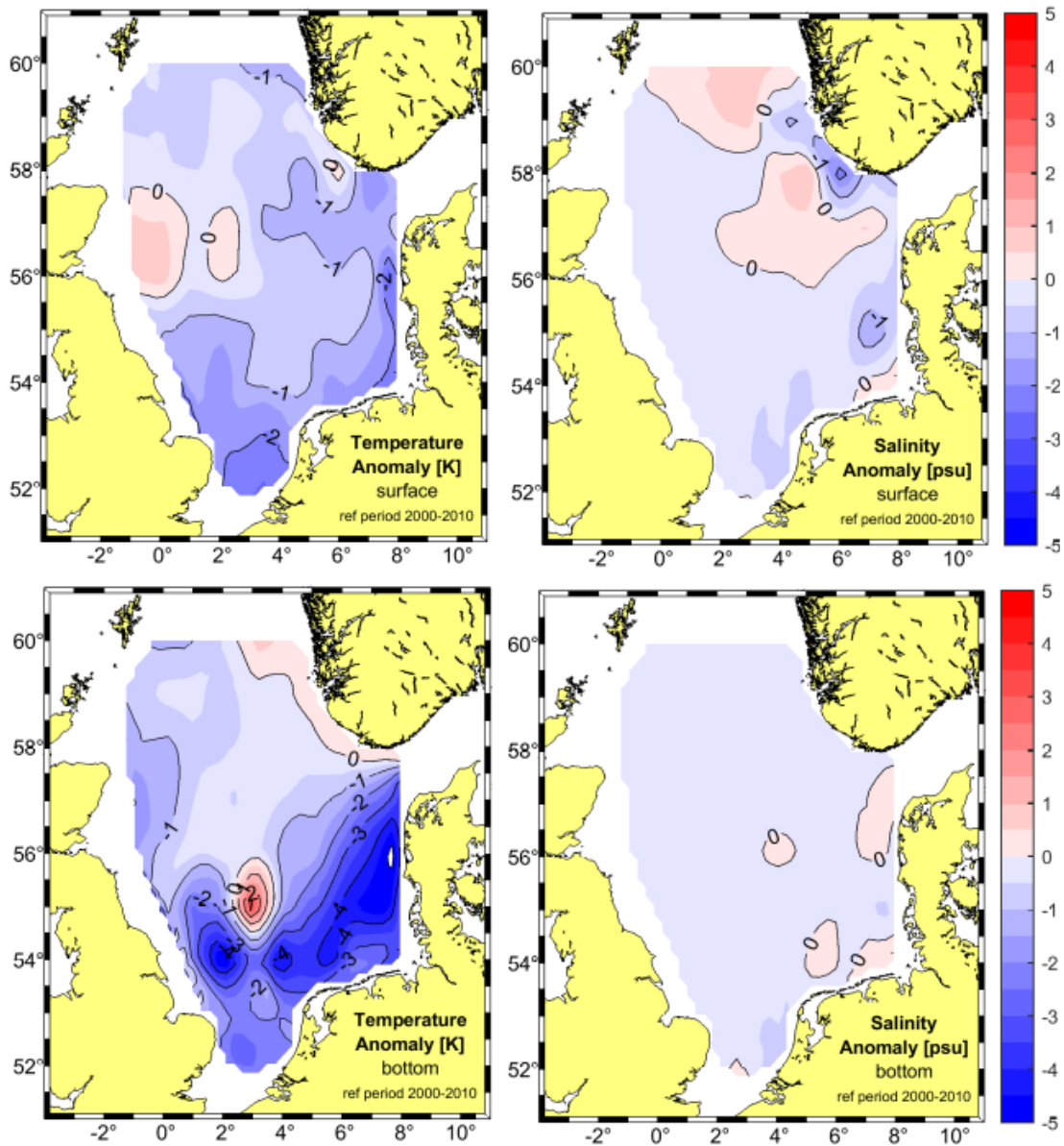


Figure 4.68. Anomalies for temperature (left) and salinity (right) shown for summer 2021 for the surface (top) and the bottom layers (bottom). Anomalies refer to the reference period 2000–2010. Data provided by BSH.

Hydrographic data were collected in 2021 for surface and bottom layers on a large-scale summer survey covering the greater North Sea region. SST generally increased from 12–14°C in the western North Sea to values > 16°C in the eastern North Sea. Bottom waters showed a north-south gradient and were generally < 12°C north of about 54°N. When compared to the 2000–2010 temperature average obtained from similar summer cruises, observed temperature anomalies in the surface layer in 2021 were mostly negative, around –0.5°C to –1.0°C (Figure 4.68). These anomalies increased from the central North Sea towards the eastern and southern boundaries of the North Sea, with extremes of up to –2°C below average. Only two patches with positive anomalies were observed of about 0.5°C east of the Firth of Forth and centred around 56.5°N to 57°N.

Compared to the surface layer, spatial differences in the bottom layer were much more pronounced. Negative temperature anomalies were observed in the southern North Sea and off the Danish coast, which gradually increased towards the coasts, exceeding  $-5^{\circ}\text{C}$  below average. Positive anomalies prevailed over Dogger Bank, where there was an isolated anomaly patch with temperatures  $+2^{\circ}\text{C}$  above average. Due to the shallow depth of Dogger Bank, the local bottom waters belong to the warm mixed layer, thus explaining this warm anomaly. The bottom layer of the Norwegian Trench showed a ribbon-like pattern, with slightly positive anomalies of about  $0.5^{\circ}\text{C}$  above average. The area-averaged summer SST (JAS) was  $16.0^{\circ}\text{C}$ , about  $0.7^{\circ}\text{C}$  above the 1991–2020 mean.

During the same summer cruise in 2021, surface salinities above 35, indicative of the presence of AW, were observed on both sides of Shetland, between about  $2^{\circ}\text{W}$  and  $1^{\circ}\text{E}$  and reaching to the south to  $59^{\circ}\text{N}$ . In the bottom layer, salinities up to 35 were present in the entire northern North Sea, with a small tip reaching southward to about  $56.5^{\circ}\text{N}$ . An intrusion of AW coming from the English Channel at the southern entrance to the North Sea was not observed in 2021. Over large areas, the surface salinity distribution showed deviations from the 2000–2010 summer mean of around  $\pm 0.5$ . These were only exceeded in the German Bight and south of Norway, where negative anomalies of up to  $-1.5$  occurred at the surface. In the bottom layer, deviations from the long-term mean were generally lower than  $\pm 0.5$  (Figure 4.68).

The ocean circulation model NORWECOM (Skogen *et al.*, 1995) has been used to quantify the flux of inflowing AW through a section between Utsira, Norway, and the Orkney Islands. Of the four inflow pathways into the North Sea (Fair Isle Gap, east of Shetland, Norwegian Trench, and the English Channel), the western slope of the Norwegian Trench is the main AW inflow pathway. The main proportion of this AW enters the Skagerrak and then recirculates anticlockwise following the direction of the Norwegian Coastal Current. NORWECOM model results showed that the total inflow of AW (the sum of all southward transport) was relatively low in 2021, ranking as the sixth lowest annual inflow since the time-series was initiated in 1985. The first half of 2021 saw a particularly low volume, while the second half had about an average inflow. Thus, the prevailing trend seen for the last decade continues with low AW inflow to the northern North Sea (Figure 4.69).

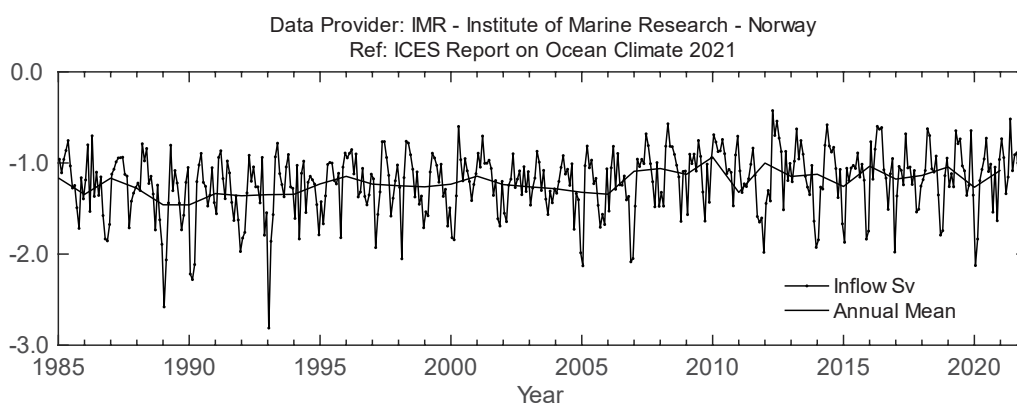


**Figure 4.69. Northern North Sea. Modelled annual mean (bold) and monthly mean volume transport of AW into the northern and central North Sea southward between the Orkney Islands and Utsira, Norway. Data provided by IMR.**

Close to the Scottish coast, annual monitoring of the properties of the Fair Isle Current and East Shetland Atlantic Inflow has been conducted since the late 1960s (Figure 4.63). The Fair Isle Current (Figure 4.70) transports a mixture of Scottish coastal waters and AW into the northern North Sea. The normalized annual mean temperature anomaly was close to the 1991–2020 mean ( $-0.13$ ), while annual mean salinity anomalies were very low ( $-1.15$ ). Low salinities were mainly observed in May and October 2021. These low salinities have been observed since 2016 and likely result from the record-low salinities in the AW spreading from the Subpolar Gyre along the circulation pathways and entering the northern North Sea.

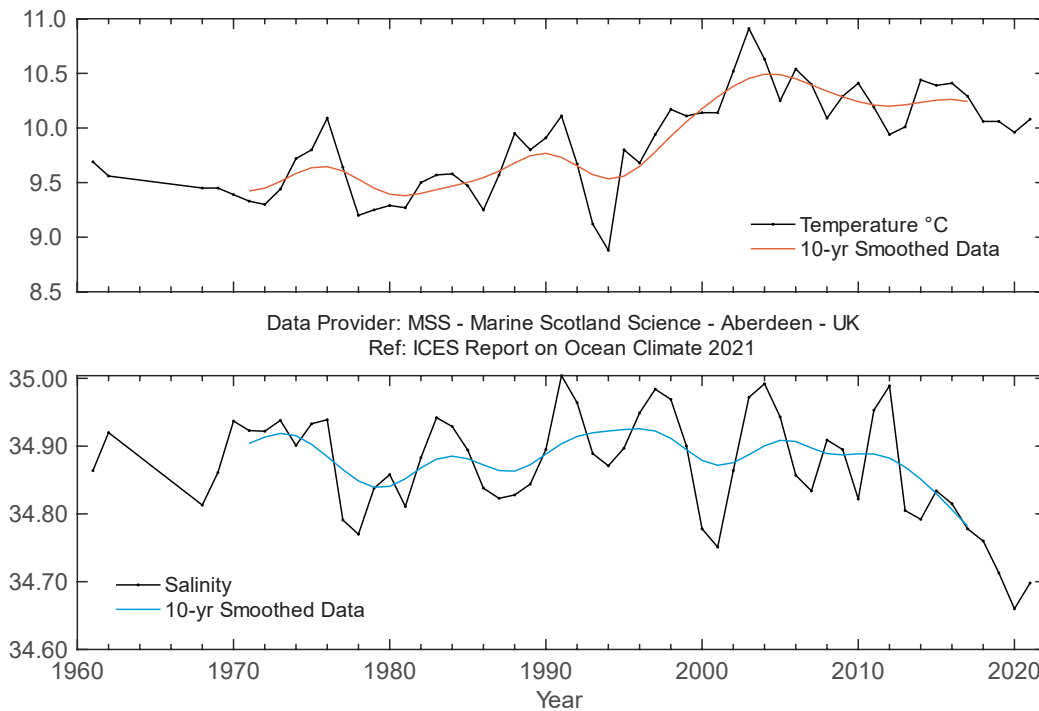
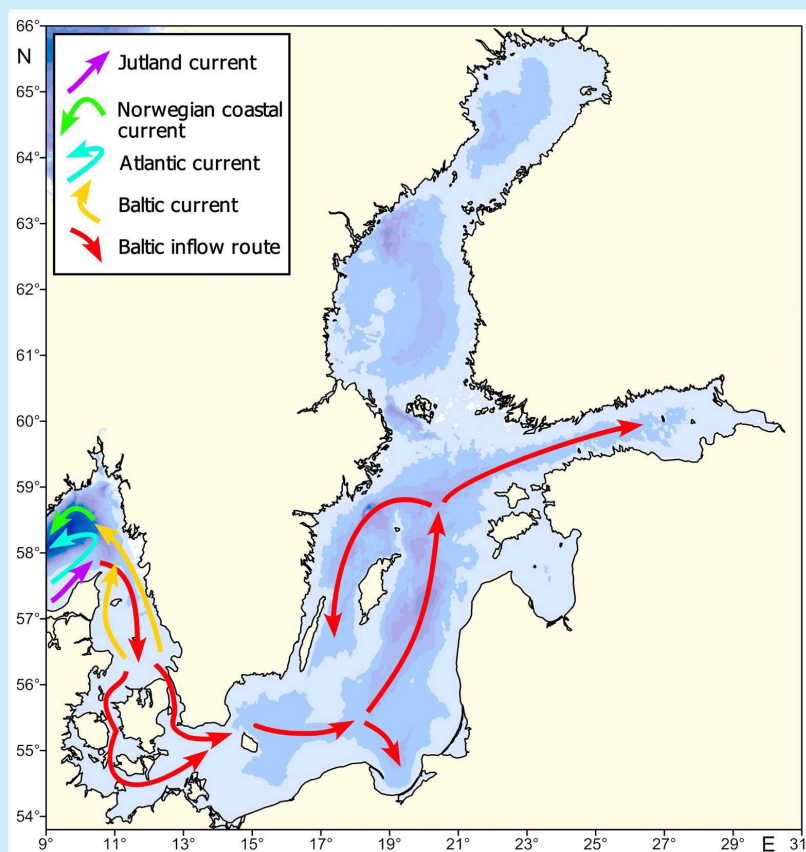


Figure 4.70. Northern North Sea. Temperature (upper panel) and salinity (lower panel) in the Fair Isle Current entering the North Sea from the North Atlantic.

## 4.19 Skaggeiak, Kattegat, and the Baltic Sea

*J. Linders, T. Liblik, and T. Wodzinowski*

The Skaggeiak, Kattegat, and Baltic Sea are characterized by large salinity variations. The Skaggeiak and Kattegat are transition areas between the Baltic and the North seas. The water in the Baltic Sea is strongly stratified with a permanent halocline. The deep water in the Baltic Sea proper enters through the Belts and the Sound and can be stagnant for long periods. In the relatively shallow area in the southern Baltic Sea, smaller inflow events pass relatively quickly, and conditions in the deep water are highly variable. Surface salinity is very low in the northern, central, and eastern Baltic Sea. The Gulf of Bothnia and the Gulf of Finland are at least partly ice-covered during winter.



**Figure 4.71. Skagerrak, Kattegat, and the Baltic Sea. Water masses circulation map.**

Owing to its central location relative to the Skagerrak, Kattegat, and the Baltic, weather in Sweden can be taken as representative for the area. Mean air temperature in Sweden, based on annual average values from 35 Swedish stations, was normal in 2021. Precipitation was also normal in the majority of Sweden, and there were no strong storms in Swedish coastal waters during all of 2021. The number of sun hours was above normal, as in previous years. Ice extent in winter 2020/2021 was normal.

In the Skagerrak and Kattegat, surface water in February was much colder than in previous years, while in the Baltic, it was close to normal. In summer, the situation reversed, and temperatures were close to normal in the Skagerrak and Kattegat, while in the Baltic, they were much warmer. SSS was mostly above normal during 2021 at most of the study sites. The relatively high salinity and temperature were not limited to the surface and extended throughout most of the water column.

Water above the seabed continued to cool, and salinity continued to drop after the maxima reached during the 2014–2015 inflows into the Baltic Sea. Results for 2021 showed that low oxygen conditions established after the regime shift in 1999 in the Baltic Sea proper continue. Almost one-fifth (20%) of the bottom area was affected by anoxia and one-third (31%) by hypoxia during 2021. In 2018, the largest bottom area and volume affected by anoxia was observed since records began in 1960. In 2018, anoxic conditions affected  $\approx 24\%$  of the bottom areas and  $\approx 33\%$  suffered from hypoxia. These conditions are novel because new areas are affected regularly. For the southern basins of the Baltic Sea proper, such as the Gulf of Gdańsk,

Hanö Bight, and the Bornholm Basin, which used to be only hypoxic (insufficient oxygen) in the deep waters, anoxia (no oxygen) is now found regularly. Hydrogen sulphide, which disappeared from the eastern and northern Gotland Basin due to the inflows in 2014–2016, is now steadily increasing again in the deep water. No major inflows have occurred since 2016.

The ice season in 2020/2021 started in November and ended in mid-May. The maximum extent of ice in the Baltic Sea occurred on 2 February 2021 and amounted to approximately 127 000 km<sup>2</sup>.

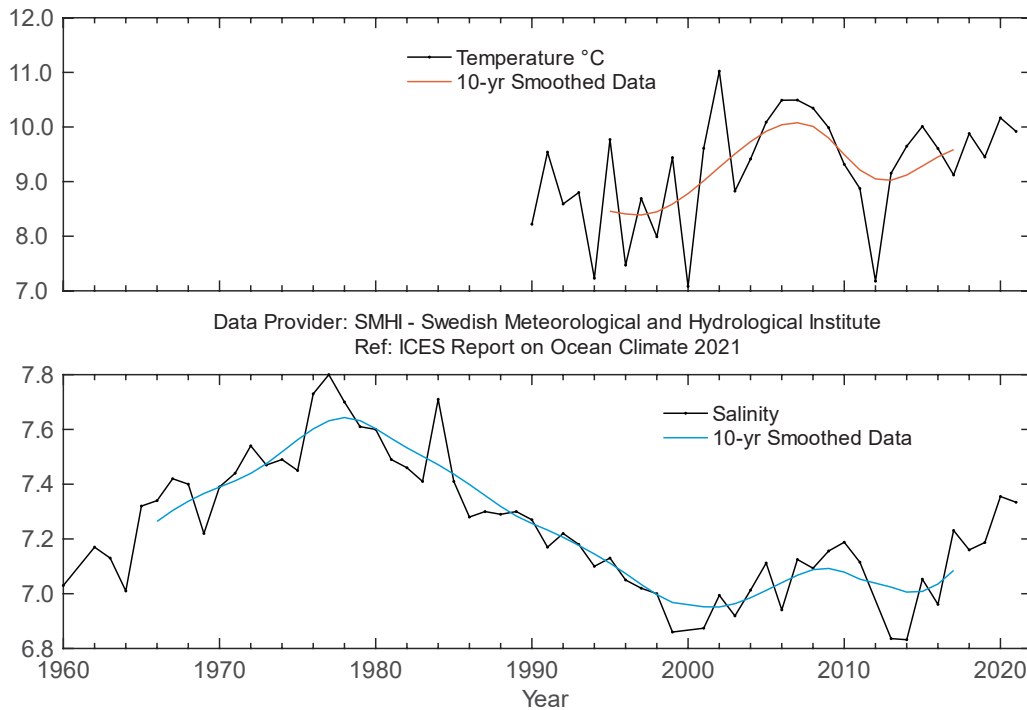


**Figure 4.72.** Skagerrak, Kattegat, and the Baltic Sea. Surface temperature, yearly mean (upper panel) and surface salinity, yearly mean (lower panel) at Station BY15 (east of Gotland) in the Baltic Sea proper.

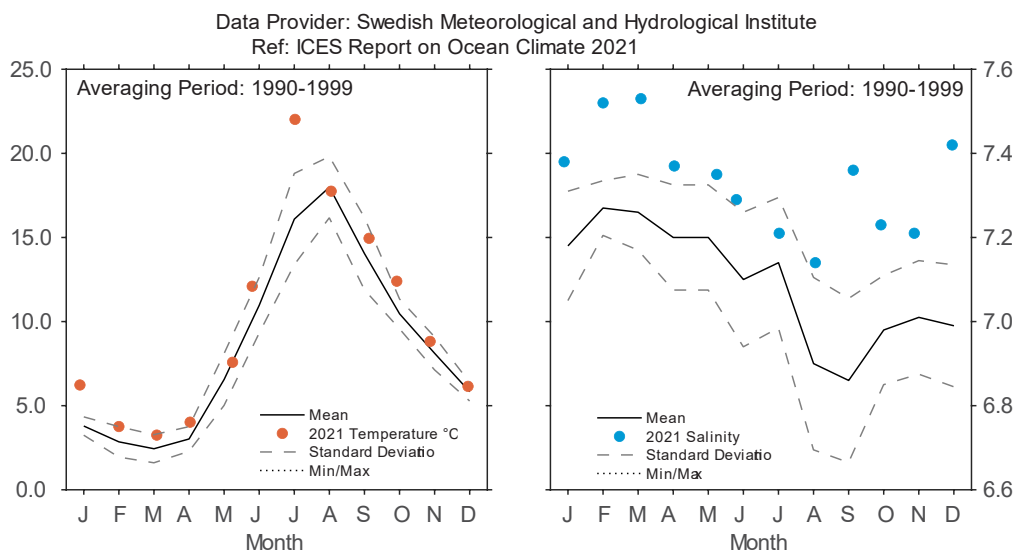


**Figure 4.73.** Skagerrak, Kattegat, and the Baltic Sea. Monthly surface temperature (left panel) and salinity (right panel) at Station BY15 (east of Gotland) in the Baltic Sea proper.

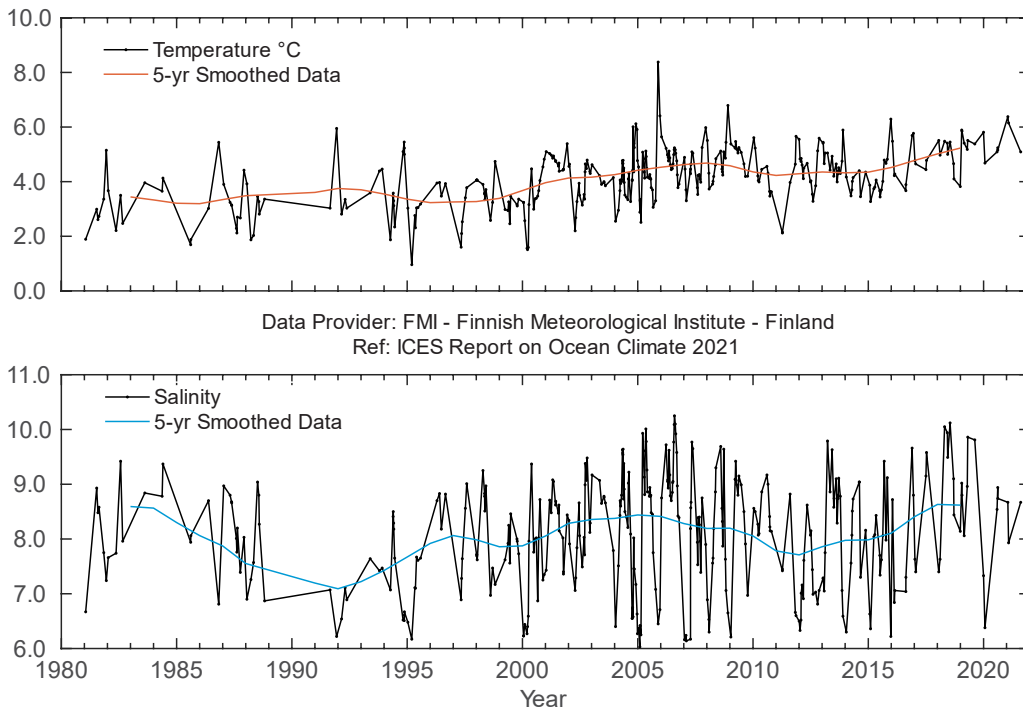


**Figure 4.74. Skagerrak, Kattegat, and the Baltic Sea. Temperature (upper panel) and salinity (lower panel) at Station LL7 in the Gulf of Finland.**

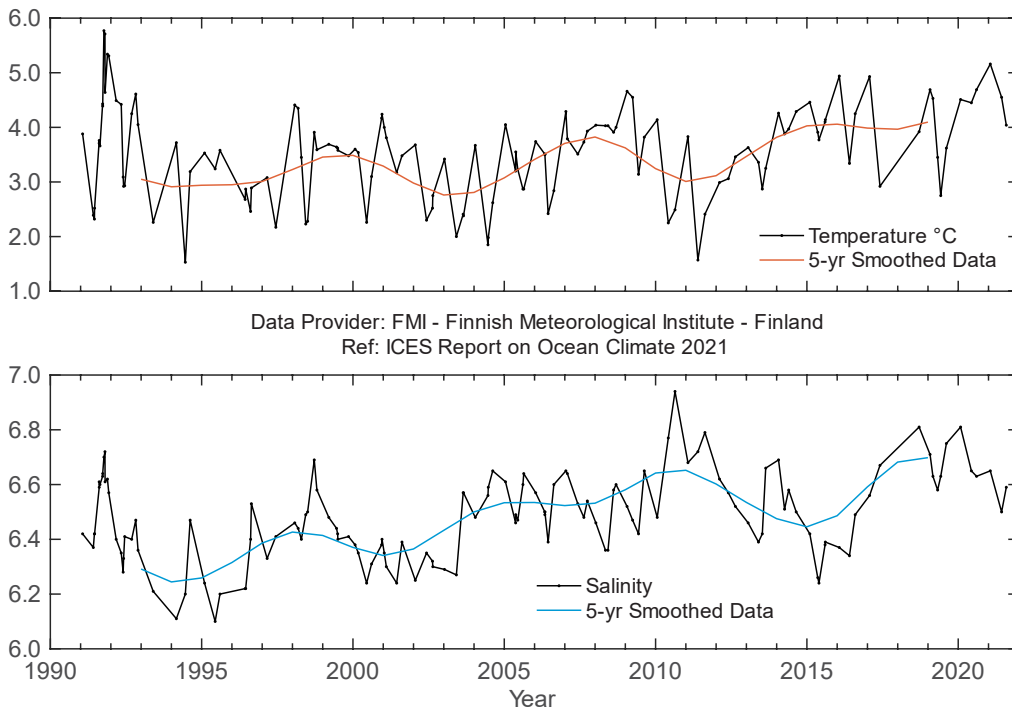


**Figure 4.75. Skagerrak, Kattegat, and the Baltic Sea. Temperature (upper panel) and salinity (lower panel) at Station SR5 in the Bothnian Sea.**

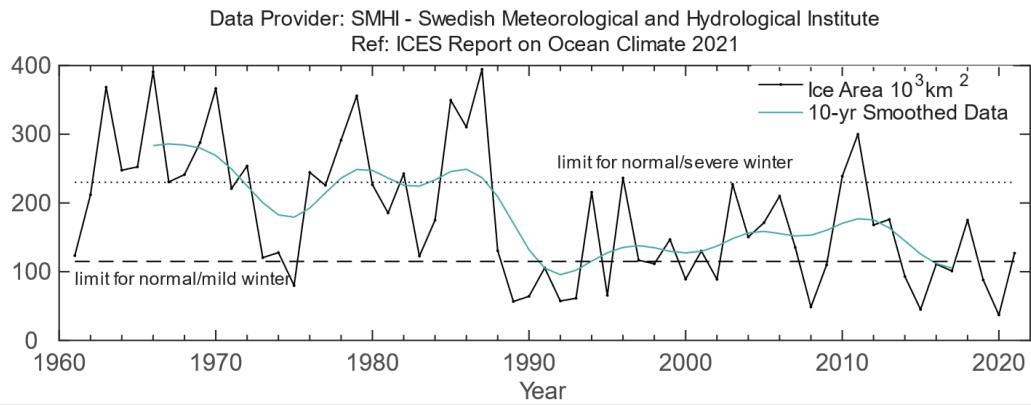


Figure 4.76. Skagerrak, Kattegat, and the Baltic Sea. The maximum ice extent in the Baltic Sea since 1960.



M6 deployment on board the R.V. Celtic Explorer. Credit: Tomasz Szumski.

## 4.20 Norwegian Sea

*K. A. Mork*

### FRESH AND NEAR-AVERAGE TEMPERATURE CONDITIONS IN THE UPPER LAYER OF THE NORWEGIAN SEA IN 2021

The Norwegian Sea is characterized by warm AW on the eastern side and cold Arctic water on the western side, separated by the Arctic front (Figure 4.77). AW enter the Norwegian Sea through the Faroe–Shetland Channel and between the Faroes and Iceland via the Faroe Front. A smaller branch, the North Icelandic Irminger Current, enters the Nordic Seas on the western side of Iceland. AW flows north as the Norwegian Atlantic Current, which splits when it reaches northern Norway; some enters the Barents Sea, whereas the rest continues north into the Arctic Ocean as the West Spitsbergen Current.

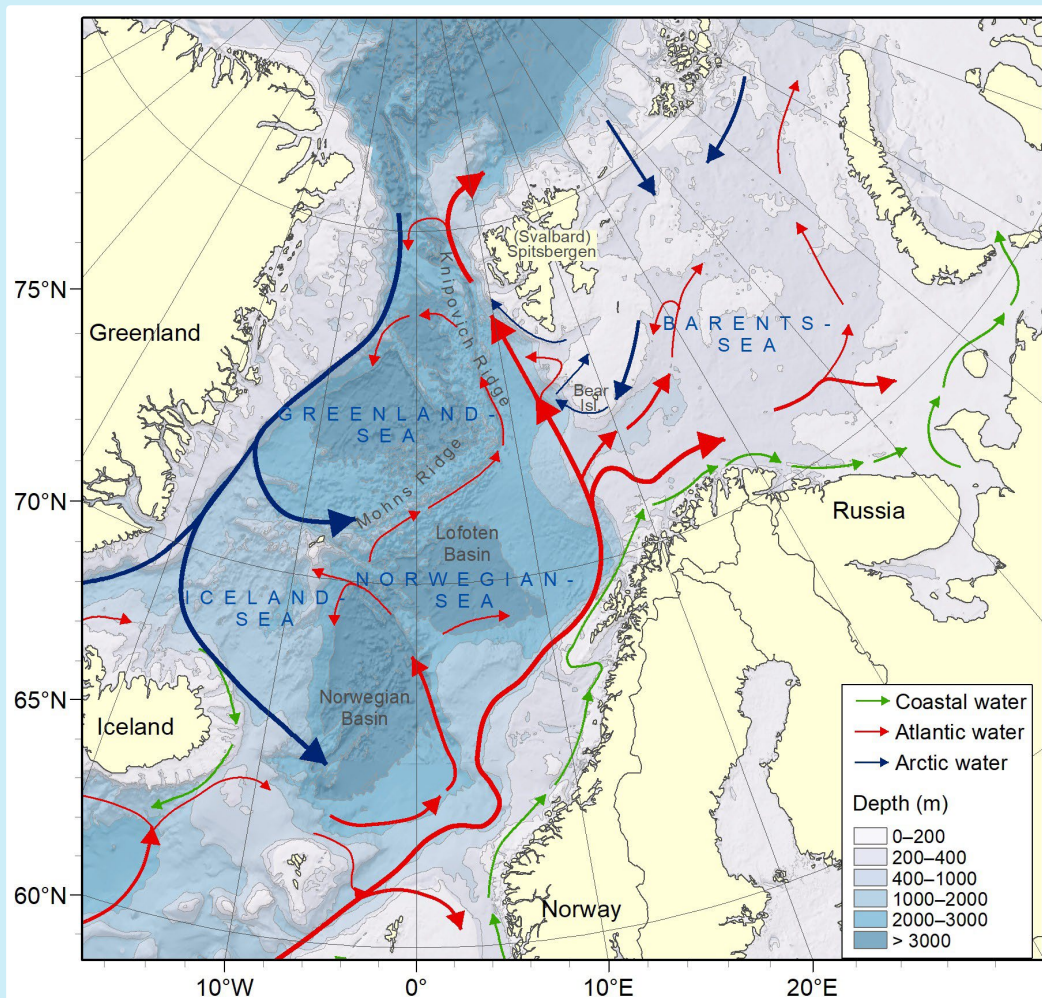
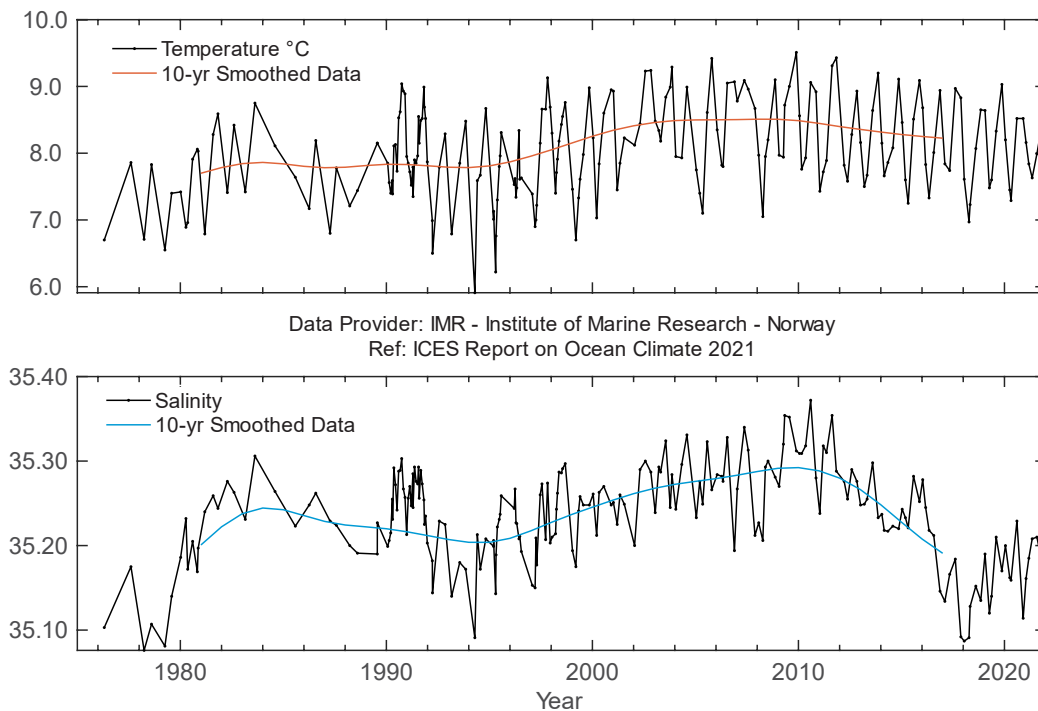


Figure 4.77. Circulation schematic for the Norwegian and Barents seas. Red lines: poleward movement of AW. Blue lines: circulation of Arctic Water. Green lines: circulation of coastal waters.

Three sections distributed from south to north in the eastern Norwegian Sea demonstrate the development of temperature and salinity in the core of the AW: Svinøy-NW (northwest; [Figure 4.78](#)), Gimsøy-NW ([Figure 4.79](#)), and Sørkapp-W (west; [Figure 4.80](#)). In general, there was an increase in temperature in all three sections from the mid-1990s to about the mid-2000s. Temperature subsequently declined in the Svinøy-NW and Gimsøy-NW sections. Annual temperature averages in 2021 were close to the long-term mean at both the Svinøy-NW and Sørkapp-W sections, while it was 0.3°C above the long-term mean at the Gimsøy-NW section.

Salinity increased at all three sections until around 2010 and decreased in recent years. In both the Svinøy-NW and Gimsøy-NW sections, salinity in 2018/2019 was the lowest observed since the end of the 1970s. Salinity has increased in recent years, but is still considerably lower than the long-term mean for all three sections. Annual salinity averages in 2021 were 0.05, 0.04, and 0.03 below the long-term means at the Svinøy-NW, Gimsøy-NW, and Sørkapp-W sections, respectively.

Ocean heat and freshwater content of Atlantic Water describe the climate variability of the Norwegian Sea. [Figure 4.81](#) provides a time-series of hydrographic data during spring since 1951. Heat content in the Norwegian Sea has been above or close to the long-term mean since 2002, reaching a record-high in 2017. Freshwater content has increased since 2010. In 2021, heat content was near the long-term mean, while freshwater content was substantially below the long-term mean.



**Figure 4.78. Norwegian Sea. Temperature (upper panel) and salinity (lower panel) above the slope at Svinøy section (63°N).**

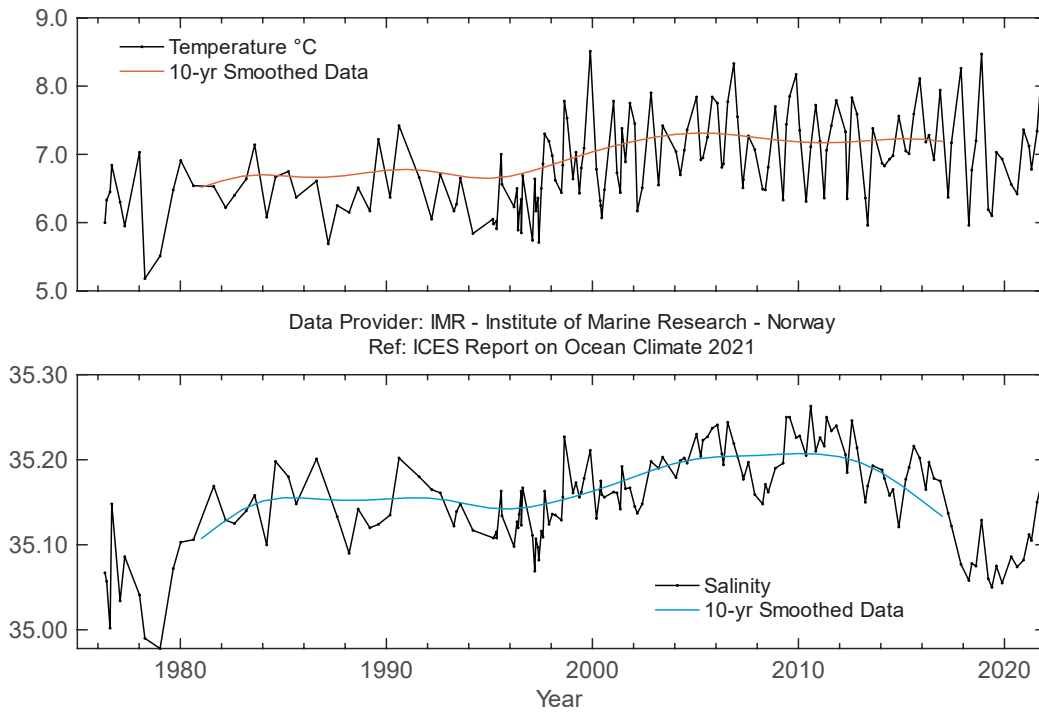


**Figure 4.79. Norwegian Sea. Temperature (upper panel) and salinity (lower panel) above the slope at Gimsøy section (69°N).**

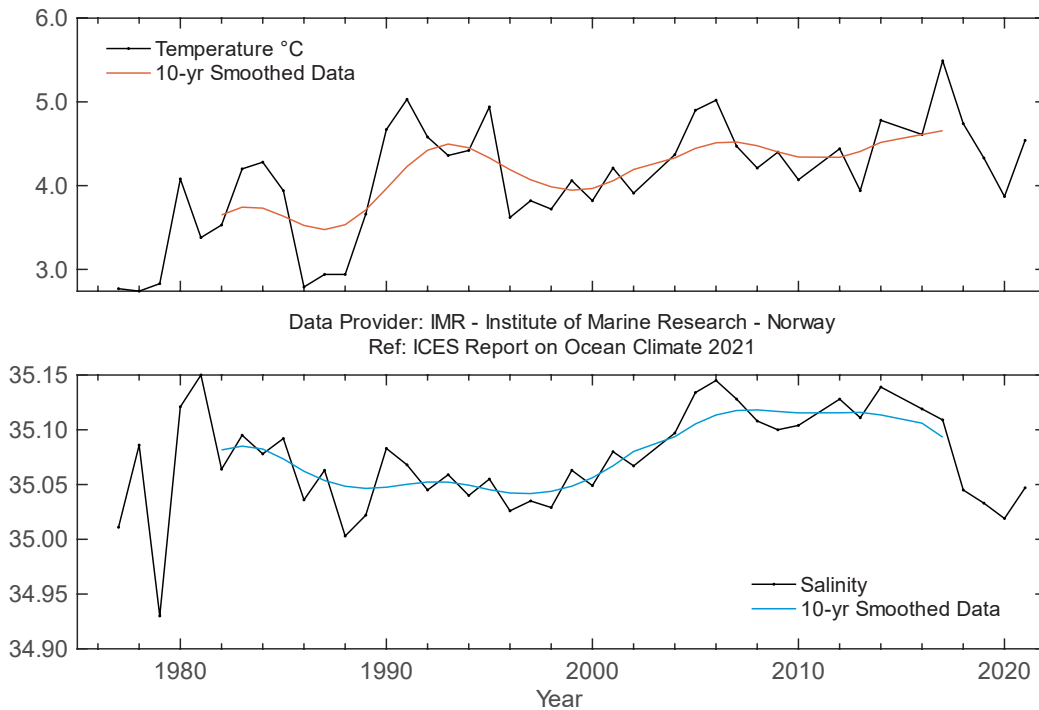


**Figure 4.80. Norwegian Sea. Temperature (upper panel) and salinity (lower panel) above the slope at Sørkapp section (76°N).**

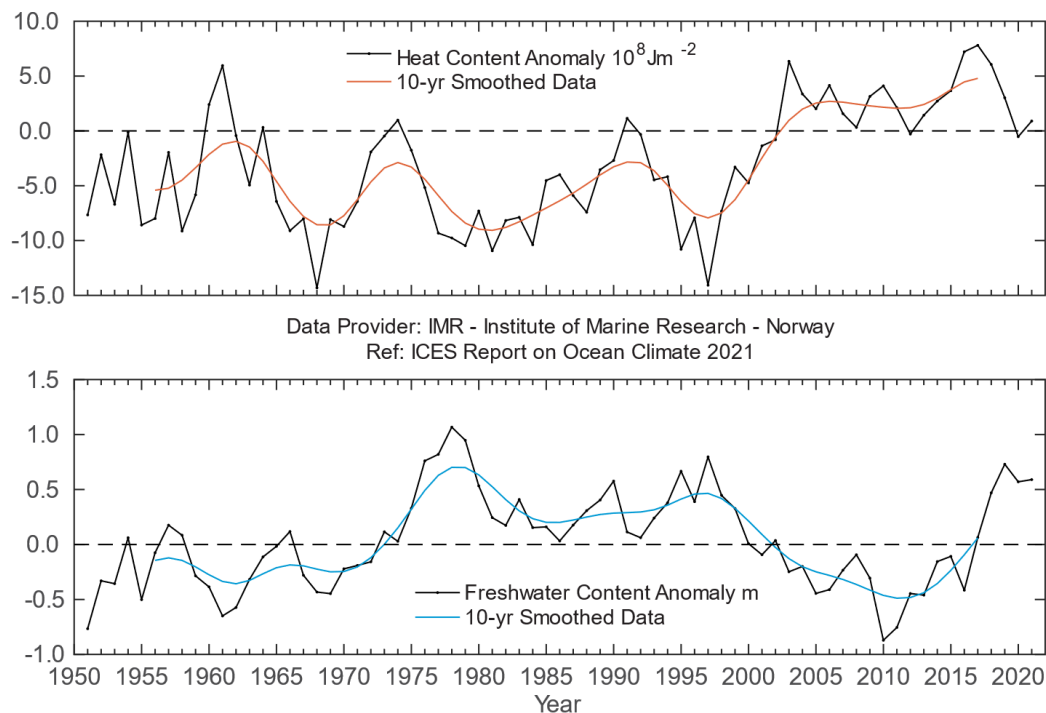


Figure 4.81. Norwegian Sea. Heat (upper panel) and freshwater (lower panel) content anomalies of Atlantic Water in the Norwegian Sea.

## 4.21 Barents Sea

*A. Trofimov and R. Ingvaldsen*

### SLIGHTLY WARM AND LOW ICE CONDITIONS IN THE BARENTS SEA IN 2021, WITH A COOLING TREND SINCE 2016.

The Barents Sea is a shelf sea that receives an inflow of warm AW from the west ([Figure 4.77](#)). The inflow exhibits considerable seasonal and interannual fluctuations in volume and water mass properties causing high variability in heat content and ice coverage of the region.

The Barents Sea showed a warming trend from the late 1970s until a peak in 2015/2016, after which temperatures decreased. From 2004 to 2017, temperature in the western Barents Sea remained mainly above the long-term mean (1991–2020), except in 2010 and 2011. In the eastern part of the sea, the same pattern was observed from 2004 to 2018, with an exception in 2011.

The Fugløya–Bear Island section covers the inflow of AW and coastal water masses from the Norwegian Sea into the Barents Sea, while the Kola section covers the same waters in the central Barents Sea. Temperature in the inflowing AW in the western Barents Sea (Fugløya–Bear Island section) peaked in 2015/2016, with temperatures  $0.6^{\circ}\text{C}$  above the long-term average (1991–2020; [Figure 4.82](#)). During 2016–2019, temperature decreased by about  $0.8^{\circ}\text{C}$  due to lower

temperatures upstream in the Norwegian Sea. However, in 2020/2021, temperatures increased slightly and were close to the long-term average in 2021 (1991–2020). AW salinity in the Fugløya–Bear Island section decreased strongly after peaking in 2011 and was 0.05 below the long-term average in 2021 ([Figure 4.82](#)). Salinity also showed a weak increase during the last years.

In the central Barents Sea (Kola section), coastal waters were still warmer than the 1991–2020 average throughout most of 2021, with an annual mean temperature anomaly of +0.2°C. AW temperature was generally close to average in the central part of the section (Murman Current) and below average (by 0.2°C on average per year) in its outer part (central branch of the North Cape Current). In January–April and December, AW in the central branch of the North Cape Current was colder than average by more than 0.3°C. The 2021 annual mean AW temperature in the central Kola Section (0–200 m) exceeded both the 1991–2020 average and that in 2020 by 0.1°C. Coastal and AW salinity in the Kola section was lower than the 1991–2020 average throughout 2021. The largest negative anomalies (> 0.10 in magnitude) were observed in coastal waters in the first half of 2021. In the second half of the year, salinity almost equalled the long-term mean. In AW, negative salinity anomalies varied from –0.06 to –0.11 during the year. The 2021 annual mean AW salinity in the central Kola section (0–200 m) was 0.08 lower than the 1991–2020 average and 0.03 lower than in 2020 ([Figure 4.83](#)). In the past decades, the areas of Atlantic and Arctic waters during August–September have changed substantially. The strongest rate of change occurred in the early 2000s, with a rapid increase in AW area and a corresponding reduction in Arctic Water area. The period from 2006 to 2016 was characterized by a small area of Arctic Water and high variability. From 2016 to 2021, the Arctic Water area increased and became comparable to that observed in 2004–2005. The area of cold bottom waters has been increasing the last five years since a record-low value in 2016 and reached the largest value since 2011 in 2021.

Ice coverage in the Barents Sea has increased since 2016 due to lower temperatures, but the area covered by ice in 2021 was still, in general, below the 1991–2020 average. The 2021 annual mean ice area was 3% below average, but 2% higher than in 2020. In January 2021, ice coverage (expressed as a percentage of the total sea area) was 32%, i.e. 10% below average. In February, the area covered by ice increased significantly (up to 52%) and exceeded the long-term mean by 6%. Due to much warmer-than-normal air temperatures in March and April, ice coverage in March remained the same (52%, i.e. only 3% above average) and ice melting began in April, a month earlier than usual. In April–July, ice coverage was 4–10% below average. By August, the Barents Sea was completely free of ice, and there was no ice in the sea from August to October. In November, ice coverage was 18%, i.e. 4% below average. However, in December, the area covered by ice increased significantly (up to 37%) and exceeded the long-term mean by 5%.

Volume fluxes into the Barents Sea show no long-term trends, but reveal pulses of stronger or weaker inflow. The years 2006 and 2015/2016 were extreme years, with high inflow during parts of the year. In these years, temperature of inflowing water was also high. After 2015/2016, inflow was lower, concurring with declining AW temperatures in the inflowing water. Another short pulse of higher winter inflow occurred from December 2019 to February 2020, while winter inflow in December 2020–February 2021 was low. The time-series currently stops in April 2021.

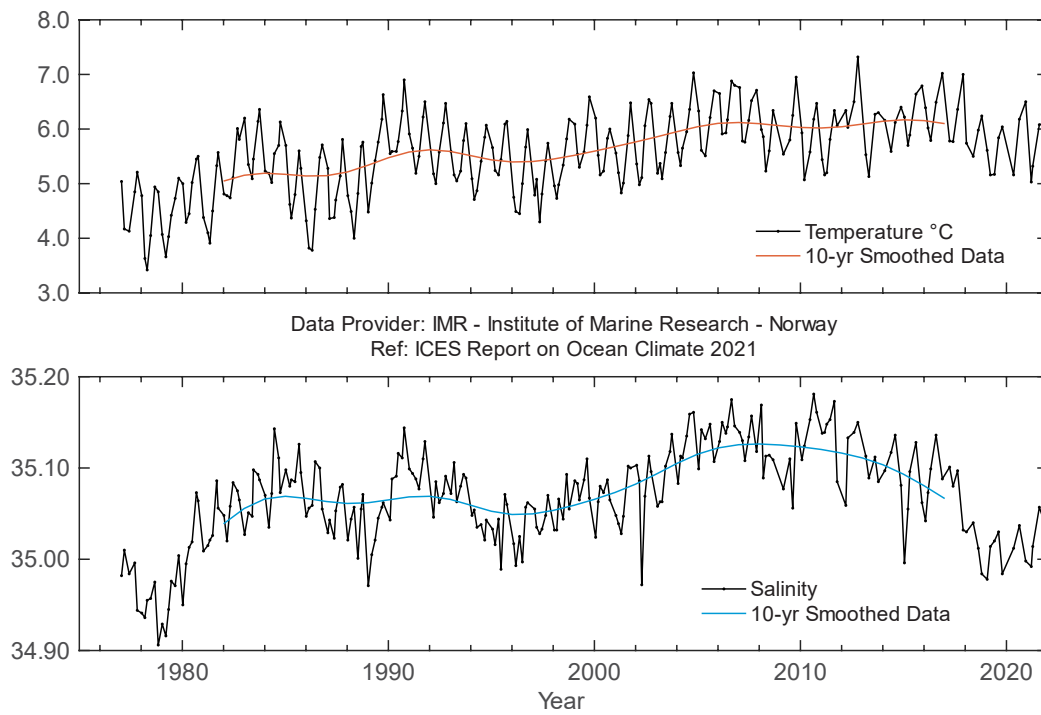


**Figure 4.82. Barents Sea. Temperature (upper panel) and salinity (lower panel) in the Fugløya-Bear Island section.**

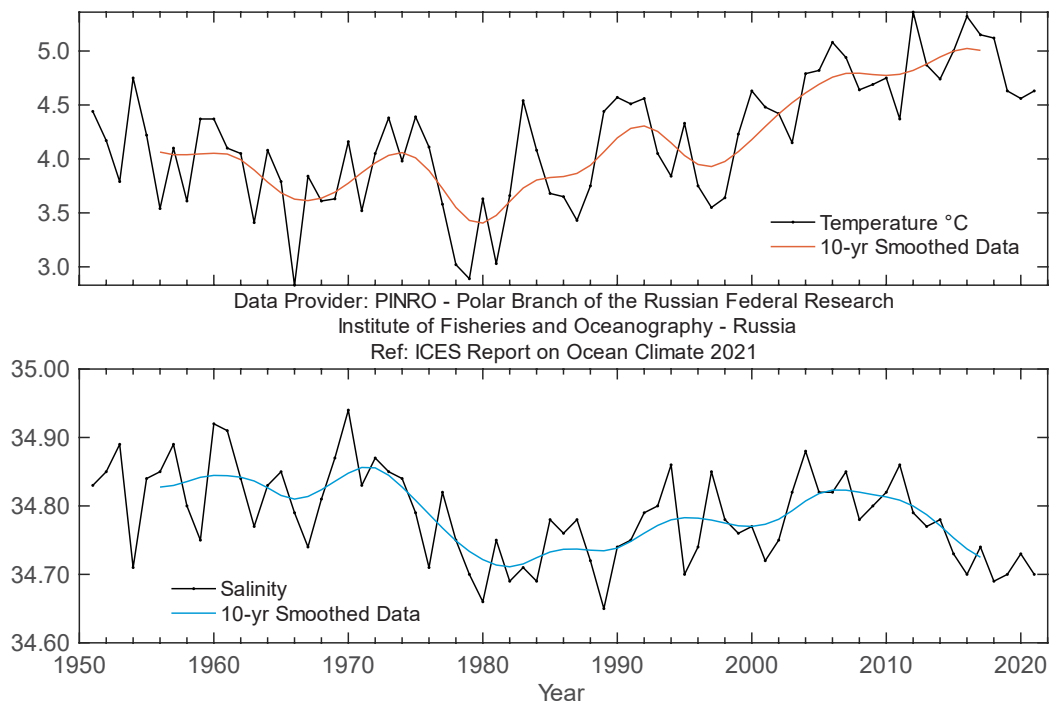


**Figure 4.83. Barents Sea. Temperature (upper panel) and salinity (lower panel) in the Kola section (0–200 m).**

## 4.22 Fram Strait

*A. Beszczynska-Möller and W. J. von Appen*

---

**IN 2021, THE TEMPERATURE OF AW CARRIED TOWARDS THE ARCTIC OCEAN ALONG THE EASTERN RIM OF THE GREENLAND SEA AND FRAM STRAIT WAS CLOSE TO OR SLIGHTLY HIGHER THAN ITS LONG-TERM MEAN, WHILE SALINITY WAS SIGNIFICANTLY BELOW. IN THE DEEP WATERS OF THE GREENLAND SEA, TEMPERATURE CONTINUED TO INCREASE, AND SALINITY REMAINED THE SAME AS IN 2020.**

---

The Fram Strait ([Figure 4.77](#)) is the northern border of the Nordic Seas. It is the only deep passage connecting the Arctic to the rest of the world oceans and is one of the main routes whereby AW enters the Arctic (the other is the Barents Sea). The AW flows along the eastern rim of the Greenland Sea, and in Fram Strait it is carried north by the West Spitsbergen Current. AW temperature, salinity, volume, and heat fluxes exhibit strong seasonal and interannual variations. A significant part of the AW also recirculates within, and shortly north of, Fram Strait and joins the flow to the south as the Return Atlantic Water (RAW). Polar Water from the Arctic Ocean flows south in the East Greenland Current (EGC) and affects water masses in the Nordic Seas.

AW temperature at the eastern rim of the Greenland Sea (along the 75°N section between 10° and 13°E) reached its highest value in 2005–2007, with a peak in 2006 ([Figure 4.84](#)). After this period, AW temperature decreased significantly in 2008/2009 and remained below its long-term mean until 2011. In 2012, AW temperature in the eastern Greenland Sea recovered and remained relatively stable with small variations (up to 0.5 s.d.) and with values exceeding the long-term mean by 0.25–0.55°C. In 2018, AW temperature slightly decreased, followed, in 2019, by a drop to 4.37°C (0.2°C below the long-term average). In 2020, AW temperature slightly increased and returned to the long-term mean (4.6°C). In 2021, it decreased again to the same value as in 2019.

A significant increase in AW salinity in the eastern Greenland Sea was observed in 2005/2006, with a maximum of 35.16 in 2006 (exceeding the long-term average by 0.06; [Figure 4.84](#)). This peak was followed by a sharp decrease in 2007 and a further slow descent until 2009, when AW salinity returned to its long-term average. In 2010, salinity started to rise again and reached its second peak in 2012 (0.06 above its long-term mean). It remained relatively steady until 2014 (with the exception of a slight decrease in 2013). Since 2015, a notable decrease in salinity has been observed and in 2020 reached the lowest value in the entire record (35.02, i.e. 0.07 below the long-term average). For 14 years (2004–2017), AW salinity in the eastern Greenland Sea was above its long-term average, but since 2018 has dropped below the long-term mean, reaching –1.8 s.d. in 2020. In 2021, salinity slightly recovered from the 2020 minimum, but still remained significantly (1.5 s.d.) below its long-term average.

The western and central part of the Greenland Sea section at 75°N has not been measured since 2010 ([Figure 4.84](#)). The temperature of Return Atlantic Water (RAW) at the western rim of the Greenland Sea reached its maximum in 2006 (2.9°C) and slowly decreased to just below the long-term average at the end of the observation period in 2010. The temperature maximum in

2006 was accompanied by a very strong peak in RAW salinity (0.13 above the long-term mean, > 3 s.d.). In 2007, RAW salinity dropped again, remained slightly higher than the long-term mean until 2008, and then decreased to close to the long-term mean in 2009 and 2010. Temperature and salinity in the upper layer of the central Greenland Basin, within the Greenland Gyre, were modified by the advection of AW and winter convection.

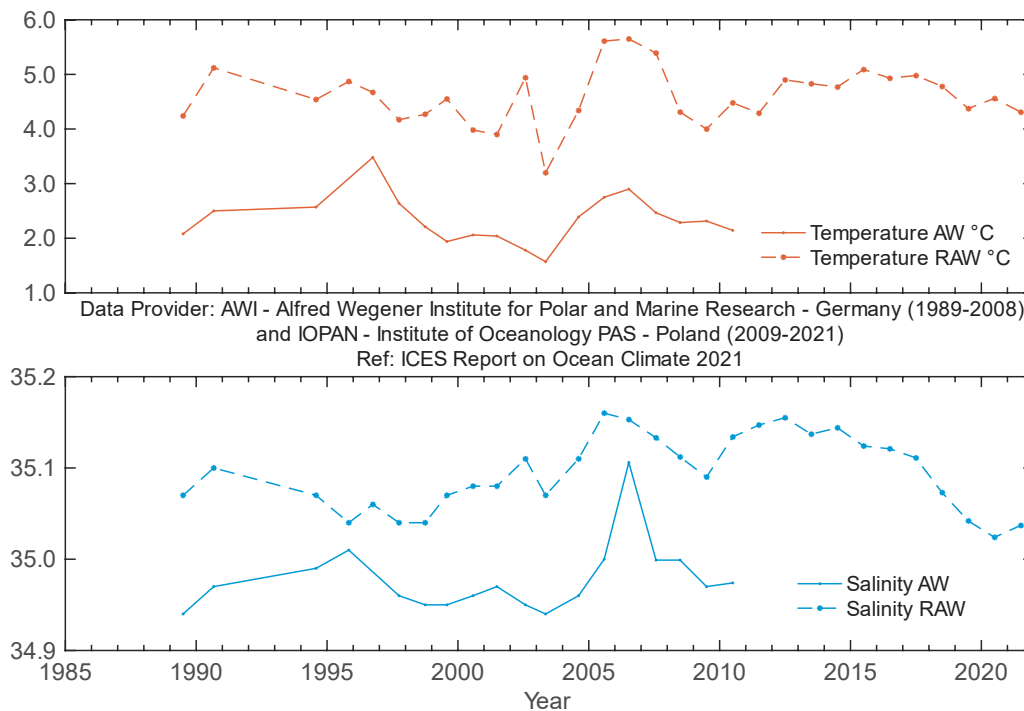


**Figure 4.84. Greenland Sea and Fram Strait. Temperature (upper panel) and salinity (lower panel) of Atlantic Water (AW) and Return Atlantic Water (RAW) in the Greenland Sea section at 75°N. AW properties are 50–150 m averages at 10–13°E. The RAW is characterized by temperature and salinity maxima below 50 m averaged over three stations west of 11.5°W. RAW has not been measured since 2010.**

In southern Fram Strait at the standard section along 76.50°N (at the level of 200 dbar, spatially averaged between 9° and 12°E), a record-high summer temperature for AW was observed in 2006 (maximum of 4.5°C, exceeding the long-term average by 1.1°C), accompanied by the highest AW salinity on record (35.13; [Figure 4.85](#)). After that peak, temperature and salinity decreased rapidly in 2007 and 2008 before increasing again in summers 2009–2012. In 2011–2015, the temperature of AW in southern Fram Strait remained relatively constant (3.7–3.8°C, exceeding its average by ca. 0.4°C) except in summer 2013, when it dropped to 3.2°C and levelled out with the long-term mean. A moderate increase has been observed since 2015, and in 2017 reached its decadal maximum of 4.1°C, the second largest value since the 2006 maximum of 4.5°C. Generally, in 2016–2018, AW temperature remained nearly constant (between 4.03°C and 4.10°C). In 2019, AW temperature dropped significantly to 3.36°C (slightly below the long-term average) and remained stable in 2020 and 2021.

In 2011, 2012, and 2014, AW salinity in southern Fram Strait was the same (35.13) as during the 2006 maximum, exceeding the long-term mean by 0.06. After recovering from a drop in 2015, AW salinity remained the same in 2016 and 2017 (0.03 above the long-term mean, about 0.7 s.d.). Since 2018, salinity has been notably decreasing, first to a minimum of 35.02 in 2019 (1.2 s.d. below the long-term average) and then in 2021 to the second lowest value on record and a minimum in the last 23 years (1.5 s.d. below the long-term average).

In northern Fram Strait at the standard section along 78.83°N, three characteristic areas can be distinguished in relation to the main flows: the West Spitsbergen Current (WSC) between the shelf edge and 5°E, the Return Atlantic Current (RAC) between 3°W and 5°E, and the Polar Water in the EGC between 3°W and the Greenland Shelf.

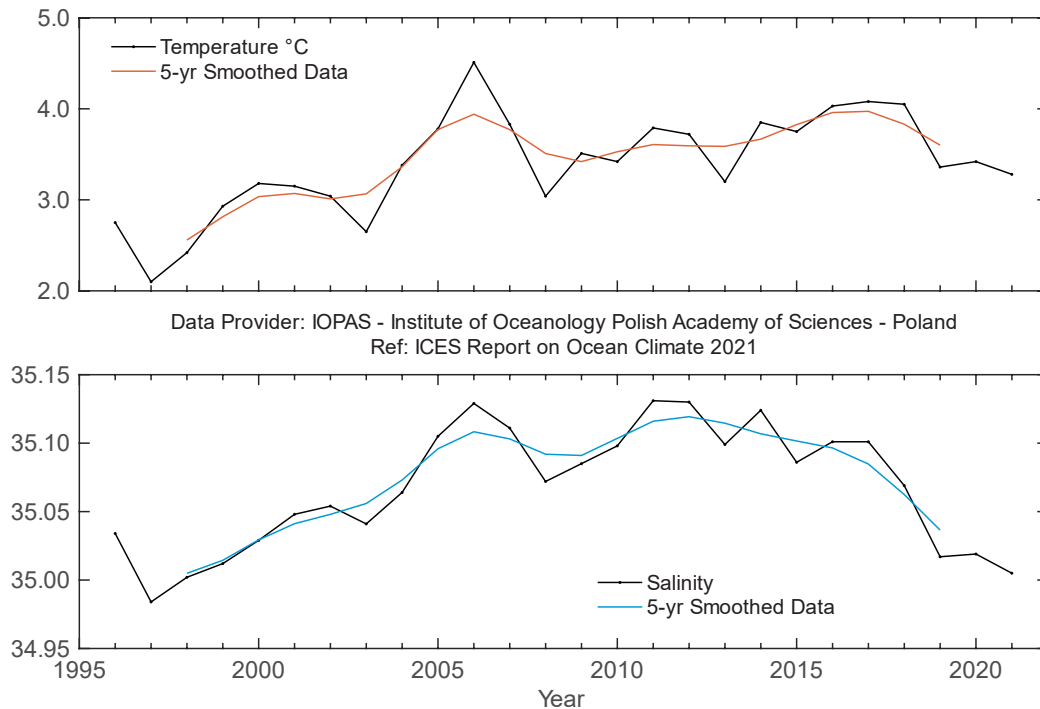


**Figure 4.85. Greenland Sea and Fram Strait. Temperature (upper panel) and salinity (lower panel) at 200 dbar in the southern Spitsbergen section (76.50°N).**

The spatially averaged mean temperature of the upper 500 m layer in the WSC reached its peak in 2006 (4.54°C) and decreased afterwards, varying in 2007–2011 within a range of ±0.4°C from the long-term average (Figure 4.86). In 2012/2013, temperature in the WSC dropped further, reaching 0.8–0.9°C below the long-term mean. From 2014 to 2017, it rose reaching the second highest value on record in 2015 (4.24°C, exceeding the long-term mean by 1°C). From 2018 to 2020, temperature decreased to 2.54°C (0.7°C colder than the long-term average), and in 2021, it rose again to 3.5°C, slightly above the long-term average.

The highest salinity in the upper 500 m in the WSC was observed in 2006 (35.11), followed by a decrease to the long-term average in 2007 and slightly below it in 2008. From 2009 to 2017, WSC salinity was high, reaching peaks in 2011 (0.43 above the long-term mean), in 2014 (35.09), and in 2017 (35.07). From 2018 to 2020, WSC salinity decreased, reaching a minimum in 2020, when the lowest salinity in over 30 years was observed (34.97; 1.8 s.d. below the long-term average). In 2021, salinity slightly increased, but still remained 1.4 s.d. below the long-term average.

At the standard section along 78.83°N, AW in the WSC core located over the upper shelf slope reached down to about 700–800 m in 2017 and 2018 (with the AW lower boundary represented by the isotherm of 2°C), while in 2016 it was found slightly shallower at about 300–600 m. In 2020, the AW layer was even shallower than in the previous year, reaching down only to 300–400 m. The core of AW flow in the WSC was also shallower in 2020 than in the three previous years, reaching down to about 300 m and being more confined to the shelf break. The offshore branch of the WSC, located over the lower shelf slope, was less pronounced and slightly

shallower in 2020 than in previous years (with the isotherm of 2°C found at the depth of about 300 m). It was also occupied by colder and significantly less saline water than in previous years. The low salinity surface layer over the WSC core, covering the upper 20–30 m in 2017, was absent in 2018–2020. In 2020, the frontal zone between Arctic- and Atlantic-origin waters in northern Fram Strait was located at about 1–1.5°E. In 2021, the AW in the WSC was significantly thicker than in 2020 and reached down to 600–700 m. The thickness of the AW layer was similar in the WSC core and its offshore branch with rather flat isopycnals, indicating wide and relatively uniform AW flow in the WSC in 2021.

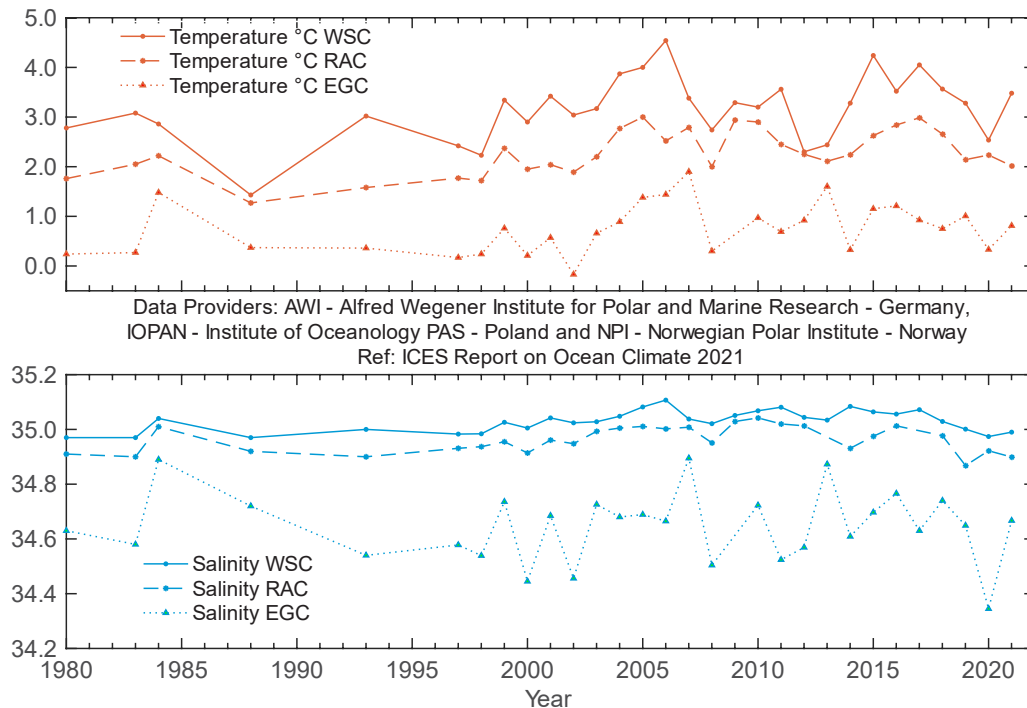


**Figure 4.86. Greenland Sea and Fram Strait. Temperature (upper panel) and salinity (lower panel) in Fram Strait (78.83°N) at 50–500 m: in the Atlantic Water (AW) in the West Spitsbergen Current (WSC; between the shelf edge and 5°E), in the Return Atlantic Current (RAC; between 3°W and 5°E), and in the Polar Water in the East Greenland Current (EGC; between 3°W and the Greenland Shelf).**

The highest temperature in the RAC was observed in 2005 (3°C) and in 2009/2010 (slightly above 2.9°C). From 2011, it decreased slowly to 2.1°C in 2013 and then increased to 2.2°C in 2014. The RAC temperature in 2016 remained close to that in 2015, but the temperature difference between AW in the WSC and that recirculating in the RAC was only half of the 2015 value (0.7°C in 2016, compared to 1.5°C). In 2017, the RAC temperature rose to the second highest value in the observation period (2.99°C), close to the 2005 maximum. Since 2018, it gradually decreased and reached 2.0°C in 2021. The maximum RAC salinity was observed in 2010. In the subsequent several years (2011, 2012, and 2014), it exceeded the long-term mean by about 0.04–0.05 before levelling out in 2015 and increasing again in 2016. In the two following years (2017–2018), RAC salinity slightly decreased; in 2019, it dropped strongly and reached a minimum in the entire observation period (34.87, 2.3 s.d. below the long-term average). In 2020 and 2021, RAC salinity was higher than the 2019 minimum, but still significantly below the long-term mean (1.7 s.d. in 2021).

In the EGC domain, temperature reached a peak in 2007 (1.9°C), decreased significantly to 0.3°C in 2008, and then remained relatively stable (within  $\pm 0.3^\circ\text{C}$  from its long-term mean) with a

slight decrease to 0.33°C in 2014 and a return to 1.0°C in 2015. In 2020, the EGC temperature dropped again to a decadal minimum of 0.33°C (the same temperature observed in 2014). In 2021, EGC temperature recovered and returned to close to the long-term average. Salinity in the EGC was highest in 2007 (34.90), close to the early maximum of 34.89 in 1984. After 2007, EGC salinity dropped and remained below the long-term average until 2020, except for an intermediate peak in 2013 (34.87), with minimum peaks in 2000 and 2002 (34.45), 2008 (close to this value), and 2020 (34.35, 2.3 s.d. below the long-term average). In 2021, salinity recovered from the 2020 minimum and exceeded the long-term average of 34.62 by 0.05 (0.4 s.d.).

## 5 Detailed area descriptions, part II: The intermediate and deep ocean

### Introduction

This section focuses on the deeper waters of the Nordic Seas and the North Atlantic, typically below 1 000 m. The general circulation scheme and dominant water masses are given in [Figure 5.1](#).



Figure 5.1. Schematic circulation of the intermediate-to-deep waters in the Nordic Seas and North Atlantic.

At the northern boundary of the region of interest, cold and dense outflow from the Arctic Ocean enters Fram Strait along its western side and reaches the Greenland Sea. The outflow is a mixture of Eurasian Basin and Canadian Basin Deep Waters and Upper Polar Deep Water (UPDW). The Eurasian Deep Water feeds the densest water in the Nordic Seas, the Greenland

Sea Bottom Water. The Canadian Basin Deep Water and UPDW supply the Arctic Intermediate Water (AIW) in the Greenland Sea, and the UPDW also includes winter convection products. The deep southward outflow from the North Atlantic in the deep western boundary current is fed by the cold and dense overflow waters. The deepest and densest is the Denmark Strait Overflow Water (DSOW). This water mass originates in the AIW produced in the Greenland and Iceland seas by winter convection and mixing with surrounding water masses. The DSOW sinks to the bottom as it passes over the Denmark Strait sill, vigorously entraining ambient water. Downstream, it is overlain by LSW, an intermediate water mass formed by deep winter convection in the Labrador Sea. The middle layer of the deep, cold-water export in the deep western boundary current is supplied by the Iceland–Scotland Overflow Water (ISOW) that originates in water masses formed in the Norwegian Sea [AIW and Norwegian Sea Deep Water (NSDW)]. While passing through the Iceland Basin, ISOW also entrains upper ocean water and LSW. The deep Antarctic Bottom Water enters the North Atlantic on the western side, but its signature is also present in eastern Atlantic abyssal basins. At intermediate levels, MW originates from vigorous mixing of Atlantic central waters and MOW at the Gulf of Cadiz. This water mass spreads at about 1 000 m depth in all directions, with a main vein progressing northwards along the European margin. Around the Canaries, MW encounters the northern limit of AAIW.

## 5.1 Nordic Seas

The deep waters of the Greenland, Iceland, and Norwegian seas are all warming. The source of the warming is the deep outflow from the Arctic Ocean, a south-flowing current of the Eurasian and Canadian Basin Deep Waters, and the UPDW found on the western side of Fram Strait at ca. 2 000 m depth. The Greenland Sea Deep Water (GSDW) is warming fastest owing to its direct contact with this Arctic outflow, whereas the Iceland and Norwegian seas are warming more slowly because they are products of the mixing of their own ambient waters with GSDW and Arctic outflow water.

### 5.1.1 Greenland Sea

#### *A. Beszczynska-Möller*

Continuous warming has been observed in the Greenland Sea deep layer at 3 000 m, both in the Greenland Sea Gyre (not measured since 2011) and in the eastern part of the deep basin (at 005°E, measured since 2001; [Figure 5.2](#)). GSDW temperature changes have been similar at both locations, with a relatively steady increase from  $-1.18^{\circ}\text{C}$  to  $-0.86^{\circ}\text{C}$  between 1993 and 2021. In 2021, deep water temperature exceeded its long-term average of  $-1.01^{\circ}\text{C}$  (for 1993–2020) by  $0.15^{\circ}\text{C}$  (1.6 s.d.). The strongest temperature increase of  $0.03^{\circ}\text{C}$  was found between 2010 and 2011, while recent year-to-year temperature changes have been lower (between 0 and  $0.02^{\circ}\text{C}$ ). Between 2020 and 2021, the deep water in the eastern Greenland Sea warmed by  $0.005^{\circ}\text{C}$ . For the entire observing period (1993–2021), the average GSDW warming rate can be estimated at  $0.11^{\circ}\text{C decade}^{-1}$ .

Warming of deep waters in the Greenland Sea is accompanied by an increase in salinity. However, the interannual variability in salinity differs between the central Greenland Sea Gyre (observation period during 1993–2010) and the eastern Greenland Sea (measured since 2001). A relatively steady increase in salinity from 34.901 in 1993 to 34.916 in 2010 was observed in the Greenland Sea Gyre. In the eastern part of the deep Greenland Sea, year-to-year changes are

much stronger than in the central gyre, but the overall trend for 2001–2020 is positive and similar to that in the central basin. The overall salinity increase is of the order of  $0.01 \text{ decade}^{-1}$ . The highest salinity on record (34.920) was recorded in 2020 and replicated in 2021, and the second highest salinity (34.919) was observed in 2015, 2017, and 2019. In the last decade, salinity in the deep layers of the eastern Greenland Sea has remained above the long-term average, exceeding it by 1.5 s.d. in 2020 and 2021.

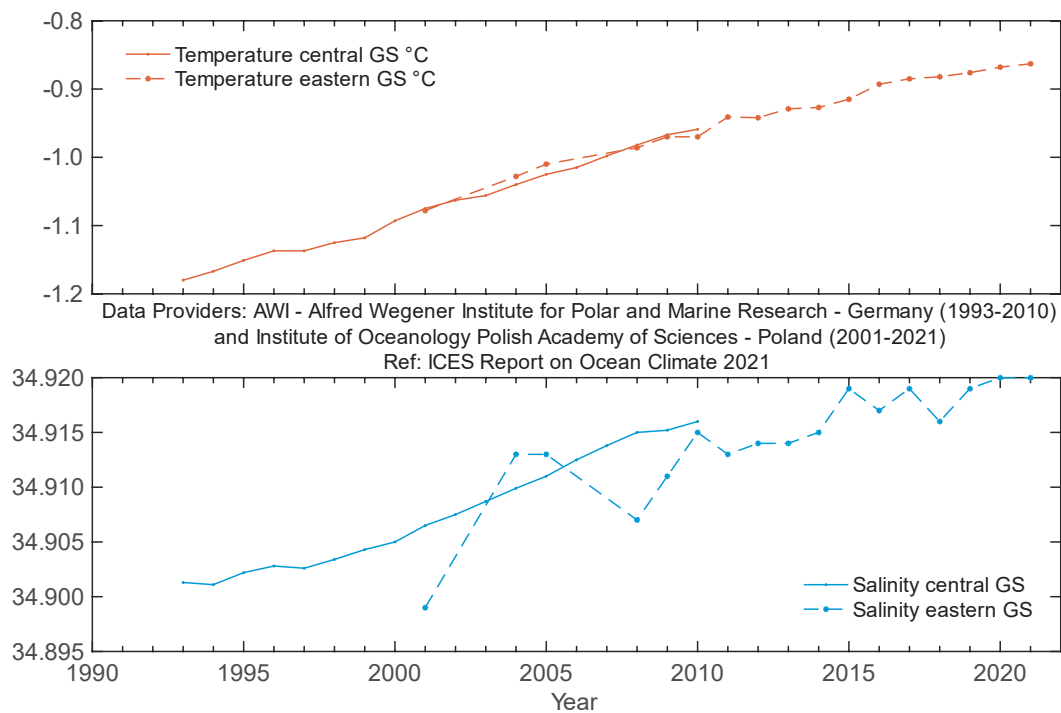


**Figure 5.2. Greenland Sea and Fram Strait. Temperature (upper panel) and salinity (lower panel) at 3 000 m in the Greenland Sea section at 75°N (solid line: in the central Greenland Sea Gyre; dashed line: in the eastern Greenland Sea at 005°E).**

## 5.1.2 Norwegian Sea

### *S. Østerhus*

The longest time-series in the Nordic Seas is from the ocean weather ship station M at 66°N 2°E in the Norwegian Sea. It reveals persistent warming from the mid-1980s (Figure 5.3). The weather-ship station M was permanently occupied by weatherships from 1948 to 2009. During this period, temperature and salinity were observed weekly in the NSDW by means of Nansen bottles equipped with reversing thermometers. Water samples were analysed for oxygen content on board and salinity concentration ashore after each cruise, which usually lasted one month. Since 2009, station M has been occupied three to eight times per year, and temperature and salinity profiles are obtained by use of a CTD. In 2021, station M was occupied three times, but only two stations contain data from 2 000-m depth. The increased variation in temperature during the last decade is probably due to the small numbers of observations.

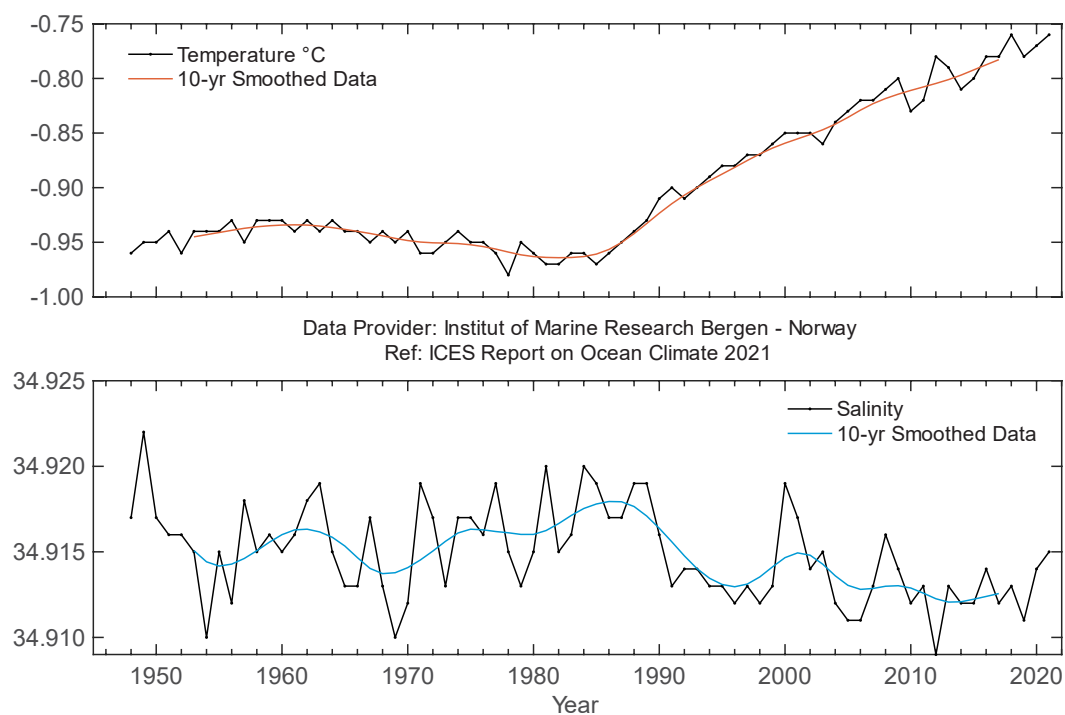
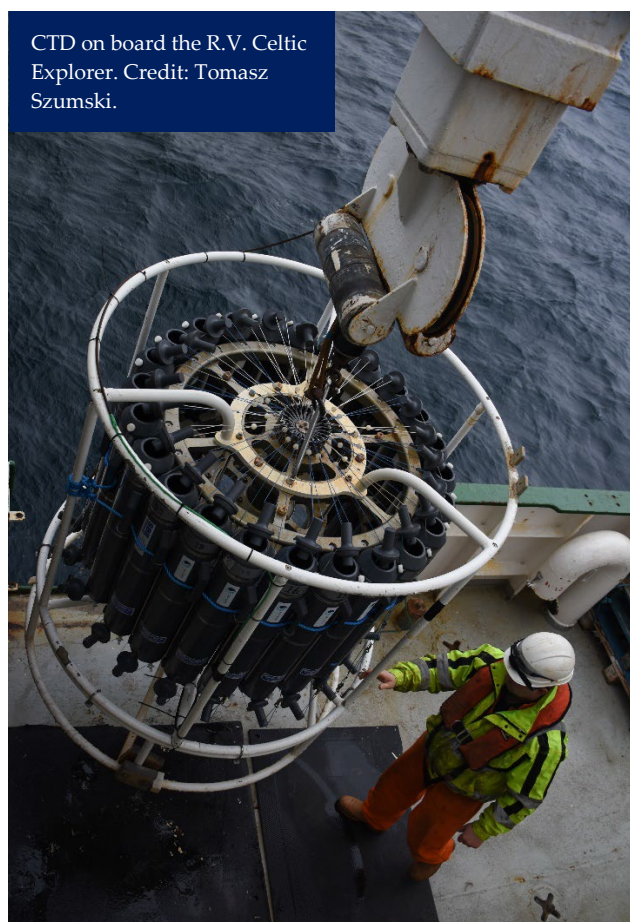


Figure 5.3. Norwegian Sea. Temperature (upper panel) and salinity (lower panel) at 2 000 m at ocean weather station M (66°N 002°E).



### 5.1.3 Iceland Sea

*S. R. Ólafsdóttir and M. Danielsen*

In the Iceland Sea, an increase in temperature in the depth range 1 500–1 800 m has been observed almost continuously since the beginning of the time-series in the early 1990s to the latest measurement at the end of 2021 (Figure 5.4). Overall, deep water in the eastern part of the Iceland Sea has warmed 0.2°C in 30 years. On average, this equates to 0.06°C decade<sup>-1</sup>, although the trend for the last decade was slightly higher. Similar trends have not been observed in salinity.

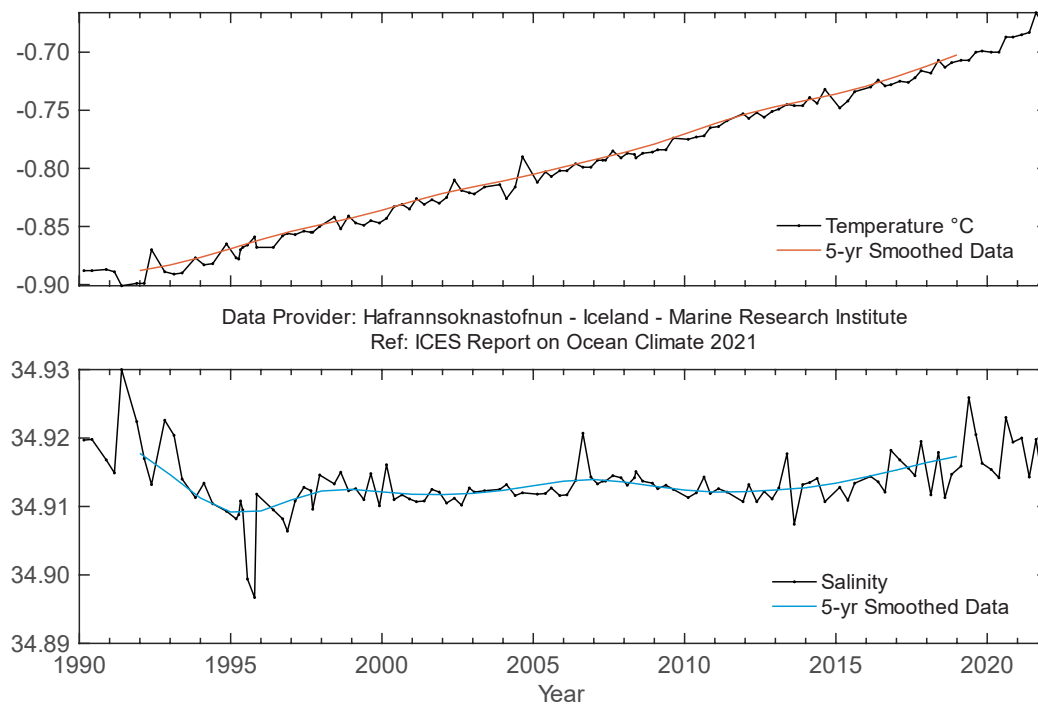


Figure 5.4. Icelandic Waters. Temperature (upper panel) and salinity (lower panel) at 1 500–1 800 m in the Iceland Sea (68.00°N 012.67°W).

## 5.2 North Atlantic

### 5.2.1 Iceland–Scotland Ridge overflow waters

*B. Berx and B. Rabe*

In the deep layers of the Faroe–Shetland Channel, the properties at 800 m correspond to NSDW that passes through the Channel back into the North Atlantic.

Due to reference levels being defined by depth coordinates rather than by water mass properties, the time-series shows some variability. In general, temperature of the deep water has decreased from the 1950s to the 1990s (Figure 5.5). Following a period of fluctuations with both increasing and decreasing temperatures, there has been an unabated increasing trend since about 2000. This warming trend continues in 2021, and temperatures are now close to the highest observed in the early 1980s. The same pattern can also be seen in the deepest layers of the Faroe–Shetland Channel (time-series data not shown).

Relatively stable salinity was observed in the first period of measurements (1950 to mid-1970s), which was followed by a slow freshening until the mid-1990s. The lowest annual mean salinity values were observed in 1997, after which there was a slow, but gradual, increase until the late 2010s (Figure 5.5). This trend in increasing salinity appears to have slowed in recent years.

The observed long-term changes in temperature and salinity in the deep waters of the Faroe–Shetland Channel are in general agreement with those observed in the Norwegian Sea, further upstream in the circulation pathway.

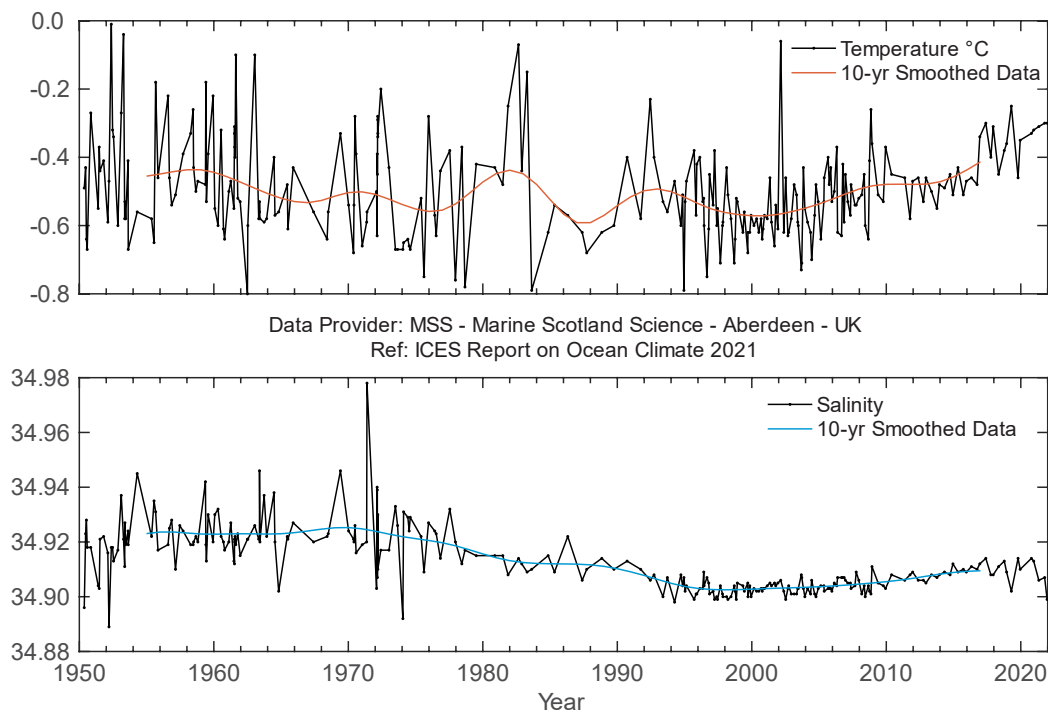


Figure 5.5. Faroe–Shetland Channel. Temperature (upper panel) and salinity (lower panel) at 800 m.

## 5.2.2 Iceland Basin

*S. Jones*

In the Iceland Basin, LSW is the dominant water mass below about 1 000 m, evident as a large recirculating body of relatively fresh and low stratified water with a core that lies between 1 700 and 2 000 m (Holliday *et al.*, 2015). After the NSDW flows through the Faroe–Shetland Channel and Faroe Bank Channel and into the Iceland Basin, it becomes known as ISOW (Figure 5.1). The dense water, supplemented by a small amount of additional flow over the sill between Iceland and the Faroes, mixes rapidly with the upper ocean and intermediate water of the Iceland Basin, entraining the lighter water and increasing the volume of the overflow plume. Therefore, ISOW properties measured at 20°W in the Iceland Basin are a product of the properties of the dense water at the sill and the entrained ambient water. ISOW temperature and salinity vary closely with the LSW and upper ocean water in the Iceland Basin. Between 1996 and 2011, the water warmed and increased in salinity, while between 2011 and 2017, there was a gradual decrease in both temperature and salinity (Figure 5.6). The Ellett Line transect has not been occupied since 2017, and Argo floats do not adequately sample the deepest waters in Iceland Basin, so no observations were possible for the deep-water time-series in 2021 (Figure 5.7). However, for the intermediate water, time-series observations from Argo floats

show that temperature and salinity remained near average from 2016 to 2021 with no evidence of the deep freshening or the partial recovery observed in the upper waters.

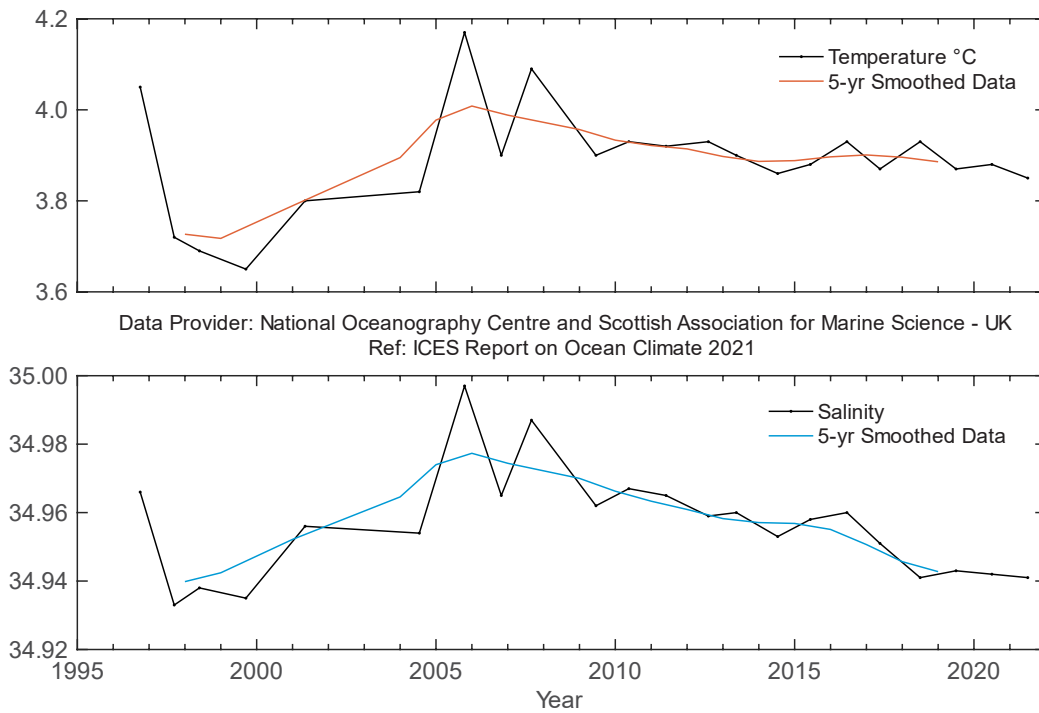


**Figure 5.6. Iceland Basin. Temperature (upper panel) and salinity (lower panel) of Labrador Sea Water (LSW;  $27.70 \leq \sigma_\theta \leq 27.85 \text{ kg m}^{-3}$ , ca. 1 200–2 000 m). Data until 2017.**

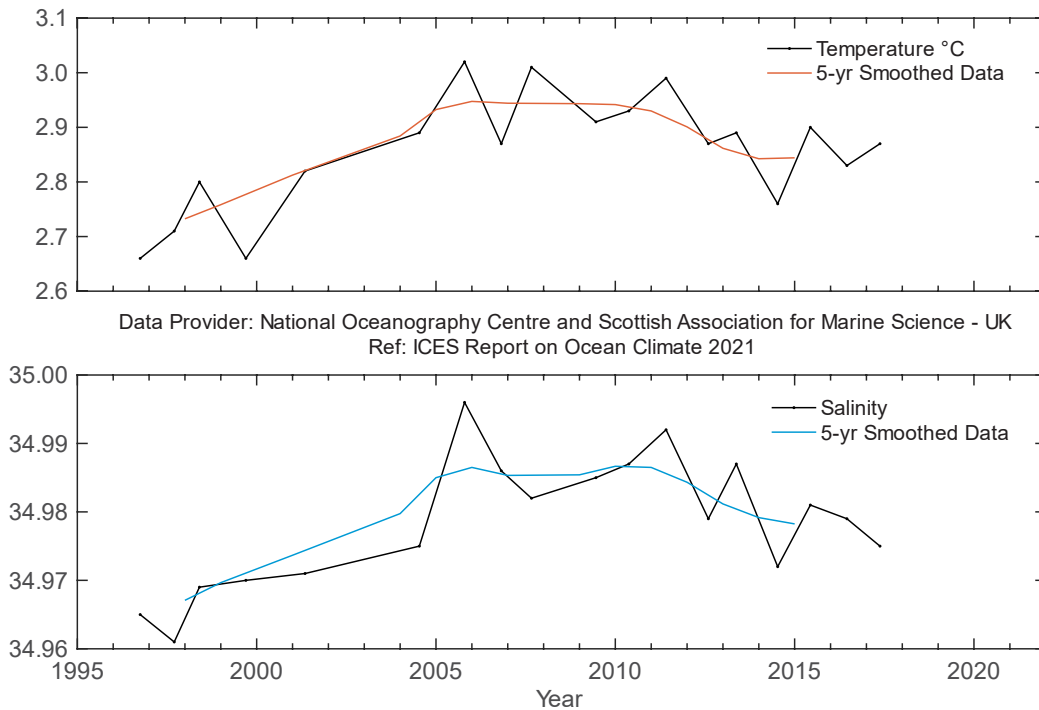


**Figure 5.7. Iceland Basin. Temperature (upper panel) and salinity (lower panel) of Iceland–Scotland Overflow Water ( $\sigma_\theta > 27.85 \text{ kg m}^{-3}$ , ca. 2 000–2 600 m).**

### 5.2.3 Rockall Trough

*S. Jones*

In Rockall Trough, the dominant water mass below about 1 500 m is LSW, which usually has its maximum concentration between 1 700 and 2 000 m. East of the Anton Dohrn seamount, LSW core tends to be characterized by a minimum in salinity and potential vorticity, although its patchy temporal distribution (possibly due to aliasing of mesoscale eddies) results in a noisy year-to-year signal. Over the time-series, there have been no significant long-term trends observed ([Figure 5.8](#)). From 1975 to the mid-1990s, there was a cooling and freshening trend, which was followed by gradual warming and increasing salinity. In 2021, LSW potential temperature and salinity derived from Argo observations were both close to the 1991–2020 mean.

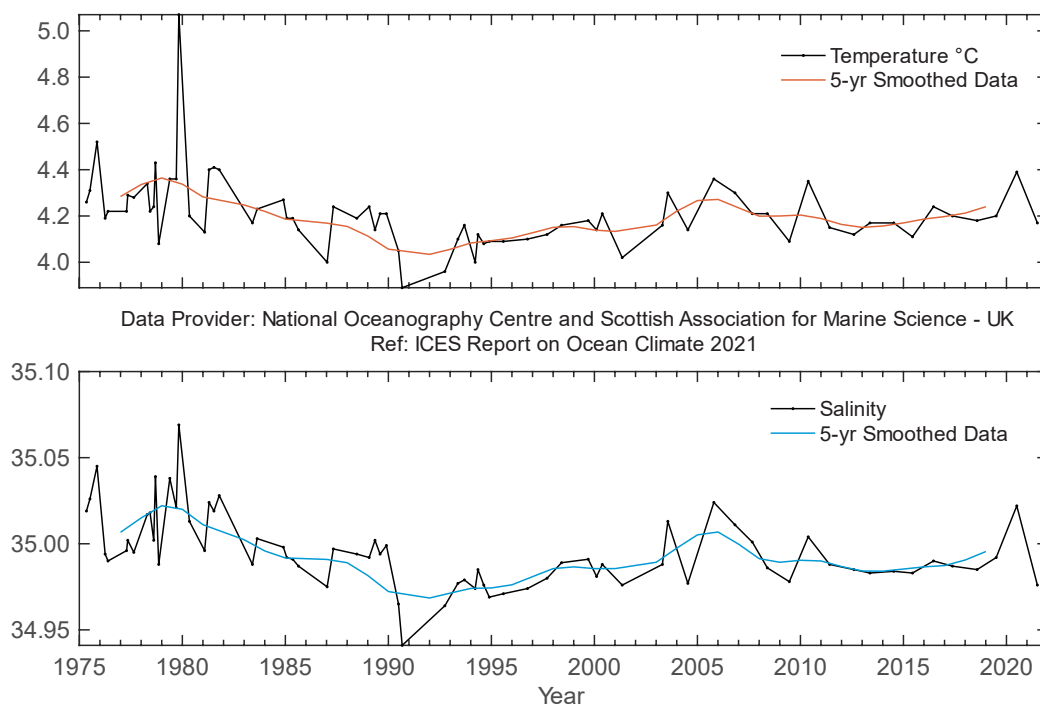


**Figure 5.8. Rockall Trough. Temperature (upper panel) and salinity (lower panel) of Labrador Sea Water ( $27.70 \leq \sigma_{\theta} \leq 27.85 \text{ kg m}^{-3}$ , ca. 1500–2000 m).**

### 5.2.4 Irminger Basin

*M. F. de Jong*

Temperature and salinity remained high in 2021 compared to most of the record. There has been a slight cooling and freshening since the maxima of salinity in 2014 and temperature in 2018 ([Figure 5.9](#)). Salinity in 2021 was 0.021 above the 1990–2020 mean (0.77 s.d.) and temperature was 0.208 above the 1990–2020 mean (1.27 s.d.). Within the overall trend of increasing temperature, slight drops in temperature were observed after winters with deep convection in the Irminger Sea in 2009 and 2013–2015. However, in most winters, convection does not reach into the 1 600–2 000 m layer. In the years leading up to 2021, moderate winters combined with strong stratification led to weak convection.

In 2020, the DSOw freshened to the lowest salinity in the last 15 years ([Figure 5.10](#)). This was likely due to entrainment of fresher upper layer waters from the subpolar fresh anomaly into

the DSOW at the overflow. In 2021, the DSOW returned to a slightly higher salinity, and the anomaly compared to the 1990–2020 mean is now  $-0.011$  (compared to  $-0.020$  in 2020). Temperature has decreased and now has a  $-0.114$  anomaly compared to the long-term mean. The higher salinity and lower temperature in 2021 lead to an increase in the overflow water density compared to 2020.

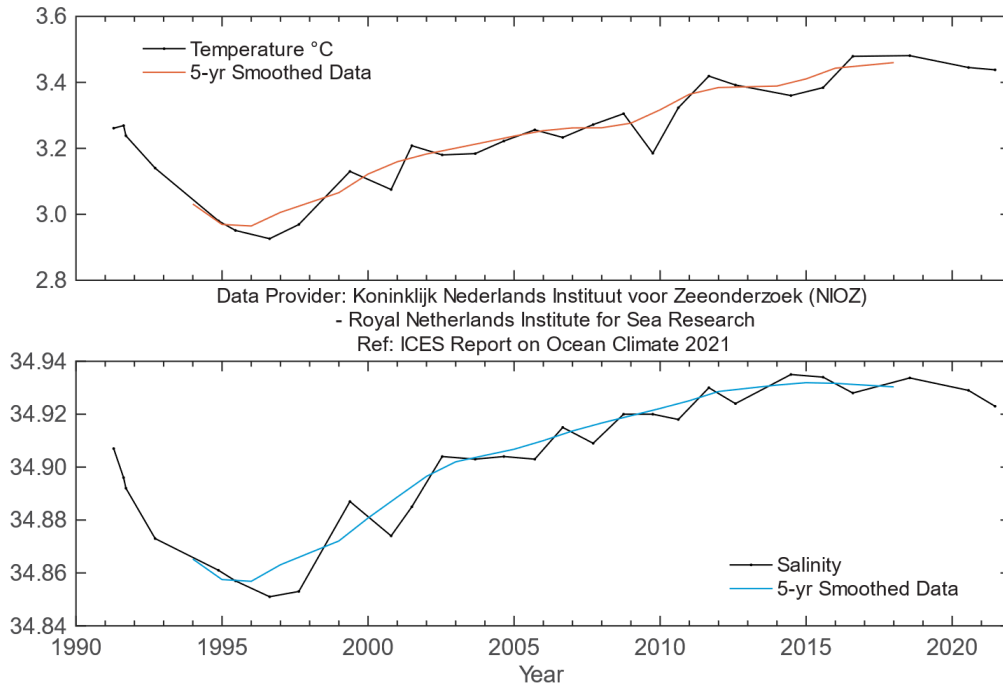


**Figure 5.9. Irminger Sea. Temperature (upper panel) and salinity (lower panel) of Labrador Sea Water (LSW; averaged over 1 600–2 000 m).**

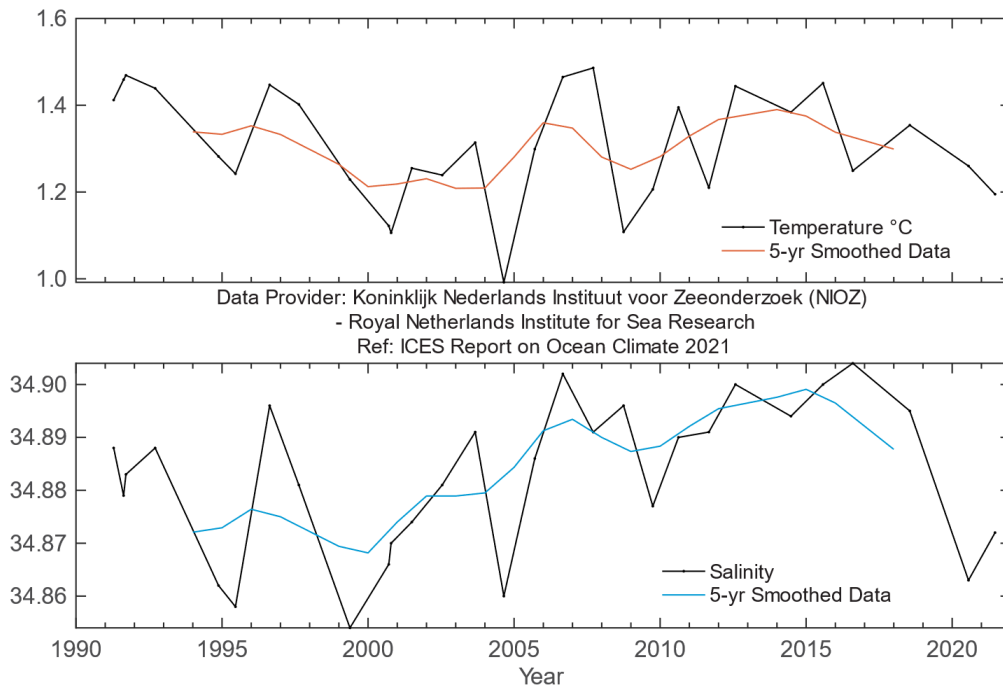


**Figure 5.10. Irminger Sea. Temperature (upper panel) and salinity (lower panel) in Denmark Strait Overflow Water (DSOW) on the East Greenland slope.**

### 5.2.5 Labrador Basin

*I. Yashayaev and B. Cisewski*

In the Labrador Sea, the 1 000–1 800 m depth layer average temperature and salinity decreased between the beginning of the 1970s and the early 1990s by about 0.9°C and 0.09, respectively. In 2011, less than two decades after reaching this record minimum, temperatures were as high as in 1970, when the previous maximum was observed, and salinity was at its highest since 1971. These increasing trends were interrupted in winter 2012 by strong convection, resulting in cooling of the deep intermediate layer (1 000–1 800 m). Its temperature continued to decrease during the five subsequent years (2013–2017), stabilized over the next three years (2018–2020), and started to increase again in 2021. A freshening trend accompanied the recent cooling of the deep intermediate layer, but ended a year earlier than the decrease in temperature in 2016. Subsequently, the 1 000–1 800 m depth layer average salinity increased slightly between 2016 and 2017/2018, decreased in 2019/2020, and stabilized, remaining nearly unchanged in 2021 (Figure 5.11).

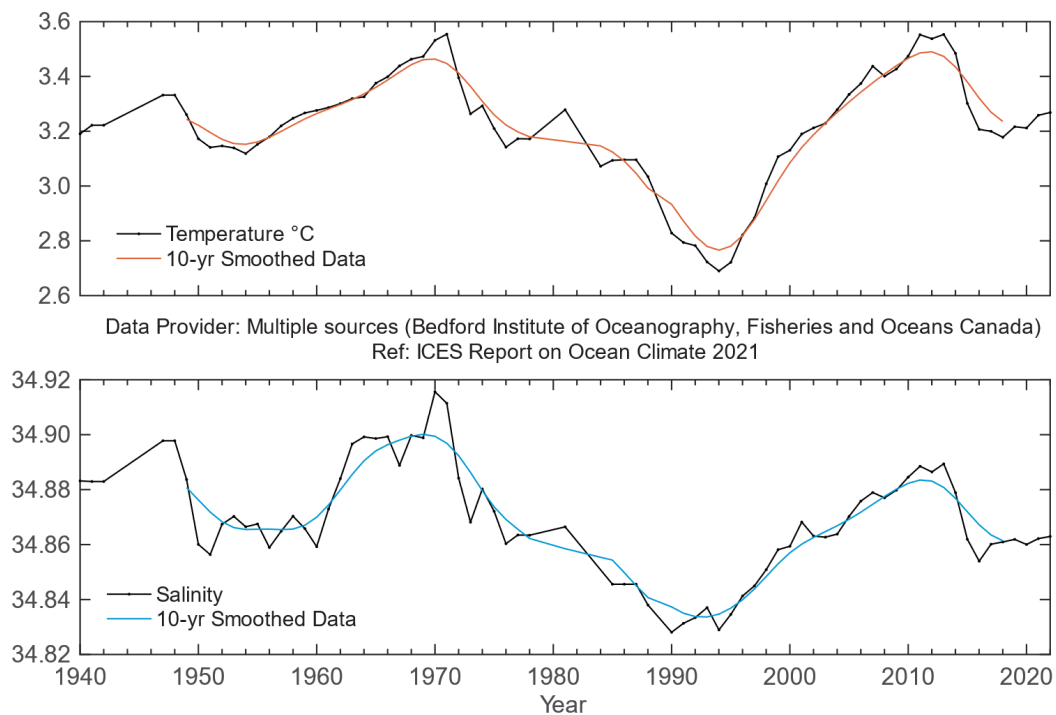
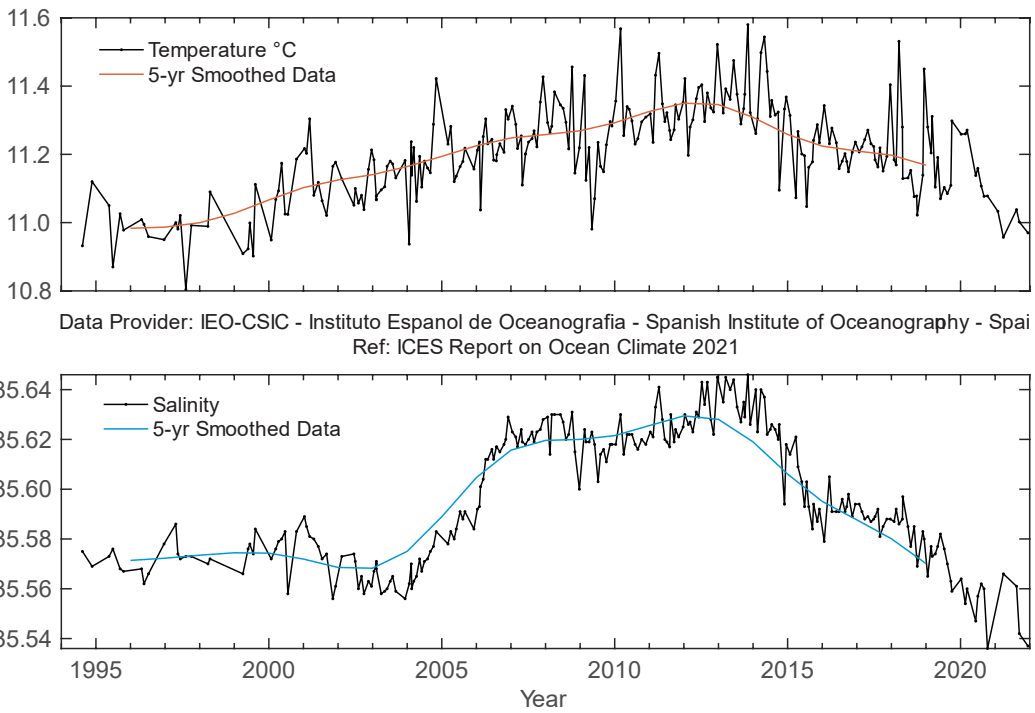


Figure 5.11. Labrador Sea. Temperature (upper panel) and salinity (lower panel) anomalies in the deep intermediate layer of the Labrador Sea (averaged over 1 000–1 800 m). Time-series are constructed as described in Figure 4.8.

### 5.2.6 West Iberian margin

*C. González-Pola, R. Somavilla, and R. Graña*

The entire water column down to 1 000 m (the depth corresponding to the core of MW) has been sampled at the outer slope stations in Santander (Figure 4.38) on a monthly basis since the early 1990s (González-Pola *et al.*, 2005). Warming for two decades, from the mid-1990s until the mid-2010s, is evident at most layers, specifically those corresponding to the ENACW (300–600 m; Figure 5.12) and upper MW (600–1 000 m; Figure 5.13).



**Figure 5.12. Bay of Biscay. Potential temperature (upper panel) and salinity (lower panel) for the 300–600 m layer at Santander Station 7.**

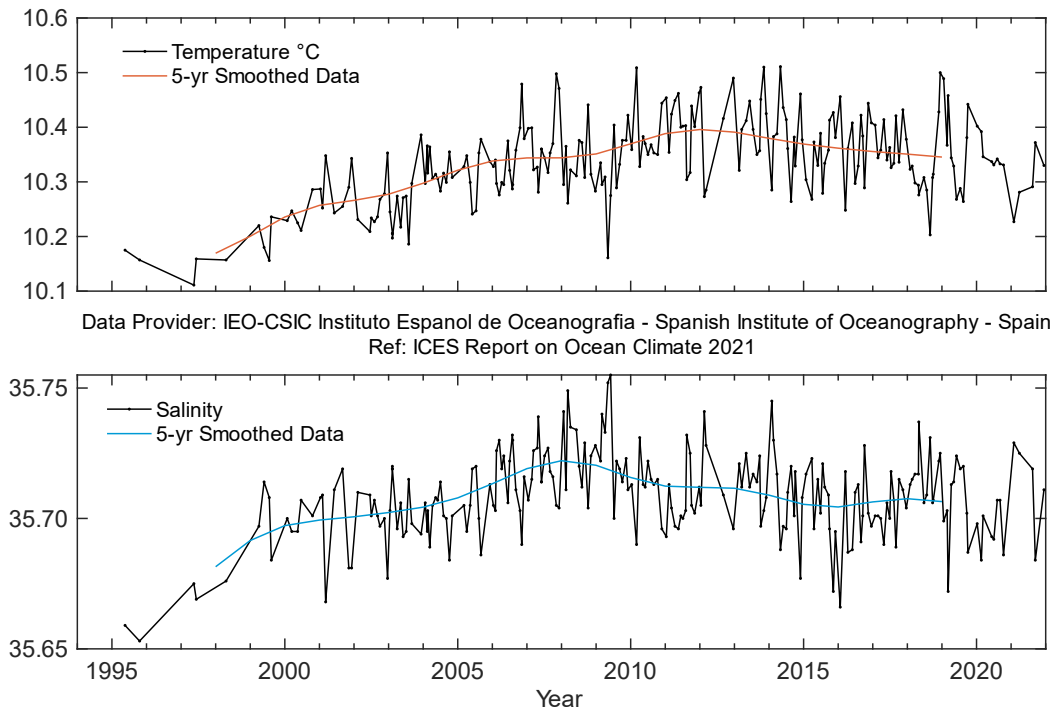


**Figure 5.13. Bay of Biscay. Potential temperature (upper panel) and salinity (lower panel) for the 600–1 000 m layer at Santander Station 7.**

The evolution of the water masses in the west Iberian margin has been strongly influenced by a significant shift in the salinity of the lower ENACW (ca. 400 m) in 2005, after the occurrence of very strong winter mixing (Somavilla *et al.*, 2009). In 2014, the upper central waters showed freshening and cooling for the first time in about a decade. The initial large drop was followed by a two-year stabilization (2016–2017) before continuing, dropping from 2018 onwards. Salinity above 400 in 2021 was at its lowest levels since the start of the record in the early 1990s, while temperature was approaching the coldest values of the time-series. Deeper water masses (at the level of the MW, ca. 1 000 m) have followed a weak freshening trend since a salinity maximum in 2007–2009.

Since 2003, a programme designed to supplement the monthly monitoring of the upper ocean in the area has monitored waters deeper than 1 000 m and the full water column (> 5 500 m) at the west Iberian margin deep (Prieto *et al.*, 2015). Cruises were carried out semi-annually during 2003–2010 and annually after that. The Finisterre section, measuring roughly ~ 400 km long, starts west of the Iberian Peninsula (43.0°N 9.3°W) and reaches the centre of the Iberian Abyssal Plain (43.0°N 15.5°W).

The Finisterre section provides information about upper, intermediate, and deep waters. The limit of the intermediate waters is considered to be near 2 000 m depth, where the core of LSW and the base of the permanent thermocline are typically centred. From the core of MW to the core of LSW, there is a strong gradient and some coherence in variability, indicating the influence of large-scale atmospheric patterns. A 3–4 year see-saw can be observed for both temperature and salinity, superimposed over a decreasing background trend ([Figure 5.14](#)).

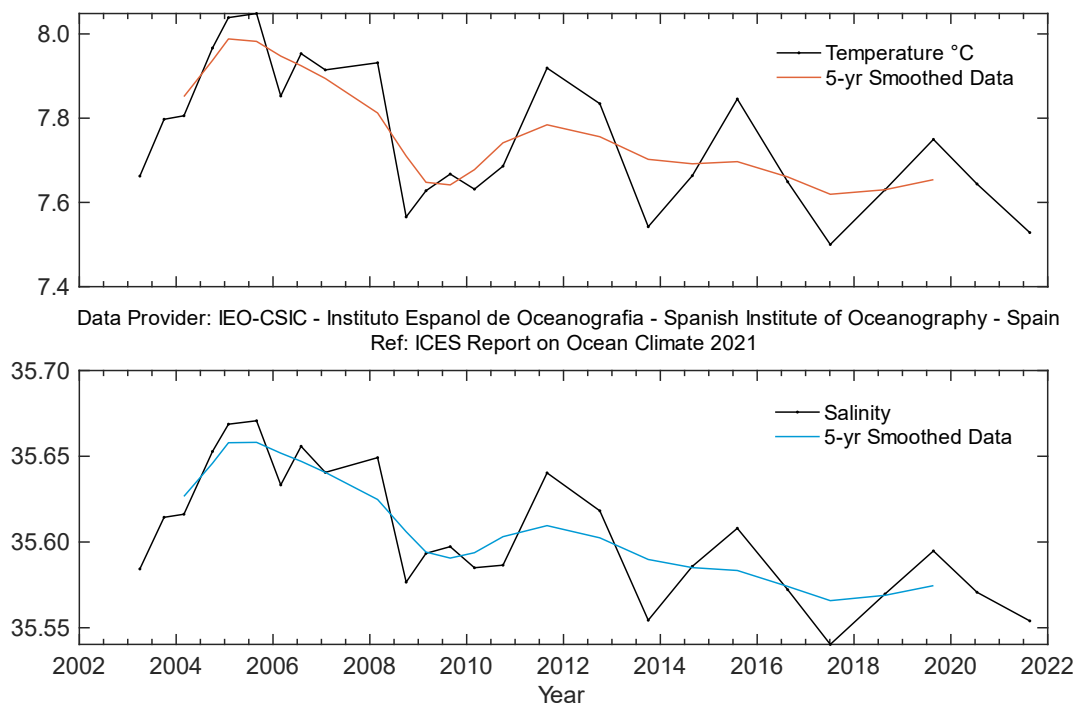


**Figure 5.14. Western Iberian margin. Potential temperature (upper panel) and salinity (lower panel) for the 800–2 000 m layer averaged across the Finisterre section.**

The abyssal waters in this basin are NADW (composed of a mixture of all Arctic water masses) and what is known as Lower Deep Water, which reflects a signature of Antarctic-origin waters. Interannual variability for these abyssal waters within the monitored period has been weak ( $<0.1^{\circ}\text{C}$  and 0.01 in salinity). A weak, but progressive, pattern of cooling and freshening around 2 000 to 3 000 m can be observed. As a whole, temperature and salinity in the water layers between 2000 m and the bottom remain close to long-term mean values ([Figure 5.15](#)).

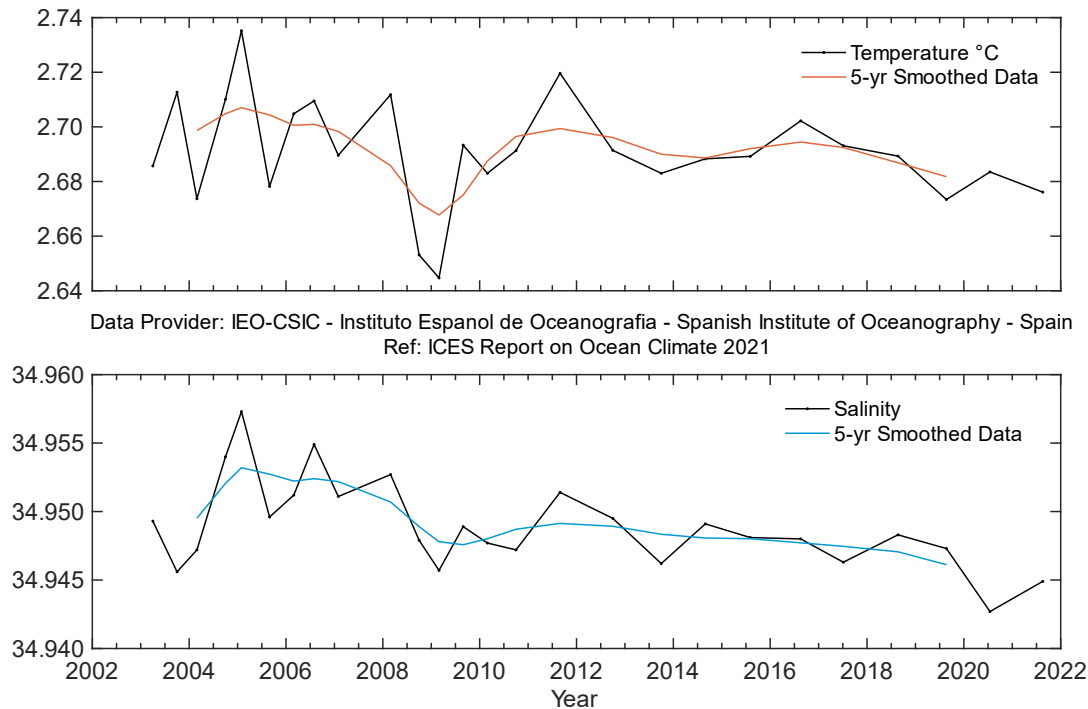


**Figure 5.15.** Western Iberian margin. Potential temperature (upper panel) and salinity (lower panel) for the 2 000–5 500 m layer averaged across the Finsiterre section.

## 5.2.7 Gulf of Cadiz

*R. Sánchez-Leal*

The outer stations in the STOCA sections ([Figure 4.43](#)) sample the ENACW (100–300 m; [Figure 5.16](#)) and the MOW (300 m–seabed; [Figure 5.17](#)).

A strong seasonal signal exists that obscures underlying patterns. However, since the commissioning of the STOCA programme in 2009, the ENACW layer has shown a consistent, statistically-significant freshening trend ( $-0.10$  to  $-0.15$  decade $^{-1}$ ) that is sustained over time. This freshening coincides with a slight statistically significant cooling trend ( $0.30^{\circ}\text{C}$  decade $^{-1}$ ). Cooling and freshening became stronger in 2020 and 2021. Since 2018, this station has been exceeding the minimum salinity on record each year, with a new minimum in 2021 of 35.8.

The depth level occupied by MOW (350–550 m) has been showing the opposite trend, with a statistically significant salinity increase during 2009–2021 ( $0.13$  decade $^{-1}$ ). This is evident in the yearly means and also in the annual (summer) minima, which increased from 36.0 in 2010 to 36.2 in 2021.

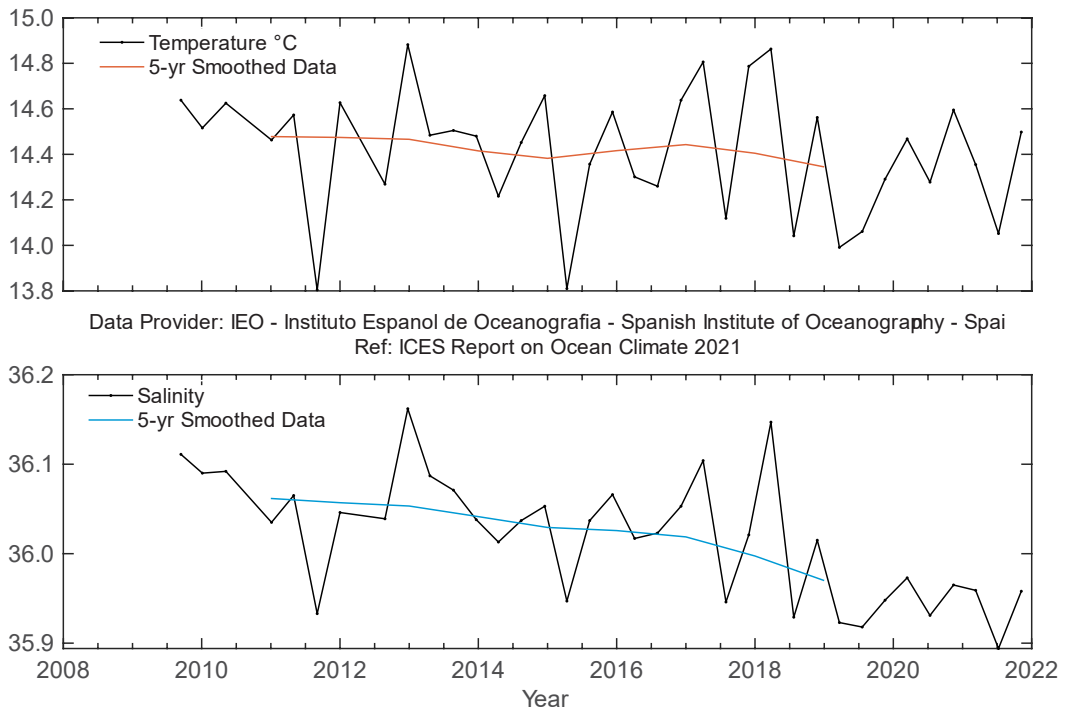


**Figure 5.16.** Gulf of Cadiz. Potential temperature (upper panel) and salinity (lower panel) for the 100–300 m layer at STOCA SP6.

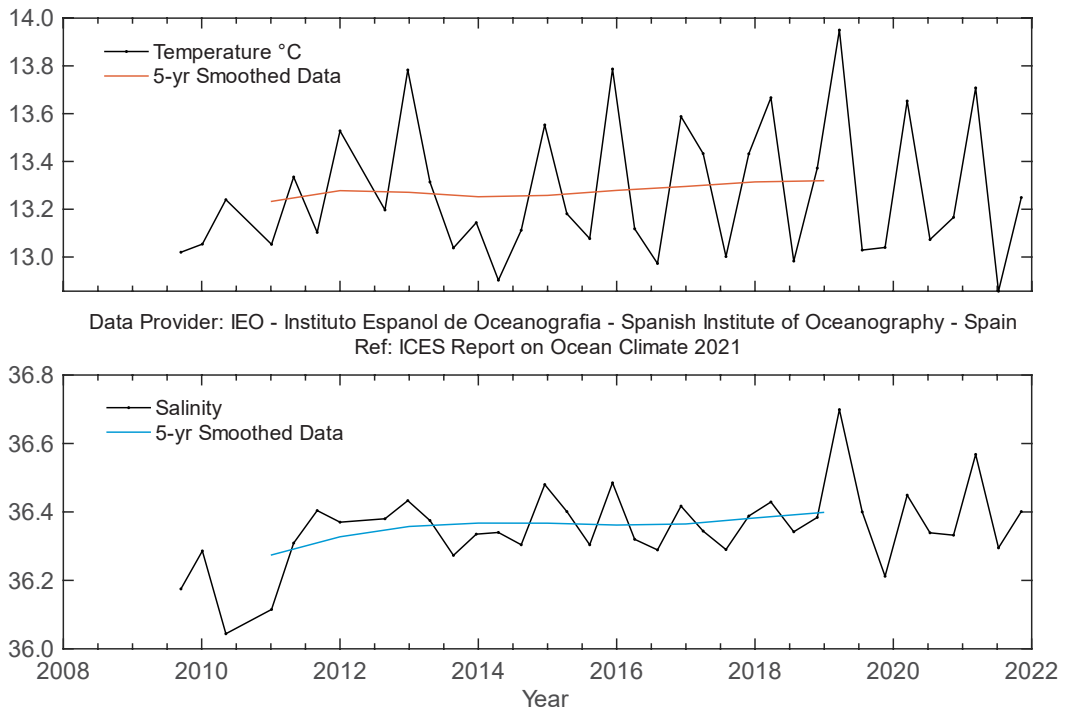


**Figure 5.17.** Gulf of Cadiz. Potential temperature (upper panel) and salinity (lower panel) for the 300–600 m layer at STOCA SP6.

### 5.2.8 Canary Basin

*P. Vélez-Belchí, A. Mosquera, and C. Presas-Navarro*

Since the 1990s, there has been an overall weak cooling and decreasing salinity trend in the Canary Basin. In the CTZ, the intermediate waters are dominated by AAIW and show a low, non-statistically significant, decrease in temperature ( $-0.01 \pm 0.06^\circ\text{C decade}^{-1}$ ) and salinity ( $-0.007 \pm 0.015^\circ\text{C decade}^{-1}$ ). Data from 2021 confirms this trend (Figure 5.18). It should be noted that in 2020, in oceanic waters for the stratum corresponding to intermediate waters (800–1 400 m), a Mediterranean water eddy (meddie) was sampled and, therefore, the values for 2020 are not representative of intermediate waters.

Both time-series show high variability due to the two very different intermediate water masses present in the region: MW and AAIW.

In the layer corresponding to the upper NADW (1 700–2 600 m), there are overall long-term weak warming and freshening trends that are not statistically significantly different from zero. In the stratum corresponding to the lower NADW (2 600–3 600 m), a small statistically significant freshening ( $-0.002 \pm 0.001 \text{ decade}^{-1}$ ) can be observed, consistent with the observation from the upper NADW (Figure 5.19). However, no trend can be confirmed for temperature ( $-0.00 \pm 0.01^\circ\text{C decade}^{-1}$ ).

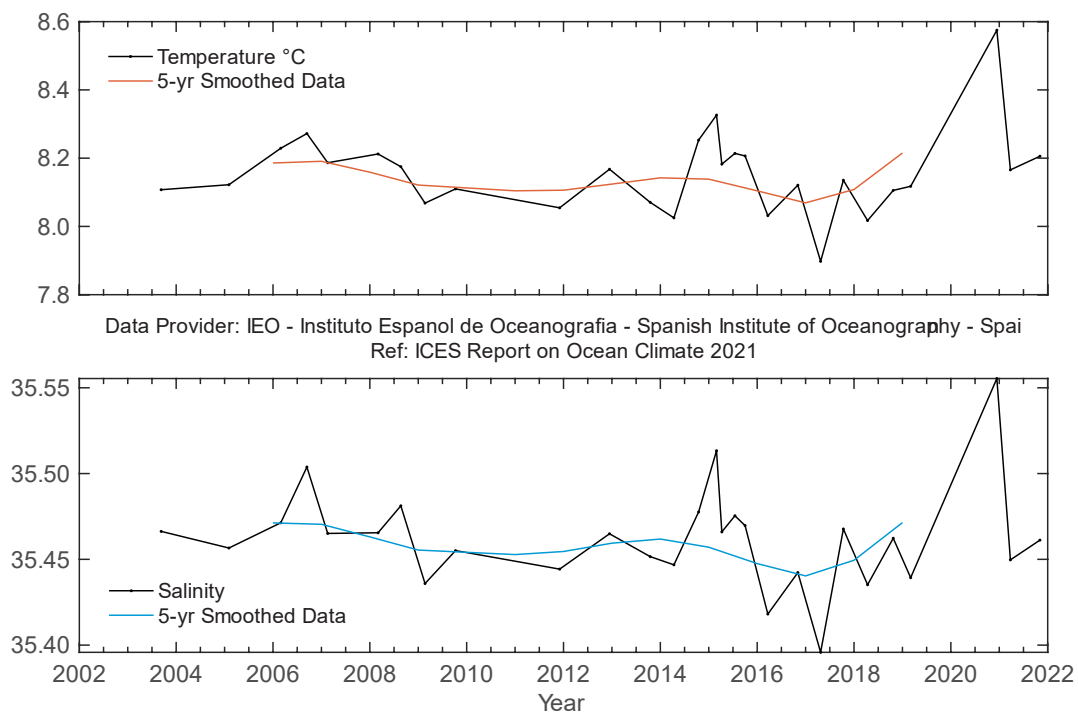


**Figure 5.18. Canary Basin. Potential temperature (upper panel) and salinity (lower panel) for the 800–1 400 m layer.**

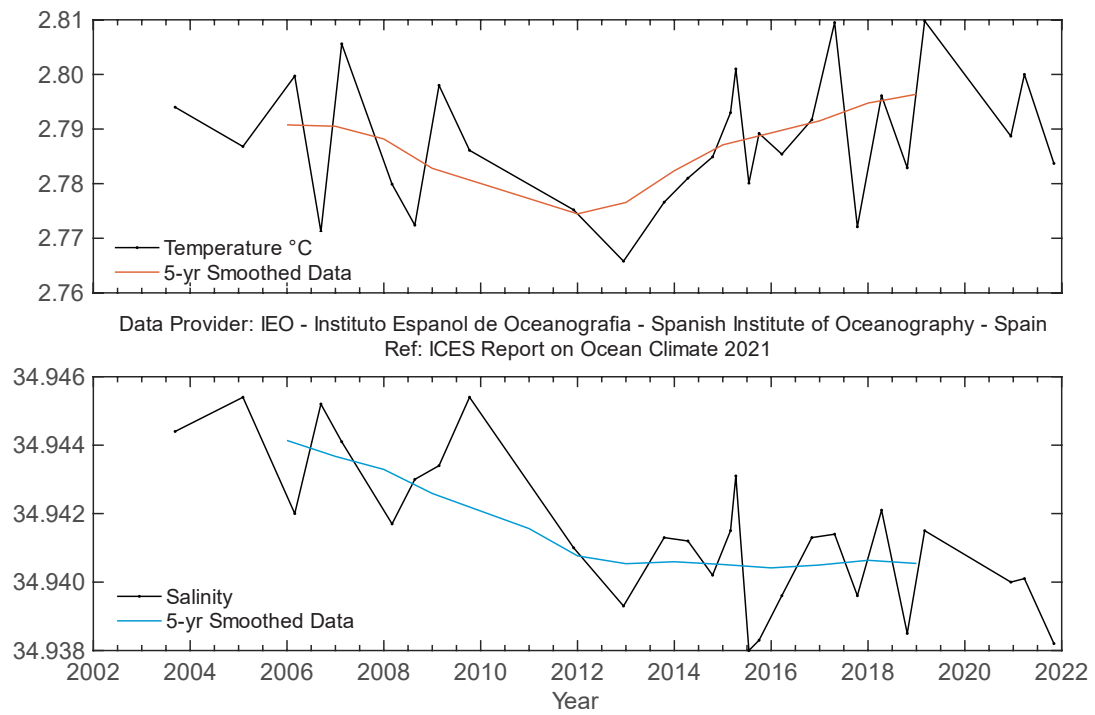


**Figure 5.19. Canary Basin. Potential temperature (upper panel) and salinity (lower panel) for the 2 600–3 600 m layer averaged across the Canaries section.**

## References

- Brakstad, A., Våge, K., Håvik, L., and Moore, G. W. K. 2019. Water mass transformation in the Greenland Sea during the period 1986–2016. *Journal of Physical Oceanography*, 49: 121–140. <https://doi.org/10.1175/JPO-D-17-0273.1>
- Cappelen, J. 2021. Greenland–DMI historical climate data collection 1784–2020. The Danish Meteorological Institute, DMI Report 21-04. 105 pp. <https://www.dmi.dk/fileadmin/Rapporter/2021/DMIREP21-04.pdf>
- Cappelen, J., and Drost Jensen, C. 2021. Climatological Standard Normals 1991–2020–Greenland. The Danish Meteorological Institute, DMI Report 21-12. 83 pp. [https://www.dmi.dk/fileadmin/Rapporter/2021/DMI\\_report\\_21\\_12\\_Greenland.pdf](https://www.dmi.dk/fileadmin/Rapporter/2021/DMI_report_21_12_Greenland.pdf)
- de Boyer Montégut, C., Madec, G., Fischer, A. S., Lazar, A., and Iudicone, D. 2004. Mixed layer depth over the global ocean: An examination of profile data and a profile-based climatology. *Journal of Geophysical Research: Oceans*, 109. <https://doi.org/10.1029/2004JC002378>
- Duchez, A., Frajka-Williams, E., Josey, S. A., Evans, D. G., Grist, J. P., Marsh, R., McCarthy, G. D., *et al.* 2016. Drivers of exceptionally cold North Atlantic Ocean temperatures and their link to the 2015 European heat wave. *Environmental Research Letters*, 11: 074004. <https://doi.org/10.1088/1748-9326/11/7/074004>
- Gaillard, F., Reynaud, T., Thierry, V., Kolodziejczyk, N., and von Schuckmann, K. 2016. *In situ*-based reanalysis of the global ocean temperature and salinity with ISAS: Variability of the heat content and steric height. *Journal of Climate*, 29: 1305–1323. <https://doi:10.1175/jcli-d-15-0028.1>
- Galbraith, P. S. 2006. Winter water masses in the Gulf of St Lawrence. *Journal of Geophysical Research: Oceans*, 111. <https://doi.org/10.1029/2005JC003159>
- Galbraith, P. S., Chassé, J., Shaw, J-L., Caverhill, C., Dumas, J., Lefaivre, D., and Lafleur, C. 2021b. Physical oceanographic conditions in the Gulf of St Lawrence during 2020. Canadian Science Advisory Secretariat, Research Document, 2021/045. 81 pp. <https://publications.gc.ca/pub?id=9.900562&sl=0>
- Galbraith, P. S., Larouche, P., and Caverhill, C. 2021a. A sea-surface temperature homogenization blend for the Northwest Atlantic. *Canadian Journal of Remote Sensing*, 47: 554–568. <https://doi.org/10.1080/07038992.2021.1924645>
- González-Pola, C., Fratantoni, P., Larsen, K. M. H., Holliday, N. P., Dye, S., Mork, K. A., Beszczynska-Möller, A., *et al.* 2019. The ICES Working Group on Oceanic Hydrography: A bridge from *in-situ* sampling to the remote autonomous observation era. *Frontiers in Marine Science*, 6: 103, <https://doi.org/10.3389/fmars.2019.00103>
- González-Pola, C., Larsen, K. M. H., Fratantoni, P., and Beszczynska-Möller, A. (Eds.). 2022. ICES Report on ocean climate 2020. ICES Cooperative Research Report Vol. 356. 121 pp. <https://doi.org/10.17895/ices.pub.19248602>
- González-Pola, C., Lavín, A., and Vargas-Yáñez, M. 2005. Intense warming and salinity modification of intermediate water masses in the southeastern corner of the Bay of Biscay for the period 1992–2003. *Journal of Geophysical Research: Oceans*, 110. <https://doi.org/10.1029/2004JC002367>
- Hernández-Guerra, A., Espino-Falcón, E., Vélez-Belchí, P., Pérez-Hernández, M. D., Martínez-Marrero, A., and Cana, L. 2017. Recirculation of the Canary Current in fall 2014. *Journal of Marine Systems*, 174: 25–39. <https://doi.org/10.1016/j.jmarsys.2017.04.002>
- Holliday, N. P., Bersch, M., Berx, B., Chafik, L., Cunningham, S., Florindo-López, C., Hátún, H., *et al.* 2020. Ocean circulation causes the largest freshening event for 120 years in eastern subpolar North Atlantic. *Nature Communications*, 11: 585. <https://doi.org/10.1038/s41467-020-14474-y>
- Holliday, N. P., Cunningham, S. A., Johnson, C., Gary, S. F., Griffiths, C., Read, J. F., and Sherwin, T. 2015. Multidecadal variability of potential temperature, salinity, and transport in the eastern subpolar North Atlantic. *Journal of Geophysical Research, Oceans*, 120: 5945–5967. <https://doi.org/10.1002/2015JC010762>
- Houpert, L., Cunningham, S., Fraser, N., Johnson, C., Holliday, N., Jones, S., Moat, B., *et al.* 2020. Observed variability of the North Atlantic Current in the Rockall Trough from 4 years of mooring measurements. *Journal of Geophysical Research: Oceans*, 125: 18. <https://doi.org/10.1029/2020JC016403>

- Hurrell, J., and National Center for Atmospheric Research Staff (Eds). 2017. Climate Data Guide: Hurrell North Atlantic Oscillation (NAO) Index (PC-based). <https://climatedataguide.ucar.edu/climate-data/hurrell-north-atlantic-oscillation-nao-index-station-based> Last accessed 24 March 2023.
- Hurrell, J. W., and Deser, C. 2010. North Atlantic climate variability: the role of the North Atlantic Oscillation. *Journal of Marine Systems*, 79: 231–244. <https://doi.org/10.1016/j.jmarsys.2009.11.002>
- Hurrell, J. W., Kushnir, Y., Ottensen, G., and Visbeck, M. 2003. An overview of the North Atlantic oscillation. *In* *The North Atlantic Oscillation: Climate Significance and Environmental Impact*, pp. 1–35. American Geophysical Union, Geophysical Monograph Series, Volume 134. <https://doi.org/10.1029/134GM01>
- Kalnay, E., Kanamitsu, M., Kistler, R., Collins, W., Deaven, D., Gandin, L., Iredell, M., *et al.* 1996. The NCEP/NCAR 40-year reanalysis project. *Bulletin of the American Meteorological Society*, 77: 437–471. [https://doi.org/10.1175/1520-0477\(1996\)077%3C0437:TNYRP%3E2.0.CO;2](https://doi.org/10.1175/1520-0477(1996)077%3C0437:TNYRP%3E2.0.CO;2)
- Kolodziejczyk, N., Prigent-Mazella, A., and Fabienne, G. 2021. ISAS temperature and salinity gridded fields. <https://doi.org/10.17882/52367>
- Mortensen, J. 2022. Report on hydrographic conditions off Southwest Greenland May 2021. Northwest Atlantic Fisheries Organization (NAFO), Scientific Council Research Document, 22/006. <https://www.nafo.int/Portals/0/PDFs/sc/2022/scr22-006.pdf>
- Mountain, D. 2012. Labrador Slope Water entering the Gulf of Maine in response to the North Atlantic Oscillation. *Continental Shelf Research*, 47: 150–155. <https://doi.org/10.1016/j.csr.2012.07.008>
- Paillet, J., and Mercier, H. 1997. An inverse model of the eastern North Atlantic general circulation and thermocline ventilation. *Deep-Sea Research Part I: Oceanographic Research Papers*, 44: 1293–1328. [https://doi.org/10.1016/s0967-0637\(97\)00019-8](https://doi.org/10.1016/s0967-0637(97)00019-8)
- Pingree, R. D. 1993. Flow of surface waters to the west of the British Isles and in the Bay of Biscay. *Deep-Sea Research Part II: Topical Studies in Oceanography*, 40: 369–388. [https://doi.org/10.1016/0967-0645\(93\)90022-f](https://doi.org/10.1016/0967-0645(93)90022-f)
- Pingree, R. D., and Le Cann, B. 1990. Structure, strength and seasonality of the slope currents in the Bay of Biscay region. *Journal of the Marine Biological Association of the United Kingdom*, 70: 857–885. <https://doi.org/10.1017/s0025315400059117>
- Piron, A., Thierry, V., Mercier, H., and Caniaux, G. 2016. Argo float observations of basin-scale deep convection in the Irminger Sea during winter 2011–2012. *Deep-Sea Research Part I: Oceanographic Research Papers*, 109: 76–90. <https://doi.org/10.1016/j.dsr.2015.12.012>
- Prieto, E., González-Pola, C., Lavín, A., and Holliday, N. P. 2015. Interannual variability of the north-western Iberia deep ocean: Response to large-scale North Atlantic forcing. *Journal of Geophysical Research: Oceans*, 120: 832–847. <https://doi.org/10.1002/2014jc010436>
- Skogen, M. D., Svendsen, E., Berntsen, J., Aksnes, D., and Ulvestad, K. B. 1995. Modeling the primary production in the North Sea using a coupled 3-dimensional physical-chemical-biological ocean model. *Estuarine Coastal and Shelf Science*, 41, 545–565. [https://doi.org/10.1016/0272-7714\(95\)90026-8](https://doi.org/10.1016/0272-7714(95)90026-8)
- Somavilla, R., Gonzalez-Pola, C., Rodriguez, C., Josey, S. A., Sanchez, R. F., and Lavin, A. 2009. Large changes in the hydrographic structure of the Bay of Biscay after the extreme mixing of winter 2005. *Journal of Geophysical Research: Oceans*, 114. <https://doi.org/10.1029/2008jc004974>
- Tel, E., Balbin, R., Cabanas, J-M., Garcia, M-J., Garcia-Martinez, M. C., Gonzalez-Pola, C., Lavin, A., *et al.* 2016. IEOS: the Spanish Institute of Oceanography observing system. *Ocean Science*, 12: 345–353. <https://doi.org/10.5194/os-12-345-2016>
- van Aken, H. M. 2002. Surface currents in the Bay of Biscay as observed with drifters between 1995 and 1999. *Deep-Sea Research Part I*, 49: 1071–1086. [https://doi.org/10.1016/s0967-0637\(02\)00017-1](https://doi.org/10.1016/s0967-0637(02)00017-1)
- Vélez-Belchí, P., González-Carballo, M., Pérez-Hernández, M., and Hernández-Guerra, A. 2015. Open ocean temperature and salinity trends in the Canary Current Large Marine Ecosystem. *In* *Oceanographic and biological features in the Canary Current Large Marine Ecosystem*, pp. 299–308. Ed. by L. Valdés, and I. Déniz-González. IOC Technical Series, 115, IOC-UNESCO, Paris, France. 383 pp.

- Vélez-Belchí, P., Pérez-Hernández, M. D., Casanova-Masjoan, M., Cana, L., and Hernández-Guerra, A. 2017. On the seasonal variability of the Canary Current and the Atlantic Meridional Overturning Circulation. *Journal of Geophysical Research: Oceans*, 122: 4518–4538. <https://doi.org/10.1002/2017jc012774>
- Yashayaev, I., and Loder, J. W. 2009. Enhanced production of Labrador Sea Water in 2008. *Geophysical Research Letters*, 36. <https://doi.org/10.1029/2008GL036162>
- Yashayaev, I., and Loder, J. W. 2016. Recurrent replenishment of Labrador Sea Water and associated decadal-scale variability. *Journal of Geophysical Research: Oceans*, 121: 8095–8114. <https://doi.org/10.1002/2016JC012046>
- Yashayaev, I., and Loder, J. W. 2017. Further intensification of deep convection in the Labrador Sea in 2016. *Geophysical Research Letters*, 44: 1429–1438. <https://doi.org/10.1002/2016gl071668>
- Yashayaev, I., van Aken, H. M., Holliday, N. P., and Bersch, M. 2007. Transformation of the Labrador Sea Water in the subpolar North Atlantic. *Geophysical Research Letters*, 34. <https://doi.org/10.1029/2007GL031812>

## Annex 1: Contact information for authors by section

Section	Area/topic	Authors	E-mail	Affiliation
<b>2. Summary of upper ocean conditions in 2018</b>				
2.3	Argo gridded temperature and salinity fields	Nicolas Kolodziejczyk	<a href="mailto:Nicolas.Kolodziejczyk@univ-brest.fr">Nicolas.Kolodziejczyk@univ-brest.fr</a>	University of Brest (UBO), CNRS, IRD, Ifremer, Laboratoire d'Océanographie Physique et Spatiale (LOPS, Laboratory for Ocean Physics and Satellite remote sensing), Brest, France
		Damien Desbruyères	<a href="mailto:Damien.Desbruyeres@ifremer.fr">Damien.Desbruyeres@ifremer.fr</a>	Laboratoire d'Océanographie Physique et Spatiale (Ifremer/LOPS) Brest, France
<b>3. The North Atlantic atmosphere</b>				
All		Stephen R. Dye	<a href="mailto:stephen.dye@cefas.gov.uk">stephen.dye@cefas.gov.uk</a>	Centre for Environment, Fisheries and Aquaculture Science (Cefas), Lowestoft, UK
		Lianne C. Harrison	<a href="mailto:lianne.harrison@cefas.gov.uk">lianne.harrison@cefas.gov.uk</a>	
<b>4. Detailed area descriptions, part I: The upper ocean</b>				
4.1	West Greenland	Boris Cisewski	<a href="mailto:boris.cisewski@thuenen.de">boris.cisewski@thuenen.de</a>	Thünen-Institut für Seefischerei (TI-SF, Thünen Institute of Sea Fisheries), Bremerhaven, Germany
		John Mortensen	<a href="mailto:jomo@natur.gl">jomo@natur.gl</a>	Institute of Natural Resources, Nuuk, Greenland
4.2	Labrador Sea	Igor Yashayaev	<a href="mailto:Igor.Yashayaev@dfo-mpo.gc.ca">Igor.Yashayaev@dfo-mpo.gc.ca</a>	Bedford Institute of Oceanography, Fisheries and Oceans Canada, Dartmouth, NS, Canada
4.3	Newfoundland–Labrador Shelf	Frédéric Cyr	<a href="mailto:Frederic.Cyr@dfo-mpo.gc.ca">Frederic.Cyr@dfo-mpo.gc.ca</a>	Northwest Atlantic Fisheries Centre, Fisheries and Oceans Canada, St. John's, NL, Canada
		Peter S. Galbraith	<a href="mailto:Peter.Galbraith@dfo-mpo.gc.ca">Peter.Galbraith@dfo-mpo.gc.ca</a>	Maurice Lamontagne Institute, Fisheries and Oceans Canada, Mont-Joli, Qc, Canada
4.4	Gulf of St Lawrence	Peter S. Galbraith	<a href="mailto:Peter.Galbraith@dfo-mpo.gc.ca">Peter.Galbraith@dfo-mpo.gc.ca</a>	Maurice Lamontagne Institute, Fisheries and Oceans Canada, Mont-Joli, Qc, Canada

Section	Area/topic	Authors	E-mail	Affiliation
4.5	Scotian Shelf	David Hebert	<a href="mailto:David.Hebert@dfo-mpo.gc.ca">David.Hebert@dfo-mpo.gc.ca</a>	Bedford Institute of Oceanography, Fisheries and Oceans Canada, Dartmouth, NS, Canada
		Chantelle Layton	<a href="mailto:Chantelle.Layton@dfo-mpo.gc.ca">Chantelle.Layton@dfo-mpo.gc.ca</a>	
		Peter S. Galbraith	<a href="mailto:Peter.Galbraith@dfo-mpo.gc.ca">Peter.Galbraith@dfo-mpo.gc.ca</a>	Maurice Lamontagne Institute, Fisheries and Oceans Canada, Mont-Joli, Qc, Canada
4.6	Northeast US continental shelf	Paula Fratantoni	<a href="mailto:paula.fratantoni@noaa.gov">paula.fratantoni@noaa.gov</a>	NOAA Fisheries, NEFSC, Oceans and Climate Branch, Woods Hole, MA, USA
4.7	Icelandic Waters	Solveig R. Ólafsdóttir	<a href="mailto:solveig.rosa.olafsdottir@hafogvatn.is">solveig.rosa.olafsdottir@hafogvatn.is</a>	Hafrannsóknastofnun (Marine and Freshwater Research Institute, MFRI), Reykjavík, Iceland
		Magnus Danielsen	<a href="mailto:magnus.danielsen@hafogvatn.is">magnus.danielsen@hafogvatn.is</a>	
4.8	Bay of Biscay and Iberian Coast	Almudena Fontán	<a href="mailto:afontan@azti.es">afontan@azti.es</a>	AZTI. Aquarium of San Sebastian (SOG) and Idalgo Meteorological Observatory (AEMet), San Sebastian, Spain
		Cesar González-Pola	<a href="mailto:cesar.pola@ieo.csic.es">cesar.pola@ieo.csic.es</a>	Instituto Español de Oceanografía (IEO, Spanish Institute of Oceanography), Gijón Oceanographic Centre, Gijón, Spain
4.9	Gulf of Cadiz	Ricardo Sánchez-Leal	<a href="mailto:rleal@ieo.csic.es">rleal@ieo.csic.es</a>	Instituto Español de Oceanografía (IEO, Spanish Institute of Oceanography), Cádiz Oceanographic Centre, Cádiz, Spain
4.10	Canary Basin	Pedro Vélez-Belchí	<a href="mailto:pedro.velez@ieo.csic.es">pedro.velez@ieo.csic.es</a>	Instituto Español de Oceanografía (IEO, Spanish Institute of Oceanography), Canary Islands Oceanographic Centre, Tenerife, Spain
		Ángela Mosquera	<a href="mailto:angela.mosquera@ieo.csic.es">angela.mosquera@ieo.csic.es</a>	
		Carmen Presas-Navarro	<a href="mailto:carmen.presas@ieo.csic.es">carmen.presas@ieo.csic.es</a>	
4.11	Southwest Approaches	Tim J. Smyth	<a href="mailto:TJSM@pml.ac.uk">TJSM@pml.ac.uk</a>	Marine Biological Association and Plymouth Marine Laboratory (PML), Plymouth, UK
4.12	Celtic Seas	Kieran Lyons	<a href="mailto:Kieran.lyons@Marine.ie">Kieran.lyons@Marine.ie</a>	Marine Institute/Met Eireann, Galway, Ireland
		Caroline Cusack	<a href="mailto:caroline.cusack@Marine.ie">caroline.cusack@Marine.ie</a>	
		Eoghan Daly	<a href="mailto:Eoghan.Daly@Marine.ie">Eoghan.Daly@Marine.ie</a>	

Section	Area/topic	Authors	E-mail	Affiliation
		Billy Hunter	<a href="mailto:Billy.Hunter@afbini.gov.uk">Billy.Hunter@afbini.gov.uk</a>	Agri-Food and Biosciences Institute, Belfast, Ireland
4.13	Rockall Trough	Sam Jones	<a href="mailto:Sam.Jones@sams.ac.uk">Sam.Jones@sams.ac.uk</a>	Scottish Association for Marine Science (SAMS), Oban, UK
4.14	Hatton–Rockall Basin			
4.15	Iceland Basin			
4.16	Irminger Sea	M. Fremke de Jong	<a href="mailto:Femke.de.Jong@nioz.nl">Femke.de.Jong@nioz.nl</a>	Koninklijk Nederlands, Instituut voor Zeeonderzoek (NIOZ, Royal Netherlands Institute for Sea Research), Texel, Netherlands
4.17	Faroese Waters and the Faroe–Shetland Channel	Karin Margretha H. Larsen	<a href="mailto:karin@hav.fo">karin@hav.fo</a>	Havstovan (Faroe Marine Research Institute, FAMRI), Tórshavn, Faroe Islands
		Barbara Berx	<a href="mailto:barbara.berx@gov.scot">barbara.berx@gov.scot</a>	Scottish Government Marine Directorate, Aberdeen, UK
		Berit Rabe	<a href="mailto:Berit.rabe@gov.scot">Berit.rabe@gov.scot</a>	
4.18	North Sea	Dagmar Kieke	<a href="mailto:Dagmar.Kieke@bsh.de">Dagmar.Kieke@bsh.de</a>	Bundesamt für Seeschifffahrt und Hydrographie (BSH, Federal Maritime and Hydrographic Agency, Hamburg, Germany)
		Holger Klein	<a href="mailto:Holger.Klein@bsh.de">Holger.Klein@bsh.de</a>	
		Peter Loewe	<a href="mailto:peter.loewe@bsh.de">peter.loewe@bsh.de</a>	
		Manuela Köllner	<a href="mailto:manuela.koellner@bsh.de">manuela.koellner@bsh.de</a>	
		Katrin Latarius	<a href="mailto:katrin.latarius@bsh.de">katrin.latarius@bsh.de</a>	
		Tim Kruschke	<a href="mailto:tim.kruschke@bsh.de">tim.kruschke@bsh.de</a>	
		Barbara Berx	<a href="mailto:barbara.berx@gov.scot">barbara.berx@gov.scot</a>	Scottish Government Marine Directorate, Aberdeen, UK
		Berit Rabe	<a href="mailto:Berit.rabe@gov.scot">Berit.rabe@gov.scot</a>	
		Jon Albretsen	<a href="mailto:jon.albretsen@hi.no">jon.albretsen@hi.no</a>	Institute of Marine Research (IMR), Bergen, Norway
	Inga Kirstein	<a href="mailto:inga.kirstein@awi.de">inga.kirstein@awi.de</a>		

Section	Area/topic	Authors	E-mail	Affiliation
		Karen Wiltshire	<a href="mailto:Karen.Wiltshire@awi.de">Karen.Wiltshire@awi.de</a>	Alfred Wegner institute, Hermholtz Centre for Polar and marine Research (AWI), Bremehaven, Germany
4.19	Skaggerak, Kattegat, and the Baltic Sea	Johanna Linders	<a href="mailto:johanna.linders@smhi.se">johanna.linders@smhi.se</a>	Swedish Meteorological and Hydrological Institute (SMHI), Göteborg, Sweden
		Tycjan Wodzinowski	<a href="mailto:tycjan@mir.gdynia.pl">tycjan@mir.gdynia.pl</a>	National Marine Fisheries Research Institute (MIR-PIB), Gdynia, Poland
		Taavi Liblik	<a href="mailto:taavi.liblik@taltech.ee">taavi.liblik@taltech.ee</a>	Tallinn University of Technology, Estonia
4.20	Norwegian Sea	Kjell-Arne Mork	<a href="mailto:kjell.arne.mork@hi.no">kjell.arne.mork@hi.no</a>	Institute of Marine Research (IMR), Bergen, Norway
4.21	Barents Sea	Alexander Trofimov	<a href="mailto:trofimov@pinro.ru">trofimov@pinro.ru</a>	Knipovich Polar Research Institute of Marine Fisheries and Oceanography (PINRO), Murmansk, Russian Federation
		Randi Ingvaldsen	<a href="mailto:randi.ingvaldsen@imr.no">randi.ingvaldsen@imr.no</a>	Institute of Marine Research (IMR), Bergen, Norway
4.22	Fram Strait	Agnieszka Beszczynska-Möller	<a href="mailto:abesz@iopan.gda.pl">abesz@iopan.gda.pl</a>	Institute of Oceanology, Polish Academy of Sciences (IOPAN), Sopot, Poland
		Wilken-Jon von Appen	<a href="mailto:Wilken-Jon.von.Appen@awi.de">Wilken-Jon.von.Appen@awi.de</a>	Alfred Wegner Institute, Hermholtz Centre for Polar and marine Research (AWI), Bremehaven, Germany
<b>5. Detailed area descriptions, part II: The intermediate and deep ocean</b>				
5.1.1	Greenland Sea	Agnieszka Beszczynska-Möller	<a href="mailto:abesz@iopan.gda.pl">abesz@iopan.gda.pl</a>	Institute of Oceanology, Polish academy of sciences (IOPAN), Sopot, Poland
5.1.2	Norwegian Sea	Svein Østerhus	<a href="mailto:svos@norceresearch.no">svos@norceresearch.no</a>	Norwegian Research Institute (NORCE), Bergen
5.1.3	Iceland Sea	Sólveig R. Ólafsdóttir	<a href="mailto:solveig.rosa.olafsdottir@hafogvatn.is">solveig.rosa.olafsdottir@hafogvatn.is</a>	Hafrannsóknastofnun (Marine and Freshwater Research Institute, MFRI), Reykjavík, Iceland
		Magnus Danielsen	<a href="mailto:magnus.danielsen@hafogvatn.is">magnus.danielsen@hafogvatn.is</a>	
5.2.1		Barbara Berx	<a href="mailto:barbara.berx@gov.scot">barbara.berx@gov.scot</a>	Scottish Government Marine Directorate, Aberdeen, UK

	Iceland–Scotland Ridge overflow waters	Berit Rabe	<a href="mailto:Berit.rabe@gov.scot">Berit.rabe@gov.scot</a>	
<b>Section</b>	<b>Area/topic</b>	<b>Authors</b>	<b>E-mail</b>	<b>Affiliation</b>
5.2.2	Iceland Basin	Sam Jones	<a href="mailto:Sam.Jones@sams.ac.uk">Sam.Jones@sams.ac.uk</a>	Scottish Association for Marine Science (SAMS), Oban, UK
5.2.3	Rockall Trough			
5.2.4	Irminger Basin	M. Fremke de Jong	<a href="mailto:Femke.de.Jong@nioz.nl">Femke.de.Jong@nioz.nl</a>	Koninklijk Nederlands, Instituut voor Zeeonderzoek (NIOZ, Royal Netherlands Institute for Sea Research), Texel, Netherlands
5.2.5	Labrador Basin	Igor Yashayaev	<a href="mailto:Igor.Yashayaev@dfo-mpo.gc.ca">Igor.Yashayaev@dfo-mpo.gc.ca</a>	Ocean Monitoring and Observation Section, Oceans and Ecosystem Division, Bedford Institute of Oceanography, Fisheries and Oceans (BIO), Bedford, Canada
		Boris Cisewski	<a href="mailto:boris.cisewski@thuenen.de">boris.cisewski@thuenen.de</a>	Thünen-Institut für Seefischerei (TI-SF, Thünen Institute of Sea Fisheries), Bremehaven, Germany
5.2.6	Western Iberian Basin	Cesar González-Pola	<a href="mailto:cesar.pola@ieo.csic.es">cesar.pola@ieo.csic.es</a>	Instituto Español de Oceanografía (IEO, Spanish Institute of Oceanography), Gijón Oceanographic Centre, Gijón, Spain
		Rocío Graña	<a href="mailto:rocio.grana@ieo.csic.es">rocio.grana@ieo.csic.es</a>	
		Raquel Somavilla	<a href="mailto:raquel.somavilla@ieo.csic.es">raquel.somavilla@ieo.csic.es</a>	Instituto Español de Oceanografía (IEO, Spanish Institute of Oceanography), Santander Oceanographic Centre, Santander, Spain
5.2.7	Gulf of Cadiz	Ricardo Sánchez-Leal	<a href="mailto:rleal@ieo.csic.es">rleal@ieo.csic.es</a>	Instituto Español de Oceanografía (IEO, Spanish Institute of Oceanography), Cádiz Oceanographic Centre, Cádiz, Spain
5.2.8	Canary Basin	Pedro Vélez-Belchí	<a href="mailto:pedro.velez@ieo.csic.es">pedro.velez@ieo.csic.es</a>	Instituto Español de Oceanografía (IEO, Spanish Institute of Oceanography), Canary Islands Oceanographic Centre, Tenerife, Spain
		Ángela Mosquera	<a href="mailto:angela.mosquera@ieo.csic.es">angela.mosquera@ieo.csic.es</a>	

---

Carmen Presas-Navarro

[carmen.presas@ieo.csic.es](mailto:carmen.presas@ieo.csic.es)

---

## Annex 2: List of abbreviations

<b>AAIW</b>	Antarctic Intermediate Waters
<b>AI</b>	Atlantic Inflow
<b>AIW</b>	Arctic Intermediate Water
<b>ARGO</b>	Not an acronym, but the name of a type of instrument used to collect data. The name ARGO is a reference to Greek mythology.
<b>Argo-GDAC</b>	Argo - Global Data Assembly Centres
<b>AW</b>	Atlantic Water
<b>BSH</b>	Bundesamt für Seeschifffahrt und Hydrographie (German Federal Maritime and Hydrographic Agency)
<b>CCLME</b>	Canary Current Large Marine Ecosystem
<b>CIL</b>	Cold Intermediate Layer
<b>CIRES</b>	Cooperative Institute for Research in Environmental Sciences, USA
<b>CTD</b>	Conductivity Temperature Depth
<b>CTZ</b>	Coastal Transition Zone
<b>DSOW</b>	Denmark Strait Overflow Water
<b>EGC</b>	East Greenland Current
<b>ENACW</b>	Eastern North Atlantic Central Waters
<b>GSDW</b>	Greenland Sea Deep Water
<b>ICES</b>	International Council for the Exploration of the Sea
<b>Ifremer</b>	Institut Français de Recherche pour l'Exploitation de la Mer (French Institute for Ocean Research)
<b>IROC</b>	ICES Report on Ocean Climate
<b>ISAS</b>	<i>In Situ</i> Analysis System
<b>ISOW</b>	Iceland Scotland Overflow Water
<b>LME</b>	Large marine ecosystem
<b>LSW</b>	Labrador Sea water
<b>MLD</b>	Mixed-layer depth
<b>MNAW</b>	Modified North Atlantic Water
<b>MOW</b>	Mediterranean Overflow Water
<b>MW</b>	Mediterranean Waters
<b>NAC</b>	North Atlantic Current
<b>NACW</b>	North Atlantic Central Waters
<b>NADW</b>	North Atlantic Deep Water

<b>NAO</b>	North Atlantic Oscillation
<b>NAW</b>	North Atlantic Water
<b>NOAA</b>	National Oceanic and Atmospheric Administration (USA)
<b>NRT</b>	Near real time
<b>NSDW</b>	Norwegian Sea Deep Water
<b>OI</b>	Optimal interpolation
<b>OISST.v2</b>	Optimum interpolation SST dataset version 2
<b>RAC</b>	Return Atlantic Current
<b>RAW</b>	Return Atlantic Water
<b>s.d.</b>	Standard deviation
<b>SPMW</b>	Subpolar mode water
<b>SLP</b>	Sea level pressure
<b>SST</b>	Sea surface temperature
<b>SSS</b>	Sea surface salinity
<b>UPDW</b>	Upper Polar Deep Water
<b>WGC</b>	West Greenland Current
<b>WGOH</b>	ICES Working Group Oceanic Hydrography
<b>WOCE</b>	World Ocean Circulation Experiment
<b>WSC</b>	West Spitsbergen Current